RIDE AND DIRECTIONAL DYNAMIC ANALYSIS OF ARTICULATED FRAME STEER VEHICLES

Alireza Pazooki

A Thesis

in

The Department

of

Mechanical and Industrial Engineering

Presented in Partial Fulfillment of the Requirements
For the Degree of Doctor of Philosophy (Mechanical Engineering) at
Concordia University
Montreal, Quebec, Canada

December 2012

CONCORDIA UNIVERSITY

SCHOOL OF GRADUATE STUDIES

This is to certify that the thesis prepared

By: **Alireza Pazooki**

Entitled: **Ride and Directional Dynamic Analysis of Articulated Steer Vehicles**

and submitted in partial fulfillment of the requirements for the degree of

DOCTOR OF PHILOSOPHY (Mechanical Engineering)

complies with the regulations of the University and meets the accepted standards with respect to originality and quality.

Signed by the final examining committee:

______________________________ Chair
Dr. Amir G. Aghdam

______________________________ External Examiner
Dr. Corina Sandu

______________________________ External to Program
Dr. S. Samuel Li

______________________________ Examiner
Dr. A. K. Waizuddin Ahmed

______________________________ Examiner
Dr. Ramin Sedaghati

______________________________Thesis Supervisor
Dr. Subhash Rakheja, Dr. Dongpu Cao

Approved by ______________________________
Dr. Ali Dolatabadi, Graduate Program Director

December 5, 2012

____
Dr. Robin A.L. Drew, Dean
Faculty of Engineering & Computer Science

ABSTRACT

Pazooki Alireza, Ph.D.
Concordia University, 2012

Articulated frame steer vehicles (ASVs), widely employed in different off-road sectors, are generally unsuspended vehicles. Owning to their complex operating environment, high mass center, relatively soft and large diameter tires, wide load variations and load distribution, and kineto-dynamics of the frame steering mechanism, these vehicles transmit higher magnitudes of low frequency whole-body vibration (WBV) to the operators and also exhibit lower roll and directional stability limits. While the superior performance potentials of axle suspension in limiting the WBV exposure have been clearly demonstrated, the implementations in ASVs have been limited due to the complex design challenges associated with conflicting requirements posed by the ride and roll/directional stability requirements. Growing concerns on human driver comfort and safety, and increasing demands for higher speed ASVs such as articulated dump trucks, however, call for alternate suspension designs for realizing an improved compromise between the ride and stability performance. This dissertation research is aimed at analysis of a torsio-elastic axle suspension concept for achieving improve ride, while preserving the directional stability limits of the ASV. For this purpose a comprehensive three-dimensional model of the articulated frame steer vehicles is developed for design and analysis of the proposed axle suspension concept. The model is formulated considering a three-dimensional tire model, tire lag, coherent right- and left-terrain track roughness, and kinematics and dynamics of the steering struts.

Field measurements were performed to characterize the ride properties of a conventional forestry skidder and that of a skidder retrofitted with the rear-axle torsio-elastic suspension under different load conditions. The measured data were analyzed to assess the ride performance potential of the suspension and to examine validity of the simulation model. Both the field measured and simulation results revealed that the proposed suspension could yield significant reductions in the magnitudes of vibration transmitted to the operator location, irrespective of the load and speed conditions. A simple yaw-plane model of the vehicle is also formulated to study the role of steering system design including the steering valve flows, kineto-dynamics of the steering struts and leakage flows on the snaking stability limits of the ASV. The results showed that the critical speeds are strongly dependent upon the kineto-dynamics of the articulated steering system.

The comprehensive three-dimensional model subsequently used for analysis of integrated ride and roll/directional stability limits of the vehicle and the axle suspension designs. The stability performance measures are defined to assess the vehicle stability limits under steady as well as transient directional maneuvers. The results show that the proposed rear-axle suspension deteriorates the stability performance only slightly, irrespective of the load condition. It is concluded that the proposed suspension concept could yield a very good compromise in ride and stability performance. The proposed model could serve as an effective and efficient tool for integrated ride and handling analysis and to seek primary suspension designs for an improved compromise between the ride and stability performance of ASVs.

ACKNOWLEDGMENTS

The author wishes to express his sincere appreciation to his thesis supervisors, Dr. Subhash Rakheja and Dr. Dangpu Cao, for initiating the study topic and for their great supports and continued guidance and efforts through the thesis work.

The author also wishes to acknowledge Quebec Government, Concordia University, Hydro Quebec and CONCAVE center for their financial support: International Tuition Fee Remission, Concordia Merit Award, Concordia Accelerator Award, Hydro Quebec Award, and Research Assistantship, respectively.

The author also thanks colleagues, faculty and staff at the department of Mechanical and Industrial Engineering, and CONCAVE center, for their contributions to this thesis work.

The author also wishes to acknowledge Dr. Thomas Heegaard Langer and Hydrema Company for their great corporations.

Finally, the author would like to express his special thanks to his family and friends, specially, Mr. Reza Ahani and Mr. Kordestani for their support and encouragement. The author would like to dedicate this thesis to the memory of his father who passed away in 2004 to keep his spirit alive and to his mother for her great support.

LIST OF CONTENTS

CHAPTER 1

CHAPTER 2

CHAPTER 3

CHAPTER 4

CHAPTER 5

CHAPTER 6

LIST OF FIGURES

Figure 1.4: Adaptive footprint tire model. 15

LIST of TABLES

NOMENCLATURE

SYMBOL	DESCRIPTION
$\bar{a}$	Frequency-weighted root-mean-square (rms) acceleration, *m/s*^{2}
a_v	Vector summation of the translational weighted accelerations, *m/s*^{2}
A_1	Effective valve outlet opening area, *m*^{2}
A_2	Effective valve inlet opening area, *m*^{2}
$A(8)$	Eight-hour energy equivalent frequency-weighted acceleration, *m/s*^{2}
A_p	Effective cross-section areas of the struts on the piston-side, *m*^{2}
A_r	Effective cross-section areas of the struts on the rod-sides, *m*^{2}
B	Bulk modulus of the hydraulic oil, *Pa*
b	Longitudinal distance of the articulation joint to the front unit *cg*, *m*
d	Longitudinal distance of the articulation joint to the rear unit *cg*, *m*
c_y, c_z, c_t	Lateral, vertical, and torsional damping coefficients of the suspension, respectively, *N.s/m*
C	Viscous damping coefficient of the adaptive tire model, *N.s/m*
C_α	Tire cornering stiffness, *N/m*
C_d	Valve discharge coefficient
C_s	Soil cone index, *Pa*
C_T, C_{TY}	Linear vertical and lateral damping coefficients of the tires, *N.s/m*
[C]	Damping matrix, *N.s/m*
$[C_F]$	Forced damping matrix, *N*
DRT	Dynamic Rollover Threshold, *g*
ELA	Effective Lateral Acceleration, *g*
$EMOB$	Mobility number

$\overline{f}$	Center frequency of the i^{th} third-octave frequency band, *Hz*
F_{dw}	Damping force of the adaptive tire model, *N*
$F_{k_{Gi}}$	Components of the gravity force of unit i $(i = f, r)$ along axis k $(k = x, y, z)$, respectively, *N*
$F_{k_{Ci}}$	Constraint forces and moments acting on unit i $(i = f, r)$ along axis k $(k = x, y, z)$, respectively, *N*
$F_{k_{Sr}}$	Total suspension forces acting on the rear unit along the axis k $(k = x, y, z)$, respectively, *N*
$F_{k_{Ti}}$	Total tires forces acting on unit i $(i = f, r)$, along axis k $(k = x, y, z)$, respectively, *N*
$F_{k_{Tl}}$	Total tires forces developed by tire l ($l=1,\ldots, 4$), along axis k $(k = x, y, z)$, respectively, *N*
F_L, F_R	Forces developed by the left and right steering struts, *N*
F_{Tx} , F_{Tz}	Resultant longitudinal and vertical forces of the adaptive tire model, *N*
F_{wn}	Resultant force act normal to the footprint, *N*
F_{y4}, F_{y3}	Lateral forces acting on the sprung mass developed due to left- and right-axle suspensions, respectively, *N*
F_{z4u}, F_{z3u}	Vertical forces acting at the unsprung mass developed due to left- and right-axle suspensions, respectively, *N*
F_{z4}, F_{z3}	Vertical forces acting on the sprung mass developed due to left- and right-axle suspensions, respectively, *N*
F_{y4u}, F_{y3u}	Lateral forces acting on the unsprung mass developed due to left- and right-axle suspensions, respectively, *N*
F_{yS_R}, $F_{yS_{jL}}$	Total suspension lateral forces acting on the right and left linkage, respectively, *N*
F_{zS_R}, F_{zS_L}	Total suspension vertical forces acting on the right and left linkage, respectively, *N*

$F_{yS_{uR}}$, $F_{yS_{uL}}$	Suspension lateral forces acting on the unsprung mass due to the right and left linkage, respectively, *N*
$F_{zS_{uR}}$, $F_{zS_{uL}}$	Suspension vertical forces acting on the unsprung mass due to the right and left linkage, respectively, *N*
$F_{yS_{sR}}$, $F_{yS_{sL}}$	Suspension lateral forces acting on the sprung mass due to the right and left linkage, respectively, *N*
$F_{zS_{sR}}$, $F_{zS_{sL}}$	Suspension vertical forces acting on the sprung mass due to the right and left linkage, respectively, *N*
$F_{y_{Sj}}$, $F_{z_{Sj}}$	Total suspension forces due to suspension linkage *j* (*j*=*L*, *R*) acting along y-, z- and x-axis of the coordinate system fixed to the linkage mass, *N*
$F_{y_{Gj}}$,$F_{z_{Gj}}$	Components of the gravity force along the y- and z-axis of the left *j*=*L*, and right, *j*=*R*, linkage masses, respectively, *N*
$F_{y_{Su}}$, $F_{z_{Su}}$	Total forces developed by the left- and right-suspension acting on the unsprung mass along the y- and z-axis, respectively, *N*
$F_{y_{Gu}}$, $F_{z_{Gu}}$	Components of the gravity force along the y- and z-axis of the unsprung mass, *N*
$F_{y_{Tu}}$, $F_{z_{Tu}}$	Total tire forces along the y- and z-axis of the axis system attached to the unsprung mass, respectively, *N*
$F_{x_{Hi}}$, $F_{y_{Hi}}$	Total hydraulic steering struts forces acting along x-, y-axis of the front (*i*=*f*) and rear (*i*=*r*) unit due to the tires, respectively, *N*
$G_Z(\Omega)$	Spatial PSD of the terrain roughness, m^3/*cycle*
h_{sf}, h_{sr}	Instantaneous cg heights of the front and rear masses, respectively, *m*
h_u	Instantaneous cg height of the rear axle unsprung mass, *m*
h_1, h_2	Vertical coordinates of the connection points of the suspension linkage and rear axle with respect to the vehicle cg and rear axle cg, *m*
h'	Vertical coordinates of the seat location with respect to vehicle cg, *m*
$[H(j\omega)]$	Complex transfer function matrices of the conventional and suspended vehicle models

$[H_{S0}(j\omega)]$	Frequency response function matrix relating the response vector at the seat to the excitation coordinates.
I_{YYS}, I_{XXS}	Pitch and roll mass moments of inertia of the unsuspended vehicle, respectively, $kg.m^2$
I'_{YYS}, I'_{XXS}	Roll and pitch mass moments of inertia of the sprung mass, respectively, $kg.m^2$
I_r	Roll mass moments of inertia of the rear axle, $kg.m^2$
I_3, I_4	Roll mass moments of inertia of the right and left suspension links, respectively, $kg.m^2$
I_1, I_2	Mass moments of inertia of the front and rear units, respectively, $kg.m^2$
$I_{xx_{si}}$, $I_{yy_{si}}$, $I_{zz_{si}}$	Mass moments of inertia about the fixed axes (i_{si}, j_{si}, k_{si}), respectively, $kg.m^2$
I_{xx_u}	Roll mass moment of inertia of unsprung mass, $kg.m^2$
k_{anti}	Equivalent torsional stiffness of the anti-roll bar, *N/rad*
k_y, k_z, k_t	Lateral, vertical, and torsional stiffness coefficients of the suspension, *N/m* or *N/rad*
K	Linear stiffness constant of the radial element of the adaptive tire model, *N/m*
K_L	Leakage coefficient
K_{φ_c}, K_{θ_c}	Torsional stiffnesses due to the structural compliance along the pitch and roll axes, *N/rad*
K_{T_l}	Vertical stiffness of tire l $(l = 1, \dots, 4)$, *N/m*
K_{Ti} , K_{TYi}	Linear vertical and lateral stiffness of tire i (i=1, 2, 3, 4), respectively, *N/m*
C_{Ti}	Linear damping coefficient of tire i (i=1, 2, 3, 4), *N.s/m*
[K]	Stiffness matrix, *N/m*
$[K_F]$	Forced stiffness matrix, *N*

l_x	Longitudinal distance of the seat location to vehicle cg, *m*
$l_1 l_2$, $r_1 r_2$	Instantaneous lengths of the left and right struts, respectively, *m*
LTR	Load Transfer Ratio
L_0	Torsio-elastic suspension linkage length, *m*
m_s	Mass of the unsuspended vehicle, *kg*
m_1, m_2	Masses of the front and rear units, respectively, *kg*
m_{ur}	Rear axle mass, *kg*
m_3, m_4	Right- and left- suspension linkage masses, *kg*
m_{si}	Masses of the front (i=f) and rear (i=r) unit, *kg*
m_u	Mass of unsprung mass, *kg*
m_j	Mass of left, j=L, and right, j=R, suspension linkages, *kg*
M	Total mass of the suspended vehicle, *kg*
$M_{k_{Ti}}$	Total tires moments acting on unit i $(i = f, r)$ along axis k $(k = x, y, z)$, respectively, *N.m*
$M_{k_{Hi}}$	Total hydraulic steering strut moments acting on unit i $(i = f, r)$ along axis k $(k = x, y, z)$, respectively, *N.m*
$M_{k_{Sr}}$	Total suspension moments acting on the rear unit along axis k $(k = x, y, z)$, respectively, *N.m*
$M_{k_{Ci}}$	Total constraint moments acting on unit i $(i = f, r)$ along axis k $(k = x, y)$, respectively, *N.m*
$M_{x_{Tu}}$	Total tire roll moment acting on unsprung mass, *N.m*
$M_{x_{Su}}$	Total resulting roll moment developed by the left- and right-suspension acting on the unsprung mass, *N.m*
$M_{x_{Sj}}$	Total suspension moment due to suspension linkage j (j=L, R) acting along x-axis of the coordinate system fixed to the linkage mass, *N.m*
$M_{xS_{sR}}$, $M_{xS_{sL}}$	Suspension moments acting on the sprung mass due to the right and

	left linkage, respectively, *N.m*
$M_{xS_{uR}}, M_{xS_{uL}}$	Suspension moments acting on the unsprung mass due to the right and left linkage, respectively, *N.m*
M_{xS_R}, M_{xS_L}	Total suspension moments acting on the right and left linkage, respectively, *N.m*
[M]	Mass matrix, *kg*
p_{si}, q_{si}, r_{si}	Roll, pitch and yaw velocities of the front (*i=f*) and rear (*i=r*) unit, respectively, *rad/s*
P_1	Pressures of fluid at the valve outlet, *Pa*
P_2	Pressure of fluid discharged by the struts, *Pa*
P_0	Reservoir fluid pressure, *Pa*
P_S	Pump working pressure, *Pa*
ΔP_m	Peak pressure drop across the steering valve, *Pa*
P_{L1}, P_{L2}	Fluid pressures within the piston- and rod-side chambers of the left strut, *Pa*
P_{R1}, P_{R2}	Fluid pressures within the piston- and rod-side chambers of the right strut, *Pa*
Q_1 , Q_2	The rates of fluid flows to and from the struts, respectively, m^3/s
Q_{max}	Maximum flow rate through the valve, m^3/s
Q_L	leakage flows through the piston seals, m^3/s
Q_{L1}, Q_{R2}	Rates of fluid flows to the piston- and rod-side chambers of the left and right struts, respectively, m^3/s
Q_{L2}, Q_{R1}	Rates of fluid flows to the rod- and piston-side chambers of the left and right struts, respectively, m^3/s
RA	Rearward amplification ratio of the yaw velocity
RSF	Roll Safety Factor
R_x, R_y	Internal forces at the articulation joint, *N*

R_w	Un-deformed tire radius, *m*
$[R]$	Transformation matrix relating the generalized coordinates with those at the operator seat
SRT	Static Rollover Threshold, *g*
$S_g(\Omega)$	PSD of road surface elevation, $m^3/cycle$
$S_g(\Omega_o)$	Roughness constant
$[S(j\omega)]$	Spectral density matrix of the generalized response coordinates
$[S_i(j\omega)]$	Matrix of the spectral density of elevations at the tire *i*-terrain interfaces
$[S_{S0}^{d}(j\omega)]$	Matrix of PSD of displacement responses at the seat
$[S_{S0}^{a}(j\omega)]$	Matrix of PSD of acceleration responses at the seat
T_e	Average daily exposure duration, *s*
T	Half-track width, *m*
T_{sf}, T_{sr}	The steering torque acting on the front and rear units, respectively, *N.m*
T_o	Torque developed by the resultant struts forces about the articulation joint, *N.m*
${}^{E}_{si}T$	The transformation matrix from the body-fixed coordinate system of the front ($i=f$) and rear ($i=r$) body masses to the inertial system
${}^{sf}_{sr}T$	Transformation from the body-fixed coordinate system of the rear unit to that corresponding to the front unit
u_i, v_i, Ω_i	Longitudinal, lateral and yaw velocities of the front ($i=1$) and rear ($i=2$) units, respectively, *m/s* or *rad/s*
u_{si}, v_{si}, w_{si}	Longitudinal, lateral and vertical velocities of the front ($i=f$) and rear ($i=r$) unit, respectively, *m/s*
v_u, w_u, p_u	Lateral, vertical and roll velocities of the unsprung mass, respectively, *m/s* or *rad/s*
v_j,w_j, p_j	Lateral, bounce and roll velocities of the left $j=L$, and right, $j=R$,

	linkage masses, *m/s* or *rad/s*
VDV	Vibration dose value, $m/s^{1.75}$
V_{L1}, V_{R2}	Instantaneous fluid volumes in the piston- and rod-side chambers of the left and right struts, respectively, m^3
V_{L2}, V_{R1}	Instantaneous fluid volumes in the rod- and piston-side chambers of the left and right struts, respectively, m^3
V_{0L1}, V_{0R2}	Initial fluid volumes in the piston- and rod-side chambers of the left and right struts, respectively, m^3
V_{0L2}, V_{0R1}	Initial fluid volumes in the rod- and piston-side chambers of the left and right struts, respectively, m^3
WB1, WB2	Longitudinal coordinates of the front and rear axles with respect to vehicle cg, *m*
W_k, W_d, W_e	Frequency weighting for assessing of vertical, horizontal and rotational vibrations
WB_1, WB_2	Longitudinal coordinates of the front and rear axles with respect to vehicle *cg*, *m*
$\vec{\omega}_R$	Rotational velocity vector at the *cg* of the right linkage mass, *rad/s*
$\vec{\omega}_L$	Rotational velocity vector at the *cg* of the left linkage mass, *rad/s*
X_V	Valve stem displacement, *m*
X_{Vmax}	Maximum valve stem displacement, *m*
X_L, X_R	Displacements of left and right strut pistons, respectively, *m*
$\dot{X}_L, \dot{X}_R$	Velocities of left- and right-strut pistons, respectively, *m/s*
z_0	Road elevation, *m*
$\mathrm{z}_{\mathrm{st}_\mathrm{l}}$	Static defection of the tire l $(l = 1, \dots, 4)$, *m*
z_l	Vertical deflection at the contact point of the tire l $(l = 1, \dots, 4)$, *m*
z_{0i}	Terrain elevation at the interface of tire i, *m*
$\dot{z}_{wc}$	Vertical velocity of the wheel center, *m/s*

α_r , β	Roughness coefficient and waviness of the terrain
α_w	One-half of the wheel-terrain contact patch angle, *rad*
α_i	Slip angle corresponding to the tire i ($i=1,\ldots, 4$) , *rad*
α_1, α_2	Instantaneous yaw angles of the left strut axis with respect to longitudinal axes of front and rear units, respectively, *rad*
θ_{sw}	Steering wheel input, *rad*
$(\theta_{sw})_{max}$	Maximum steering input corresponding to the locked position, *rad*
β_1, β_2	Instantaneous yaw angles of the right strut axis with respect to longitudinal axes of the front and rear units, respectively, *rad*
Ω_o	Spatial frequency, *cycle/m*
$\sigma(\omega)$	Amplitude of the terrain elevation
τ_θ	Correlation between the front and rear wheels in the pitch plane, *s*
τ_ϕ	Correlation between the right- and left- wheels in the roll plane, *s*
δ_{st}	Static tire deflection (adaptive model), *m*
γ_{LR}^2	Coherence between the left and right tracks of a terrain
φ	Articulation angle, *rad*
φ_o	Articulation angle corresponding to a steer input in the absence of the vehicle resistances, *rad*
$(\varphi_o)_{max}$	Open-loop articulation angle corresponding to maximum steering input, *rad*
δ_{char}	Characteristic articulation angle error corresponding to valve saturation, *rad*
ρ_m	Fluid mass density, kg/m^3
τ_y	Relaxation time, *s*
σ_y	Relaxation length, *m*

ρ	Rate of decay of the articulation angle response oscillations, *1/s*
$(\dot{\phi}_{si}, \dot{\theta}_{si}, \dot{\varphi}_{si})$	Euler angular velocities along x-, y- and z-axis of the coordinate system fixed to the front (*i=f*) and rear (*i=r*) unit sprung mass, *rad/s*
$(\dot{\phi}_u)$	Euler angular roll velocity of the unsprung mass, *rad/s*
$(\dot{\phi}_j)$	Euler angular roll velocity of the suspension linkage mass, *rad/s*
$\mathit{\Delta}_l$	Total vertical deflection of tire l $(l = 1, \dots, 4)$, *m*

CHAPTER 1

LITERATURE REVIEW AND SCOPE OF THE DISSERTATION

1.1 Introduction

Articulated steer vehicles (ASVs), commonly employed in agricultural, construction, forestry and mining sectors, are known to transmit comprehensive higher magnitudes of low frequency whole-body vibration (WBV) along the translational as well as rotational axes to the drivers, which can be attributed to vehicle interactions with the uneven off-road terrains, and lack of adequate primary and/or secondary suspensions. Furthermore, owing to their relatively soft tires, extreme variations in the load and load distributions during work cycles, and high mass center, the articulated steer vehicles (ASV) exhibit lower roll and directional stability limits. The WBV exposure of many off-road vehicles widely characterized through field measurements [1,2], is known to exceed the health-caution guidance zone defined in ISO-2631-1 [3] and the exposure limit of the EN14253 [4]. Prolonged occupational exposure to such WBV has been directly associated with various health and safety risks among the vehicle drivers [5,6], while the operators of ASVs are exposed to far greater magnitudes of WBV compared to other off-road vehicles [1,7]. Furthermore, there exists as increasing demand for operations at relative higher speeds, which would yield even greater magnitudes of WBV.

Owing to the high inertia (load carrying capacity) and high center of gravity (*cg*), the vast majority of ASVs have been designed without a primary suspension. The inhibition of ground-induced vibration is thus generally limited to large-diameter and soft tires, suspension seat and elastic operator cabin mounts [8-10]. The large tires, however, tend to increase the vehicle *cg* height and reduce the vehicle track width, leading to potentially greater fore-aft and lateral motions of the driver, and lower roll stability limit. Moreover, pneumatic tires yield very light damping. A combination of these factors suggests that the design and property tuning of tires could help achieve only limited gains in the ride performance and roll/directional stability limit, partly due to the constraint imposed by the off-road tractive performance. A suspension seat, on the other hand, could yield limited isolation of high intensity vertical vibration, when the suspension is adequately tuned for the specific target vehicle vibration [10-12]. A few studies have shown that the suspension seats yield only limited control of vehicle vibration in some vehicles, and amplify the vibration in many large size off-road vehicles [1,9,10,13]. Furthermore, a suspension seat is not effective in limiting the transmission of fore-aft and lateral vibration, whose magnitudes are known to be either comparable to or exceed that of the vertical vibration [10,11]. A suspension at the cab, generally limited to elastic mounts, also yields attenuation of only high frequency vibration [14,15]. Furthermore, the implementation of a cab suspension could pose many complexities in the ASV design, where the cab is often welded to the chassis along with the ROP structure.

Although axle suspensions offer greater potential to reduce the transmission of terrain-induced translational as well as rotational vibrations, relatively fewer studies have attempted the design and performance analyses of such suspensions, where the enhancements in ride have been clearly demonstrated [16-21]. This may in-part be attributed to the strong couplings between the ride and roll/directional stability properties of such vehicles, which pose complex design challenges associated with conflicting requirements posed by the ride and roll stability measures, and wide variations in the axle loads, particularly in view of design and property tuning of the main vehicle cushioning systems. While a soft axle suspension would be highly desirable for attenuation of WBV arising from the tire-ground interactions, it tends to reduce the vehicle roll stability limit. Anti-roll suspension concepts with a ride-height levelling function and interconnected hydro-pneumatic suspensions [22,23] would offer promising alternative solutions for off-road vehicle applications. However, their performance analyses in view of both the ride and roll/directional stabilities have not been thoroughly explored.

A number of design and operating factors contribute to relatively lower directional and roll stability limits of ASVs. These include the multi-axle articulated vehicle design, large diameter tires and thus high mass centre (cg), operation on complex terrain conditions, wide range of operating speeds, and large vehicle load and load variations, in addition to kinematics and dynamics of the articulated steering system [24-26]. Moreover, a class of the ASVs such as dump trucks also operate on paved roads at relatively higher speeds and thus pose difficult handling and directional performance requirements. Such vehicles are known to exhibit relatively lower directional stability thresholds, particularly greater jack-knife and snaking tendencies at medium-high speeds [27]. Moreover, the stability limits are known to be sensitive to kinematic and dynamic properties of the steering system in addition to the cg positions of the front and rear body, and rear body inertia [24-26,28-31]. The articulated frame steering mechanisms have been invariably represented by equivalent linear torsional spring and damping constants, which do not adequately reflect the kineto-dynamic effects of the steering struts [24-26,28-31].

The ride, handling and directional response characteristics of heavy road and off-road vehicles have been widely investigated using different multi-body dynamic models [32-

39]. The simulation models focusing on handling, dynamic roll and directional characteristics generally ignore the vertical tire integrations with random rough roads. The models aimed at ride dynamic evaluation, on the other hand, ignore the steering dynamics. The tire-terrain interactions, however, is vital for both the handling and ride dynamic evaluation, particularly for off-road vehicles, including the ASVs. It is thus desirable to develop integrated ride and handling multi-body dynamic models incorporating tire interactions with randomly rough terrains and kineto-dynamic of the steering system. Furthermore, the handling and directional properties of off-road vehicles have been addressed in only a few studies, which is partly attributed to their low speed operation. However, the growing demands for higher speed ASVs such as articulated dump trucks necessitate the developments of a comprehensive three-dimensional model to facilitate the design of high speed ASVs and to identify desirable axle suspension designs to achieve an improved compromise between the ride and stability limits.

This dissertation research focuses on: (i) development of an integrated ride and handling dynamic model of an articulated frame steer vehicle incorporated a kineto-dynamic model of the frame steering mechanism; and (ii) an advanced axle suspension design for enhancement of both the ride and roll stability limits of the ASVs. The ride performance potentials of a torsio-elastic axle suspension are investigated through field measurements and simulations of a ride dynamic model. A kineto-dynamic model of the frame steering struts is developed and integrated to the vehicle model to study the directional dynamics and stability characteristics and the influences of steering system design on the vehicle stability limits.

1.2 Review of Relevant Literature

Vehicles using articulated frame steering (ASVs) have been tested as early as 1836 and were first patented in the beginning of the 20th century [40]. These vehicles include two separate units coupled through an articulation joint, while the steering is attained by altering the angle between the two bodies in the yaw plane using two hydraulic cylinders, as seen in Fig. 1.1. ASVs offer enhanced maneuverability and drawbar pull performance but yield complex ride and stability characteristics. Such vehicles operate on both paved and unpaved surfaces and are known to yield comprehensive magnitudes of whole body vibration and lower directional and roll stability limits.

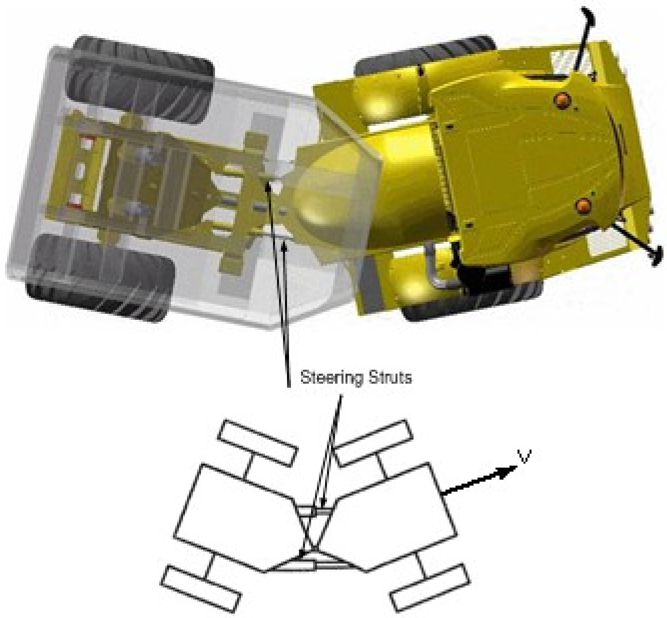

Figure 1.1: A pictorial view and a schematic of an articulated frame steer vehicle (ASVs).

Strong coupling between the ride and stability performance measures poses significant design challenges for ASVs, particularly for the axle suspensions. A study of ASV ride and stability characteristics encompasses numerous measurement and modeling challenges and necessitates a thorough knowledge of the characteristics of various vehicle subsystems, analytical and experimental methods, analysis and assessments of ride vibration, and roll and directional stability limits, and performance measures and requirements. The reported relevant studies are reviewed and discussed in the following subsections to build the essential knowledge and formulate the scope of the dissertation research.

1.2.1 Characterization of vibration and vibration assessment of off-road vehicles

ASVs are generally unsuspended vehicles that are directly supported on large-diameter soft tires. These vehicles operate on both the paved roads and relatively rough terrains with large localized slopes and cross-slopes, and yield comprehensive magnitudes of translational and rotational whole-body vibrations (WBV) at the operator location [7,41,42]. The WBV exposure of operators of various off-road vehicles has been widely characterized through field measurements over the past five decades [43-47]. These have demonstrated that the WBV of off-road wheeled vehicles generally dominates in the 0.5-5 Hz and that the magnitudes of vibration encountered by ASVs operators are generally higher than those observed in conventional steering off-road vehicles [1,7]. A number of epidemiologic studies have established a strong association between the WBV exposure and various health risks among the operators [42,48]. A number of standardized methods have thus been defined to assess the vibration exposure risks considering the human sensitivity to frequency and magnitude of vibration and exposure duration [3,4,49,50]. The international (ISO-2631-1[3]) and British (BS 6841) [49] define the frequency weightings to account for human sensitivity to vibration and method of assessing the exposure. The standards define frequency weighting W_k , W_d and W_e for assessing of vertical, horizontal and rotational vibrations, while the exposure is expressed in terms of frequency-weighted root-mean-square (rms) acceleration, $\bar{a}$, or vibration dose value (*VDV*), when the ride vibration environment involves high intensity vibration or shock motions, given by:

$$\bar{a} = \sqrt{\frac{1}{T}\int_0^T a_w^2 dt} \quad ; \qquad VDV = \left[\int_0^T a_w^4 dt\right]^{1/4} \tag{1.1}$$

where a_w is the frequency-weighted acceleration along a given axis and T is the exposure duration considered. The frequency-weightings employed in the standardized exposure assessment methods suggest that human body is most sensitive to horizontal and rotational vibration in the 0.5-2 Hz range, and to vertical vibration in the 4-10 Hz range. The comfort perception of vibration and the health effects are directly related to overall rms acceleration computed from the above equation. The overall frequency-weighted rms acceleration due to WBV can also be evaluated from:

$$\bar{a} = \sqrt{\sum_i \left[W_i a_i(\bar{f})\right]^2} \tag{1.2}$$

where $a_i(\bar{f})$ is the rms acceleration corresponding to center frequency $\bar{f}$ of the i^{th} third-octave frequency band, and W_i is the corresponding weighting factor. The standard also requires the evaluation of total WBV exposure through vector summation of the translational weighted accelerations, when the dominant ride vibrations occur along multiple axes, such that:

$$a_v = \sqrt{\left(k_x^2 \bar{a}_x^2 + k_y^2 \bar{a}_y^2 + \bar{a}_z^2\right)} \tag{1.3}$$

where $\bar{a}_x$ and $\bar{a}_y$ are W_d-weighted rms longitudinal and lateral accelerations, respectively, and $\bar{a}_z$ is the W_k-weighted rms vertical acceleration. In the above equation, $k_x = k_y = 1.4$ are the constants applied to account for relatively higher human sensitivity to horizontal vibrations. In addition, the exposure assessment guidelines of the European Commission (EC, 1992) defines an eight-hour energy equivalent frequency-weighted acceleration, *A*(*8*), for assessing the WBV exposure. The *A*(*8*) value represents the equivalent exposure to continuous vibration over an eight-hour work period, given by:

$$A(8) = a_v \sqrt{T_e / T_0} \tag{1.4}$$

where T_0 is the reference duration of 8 hours and T_e is the average daily exposure duration. The EC has also set for the 'action' and 'limiting' values of *A*(*8*) as 0.5 m/s^2 and 1.15 m/s^2, respectively. The studies on assessment of ride vibration of different off-road vehicles generally report frequency-weighted overall rms acceleration levels, and exhibit wide variations in the measured magnitudes even for the same class of vehicles, as evidenced in Table 1.1.

Table 1.1: Summary of the WBV levels reported in different studies for different off-road vehicles.

Vehicle	**a_v (m/s^2)**	**VDV(m/s$^{1.75}$)**	**Source(s)**
Excavator	0.51[c]-0.91[c]	5.76	[41,52,53]
Scraper	1.61[e]	14.9	[53]
Grader	0.55[c]-1.4[e]	7.25	[52-54]
Skid-steer vehicle	1.18[d]	9.64	[53]
Compactor	0.91[c]	7.86	[53]
Wheel-Loader	0.95[c]-1.22[e]	31.7	[52,53,55]
Mobile Crane	0.15-0.59[c]	-	[41,53,55-57]
Off-road dump truck	1.21[d]-1.93[e]	17.2	[41,53,54]
Skidder loaded	1.8[e]-1.83[e]	-	[1,58]
unloaded	1.96[e]-2.10[e]		
Agricultural Tractor	0.50[c]-1.93[e]	-	[41,54,59-62]
Crawler loader	1.01[c]	8.71	[53]

[c] exceeds ISO 2631-1 (1997) health caution zone lower limit for an 8-h day;
[d] exceeds ISO 2631-1 (1997) health caution zone upper limit for an 8-h day;
[e] exceeds ISO 2631-1 (1997) health caution zone upper limit for a 4-h day.

Table 1.2: Summary of reported WBV levels along *x, y, z* axes of different off-road vehicles.

Vehicle	$\bar{a}_x$ **(m/s^2)**	$\bar{a}_y$ **(m/s^2)**	$\bar{a}_z$ **(m/s^2)**	**Source(s)**
Load-haul dump truck	0.81	0.49	1.57	[42,63]
Heavy-haul mining trucks	0.13-0.57	0.14-0.48	0.40-1.52	[64]
Agricultural tractors (various tasks)	0.07-1.12	0.11-1.40	0.16-1.35	[65-70]
Underground mining dumpers (loaded and unloaded)	0.63-1.50	0.54-0.84	0.87-2.50	[63]
Cranes – mobile and overhead	0.07-0.66	0.11-0.67	0.22-0.52	[6,57,71]
Grader	0.38	0.45	0.79	[54]
Construction machinery				[6,42,67,71-74]
Loaders-wheeled	0.21-1.40	0.22-1.30	0.29-1.26	
Loaders-tracked	0.65-1.12	0.34-0.76	0.51-0.96	
Dumpers	0.51-1.12	0.30-0.78	0.46-1.18	
Excavators	0.24-0.52	0.20-0.26	0.30-0.52	
Forestry machines				[1,75-78]
Skidders	0.54-0.86	0.49-1.42	0.72-1.15	
Forwarder	0.64-0.75	0.80-1.52	0.39-0.68	
Snow vehicles				[58,79]
Side-walk ploughs	0.35-1.03	0.20-0.86	0.81-2.23	
Snowmobiles	0.43-1.00	0.50-1.00	0.30-1.00	
Groomers	0.15-0.36	0.15-0.36	0.40-1.10	
Compactor	0.37-0.50	-	0.78-1.49	[80]

Table 1.2 further summarizes the reported frequency-weighted rms accelerations due to vibration along the x-, y- and z-axis of different vehicles. The wide range of reported acceleration values are attributed to variations in the design and operating conditions, local terrain condition and the tasks. The results further reveal significantly higher magnitudes of WBV of off-road vehicles, while those of the articulated steer vehicles, such as wheel loader, off-road dump truck, tractor and skidder are relatively higher [7,51]. The results in the table also show that WBV levels of many vehicles either

approach or exceed the *'health caution zone'* defined in ISO-2631-1. These are indicated by the superscripts *'c', 'd',* and *'e'* in Table 1.1. The results in Table 1.2 also shown that the magnitudes of horizontal vibration of ASVs are either comparable or exceed the vertical vibration magnitudes.

Teschke et al. [51] also conducted a review of reported studies on WBV and back disorders among the heavy equipment operators and motor vehicle drivers. The study concluded that operation of excavators, forestry vehicles, tractors, dump trucks, bulldozers, graders, cranes, etc., are typically exposed to higher levels of vibration than the limiting values recommended in ISO 2631. Boshuizen et al. [59] conducted a cross-sectional study with 450 tractor drivers exposed to 0.75 m/s^2 for at least 10 years and a control group of 110 people, and concluded that the low back pain (LBP) symptoms were 50% greater among the control group. Considering the reported health risks of WBV exposure among the operators and high magnitudes of off-road vehicles vibration, numerous studies have emphasized the need for control of WBV transmitted to the operator by means of primary and secondary suspensions [21,76,84,85]. The vast majority of these concepts, however, have met limited success in off-road vehicles partly due to complexities associated with the design compromises and their integrations.

1.2.2 Ride dynamic analyses and vibration control

The designs of primary and secondary suspensions require a comprehensive understanding of ride dynamic characteristics of the target vehicle. The ride dynamic responses of an off-road vehicle are a complex function of multiple design and operating factors such as terrain roughness, speed, tire-terrain interactions, vehicle weight and dimensions, and suspension and tire properties. A number of studies have proposed ride dynamic models of different vehicles to evaluate ride vibration responses, and the contributions and significance of various design and operating factors [86-90]. The vast majority of these studies, however, focus on road vehicles, while the efforts on off-road vehicles have been mostly limited to tracked military vehicles and agricultural tractors [43,91-100]. The lack of efforts in ride dynamic modeling of ASVs may be partly attributed to complex dynamics of these vehicles.

The reported off-road ride dynamic models have employed different tire and suspension models, while the objectives differ such as the characterization of ride dynamic properties [91,92,100] or developments in cab and seat suspensions [91,102,103]or active and passive axle suspensions [21,100,104,105]. The vast majorities of the reported ride dynamic models are planar model and assume negligible tire-terrain interactions in the fore-aft and lateral modes, constant forward speed, and negligible contributions due to articulation mechanism in the case of ASV [101,106-108]. Such simplifying assumptions, especially the negligible tire-terrain interaction in the shear modes and lack of articulation frame steering are the main sources of the error in ride dynamic predictions of off-road vehicles [109]. Only a few studies have considered three-dimensional ride dynamic models of off-road wheeled vehicles while the agricultural tractors being the primary focus, as seen in Fig. 1.2 (a) [100].

A three-dimensional analytical model of an articulated frame steer vehicle could not be found in the literature. A few studies, however, have explored a simplified virtual multi-body model of an ASV using MSC/ADAMS. Rehnberg and Drugge [21] developed the virtual multi-body model of a wheel loader with and without an axle suspensions using MSC/ADAMS software to investigate the effect of introducing axle suspension on the vehicle ride performance. The 19 degrees-of-freedom (DOF) unsuspended wheel loader model comprised five rigid bodies apart from the wheels, as shown in Fig. 1.2 (b). The wheel loader with front and rear axle suspensions was modeled considering eight rigid parts besides wheels, and 22-DOF [21,30]. The validity of an off-road vehicle ride dynamic model strongly relies on the accuracy of the component models, particularly the tire modeling, terrain roughness, and secondary and primary suspension models, which are reviewed and summarized below.

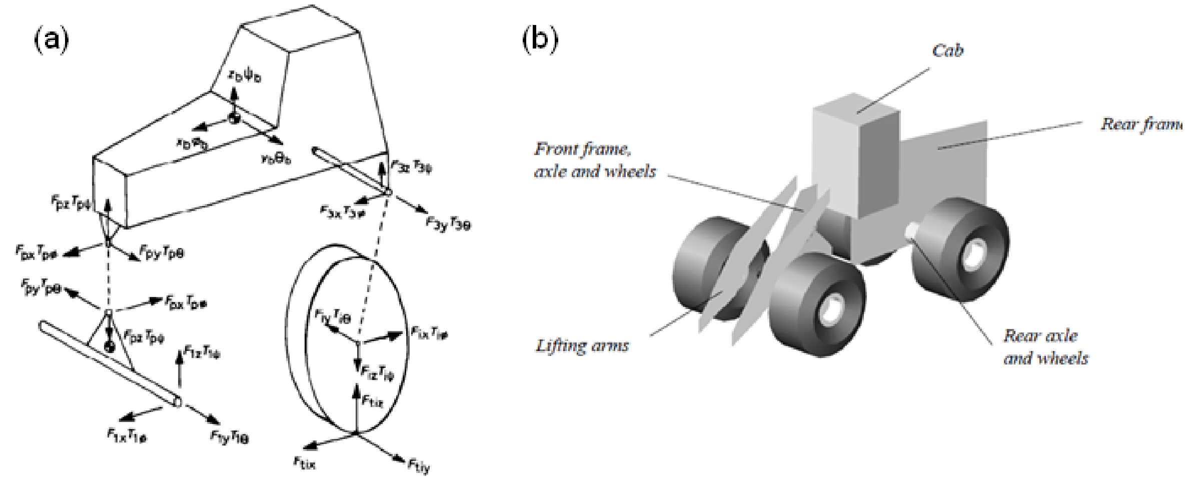

Figure 1.2: (a) Three-dimensional tractor model and the related forces and torques acting on the body, axle, and wheel [100]; and (b) virtual multi-body model of a wheel loader [21].

1.2.3 Tire modeling

Off-road vehicle tires play the most important role in different vehicle performance measures such as ride, handling, directional stability, traction/mobility and the operational economy. These measures, however, impose conflicting requirements on the tuning of tire properties. Soft tires would be highly desirable for absorption of vibration energy [21,110] but lower effective roll stiffness and thus reduced stability, and poor fuel economy due to higher rolling and shear resistances [21,111-114]. Alternatively, stiff tires would be desirable for improved handling and directional stability on roads, but could yield limited mobility performance on soft terrains. Vertical properties of the tires affect the vehicle ride responses, while vehicle handling and directional stability analyses necessitate characterization of longitudinal and lateral force properties of the tires. The characterizations of tire forces and moments, however, are quite complex due to highly nonlinear tire properties, and continue to be the focus of many studies.

The reported studies on off-road vehicle ride dynamics have employed tire models ranging from the simplest linear point-contact model to a complex adaptive footprint tire model, as shown in Fig. 1.3 [91,94,97,115-118]. The simple linear point-contact model, however, has been most widely used, where the tire is represented by its equivalent vertical stiffness and viscous damping constants with a single contact point with the terrain surface. Such tire models have proven to be effective for studies on road vehicles, particularly for relative analyses of different suspension concepts. Such a model, however, would not be adequate for off-road vehicles operating on highly rough and deformable terrains. This is partly attributed to overestimation of the contact pressure and thus the sinkage of the point-contact tire model together with lack of consideration of tire-terrain interactions in the shear mode loss of tire-terrain contact [115-119]. A few studies have also incorporated a nonlinear point-contact model of the tire in order to account for tire-ground loss of contact, while such models invariably assume undeformable terrains [120].

Captain et al. [115] and Xiding et al. [116] employed fixed footprint tire models to describe the vertical tire-terrain contact force distributed over a fixed footprint length. These models are also limited to vertical tire-terrain interactions only, while the terrain deformation is ignored. Alternatively, adaptive footprint models comprising radial spring elements distributed uniformly over the contact patch have been proposed to characterize both the resultant vertical and horizontal forces within the contact patch, as shown in Fig. 1.4 [115,116,121]. It has been shown that the linear point-contact and fixed footprint models could provide good estimations of the vehicle ride response only in the low frequency range, while the adaptive footprint model yields better predicts of in the entire frequency range.

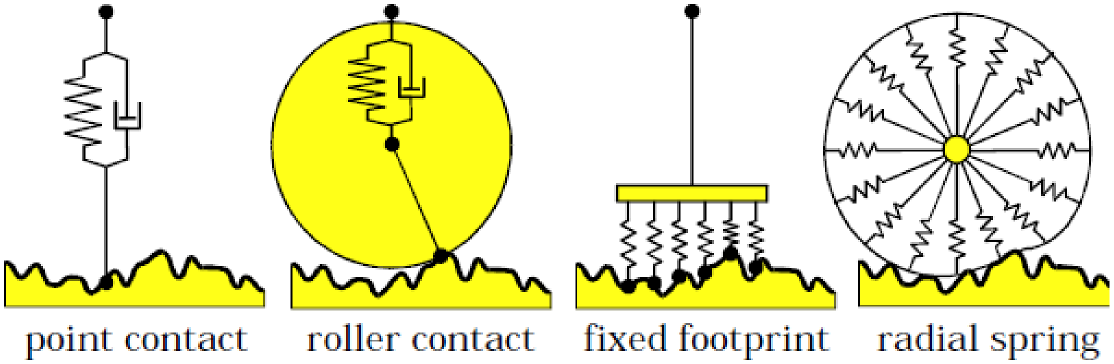

Figure 1.3: Tire models used for ride dynamic analysis [117].

Three-dimensional point-contact tire models have also been proposed to generate horizontal and vertical forces developed at the tire-terrain interface [101,110,112]. These models employ linear stiffness and damping components in either parallel or series arrangements, as shown in Figs. 1.5 (a) and 1.5 (b). It has been shown that the point-contact tire model in series yield better agreements with measured acceleration responses of an agricultural tractor along all the translational axes [101]. It has been shown based on the measurements that the carcass characteristics in the lateral direction could be modelled by a parallel spring/damper unit (Kelvin unit), and the tire-ground interaction could be represented by a viscous damper in series with the Kelvin unit, which is called as visco-plastic model, as seen in Fig. 1.5(c) [110,119]. Although comprehensive finite element tire models have been widely reported for characterizing multi-axis tire-terrain interactions [122], such models could find only limited applications in ride dynamic analysis of vehicles due to associated complexities and high computational demands.

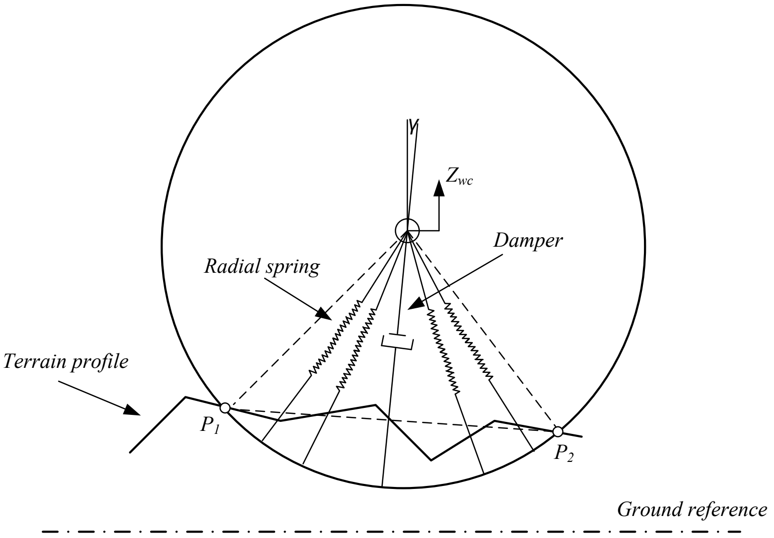

Figure 1.4: Adaptive footprint tire model.

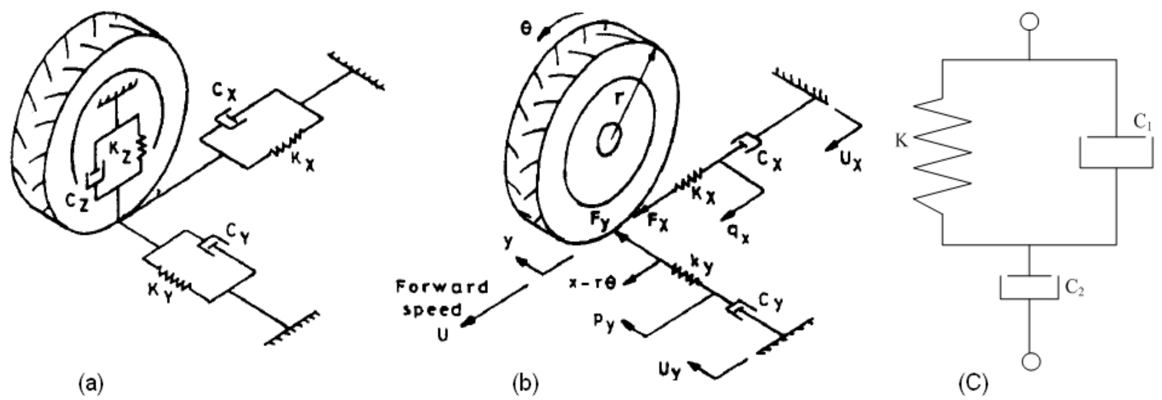

Figure 1.5: (a) tire model consisting of spring and damper in parallel [100]; (b) tire model consisting of spring and damper in series [101]; and (c) visco-plastic model [110, 119].

A number of regression-based empirical models have been developed for describing longitudinal and lateral forces developed by the tires. Among these the Magic Formula (MF) tire model, developed by Pacejka [123,124], has been widely employed in handling and directional dynamics analyses of road vehicles. The MF tire model is a complex regression relation, which can be calibrated using the experimental tire data that yields the relationships between the tire cornering force and slip angle, braking force and longitudinal slip (skid), or self-aligning torque and slip angle. The MF tire model is described:

$$y(x) = D\sin[C\,tan^{-1}\{Bx - E(Bx - tan^{-1}[Bx])\}] \qquad (1.5)$$

$$Y(X) = y(x) + S_v\,; \qquad x = X + S_h$$

where *Y*(*X*) represents the result such as tire cornering force or braking force, or self-aligning torque, and *X* is the side-slip angle or the longitudinal slip. The constants *B*, *C*, *D* and *E* are the stiffness, shape, peak and the curvature factors, respectively, and *Sv* and *Sh* are the slip variables. The cornering force due to off-highway vehicle tires has been also described by Metz [125] proposed a cornering force model in the result and empirical relation assuming negligible camber effect and longitudinal wheel slip, given by:

$$F_y = A \times F_Z(1 - e^{-B\alpha}) \qquad (1.6)$$

where F_y and F_z are cornering and the normal tire forces, respectively, and α is the tire slip angle. *B* is a constant dependent upon the tire load and terrain surface, such that:

$$B = \frac{C}{A}\left(\frac{F_{ZT}}{FZ}\right)^m + \frac{D}{A} \qquad (1.7)$$

where F_{ZT} is the nominal tire design load at the design operating pressure, *m* is an exponent (equal to 0.14), and *A*, *C* and *D* are constants dependent upon the terrain condition, as seen from Table 1.3. The tire cornering stiffness $C_{F\alpha}$ for small slip angles can thus be estimated from:

$$C_{F\alpha}=A\times B\times F_z \qquad (1.8)$$

The MSC.ADAMS software integrates the longitudinal and lateral tire forces relations denoted as the ‘Fiala model’ [126]. The Fiala tire model uses mathematical equations to represent the tire force and moment characteristics assuming rectangular contact patch or footprint, uniform pressure distribution across the contact patch, and negligible tire relaxation and camber effects. The Fiala model is considered meritorious over the other models since it requires only a few directly measurable physical and geometrical parameters. The model also provides estimations of vertical force on the basis of the vertical stiffness, unloaded radius, and damping ratio.

Table 1.3: Parameters for the Metz tire model for different types of terrain surfaces [125].

Constants	**Highway**	**Plowed field**	**Gravel**	**Corn field**	**Meadow**
A	0.67	0.65	0.52	0.53	0.88
C	0.677	0.267	0.588	0.440	0.784
D	-0.563	-0.222	-0.489	-0.365	-0.652

The off-road vehicles tires penetration into the deformable soils, however, influences the tire forces significantly. The tire-tread penetration is a function of soil shear strength expressed by soil cone index, soil cohesion and internal shearing resistance [101,118]. The forces developed by tires operating on deformable soils have been estimated on the basis of a parameter known as the mobility number ($EMOB$), which defined through a dimensional analysis of the measured data considering the effects of tire size, load and soil cone index [118], the mobility number of a tire is derived from:

$$EMOB = \frac{C_s w d_T \sqrt{\delta/h}}{F_z\left[1+\left(w/2d_T\right)\right]} \tag{1.9}$$

where C_s is soil cone index, and $w,\ d_T$ and h are the tire width, diameter and section height, respectively. δ is the tire deflection and F_z is the tire normal load.

The lateral force developed by the tire is defined as a function of two constants, K_y and B_y, dependent upon $EMOB$, vertical load and corresponding slip angle α , such that [118]:

$$F_y(t) = -F_z K_y \left(1 - e^{-B_y \alpha(t)}\right) \tag{1.10}$$

$$K_{yi} = \left(\frac{0.69}{EMOB_i}\right) + 0.61; \qquad B_{yi}\, K_{yi} = 2.34 + 0.088\, EMOB_i \tag{1.11}$$

The above model can also accounts for tire lag associated with buildup of the lateral force, which is notable in off-road vehicle tires [101]. The lateral force developed by a tire can be thus derived assuming the first-order tire dynamics, where the relaxation time constantτ_y, directly relates to the relaxation length σ_y and the forward speed u ($\tau_y = \sigma_y/u$) [118]:

$$\tau_y \dot{F}_y(t) + F_y(t) = -F_z K_y \left(1 - e^{-B_y \alpha(t)}\right) \tag{1.12}$$

1.2.4 Terrain roughness

The characterization of off-road terrains roughness is quite complex since it varies with the local conditions of a region, soil properties and the number of vehicle passes [127-129].The terrain roughness properties are thus generally estimated from surface elevation measurements. International standard organization (ISO) has proposed relationships between the power spectral densities (PSD) of roughness of various classes of undeformable roads with the spatial frequency, as [114]:

$$S_g(\Omega) = \begin{cases} S_g(\Omega_o)\left(\Omega/\Omega_o\right)^{-N_1} & ; \quad \Omega \le \Omega_o \\ S_g(\Omega_o)\left(\Omega/\Omega_o\right)^{-N_2} & ; \quad \Omega > \Omega_o \end{cases} \tag{1.13}$$

where $S_g(\Omega)$ is PSD of road surface elevation, $S_g(\Omega_o)$ is a roughness constant defined for different classes of roads at the spatial frequency $\Omega_o = 1/2\pi$, and N_1 and N_2 are waviness of the terrain. The surface roughness properties of various undeformable off-road terrains have also been characterized and expressed by the following power relations

[114,130-132]:

$$G_Z(\Omega) = \alpha_r \Omega^{-\beta}; \quad \alpha_r > 0 \text{ and } \beta > 0 \tag{1.14}$$

where the constants α_r and β are the roughness coefficients and wavinesses of the terrain, respectively, which are generally identified from the measured terrain profiles.

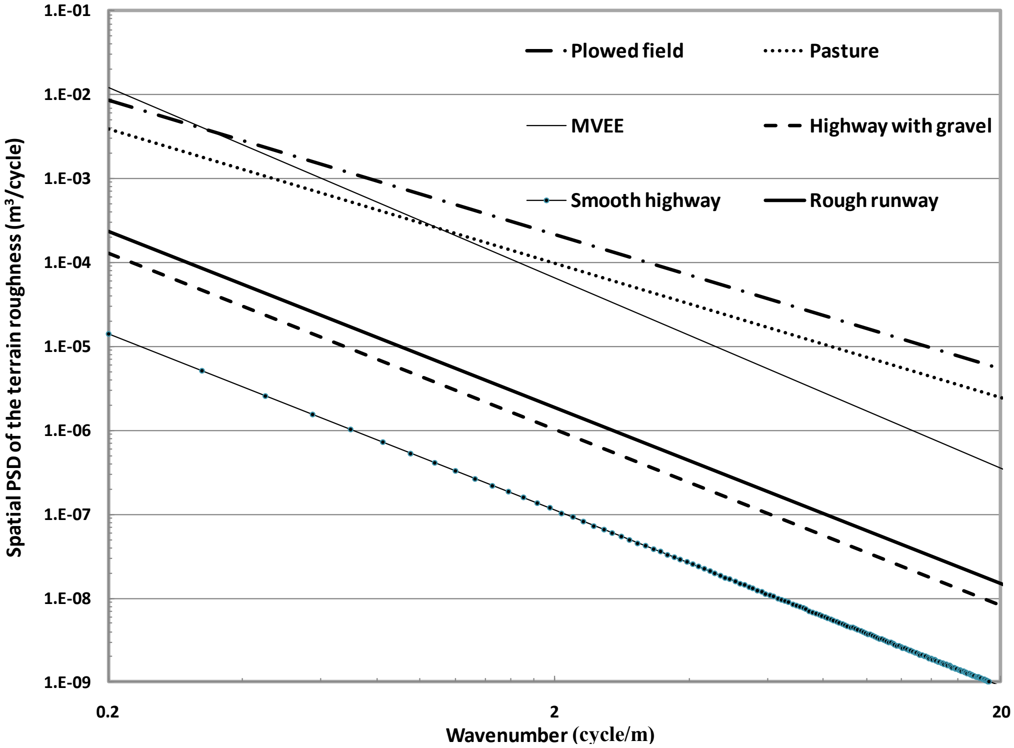

Figure 1.6: Roughness characteristics of different surfaces.

The roughness characteristics of the terrain profiles reported for the plowed field, pasture, highway with gravel, smooth highway, and rough runway [114], and the MVEE (Military Vehicle Engineering & Establishment) random course [131,132] are compared in Fig. 1.6. The results clearly show that the unpaved terrains exhibit greater roughness compare to the paved roads. The spatial power spectral density (PSD) of the terrain roughness may also be expressed by a rational PSD function in temporal frequency and operating speed to synthesize the time-history of the terrain roughness by applying a random white noise signal of unity power [133]. The reported models describe the average roughness of the terrain profile, while the roughness of the two tire tracks has been addressed in only a few studies [134,135]. The correlations between the terrain roughness encountered by the two tires tracks is vital for the study of roll ride and roll dynamics of the vehicle.

1.2.5 Vehicle Suspensions

Owning to increasing demands on higher speeds and operating capacity, the current design practices for ASVs seem to be converging towards large-diameter soft tires, while employing suspended seat and/or cab suspension for cushioning the vibrations/shocks transmitted to human operators, instead of axle suspensions that can deteriorate the vehicle roll stability limits [103,111,136-138]. The suspension seats are most widely used in such vehicles to limit the vertical vibration exposure of the operator. There are designed with low natural frequency, in the order of 1.5 Hz, with suspension travel generally limited to ± 5 cm by introducing elastic end-stops [8-10,139-143]. Although some studies have considered active seat suspensions in the bounce, roll and pitch modes [144,145], the associated cost and power consumption are considered prohibitive for their implementation.

The off-road vehicles vibration along the lateral and vertical axes predominate around 1 and 2.5 Hz, respectively. The design of a passive seat suspension for limiting the low-frequency lateral vibration is considered infeasible due to very low frequency of lateral vibration [136,146,147]. It has been shown that multi-axis passive seat suspension could provide attenuations of bounce, pitch and longitudinal vibrations in off-road tractors, while the reductions in low frequency roll and lateral modes would impose extreme design challenges [136]. The suspension seats applications in off-road vehicles, including

ASVs, have been mostly limited to a vertical suspension. The performance of such suspension seats are generally limited under high intensity ride vibration, which cause suspension seat to exceed its free travel and thus transmit high intensity vibration or shock motions to the operator due to the end-stop impacts. A few studies have shown that the suspension seat does not offer significant reduction in high intensity vertical vibration, which is attributed to lack of suspension tuning with regard to the intensity and frequency contents of the target vehicle vibration [14,15]. Cation et al. [1] measured the vibration encountered at the occupant-seat interface and the cabin floor of forestry skidders, and found no evidence of reduction in transmitted vertical vibration. This finding was also confirmed by Wegscheid [107] for the skidders. These studies further concluded that a vertical suspension seat may even amplify the vibration transmitted to the operators.

Alternatively, various concepts in cab suspension have also evolved to attenuate vibration along the translational as well as rotational axes [91,102,136,138]. Different concepts in cab suspension involving vertical (natural frequency range of 0.8 and 1 Hz), pitch (0.6, 0.85 and 1.2 Hz) and roll (0.5 Hz) suspensions have been investigated for off-road vehicles, particularly agricultural tractors [91,103]. The studies have shown that the vertical and pitch vibrations could be effectively attenuated by a passive cab suspension, while same challenges exist for control of low frequency lateral and roll vibration. The performance potentials of rubber, air and hydro-pneumatic mounts, and spring-damper suspension, at the cabin have been investigated analytically and experimentally [136]. It is shown that the ride improvement obtained via cab suspension is significantly superior to that obtained from a vertical seat suspension in the low frequency region. However, the studies illustrated that isolation of the lateral and roll modes still remains quite complex by means of a cab suspension [103]. It has also been shown that suspension design with nonlinear damping elements is more effective than those with linear damping [102,103]. The implementation of a suspension at the cab is also considered to be complex in small-size vehicles, where the cab is generally directly welded to the chassis along with the ROP structure. It can thus be concluded that the secondary suspensions are not effective in limiting the transmission of fore-aft and lateral vibration, whose magnitudes are known to be either comparable to or exceed that of the vertical vibration [1,11]. In addition, performance of secondary suspensions, generally derived from subsystem models of the seat and cab suspensions [9,10,13,14], may be also limited due to lack of consideration of dynamics of the target vehicle [14,15].

Owning to increasingly demand for high-speed work vehicles and enhanced ride comfort, the axle suspensions have been regarded to be most promising, particularly for the ASVs. These can help limit the stresses in the vehicle structure and components, apart from improved ride performance [20,30,94,97,105,139,140]. Although axle suspensions offer greater potential to reduce translational as well as rotational vibrations, relatively fewer studies have attempted design and performance analyses of such suspensions, where the enhancements in ride have been clearly demonstrated [17-21]. This may in-part be attributed to design challenges associated with conflicting requirements posed by the ride and roll stability measures, and wide variations in the axle loads. A number of studies have investigated various concepts in passive and semi-active anti-roll bars to enhance roll stability of heavy vehicles, while minimizing the negative effect on vehicle ride performance [148-150]. The use of anti-roll bars tends to add weight and could not provide additional roll mode damping which is very important for dynamic roll stability [147].

A few studies have shown that tractors with both the front and rear axle suspensions could enhance the ride performance, when compared with those with only seat, cab or front axle suspension [20,94]. Although a soft rear axle suspension with light damping could provide good vibration reduction along the translational axes, it necessitates large suspension travel space and affects the roll stability in an adverse manner [20,97]. Various control strategies have also been investigated to develop semi-active and active suspension systems for heavy road and off-road army vehicles to achieve improved compromise between the vehicle ride, handling and roll stability performance [20,60,99,100,105,151]. The applications of such suspensions, however, are very limited, particularly for heavy commercial vehicles (both road and off-road), due to the associated high cost and weight, and reliability concerns.

Rehnberg and Drugge [21] developed the virtual multi-body models of a wheel loader with and without axle suspensions to investigate the effect of introducing axle suspension on the vehicle ride performance. The simulation results revealed about 50% reduction in the longitudinal and vertical accelerations by using the front and rear axle suspensions. Only limited improvement in the lateral acceleration, however, was observed due to the high effective roll stiffness and the high location of the driver. Alternatively, anti-roll suspension concepts with a ride-height leveling function, such as interconnected hydro-pneumatic suspensions [152-154], could be promising for ASVs.

A few recent studies have explored passive interconnected mechanical or hydraulic/pneumatic suspension concepts to improve the roll dynamic performance of heavy road vehicles without affecting the vehicle vertical ride [153-155]. The results demonstrated considerable potential of passive interconnected suspensions in enhancing vehicle roll stability. Ride and handling dynamics of a heavy vehicle involving different full-vehicle interconnected suspension arrangements have also been investigated based on a three-dimensional vehicle model [154,156]. Some of the proposed inter-connected suspension arrangements are shown in Fig. 1.7 [154]. The simulation studies suggest that a full-vehicle coupled hydro-pneumatic suspension could provide considerable benefit in realizing enhanced ride and handling performance, as well as improved anti-roll and anti-pitch properties in a flexible manner.

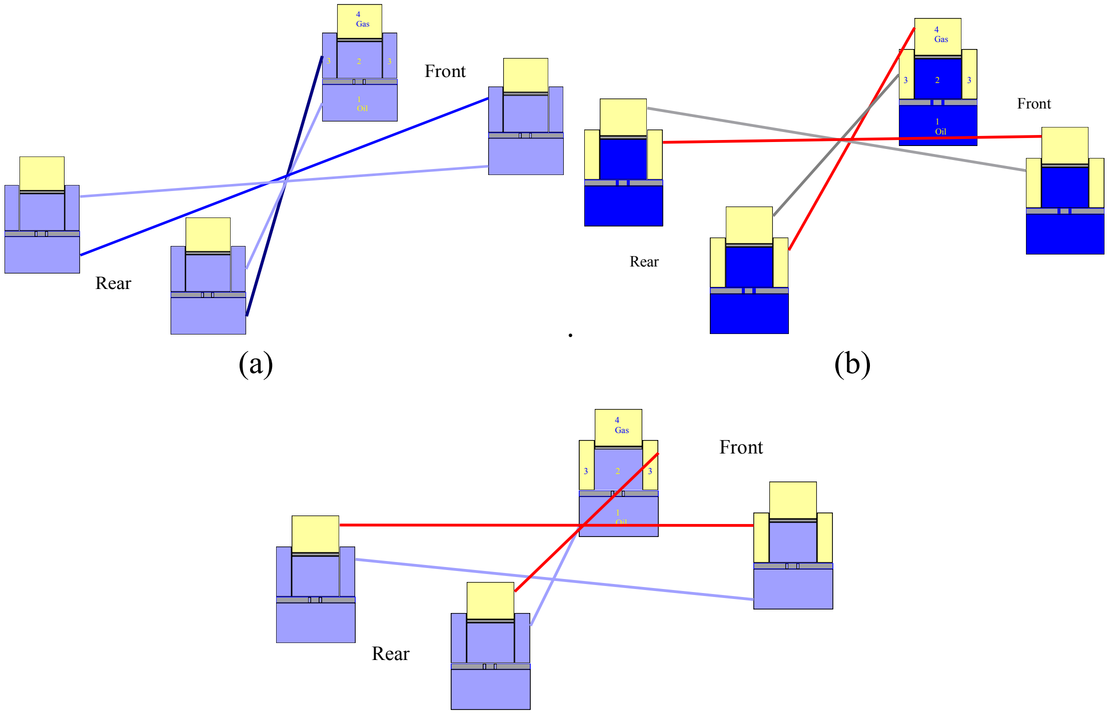

(a) (b)

(c)

Figure 1.7: Full-vehicle interconnected suspension arrangements: (a) hydraulic; (b) pneumatic; and (c) hybrid [154].

1.2.6 Directional/roll stability dynamics

Articulated frame steer vehicles with their enhanced mobility and manoeuvrability on off-road terrains are widely used in the agricultural, construction, forestry and mining sectors. These vehicles also operate on paved roads at relatively higher speeds and thus pose difficult handling and directional performance requirements. Such vehicles are known to exhibit relatively lower stability thresholds, particularly greater jack-knife and snaking tendencies, which are attributable to a number of factors [157-159]. These include the multi-axle vehicle design, large diameter tires and thus high mass centre (cg), operation on complex terrain conditions, wide range of operating speeds, and large vehicle load and load variations, in addition to the kinematics and dynamics of the articulated steering system.

The ASVs also exhibit a strong coupling between the roll and yaw motions, which could cause yaw divergence leading to a potential rollover in the absence of a corrective steering action or speed reduction [151]. The vehicle is generally stable in roll when the lateral acceleration is lower than the rollover threshold, while a yaw instability could occur at a relatively low lateral accelerations levels at higher speeds [160]. The roll instability could thus be prevented by limiting the vehicle lateral acceleration, while the yaw instability may still occur [161]. The ground vehicles employing axle suspensions exhibit lower rollover threshold compared to unsuspended vehicles, which is attributed to greater sprung body roll motion and thus the lateral displacement roll moments. The roll and yaw directional dynamics of the vehicle are further affected by variations in tire loads due to varying terrain roughness and possible loss of tire-terrain contact [162].

The directional dynamics of road vehicles have been extensively evaluated using analytical and simulation-based methods [163-169]. While the industrial analysts often develop complex models to achieve greater accuracy, the academic researchers have put forward the view that typical industry-used vehicle models are too complex and inefficient as design tools [170-172]. An ideal model should be capable of providing the concerned assessments and design evaluation with an acceptable accuracy with minimal complexity [172]. However, only a few reported studies could be found on directional analysis off-road vehicles, particularly the articulated steering vehicles. This is partly attributed to complexities associated with the dynamic modeling of the ASVs and low operating speeds of the ASVs. The vast majority of the reported studies on ASVs are limited to 3-DOF yaw-plane linear models to evaluate the yaw responses of the vehicle, assuming negligible contributions due to vehicle roll, vertical tire-terrain interactions and linear stiffness representation of the frame steering [28,29,157-159]. Furthermore, while a number of roll and yaw directional performance measures have also been defined for heavy road vehicles for assessing their safety dynamics [173], only a few efforts have been made on roll stability measures of the off-road vehicles. These are mostly limited to static slope/cross-slope stability margins for developments in various ROP structures and rollover early-warning devices [174-176].

Considering the increasing demand for high-speed ASVs, it is essential to develop comprehensive directional dynamic models of the ASVs. Furthermore, the articulated frame steer vehicles are known to be inherently directionally unstable and exhibit jack-knife tendency about the pivot, particularly at higher speeds [158,159]. Some of the reported studies on the directional dynamic of the ASVs have established that the hydraulic steering system is the most essential design factor in view of the vehicle steering responses and stability [158,159]. Apart from the steering of the vehicle, the kinematics and dynamics of the hydraulic articulated frame steering system play a critical role in retaining directional stability of the vehicle. This suggests the need to enhance understanding of contributions of the kinematics and dynamics of the steering mechanism behaviour to the directional dynamic responses of the articulated frame steer vehicles.

The articulated frame steering responses are strongly dependent on both the kinematics and dynamics of the steering system and it's coupling with the dynamics of the vehicle. The vast majority of the reported studies on characterization of directional responses have employed linearized low-order vehicle models together with a simplified articulated steering model characterized by an equivalent linear torsional stiffness and damping, while the kinematics properties of the steering mechanism are entirely ignored [28,29,157-159]. The reported studies have generally investigated three modes of instabilities namely the 'Snaking', 'Jack-Knife' and 'Oversteer', which have been observed with articulated frame steer vehicles [157,159]. Crolla and Horton [157] investigated the steering behavior and directional responses through an eigenvalue analysis of the 3-DOF linear yaw-plane model of the articulated steer vehicle, while the steering system was described by linear torsional spring and damping constants, as shown in Fig. 1.8. The study concluded that snaking and jack-knife types of instabilities could occur even at low speeds when the steering torsional stiffness is low. A higher torsional stiffness and damping of the articulated steering was thus suggested for enhanced vehicle stability limits.

Horton and Crolla [158] further extended the model by replacing the equivalent torsional stiffness and damping by a linear model of the hydraulic steering system, although the kinematics of the steering struts and the joint was not considered. The results showed that an oversteer instability could occur at a speed above 24 m/s, which would lead to snaking mode as the driver attempts a steering correction, which was confirmed through a full vehicle test conducted by Lopatka and Muszynski [27]. The study also concluded that the stability limits are more sensitive to the steering system properties, cg positions of the front and rear body, and rear body inertia [27,158,159].

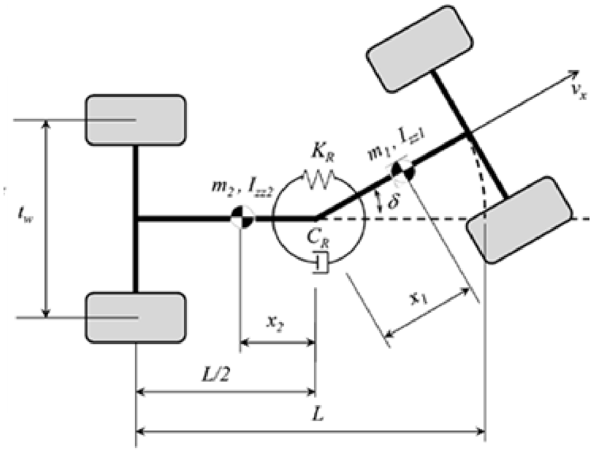

Figure 1.8: A three-DOF linear yaw-plane model of the articulated steer vehicle [159].

He et al. [159] investigated the oversteer jack-knife types of instabilities of an articulated forestry vehicle using the model reported in [158], and showed that an oversteer mode could evolve into jack-knife with low torsional stiffness at the articulation. Azad et al. [29,177,178] used the same 3-DOF planar linear model and a virtual multi-body dynamic model of the articulated forestry vehicle, as shown in Figs. 1.9 (a) and 1.9 (b), to study the snaking instability of the vehicle. The study concluded that the rear-mounted load would negatively affect the snaking stability mode of the vehicle. The reported studies have also shown that an increase in tire lateral force would yield a moderate stabilizing effect, while the effects of tire longitudinal forces and aligning moments were negligible [158,177,178].

The above studies have mostly considered yaw-plane models of the vehicle, where the contributions of roll motions of the articulated units are assumed to be small. A recent study [30] has developed a three-dimensional multi-body simulation model of an articulated wheel loader with an axle suspension to study snaking and roll responses, while the steering mechanism was represented by equivalent linear stiffness and damping constants, as in the earlier studies. The results showed a slightly negative effect of axle suspension on the snaking mode of the vehicle, which could be compensated by a refined design of the steering system. For a given pulse steering torque, a snaking instability could occur at speeds above 12.6 *km/h*, which was strongly influenced by the rear-body inertia and cg position, where the loaded vehicle with heavy rear-unit is most prone to snaking instability. The study suggested that an axle suspension would yield improved ride comfort, while the vehicle directional stability is mostly managed by the design of the steering system.

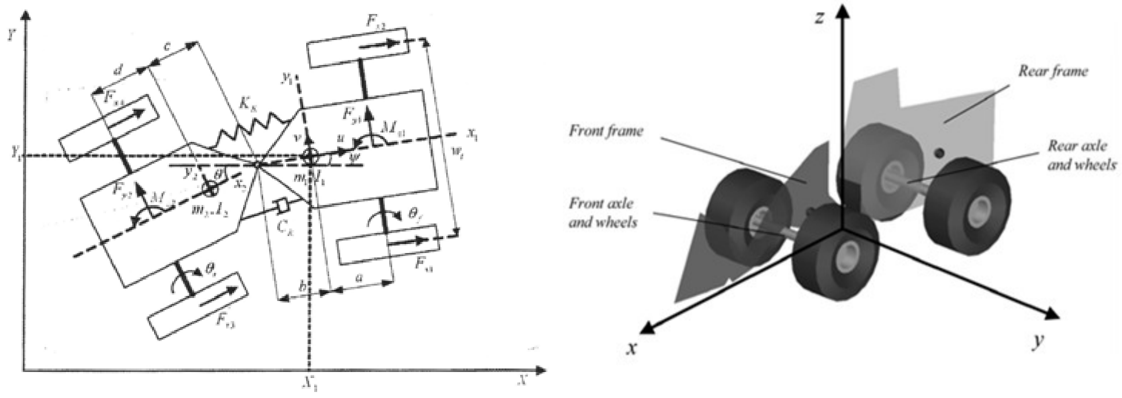

(a) **(b)**

Figure 1.9: (a) Planar models of a forestry skidder [29]; and (b) a multibody model of an ASV for stability analysis [21].

The steering response of an ASVs is a nonlinear function of the steering valve flows, kinematic and dynamic responses of the steering struts, which may not be adequately reflected by the equivalent linear torsional spring and damping constants that have been invariably employed in the reported models. Kineto-dynamic analysis, comprising kinematic motions of the struts and dynamics of the vehicle bodies, is thus vital to identify desirable design of the steering system for enhancement of the lateral stability of the vehicle. The kinematic model of the articulation dampers used in the articulated highway buses has been investigated by Rakheja et al. [179], which showed that the additional articulation damping forces, which are strongly dependent on the geometry of the damper struts, help improve the yaw stability of the articulated freight vehicle and reduce the side force demand on the tires. Although the study considered linear dampers at the articulation joint, the dampers configuration was similar to the hydraulic struts of the articulated frame steering system.

While heavy road vehicles may exhibit a directional instability at relatively high speeds, the off-road vehicles can undergo roll instability at very low speeds. This is attributable to tire interactions with rough terrains with relatively large slopes and cross-slopes. Moreover, uneven sinkages of left and right wheels on deformable terrains could yield greater sprung mass roll displacement and additional lateral load transfers leading to a lower roll stability limit. The static slope stability of an ASV could be 13º less when steered compared to that of the non-steered [30,175]. Hunter [175] summarized the primary causes of reduced roll and slope stabilities of ASVs as excessive tip angle, exceeding the static stability limit, high *cg* position, travelling at high speed over rough ground, and operations on terrain with steep slopes and cross-slopes. However, a large number of off-road vehicles tip- and roll-over have been attributed to driver's misjudgments [175].

The roll stability of the ASVs is affected by a number of design and operating factors such as front and rear track widths, *cg* heights and locations of the front and rear vehicle bodies, tire stiffness, articulation angle, and suspension spacing and effective roll stiffness (if employed). It has been shown that the tire stiffness has considerable effects on the vehicle roll stability [111], and tires with high vertical stiffness would be desirable. Softer tires, however, are desirable for enhanced ride comfort and tractive performance on deformable terrains. This suggests the conflicting requirements on the tire property tuning and promising potentials of using axle suspensions. A stability triangle for 4-wheel drive logging machines with a pinned front axle during operation on inclined grounds at low speeds was defined by Gibson et al. [35]. The study was based on the static analysis using three support points including rear tires contact points and the front axle pin joint. An ASV is assumed to be potentially instable when the weight vector of the vehicle intersects the line forming a side of the defined stability triangle. For a given articulation angle and orientation of the vehicle on a slope, the slope at which rollover or tip-over may occur can be estimated based on this measure. The minimum stability point (i.e. the lowest slope when rollover or tip-over occurs) for a given articulation angle can also be determined. The stability triangle concept is similar to static stability factor (SSF) defined for heavy road vehicles, both of which do not consider the compliance of tire and the suspension system [35,175].

The extensive efforts on directional dynamics of heavy road vehicles have also evolved a number of safety dynamic measures [180-186]. The reported simulation models [187-191], the performance measures and the methods could also be applied for analysis of articulated off-road vehicles. For instance, the overturning roll- and tip-over potentials of heavy road vehicles have been assessed using three different measures: Rollover Prevention Energy Reserve (RPER), Rollover Prevention Metric (RPM) and Critical Sliding Velocity (CSV) [192-194]. The static rollover threshold, however, is most widely used to assess the steady-turning roll stability of heavy vehicles. The static rollover threshold of such vehicles is well below the normal road adhesion factor (0.6-0.85), the lateral skid of the vehicle is thus not expected prior to a rollover. The roll instabilities in heavy vehicles are thus generally maneuver-induced. Two different measures have thus been proposed by El-Gindy [195] for assessing maneuver-induced rollover potentials: (i) Lateral Load Transfer Ratio (LTR), defined as the ratio of the absolute value of the difference between the sum of right wheel loads and sum of the left wheel loads, to the sum of all the wheels loads; and (ii) Rearward Amplification Ratio (RAR), a frequency dependent measure defined as the ratio of the peak lateral acceleration at the center of the gravity of the rearmost trailer to that at the cg of the tractor. Another dynamic measure was further proposed, which describes the effective damping or decay rate of the lateral acceleration response oscillations of the rearmost trailer of the articulated vehicle under a pulse steer input [195]. This measure, referred to as the 'Yaw Damping Ratio' is evaluated at a vehicle speed of 100 km/h, by applying a half-sine steering pulse of 80° over 0.1s interval. A rearward amplification of 2 or less at a speed of 88 km/h has been suggested acceptable for articulated vehicles by Winkler et al. [196].

1.3 Scope and Objective of the Dissertation

From the literature review, it is apparent that the articulated frame steer vehicles transmit high magnitudes of translational and rotational vibration to the human operator, which could adversely affect the comfort, performance and the health of the operator. Furthermore, directional stability limits of such vehicles are considerably lower than the heavy road vehicles due to their operating environment involving complex terrain conditions. Despite of complex ride and directional performance of the articulated frame steer vehicles, only a few studies have investigated the ride and directional response characteristics of ASVs. The reported studies have focused either on the ride dynamic evaluations or on the handling and directional properties. Moreover, the vast majority of the ride studies are based on field measurements, and the directional response studies are limited to planar models assuming negligible contributions due to roll motions and vertical tire interaction with random rough terrains. The tires-interactions with off-road terrains are most significant in view of both the handling and ride performance of off-road vehicles. Moreover, the developments in primary suspensions for wheeled off-road vehicles including ASVs have been lacking due to the complex design challenges associated with conflicting requirements posed by the ride and roll/directional stability properties of the vehicle.

Owning to increasing demands for high speed ASVs such as articulated dump trucks, it is vital to seek promising axle suspension designs for preservation of ride quality, and comprehensive vehicle models for assessment of both the ride and directional performance. It is thus desirable to develop integrated ride and handling multi-body dynamic models incorporating tire interactions with randomly rough terrains and kineto-dynamics of the frame steering system to facilitate the design of high speed ASVs, and to identify desirable axle suspension designs to achieve an improved compromise between the ride and stability limits, which cannot be found in the literatures.

1.3.1 Objectives of the dissertation research

This proposed dissertation research is aimed at development of ride and handling model of an articulated frame steer vehicle, and an advanced axle suspension design concept, namely the torsio-elastic suspension, for enhancement of ride and stability performance of ASVs. The overall goal of the dissertation research is to develop analytical/simulation tools for assessment of ride and handling properties of ASVs operating on both the paved and unpaved terrains. The specific objectives of the proposed dissertation are as follows:

1. Investigate ride performance potentials of an advanced suspension concept, namely the torsio-elastic suspension, for applications in ASVs through field measurements and simulations, and to seek design guidelines for the proposed suspension through multi-objective optimization;

2. Develop a comprehensive off-road vehicle ride dynamics model integrating a three-dimensional adaptive tire model for characterizing tire-terrain interactions along all the three translational axes considering coherence of the two terrain tracks;

3. Formulate a kineto-dynamic model of the frame steering mechanism in conjunction with a nonlinear yaw-plane model of an articulated dump-truck, and investigate steering responses and stability limits of the ASVs;

4. Develop an integrated ride and handling dynamic model of an articulated frame steer vehicle incorporating kineto-dynamic model of the frame steering mechanism, axle suspension, tire-terrain interactions and roughness properties of the two tire tracks for analyses of ride and directional response characteristics of the vehicle;

5. Formulate performance indices, and investigate the effects of selected design and operating parameters on both the ride and directional stability measures so as to develop essential design guidance for the articulated steering mechanism and axle suspension.

1.3.2 Organization of the dissertation-manuscript based format

This dissertation has been written according to the manuscript-based format based on the requirements described in “Thesis Preparation and Thesis Examination Regulation” booklet of the School of graduate Studies of Concordia University. This dissertation research is organized into 6 chapters including a literature review chapter (Chapter 1) describing systematic developments and analysis in achieving the above-stated objectives:

Chapter 2 presents systematic developments in ride dynamic modeling of an articulated off-road vehicle, the axle suspension design, field assessments of the prototype suspension and ride simulation results. The results obtained during this initial phase of the study have been published in two different articles, which are listed below:

1. A. Pazooki, D. Cao, S. Rakheja, and P-É. Boileau, “Experimental and Analytical Evaluations of a Tosio-Elastic Suspension for Off-Road Vehicles”, *SAE International Journal of Materials and Manufacturing*, 3 (1), 326-338, 2010.
2. A. Pazooki, D. Cao, S. Rakheja, and P-É. Boileau, “Ride Dynamic Evaluations and Design Optimization of a Torsio-Elastic Off-Road Vehicle Suspension”, *Journal of Vehicle System Dynamics,* 49 (9), 1455-1476, 2011.

These two articles describe torsio-elastic linkage suspension concept to achieve improved ride performance coupled with high lateral and roll stiffness. Analytical models of a forestry skidder with and without the torsio-elastic suspension at the rear axle were formulated assuming negligible contributions of the articulation. The data acquired from a comprehensive field test program involving a conventional skidder and a skidder equipped with the prototype suspension were analyzed to identify terrain properties and the ride characteristics. The data were used to verify the model and derive ride performance potentials of the prototype suspension. The model was further used to identify optimal suspension parameters. For this purpose, a sensitivity analysis is performed to study the influences of variations in suspension design parameters on the ride performance evaluated under different operating conditions. The Pareto optimization based on the genetic algorithm method was further used to identify optimal suspension parameters in the second article. The second article, published in *Journal of Vehicle System Dynamics*, alone is presented in the thesis, which presents a more refined vehicle model together with suspension optimization.

The limitations of the tire model used in the preliminary model were subsequently identified. The point-contact tire model, used in the above articles, lacked the tire-ground interactions in the shear directions and thereby provided poor predictions of longitudinal and lateral ride performance of the vehicle. The vehicle vibration along the lateral and longitudinal axes was observed to be quite high, and it became evident that a three-dimensional tire model would be needed to predict the ride responses along the horizontal axes. Subsequently, an adaptive contact radial tire model was formulated and coupled with a lateral force model to incorporate tire interactions with the terrain along all the three-translational axes. Assuming small side slip angles and contact normal load, the lateral force developed by the tire was derived considering first order tire dynamics, and thus the tire lag. The time constant relates to the forward speed and the tire relaxation length. The three-dimensional tire model was integrated to the vehicle model with and without the rear axle suspension.The time-history of an equivalent undeformable forestry terrain was considered to synthesize roughness profiles of the two tire tracks through a proposed coherence function. This permitted better predictions of the vehicle roll and lateral ride responses.

The ride dynamic responses of the model were evaluated under excitations representing the proposed forestry terrain. The model validity was demonstrated by comparing the simulation results with the measured data. The ride responses were obtained for the vehicle model with and without a rear-axle suspension to further illustrate the ride performance potentials of the torsio-elastic suspension. The ride vibration response of the vehicle deriver was subsequently assessed on the basis of total whole-body vibration (WBV) exposure in accordance with the ISO-2631-1 guidelines [3]. The results of this segment of the study have been published in the following article, which is presented in chapter 3.

3. A. Pazooki, S. Rakheja, and D. Cao, "Modeling and Validation of Off-Road Vehicle Ride Dynamics", *Mechanical Systems and Signal Processing,* 28, 679–695, April 2012.

A yaw-plane model of the vehicle was subsequently developed to study directional response characteristics of the articulated frame steer vehicle. Owing to the significant effects of the frame steering design on the vehicle directional stability, a comprehensive kineto-dynamic model of the steering system was formulated and integrated to the vehicle model. The model was analyzed to identify yaw stability limits and steering responses of the vehicle. The model and the simulation results have been presented in the following article submitted for publication in the *International Journal of Vehicle Design*.

4. A. Pazooki, S. Rakheja, and D. Cao, "Kineto-Dynamic Directional Response Analysis of an Articulated Frame Steer Vehicle" *Journal of Vehicle System Design,* Ref: IJVD-38698 (Accepted subject to minor revisions, September 2012).

The above manuscript is presented in chapter 4 of the dissertation. The manuscript presents a comprehensive kineto-dynamic model of the frame steer system incorporating the closed-loop steering valve dynamics and kinematics and dynamics of the steering struts considering fluid flows through the control valve, leakage flows and fluid compressibility. The kineto-dynamic model of the frame steering system was integrated to a nonlinear 3-dof yaw plane model of an articulated dump truck to investigate the effects of the combined kinematic and dynamic characteristics of the steering system on the vehicle directional dynamics and stability characteristics. The model also incorporated the tire-lag effect, as describe in the article in chapter 3. The proposed kineto-dynamic model of the steering system was validated on the basis of the limited measured data obtained from Hydrema [235]. The vehicle model integrating the kineto-dynamic steering system model is then applied to evaluate directional response and yaw stability limits of the vehicle. The influences of selected steering and vehicle system parameters on the response measures were further evaluated. The relative stability limits were identified from the rate of decay of the articulation angle under a pulse steering input. The results revealed most significant effects of leakage flows, maximum flow rate and characteristic articulation angle error. The steering value saturation was observed under abrupt steering inputs, which caused weaving/snaking of the vehicle.

In the final phase of the dissertation research, Chapter 5, a three-dimensional vehicle model is formulated in order to study integrated ride, roll and directional dynamic characteristics of the frame steer vehicle. The proposed model integrates the kineto-dynamic model of the frame steering system to the three-dimensional ride dynamic model of the vehicle. The model, therefore, permits the coupled ride and handling analysis in the presence of vertical tire interactions with off-road terrains, and the effects of axle suspension on both the ride and roll dynamic responses. The model also permits the analyses of effects of terrain roughness on directional responses and stability limits of the vehicle. The study also presents a set of performance measures for relative assessments of vehicle directional performance, which were established from the measures reported for heavy road vehicles. Simulations were performed to evaluate ride dynamic responses, together with the directional responses of the vehicle under different operating conditions. The model together with the simulation results have been presented in the following article that has been submitted to the *International Journal Vehicle Performance*.

5. A. Pazooki, S. Rakheja, and D. Cao, “A Three-Dimensional Model of an Articulated Frame-Steer Vehicle for Coupled Ride and Directional Dynamic Analyses”, Submitted, October 2012.

The published/submitted manuscripts presented in the thesis have been reformatted, while the article references have been grouped together are re-numbered. The highlights of the dissertation research together with the major conclusions and recommendations for future works are presented in Chapter 6.

CHAPTER 2

RIDE DYNAMIC EVALUATIONS AND DESIGN OPTIMIZATION OF A TORSIO-ELASTIC OFF-ROAD VEHICLE SUSPENSION

2.1 Introduction

Wheeled off-road vehicles, employed in forestry, agriculture, mining, construction as well as military sectors are known to yield comprehensive magnitudes of low frequency ride vibration of whole-body nature. The logging tractors used for harvesting of trees in the forestry sectors, commonly known as the skidders, are unsuspended vehicles, which yield highly complex ride vibration along translational and rotational axes arising from dynamic interactions of the vehicle with uneven terrains. The whole-body vibration (WBV) environment of such vehicles exhibits predominance of shocks and jolts, characterized by high crest factors, particularly along the vertical and lateral axes [137,3]. It has been established that exposure to low frequency WBV derived from skidder's operation, may well exceed the fatigue decreased proficiency limits defined in ISO-2631 for all the three translational axes [137]. On the basis of extensive field measurements, Cation et al. [1] showed that the skidder operators' vibration exposure exceeds the health caution guidance zone for a 4-h work day, as defined in the current international standard, ISO-2631-1[3]. The measured data revealed predominance of shocks, which was characterized by a high crest factor in the vicinity of 12 in the vertical axis. Neitzel and Yost [2] further showed that the 8-h equivalent vibration exposure of forestry workers, including the skidder operators, exceeds the 8-h exposure limit defined by the Commission of the European Communities [198]. The measured data further suggest that the WBV of a forestry skidder tends to dominate in the low frequency range (up to 5 *Hz*), which can be partly attributed to large diameter soft tires with light damping.

Exposure of high intensity and low frequency WBV has been widely associated with several musculoskeletal disorders among the human drivers [5,78,83]. Several epidemiological studies have established strong relation between exposure to WBV and low back pain (LBP) among the off-road vehicle operators [6,48,57,199,200]. A few studies have also established high prevalence of LBP among the forestry vehicle operators [57,199]. Despite the high intensity WBV environment of forestry skidders and the associated health and safety risks, only limited efforts have been made to control the transmission of vibration to the human operator. A forestry skidder is directly suspended on large diameter soft tires, which provide only very light damping. The ride vibration properties may thus be characterized by the response of a lightly damped mechanical system. Furthermore, vehicle operations on relatively rough terrains coupled with large size tires and high location of the operator contribute to high magnitudes of lateral and fore-and-aft vibration at the operator's location. Although a number of primary and secondary suspension designs have evolved for different wheeled off-road vehicles [20,94,97,106], the implementation in forestry skidders has been mostly limited to low natural frequency vertical seat suspension [137]. This may be partly attributed to increased vehicle rollover or tipover risk associated with a primary suspension operating on forestry highly uneven terrains with considerable grade and cross-grade [201,202].

Suspension seats, designed with low natural frequency in the order of 1.5 *Hz* and free travel of ± 5 *cm*, are generally employed to attenuate vertical vibration in such vehicles [139,203,204]. The vehicle interactions with rough forest terrains may cause the suspension seat to exceed its free travel and transmit high intensity vibration or shock motions due to end-stop impacts. Furthermore, a few studies have shown that the suspension seats used in skidders do not offer reductions in vertical vibration [1,107]. These studies also concluded that a vertical suspension seat may amplify the vibration transmitted to the operators. Alternatively, various concepts in cab suspension have evolved to attenuate vibration along the translational as well as rotational axes [103,131,136,205,206]. The vibration isolation performance characteristics of a prototype skidder cab supported on rubber and hydro-pneumatic mounts, and spring-damper suspension units have been investigated analytically and experimentally [136]. The study showed that the low frequency lateral vibration (predominant around 1 *Hz*) could not be attenuated by a suspension at the cab. Furthermore, the implementation of a suspension at the cab was considered to be quite complex in small size forestry vehicles, where the cab is often welded to the chassis along with the ROP structure.

Alternatively, a number of primary suspension designs have been explored for agricultural and construction vehicles to achieve improved ride comfort for operators and reduce stresses in the vehicle structure and components [43,93,94,97,207]. Similar developments in primary suspensions for forestry skidders have been lacking, which may be partly attributed to concerns related to reduced roll and lateral stability due to low natural frequency suspension, the requirements of high roll and pitch stiffness, complexities associated with implementation of a wheel suspension since the axles are generally welded to the chassis structure; and extreme variations in the axle loads that would pose considerable design challenge.

In this chapter (paper), a concept in a torsio-elastic linkage suspension is presented to achieve improved ride performance coupled with high lateral and roll stiffness. The performance potentials of the proposed concept are investigated analytically and through field measurements of a prototype suspension. The influences of variations in the suspension design parameters on the ride performance are further presented through a parametric study and optimal suspension parameters are identified using the Pareto optimization based on the genetic algorithm method.

2.2 Ride Dynamic Modeling of an Off-Road Skidder

Fig. 2.1 schematically shows a wheeled log skidder with a single articulation. A 3 degree-of-freedom (DOF) ride dynamic model of the conventional skidder is formulated assuming constant speed operation and negligible contributions of the articulation mechanism to the vertical, roll and pitch responses. Considering that the axles are welded to the vehicle frame, the frame together with the axles and the cabin can be considered as a rigid mass supported on four tires, which are modeled by linear damped springs with point contact with the terrain, as illustrated in the pitch and roll-plane models in Fig. 2.2 The equations of motion for the vehicle model subject to terrain excitations at the four tire-terrain contact points are derived as follows:

$$m_s\ddot{z}_s + \sum_1^4 F_{Ti} = 0;\ I_{YYS}\ddot{\theta}_s - WB_1[F_{T1} + F_{T2}] + WB_2[F_{T3} + F_{T4}] = 0$$

$$I_{XXS}\ddot{\phi}_s + T[F_{T1} + F_{T3}] - T[F_{T2} + F_{T4}] = 0 \tag{2.1}$$

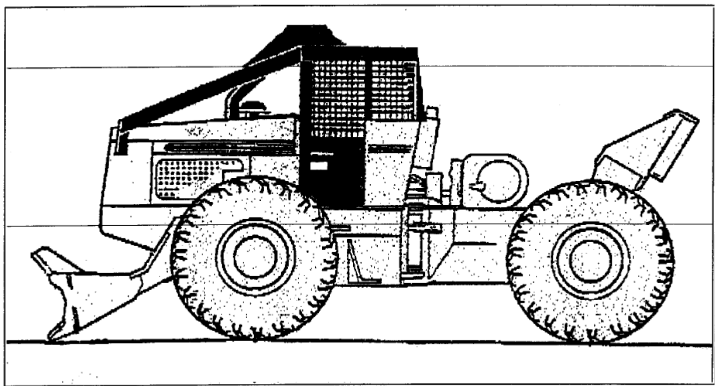

Figure 2.1: Schematic of a wheeled forestry skidder.

where m_s, I_{YYS} and I_{XXS} are the mass, and pitch and roll mass moments of inertia of the vehicle, respectively. T is the half-track width, assumed to be identical for both axles, and WB_1 and WB_2 are longitudinal coordinates of the front and rear axles with respect to vehicle center of gravity (*cg*). z_s, θ_s and ϕ_s are vertical, pitch and roll displacements, respectively, of the sprung mass about a static equilibrium, and $F_{Ti} = K_{Ti}q_i + C_{Ti}\dot{q}_i$ is the force developed by tire i (i=1,2,3,4), where K_{Ti} and C_{Ti} are the linear stiffness and damping coefficients of tire i, and q_i is its deflection, given by:

$$q_i = z_s + (-1)^j WB_j\theta_s + (-1)^i T\phi_s - z_{0i}; \qquad j=1 \; for \; i=1,2; \; and \; j=2 \; for \; i=3,4. \quad (2.2)$$

where z_{0i} is the terrain elevation at the interface of tire i.

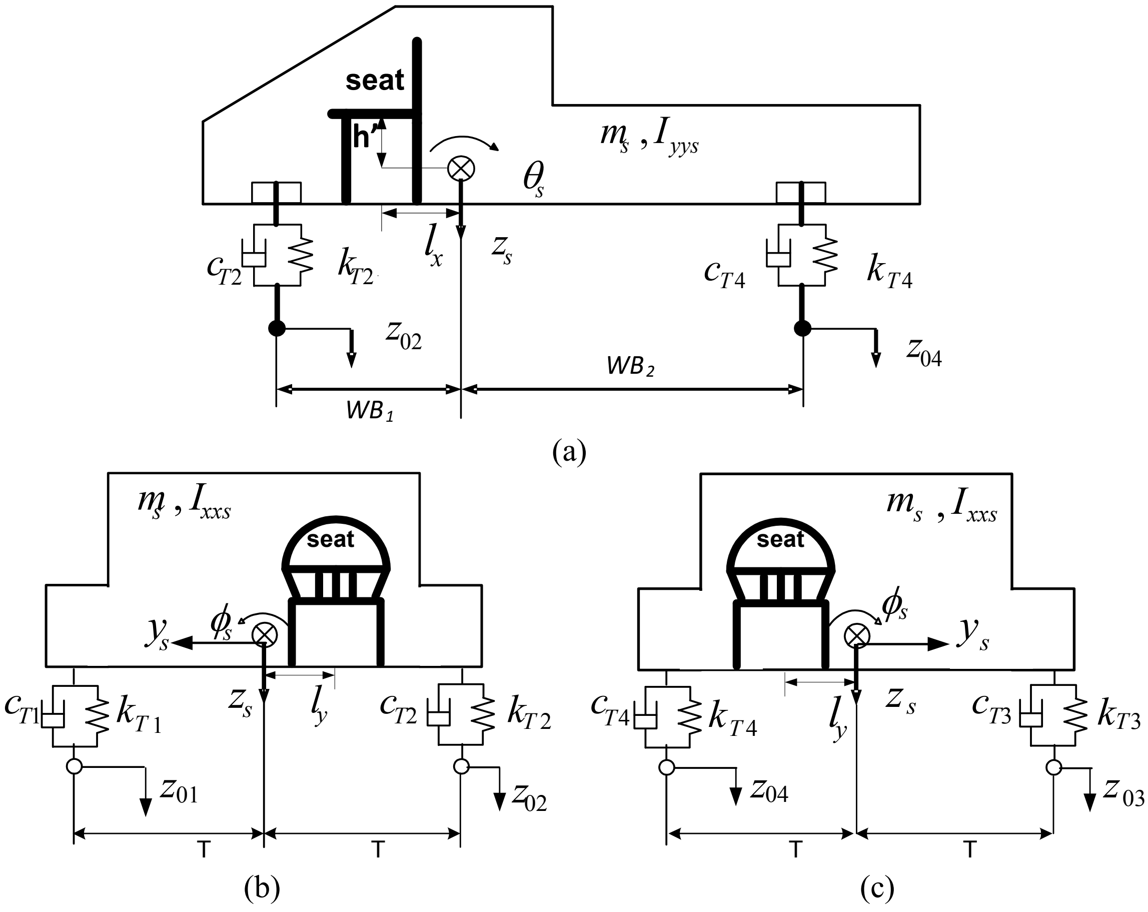

(a)

(b) (c)

Figure 2.2: Pitch- and roll-plane representations of a conventional skidder: (a) Pitch-plane; (b) Roll-plane, (front axle; front view); and (c) Roll-plane, (rear axle; rear view).

2.3 Torsio-Elastic Suspension Concept

The torsio-elastic suspension consists of a linkage that is oriented along the vehicle lateral axis and couples the vehicle body (sprung mass) with the unsprung mass. The suspension linkage mechanism envelopes two 0.6 *m* long tubular shafts of elliptical cross section (43 *mm* × 38 *mm*), oriented along the vehicle longitudinal axis, directly coupling the sprung and unsprung masses through a series of clevises, as illustrated in Fig. 2.3(a). Each tubular shaft comprises an elastomeric bar reinforced with a 16 *mm* metallic shaft in the center. The nominal width of the suspension link is 160 *mm*, while its length could be varied depending upon the desired load carrying capacity.

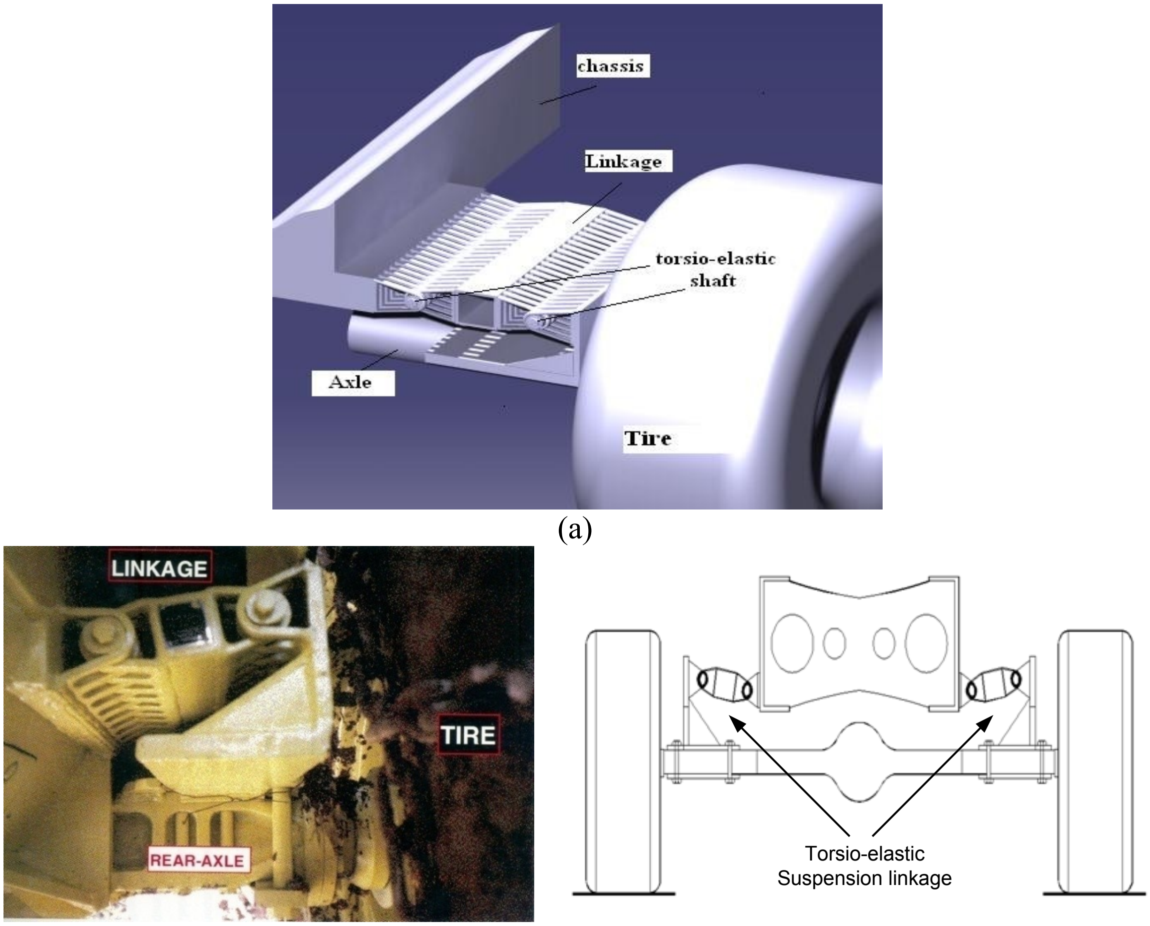

(a)

(b) (c)

Figure 2.3: The prototype rear-axle torsio-elastic suspension: (a) isometric schematic; (b) pictorial view; (c) roll-plane illustration of the suspension.

The torsio-elastic suspension is introduced at the rear axle of the vehicle by eliminating the rigid coupling between the chassis and the rear axle, while providing high effective roll stiffness due to restoring moment capability of the torsional shafts. A pictorial view of the suspension fitted to the rear axle of a skidder is shown in Fig. 2.3(b), while the suspension with the sprung and unsprung masses in the roll plane is schematically shown in Fig. 2.3(c). The laterally-oriented linkage suspension undergoes relative roll motions between the unsprung and sprung masses, which yields a kinematic advantage and absorption of energy due to torsional deflections of each composite shaft. In addition, the composite shaft could also undergo radial deflection.

2.4 Development of a Ride Dynamic Vehicle Model with Rear-Axle Suspension

The log skidder, retrofitted with the proposed torsio-elastic suspension at the rear-axle, is analytically modeled as a 13-DOF dynamic system. Figures 2.4(a) and 2.4(b) illustrate the pitch and roll planes of the full-vehicle model with the rear-axle suspension, respectively, while the detailed linkage suspension model is shown in Fig. 2.4(c). The vehicle body, chassis, cab, and the mounted equipment together with the front axle are represented by a lumped sprung mass (m_s') with four-DOF: vertical (z_s), roll (ϕ_s), pitch (θ_s), and lateral (y_s). The rear axle is represented by a rigid body with three-DOF: vertical (z_{ur}), lateral (y_{ur}), and roll (ϕ_{ur}). Each suspension link on the right and left sides is considered to possess three-DOF motion along the vertical (z_3, z_4), roll (ϕ_3, ϕ_4), and lateral (y_3, y_4) directions. Each tire is modeled as a parallel combination of linear energy restoring and dissipative elements, assuming that the tire remains in contact with the terrain through a point contact model. The torsio-elastic suspension is characterized by its radial and torsional visco-elastic properties.

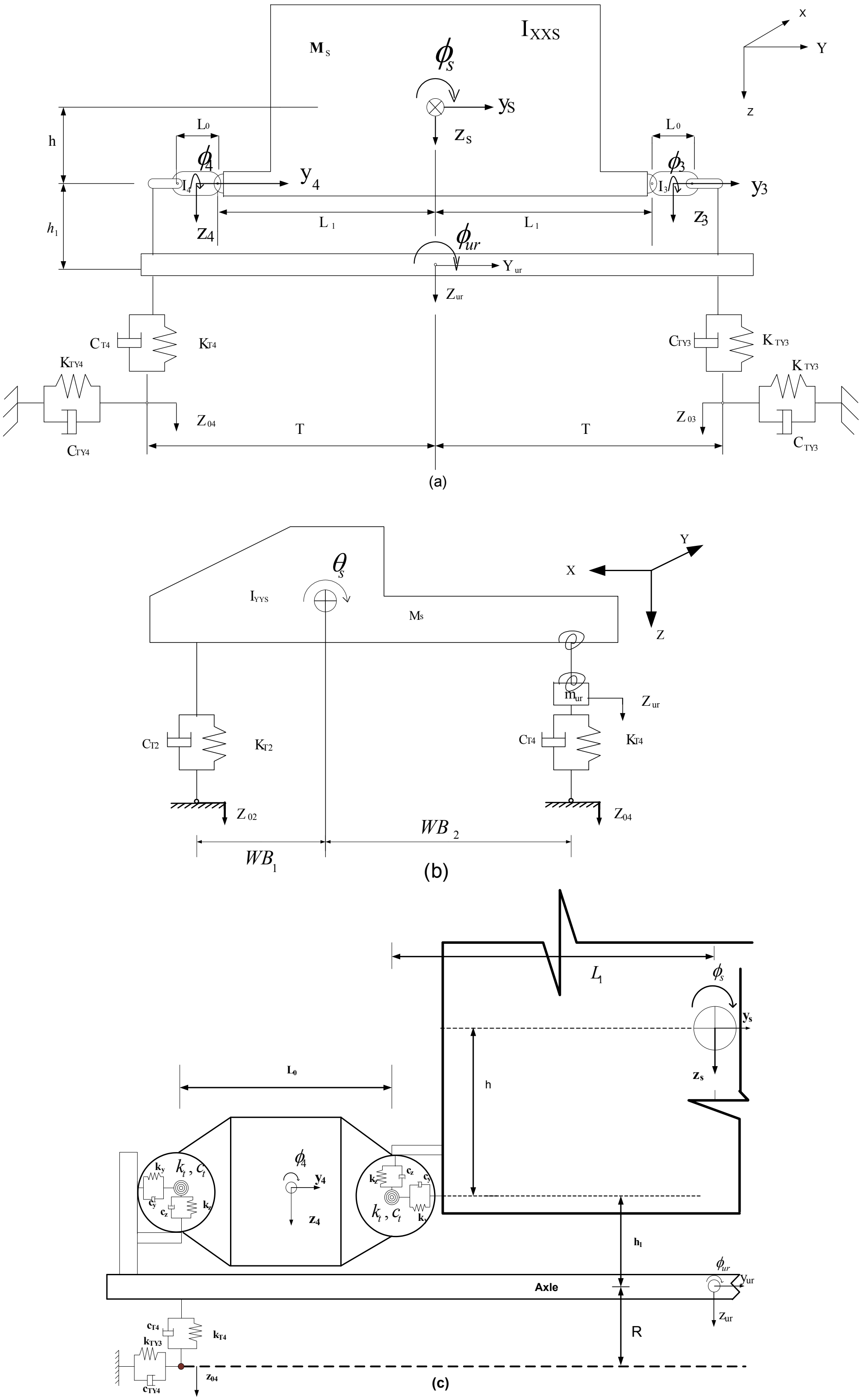

Figure 2.4: Schematic representation of the 13-DOF suspended vehicle model: (a) roll plane; (b) pitch plane; and (c) torsio-elastic suspension linkage mechanism.

The radial visco-elastic properties are represented by linear stiffness and damping elements along the vertical (k_z, c_z) and lateral (k_y, c_y) axes, while the torsional properties are characterized by linear torsional stiffness and damping coefficients (k_t, c_t). The equations of motion for the vehicle model subject to terrain excitations at the four tire-terrain contacts points are formulated as follows:

$$m'_s\ddot{z}_s + \sum_{i=1}^{2} F_{Ti} + \sum_{i=3}^{4}\left(F_{zi}\right) = 0\,; \qquad m'_s\ddot{y}_s + \sum_{i=3}^{4} F_{yi} + \sum_{i=1}^{2} F_{TYi} = 0$$

$$I'_{XXS}\ddot{\phi}_s + M_{\theta 4s} + M_{\theta 3s} - \left(F_{z4} - F_{z3}\right)L_1 - \sum_{i=3}^{4} F_{yi}h - T\left(F_{T2} - F_{T1}\right) + \sum_{i=1}^{2} F_{TYi}\left(h + h_1 + R\right) = 0$$

$$I'_{YYS}\ddot{\theta}_s + \sum_{i=3}^{4} F_{zi}WB_2 - \sum_{i=1}^{2} F_{Ti}WB_1 = 0$$

$$m_{ur}\ddot{z}_{ur} + \sum_{i=3}^{4} F_{Ti} - \sum_{i=3}^{4} F_{ziu} = 0\,; \qquad m_{ur}\ddot{y}_{ur} - \sum_{3}^{4} F_{yiu} + \sum_{i=3}^{4} F_{TYi} = 0$$

$$I_r\ddot{\phi}_{ur} + \left(F_{T3} - F_{T4}\right)T - \sum_{i=3}^{4}\left[RF_{TYi} + F_{yiu}h_1 - F_{ziu}\left(L_1 + L_0\right)\right] - M_{\theta 3u} - M_{\theta 4u} = 0$$

$$m_3\ddot{z}_3 + F_{z3u} - F_{z3} = 0; \qquad m_4\ddot{z}_4 + F_{z4u} - F_{z4} = 0$$

$$I_3\,\ddot{\theta}_3 + \left(F_{z3u} + F_{z3}\right)\frac{L_0}{2} - M_{\theta 3s} + M_{\theta 3u} = 0; \qquad I_4\ddot{\theta}_4 + \left(F_{z4u} + F_{z4}\right)\frac{L_0}{2} - M_{\theta 4s} + M_{\theta 4u} = 0$$

$$m_3\ddot{y}_3 + F_{y3u} - F_{y3} = 0; \qquad m_4\ddot{y}_4 + F_{y4u} - F_{y4} = 0 \qquad (2.3)$$

whereI'_{XXS} and I'_{YYS} are roll and pitch mass moments of inertia of the sprung mass, respectively. I_r, I_3 and I_4 are the roll mass moments of inertia due to rear axle, and right and left suspension links, respectively. The geometric parameters L_0, L_1, R, h and h_1 are illustrated in Fig. 2.4 In the above equations, subscripts "3" and "4" of the forces or moments refer to those developed by the right- and left-suspension units, respectively. F_{z4} and F_{z3} are vertical forces acting on the sprung mass developed due to left- and right-axle suspensions, respectively. F_{z3u} and F_{z4u} are the corresponding forces acting at the unsprung mass attachments. (F_{y3}, F_{y4}) and (F_{y3u}, F_{yu4}) are the lateral forces acting on the sprung and unsprung masses, respectively, due to radial stiffness and damping properties of the torsio-elastic suspension, and ($M_{\theta 3s}$, $M_{\theta 4s}$) and ($M_{\theta 3u}$, $M_{\theta 4u}$) are the respective roll moments acting on the sprung and unsprung masses. F_{TYi} ($i=1,\ldots,4$) are lateral forces developed at the tire-terrain interfaces. The forces and the moments developed due to the tire and suspensions are described in details in the Appendix 2-A.

The coupled differential equations of motion of the 13-DOF skidder model can be expressed in the following matrix form:

$$[M]\{\ddot{q}\}+[C]\{\dot{q}\}+[K]\{q\}=[C_F]\{\dot{q}_0\}+[K_F]\{q_0\} \tag{2.4}$$

where [M], [C] and [K] are (13×13) mass, damping and stiffness matrices, respectively, and [C_F] and [K_F] are (13×4) forced damping and stiffness matrices. $\{q\}$ and $\{q_0\}$ are the vectors of generalized and excitation coordinates, given by:

$$\begin{aligned}\{q\}&=\{z_s,\phi_s,y_s,\theta_s,z_{ur},\phi_{ur},y_{ur},z_3,\theta_3,y_3,z_4,\theta_4,y_4\}'\\ \{q_0\}&=\{z_{01},z_{02},z_{03},z_{04}\}'\end{aligned} \tag{2.5}$$

The superscript “ ' ” in the above equations denotes the transpose. The equations of motion of the 3-DOF unsuspended vehicle can also be presented in the matrix form of Eq. (2.4), where the generalized coordinate vector is $\{q\}=\{z_s, \theta_s, \phi_s\}'$.

2.5 Field Measurements of Vehicle Ride Vibration Responses

Field tests were performed to measure and compare the ride vibration characteristics of a conventional unsuspended skidder and a skidder fitted with the proposed torsio-elastic suspension at the rear axle. The two vehicles (TREE FARMER C6D) were identical in all respects except for the rear-axle suspension. Both the vehicles employed a cushioned seat without a suspension and were instrumented to measure the vibration responses at the cabin floor along the vertical, fore-aft, lateral, roll and pitch directions during the transport operation under loaded and unloaded conditions. The measured data were analyzed to obtain relative ride properties of the suspended and unsuspended vehicles. The data acquired with the unsuspended vehicle were further applied to obtain an estimate of the terrain properties, while those with the suspended vehicle were used to examine validity of the 13-DOF ride dynamic model and to assess the potential ride benefits of the proposed suspension.

2.6 Measurement Methods and Data Analyses

A total of six accelerometers were installed on the cabin floor of each vehicle to measure vibration responses along the fore-aft (x), lateral (y), vertical (z), roll (ϕ) and pitch (θ) axes. Fig. 2.5 illustrates a schematic of the accelerometers located at the cab floor, together with the distances between the various accelerometers. One accelerometer was mounted beneath the driver seat to capture vertical vibration near the driver seat, indicated as “4”. Three accelerometers, “1”, “2” and “3”, oriented along x, y and z-axes, respectively, were installed at rear-left of the cabin, and two single-axis accelerometers were mounted at the front-left, “5”, and front-right, “6”, of the cabin at the floor level. The roll and pitch acceleration response characteristics of each vehicle were derived from the measured vertical accelerations using kinematic relations, while assuming small angular motions and negligible contribution due to structure flexibility, such that:

$$\ddot{\phi}_c = \frac{\ddot{z}_5 - \ddot{z}_6}{L}\ ; \quad and \quad \ddot{\theta}_c = \frac{\ddot{z}_3 - \ddot{z}_5}{L} \qquad (2.6)$$

where $\ddot{\phi}_c$ and $\ddot{\theta}_c$ are roll and pitch accelerations of the vehicle cabin, respectively, and $\ddot{z}_5$, $\ddot{z}_6$ and $\ddot{z}_3$ are vertical accelerations measured at locations 5, 6 and 3, respectively, as shown in Fig. 2.5 The lateral spacing between accelerometers 5 and 6 is denoted by B_{ac}, and L_{ac} is longitudinal spacing between accelerometers 3 and 5.

It should be noted that measurements of vibration levels at the operator seat were not attempted, since such vehicles may employ widely different types of seats with or without a suspension. The vibration transmitted to the driver's seat, however, was evaluated for exposure assessment. For this purpose, the fore-aft ($\ddot{x}_{m0}$) and lateral ($\ddot{y}_{m0}$) acceleration levels at the driver-seat interface were estimated from those measured at the cab floor, assuming small rotations and negligible effects of the seat cushion, such that:

$$\ddot{x}_{m0} = \ddot{x}_1 - h\ddot{\theta}_c; \quad \mathit{and} \quad \ddot{y}_{m0} = \ddot{y}_2 + h\ddot{\phi}_c \tag{2.7}$$

where h is the seat height from the cabin floor, and $\ddot{x}_1$ and $\ddot{y}_2$ are the longitudinal and lateral accelerations measured at the cab floor using accelerometers 1 and 2, respectively (Fig. 2.5). Although the seat cushion was expected to influence the cab floor vibration transmitted to the operator, particularly at frequencies above 3 *Hz*, the vertical acceleration ($\ddot{z}_4$), measured beneath the seat, was considered for the exposure assessment, such that $\ddot{z}_{m0} = \ddot{z}_4$, where $\ddot{z}_{m0}$ is the vertical acceleration at the operator-seat interface.

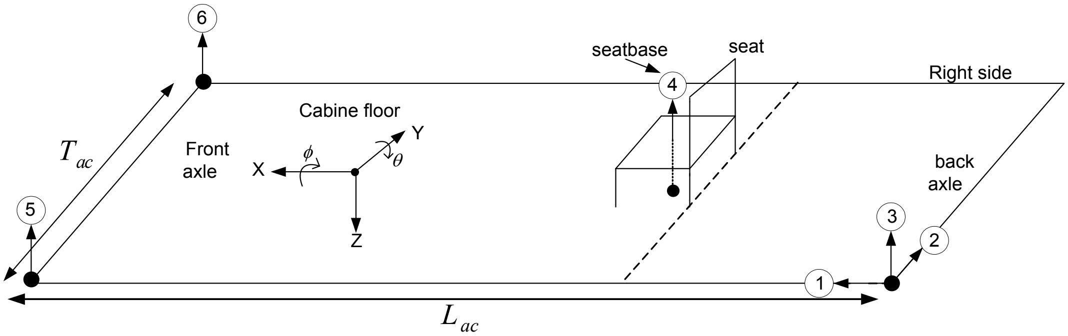

Figure 2.5: Locations of accelerometers on the cabin floor: “1”, “2”and “3”, oriented along the x, y and z -axes at the rear-left, respectively; “4” at the seat base along z -axes; “5” front-left along z -axes; and “6” front-right along z -axes.

The measurements were performed while the two vehicles were driven in a forest in Eastern Quebec (Canada) by the same driver. The driver was advised to operate the vehicle at a steady speed near 5 *km/h*, and the accelerometers signals were acquired in a multi-channel data recorder. The measurements were acquired while the vehicles were driven forward along the selected trails and return to the start location. The duration of each measurement ranged from 5 to 15 minutes. The measured signals were manipulated to compute the roll and pitch accelerations of the cabin using Eq. (2.6), and the acceleration responses at the seat ($\ddot{x}_{m0}$, $\ddot{y}_{m0}$, $\ddot{z}_{m0}$) using Eq. (2.7). The time histories of the resulting acceleration signals were subsequently analyzed using a multi-channel signal analyzer to derive power spectral density (PSD) spectra of accelerations along the fore-aft, lateral and vertical-axes at the seat, and along the fore-aft, lateral, vertical, roll and pitch axes at the cab floor.

The spectra were evaluated using a bandwidth of 100 *Hz* and frequency resolution of 0.125 *Hz* considering a 75% overlap. The overall unweighted and frequency-weighted rms accelerations at the seat were also obtained for relative ride assessments of the suspended and unsuspended vehicles. The frequency-weighted rms accelerations were computed using the W_k–, W_d– and W_e–weighting filters defined in ISO-2631-1 [3] for vertical, horizontal and angular accelerations, respectively.

2.7 Response Analyses of the Vehicle Model

The coupled differential equations of motion for the 3-DOF and 13-DOF models of the conventional and suspended vehicle models, respectively, were solved in the frequency-domain to obtain ride vibration responses at the operator seat and cab floor. The spectral densities of the generalized response coordinates could be derived from the complex frequency response function of the models, such that:

$$[S(j\omega)] = [H(j\omega)][S_i(j\omega)][H(j\omega)]^{T*} \tag{2.8}$$

where $[H(j\omega)]$ is the (3×4) and (13×4) complex transfer function matrices of the conventional and suspended vehicle models, respectively. The superscript “'*” denotes the transposed complex conjugate of the transfer function matrix. In the above equation, $[S(j\omega)]$ is the spectral density matrix of the generalized response coordinates, and $[S_i(j\omega)]$ is the (4×4) matrix of the spectral density of elevations at the four tire-terrain interfaces, given by:

$$[S_i(j\omega)] = \sigma \begin{bmatrix} 1 & e^{-i\omega\tau_\phi} & e^{-i\omega\tau_\theta} & e^{-i\omega(\tau_\phi+\tau_\theta)} \\ e^{i\omega\tau_\phi} & 1 & e^{-i\omega(\tau_\phi-\tau_\theta)} & e^{-i\omega\tau_\theta} \\ e^{i\omega\tau_\theta} & e^{i\omega(\tau_\phi-\tau_\theta)} & 1 & e^{-i\omega\tau_\phi} \\ e^{i\omega(\tau_\phi+\tau_\theta)} & e^{i\omega\tau_\theta} & e^{-i\omega\tau_\phi} & 1 \end{bmatrix} \tag{2.9}$$

where σ is the amplitude of the terrain elevation, which is related to the vehicle speed U and the spatial PSD of the terrain roughness $G_Z(\Omega)$ as a function of the spatial frequency Ω of the terrain profile, such that: $\sigma(\omega) = G_Z(\Omega)/U$. τ_θ defines the correlation between the front and rear wheels in the pitch plane, and τ_ϕ describes the correlation between the right- and left- wheels in the roll plane. The correlation between the front and rear wheels excitation can be expressed as a function of the vehicle speed and the wheelbase [208], such that: $\tau_\theta = WB/U$.

The roll excitation due to unevenness of the two tracks of the terrain is estimated by generating a randomly distributed cross-slope function in the following manner:

$$\chi = 2T\,(0.5 - rnd) \tag{2.10}$$

where *rnd* is a Gaussian random number generated between 0 and 1. The random cross-slope is expressed in terms of an equivalent time delay between the right- and left-wheels in a manner similar to that described for the front- and rear-axle wheels, such that: $\tau_\phi = \chi/U$.

The response characteristics at the driver-seat location ($\ddot{x}_{S0}$, $\ddot{y}_{S0}$, $\ddot{z}_{S0}$) are evaluated using the coordinate transformations. The frequency response transfer function matrix relating displacement responses at the seat (x_{s0}, y_{s0}, z_{s0}, θ_{s0}, ϕ_{s0}) to the generalized coordinates is formulated as:

$$[H_{S0}(j\omega)] = [R][H(j\omega)] \tag{2.11}$$

where $[R]$ is (5×3) or (5×13) coordinate transformation matrix relating the generalized coordinates with those at the operator seat for the conventional and suspended vehicle models, respectively. $[H_{S0}(j\omega)]$ is the (5×4) frequency response function matrix relating the response vector at the seat to the excitation coordinates. The PSD of displacement responses at the seat can be subsequently evaluated from:

$$[S_{s0}^{d}(j\omega)] = [H_{s0}(j\omega)][S_{i}(j\omega)][H_{s0}(j\omega)]^{T*} \tag{2.12}$$

where $[S_{S0}^{d}(j\omega)]$ is the (5×5) matrix of PSD of displacement responses at the seat. The PSD of acceleration response at the seat $[S_{S0}^{a}(j\omega)]$ is subsequently computed from:

$$[S_{s0}^{a}(j\omega)] = \omega^{4}[S_{s0}^{d}(j\omega)] \tag{2.13}$$

2.8 Estimation of an Equivalent Terrain Profile

The analysis of ride dynamic model of the forestry skidder requires characterization of roughness properties of the forestry terrain. Although the surface roughness properties of various undeformable off-road terrains have been characterized and expressed by regression models in many studies [130-132], a description of a forestry terrain could not be found. Furthermore, the surface roughness of a forestry terrain may vary with local soil properties and number of passes of the vehicle [127, 128]. In this study, roughness of the forestry terrain is estimated from the measured responses of the unsuspended vehicle in conjunction with its 3-DOF model. For this purpose, the 3-DOF vehicle model was initially analyzed by considering a random terrain excitation derived from a roughness model of the form [114]:

$$G_Z(\Omega) = \alpha_r \Omega^{-\beta}; \quad \alpha_r > 0 \text{ and } \beta > 0 \tag{2.14}$$

where constants α_r and β are the roughness coefficient and waviness of the terrain, respectively, which are generally identified from measured roughness profiles. The temporal frequency of the terrain excitation is computed from $f=\Omega U$. The constants α_r and β were identified from the measured responses of the conventional skidder. For this purpose, a minimization problem was formulated to minimize sum of squared normalized errors between the model and the measured responses at the vehicle *cg* at several discrete frequencies, such that:

$$\varepsilon(\omega, \alpha, \beta) = \sqrt{\left(\frac{\mathrm{Re}\left(S^a(1,1)\right) - \ddot{z}_c}{\ddot{z}_c}\right)^2 + \left(\frac{\mathrm{Re}\left(S^a(2,2)\right) - \ddot{\theta}_c}{\ddot{\theta}_c}\right)^2 + \left(\frac{\mathrm{Re}\left(S^a(3,3)\right) - \ddot{\phi}_c}{\ddot{\phi}_c}\right)^2} \tag{2.15}$$

where ε is the error function corresponding to a discrete circular frequency ω. $S^a(i,i); i = 1,2,3$ are the vertical, pitch and roll acceleration responses of the unsuspended vehicle model, respectively.

In the error function, $\ddot{z}_c$ refers to the measured vertical acceleration transformed to the vehicle *cg*, which is estimated from the measured vertical acceleration beneath the seat ($\ddot{z}_4$), and measured roll ($\ddot{\phi}_c$) and pitch ($\ddot{\theta}_c$) accelerations of the cabin:

$$\ddot{z}_c = \ddot{z}_4 + l_x \ddot{\theta}_c + l_y \ddot{\phi}_c \tag{2.16}$$

where l_x and l_y are longitudinal and lateral distances between the vehicle *cg* and the seat base, respectively, as shown in Fig. 2.2.

The minimization problem was solved at 150 different discrete frequencies of excitation in the 0.375 to 25 *Hz* range using Matlab optimization toolbox [210], assuming a constant forward speed of 5 *km/h*. The starting values of parameters were taken as those for a plowed field (α_r=6.5×10^{-4}; β=1.6) [114]. The solutions were also attempted for different starting values, which converged to very similar values of the parameter vector at each frequency. The solutions of the minimization problem provided the parameter vector values corresponding to each discrete frequency, which showed considerable variation with the frequency. The identified coefficients were subsequently applied to the roughness model in Eq. (2.14) to determine terrain roughness in terms of spatial PSD of the profile, $G_Z(\Omega)$. Fig. 2.6 illustrates variations in spatial PSD as a function of the spatial frequency Ω. The results clearly show considerable scatter in the spatial PSD data. A power regression function of the form, defined in Eq. (2.14), was subsequently fitted to the data to obtain estimates of the probable roughness coefficients, which resulted in the following roughness model with a correlation coefficient (r^2) value of 0.6425.

$$G_Z(\Omega) = 1\times 10^{-4}\,\Omega^{-1.7528} \tag{2.17}$$

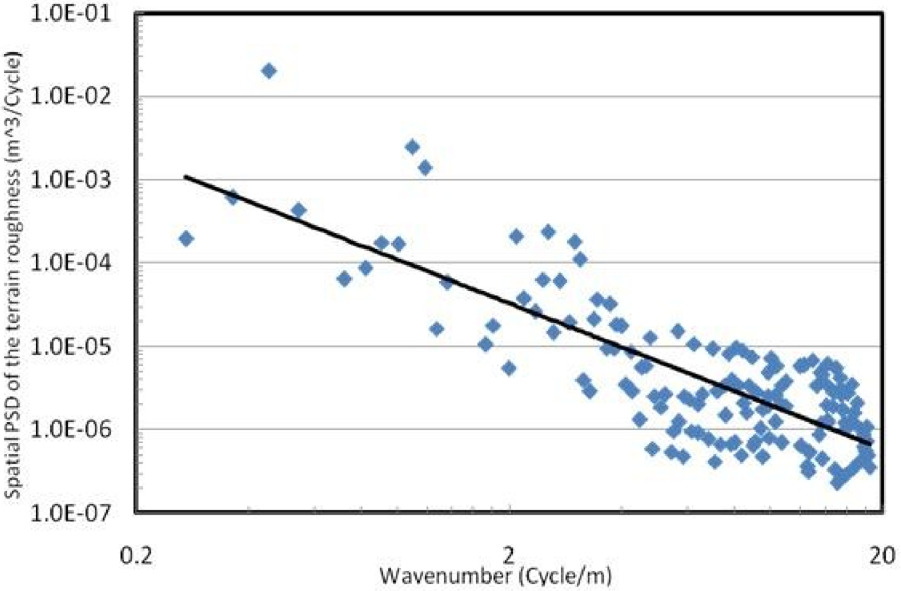

Figure 2.6: Spatial spectral density of terrain elevation identified from measured data at various discrete frequencies and the power regression curve (r^2=0.6425).

The above roughness model of the forestry terrain may be considered to represent roughness profile of an equivalent undeformable terrain. The identified roughness model coefficient and the roughness profile are compared with those reported for the plowed field and pasture [114], and the MVEE (Military Vehicle Engineering & Establishment) random course [131, 132], in Table 2.1 and Fig. 2.7, respectively. The comparisons suggest lower roughness of the forestry terrain compared to the profiles considered, particularly corresponding to the lower wave numbers. This may also be attributed to relatively soft forestry terrain since the measurements were performed during late fall season. The waviness of the forestry terrain, however, is quite comparable to those of the plowed field and the pasture.

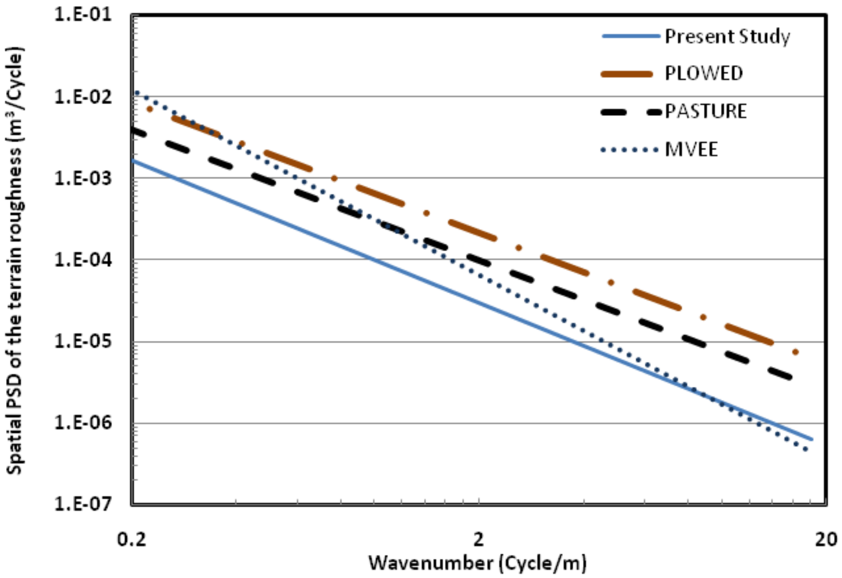

Figure 2.7: Comparisons of roughness profiles of some of the off-road terrains with that estimated for the forestry terrain.

Table 2.1: Comparisons of roughness model coefficients (α_r, β) with those reported for some of the off-road terrains [114,131,132].

Terrain	α_r	β
Plowed	6.50×10^{-4}	1.60
Pasture	3.00×10^{-4}	1.60
MVEE	3.16×10^{-4}	2.27
Present Study	1.00×10^{-4}	1.76

2.9 Results and Discussions

The measured vibration responses of both the suspended and unsuspended vehicles were compared to assess effectiveness of the proposed torsio-elastic suspension in reducing transmission of terrain-induced vibration to the cabin and the human driver's location. The responses were evaluated in terms of power spectral densities of accelerations, overall rms accelerations along all the axes, as well as 8-hour energy frequency-weighted acceleration [3, 202]. Fig. 2.8 compares PSD of accelerations measured at the cabin floor of both the suspended and unsuspended loaded vehicles along the fore-aft, lateral, vertical, pitch and roll axes. The results suggest that the predominant fore-aft and lateral vibration occur at frequencies near or slightly below 1 *Hz*, which are attributable to the pitch and roll modes resonances, respectively. For both the vehicles, the roll, pitch, and vertical acceleration peaks occur near the respective resonance frequencies of 1.0 *Hz*, 0.9 *Hz* and 1.6-2.1 *Hz* range, respectively. Although the resonance frequencies of both the vehicles appear to be quite comparable, the suspended vehicle yields significantly lower magnitudes of vibration in all the axes when compared to those of the unsuspended vehicle.

The potential benefits of the proposed torsio-elastic suspension were also evaluated from the overall unweighted and weighted acceleration responses, computed in the 0.5-20 *Hz* frequency range, and the 8-hour energy frequency-weighted acceleration. The frequency-weighted rms accelerations along the x-, y- and z-axis at the driver's location were evaluated through applications of the appropriate weighting functions defined in ISO-2631-1 [3]. The total WBV exposure was also evaluated in terms of vector summation of the weighted accelerations along the three translational axes, such that:

$$a_v = \sqrt{\left(k_x^2 a_{wx}^2 + k_y^2 a_{wy}^2 + a_{wz}^2\right)} \tag{2.18}$$

where $a_{w\mathrm{x}}$ and a_{wy} are W_d-weighted rms fore-aft and lateral accelerations, respectively, and a_{wz} is the W_k-weighted rms vertical acceleration. The constants k_x and k_y are additional weightings used to account for human sensitivity to horizontal vibration, as recommended in ISO-2631-1 [3]. Eight-hour energy equivalent frequency-weighted acceleration $A(8)$ is also computed in accordance with the exposure assessment guidelines of EC [202], which is computed from:

$$A(8) = a_v \sqrt{\frac{T_e}{T_0}} \tag{2.19}$$

where T_0 is the reference duration of 8 hours and T_e is the average daily exposure duration. In this study, the average daily exposure duration is taken as 4 hours on the basis of the information attained from the Forestry Engineering Research Institute of Canada [211].

Table 2.2 summarizes the unweighted and frequency-weighted rms accelerations along each axis of the suspended and unsuspended vehicles with and without the load. The Table also presents the total exposure a_v and $A(8)$ values. The results show that the torsio-elastic suspension could significantly decrease the vibration exposure levels in all the directions. The suspended vehicle yields 35%, 43% and 57% lower frequency-weighted rms accelerations in x-, y- and z-axis, respectively, compared to the unsuspended vehicle, when loaded. The suspended vehicle, however, exhibits relatively higher unweighted pitch and roll vibration, when unloaded, while the unweighted rms accelerations along the x, y, and z directions are 44%, 27% and 45% lower, respectively, compared to those of the unsuspended vehicle. The higher pitch response of the suspended vehicle is attributed to the pitch dynamic response of the vehicle with a relatively soft suspension at its rear axle. This phenomenon has been illustrated by Cao et al. [212]. The results further show that the weighted magnitudes of horizontal vibration transmitted to the operator location are either comparable to or exceed vertical vibration magnitude. The results also suggest that both the a_v and $A(8)$ values for the suspended vehicle are 41% and 37% lower than those of the unsuspended vehicle under the loaded and no-loaded conditions, respectively. The results thus suggest that the proposed torsio-elastic suspension could offer considerable benefits in reducing the WBV exposure of the vehicle operators.

Table 2.2: Comparisons of unweighted and frequency-weighted rms accelerations along individual axes, the overall rms acceleration and 8-hour energy equivalent values of the suspended and unsuspended vehicles with/without load at the driver location.

Axis	Unweighted rms acceleration, m/s^2				Frequency-weighted rms acceleration, m/s^2			
	Loaded		Unloaded		Loaded		Unloaded	
	Unsusp	**Susp.**	**Unsusp.**	**Susp.**	**Unsusp.**	**Susp.**	**Unsusp.**	**Susp.**
x	1.39	0.85	1.59	0.89	1.16	0.75	1.43	0.78
y	2.12	1.26	1.79	1.30	1.67	0.95	1.52	1.07
z	2.34	1.00	1.83	1.00	1.41	0.60	1.12	0.62
θ	1.01	0.74	0.70	0.82	0.72	0.52	0.46	0.43
ϕ	2.01	0.79	1.10	0.87	1.53	0.56	0.75	0.44
a_v					3.03	1.80	3.13	1.96
$A(8)$					2.14	1.27	2.21	1.40

2.9.1 Vehicle model validation

Validity of the 13-DOF ride dynamic model was examined using the field-measured data corresponding to the unloaded case, which could serve as a design tool for deriving an optimal suspension design. The ride dynamic responses of the vehicle model were obtained under terrain excitation defined in Eqs. (2.9) and (2.17), assuming a constant vehicle speed of 5 *km/h*, which is identical to that used for the field measurements. The simulation parameters of the vehicle model are summarized in Table 2.3, which were obtained partly from the data sheets provided by the manufacturers, and partly estimated from the measured natural frequencies of the vehicle [213].

The results obtained from the eigenvalue problem for the vehicle model revealed vertical, pitch and roll mode resonance frequencies of the sprung mass near 2 *Hz*, 1.1 *Hz* and 0.9 *Hz*, which are quite close to the frequencies corresponding to the peaks in the measured acceleration spectra (Fig. 2.8), while the resonant frequencies of the unsprung mass and the suspension linkage mechanisms were significantly higher. The ride vibration responses of the vehicle model near the operator seat were subsequently obtained in terms of acceleration PSD and the rms values.

Table 2.3: Simulation parameters

Parameter	**Value**	**Parameter**	**Value**
m_s	*8016 kg*	k_z	*185 kN/m*
m_3	*42.6 kg*	k_y	*185 kN/m*
m_4	*42.6 kg*	k_t	*125kNm/rad*
m_{ur}	*1500 kg*	c_z	*4000 Nm.s/rad*
I'_{XXS}	$10495\ kgm^2$	c_y	*4000 Ns/m*
I'_{YYS}	$16353\ kgm^2$	c_t	*3500 Ns/m*
I_3	$3500\ kgm^2$	$K_{Ti},\ i=1,\ldots,4$	*340 kN/m*
I_4	$3500\ kgm^2$	$C_{Ti},\ i=1,\ldots,4$	*1935 Ns/m*
WB	*3.13 m*	$K_{TYi},\ i=1,2$	*256.2 kN/m*
WB_1	*1.23 m*	$K_{TYi},\ i=3,4$	*316.2 kN/m*
WB_2	*1.9 m*	$C_{TYi},\ i=1,\ldots,4$	*1800 Ns/m*
T	*1.25m*	$h+h_1$	*0.8 m*
R	*0.8 m*	l_y	*0.0 m*
l_x	*0.291 m*	L_0	*0.16 m*

The response acceleration spectra obtained along the vertical, pitch and roll axes are compared with those of the measured data in Fig. 2.9. The comparisons along the fore-aft and lateral axes, however, were not attempted due to simplifying assumption of constant forward speed, negligible articulation forces and lack of consideration of the tire-terrain interactions in the fore-aft direction. It should be noted that the spectra of the measured accelerations are quite smooth in relation with those derived from the model responses, as seen in Fig. 2.9. This is attributed to the number of averages performed and signal overlap used during processing of the measured data. While the results suggest comparable trends between the model responses and the measured spectra, considerable deviations are also evident.

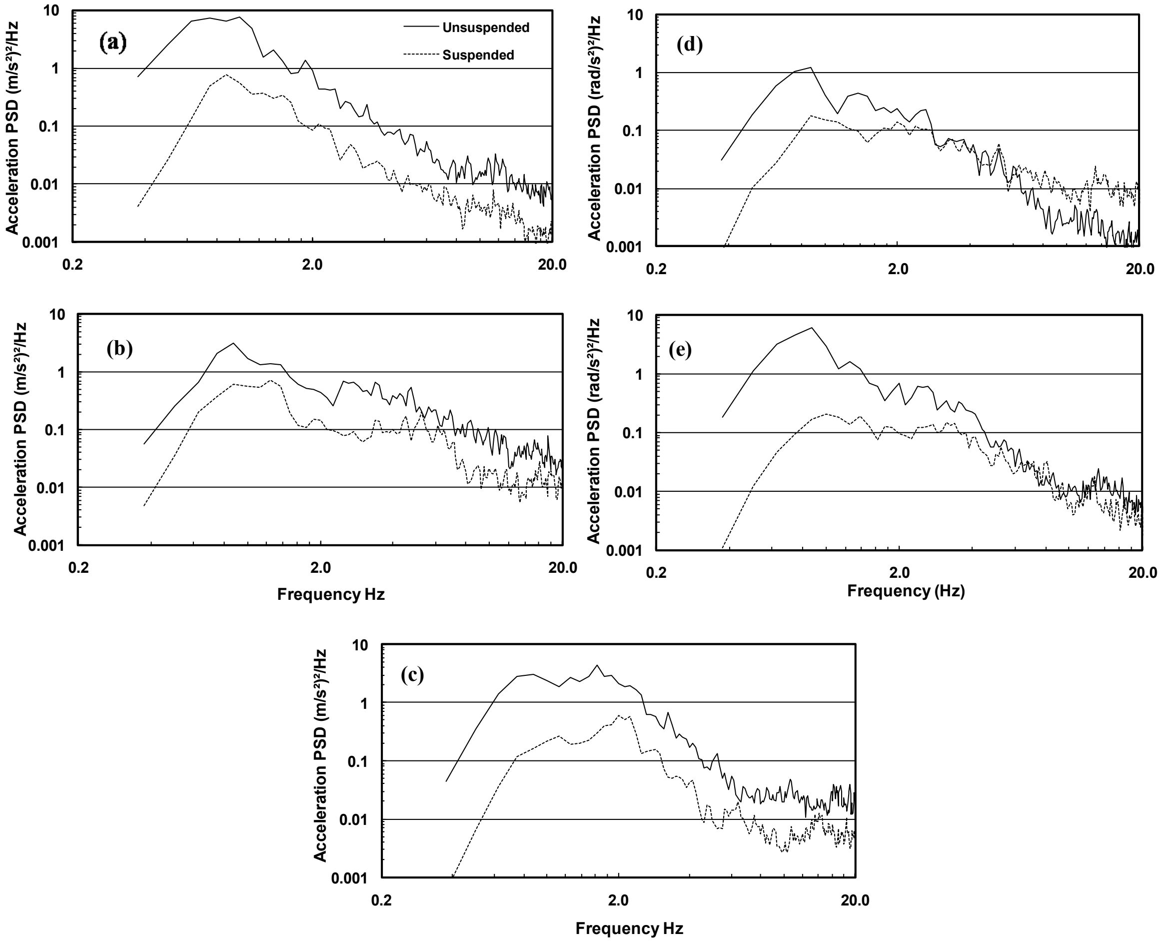

Figure 2.8: Comparisons of measured acceleration PSD responses at the cab floor of the suspended and unsuspended vehicles: (a) fore-aft; (b) lateral; (c) vertical; (d) pitch; and (e) roll.

The model responses exhibit significant troughs near 2 *Hz* and at higher frequencies, which are attributed to the wheelbase filtering effect [212,214,215]. The deviation in the responses are also attributable to various simplifying modeling assumptions, particularly the consideration of negligible contributions due to articulation forces and moments, absence of wheel hop, and linear tire and suspension properties. Despite the observed deviations, the results in general suggest reasonably good validity of the model for predicting vertical, roll and pitch ride responses of the sprung mass. The model may thus be considered applicable for identifying desirable suspension design parameters for enhanced attenuation of the terrain-induced whole-body vibration.

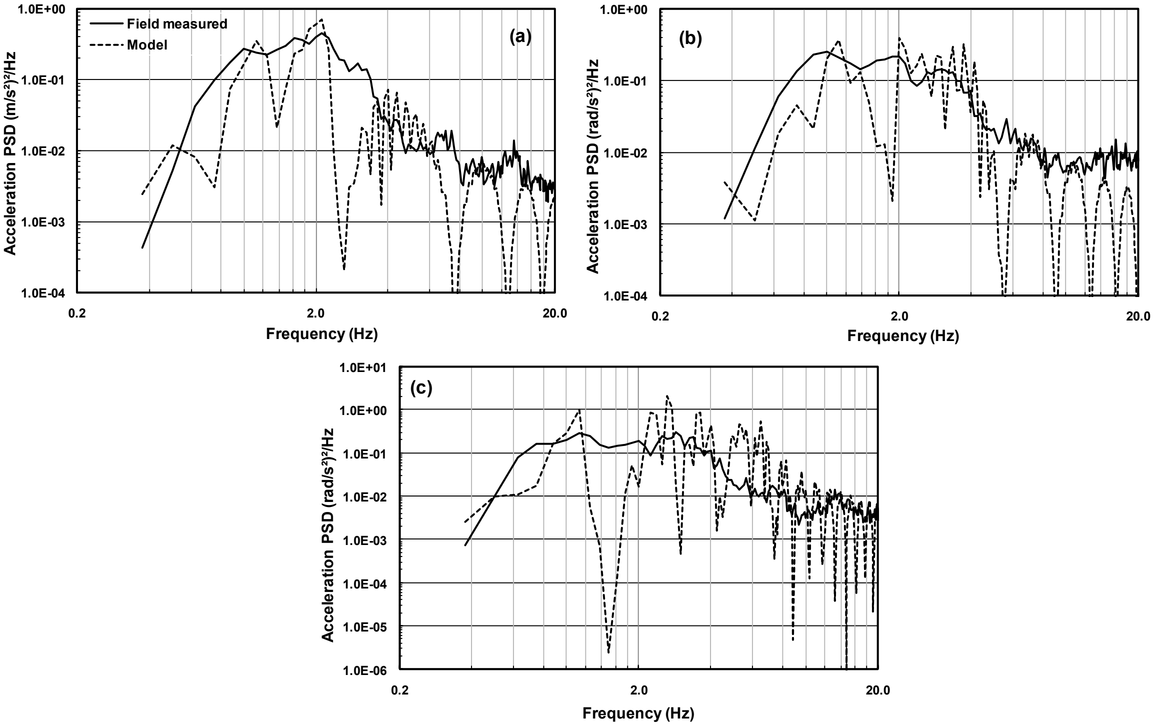

Figure 2.9: Comparisons of acceleration PSD responses of the suspended vehicle model with those of the measured data: (a) vertical; (b) pitch; and (c) roll.

The ride dynamic responses of the model were further evaluated in terms of unweighted and frequency-weighted vertical, roll and pitch rms accelerations. The computed values of the rms accelerations are compared with those derived from the measured data of the suspended vehicle corresponding to the unloaded condition in Table 2.4. The results presented in Table 2.4 suggest good correlations between the frequency-weighted acceleration values of the model and the measured data in the pitch and roll axes. Considerable discrepancy, however, is observed in the vertical acceleration values. Higher vertical acceleration response of the model at frequencies above 3 *Hz* (Fig. 2.9), where the magnitude of W_k-weighting is relatively larger, contributed to higher frequency-weighted rms value. This is evident from relatively smaller difference in the unweighted vertical acceleration values. The results also illustrate considerably higher values of the unweighted roll and pitch accelerations compared to the weighted values. This is mostly attributed to the properties of the W_e-weighting. Considering the promising potentials of the suspension concept, further efforts would be desirable to formulate a more reliable model so as to derive an optimal suspension design for different classes of off-road vehicles.

Table 2.4: Comparisons of weighted and unweighted rms accelerations of the suspended vehicle model with the corresponding measured values.

Axis	Unweighted rms accelerations			Frequency-weighted rms accelerations		
	Model	Measured	%Deviation	Model	Measured	%Deviation
z	1.28	1.00	28.0	0.98	0.62	58.0
θ	0.77	0.82	-6.1	0.41	0.43	-3.2
ϕ	1.01	0.87	14.5	0.49	0.44	10.6

2.9.2 Sensitivity analysis and optimization of the torsio-elastic suspension design

Ride performance potentials of the proposed toriso-elastic suspension would be dependent on a number of vehicle design and operating parameters. The stiffness properties and geometry of the torsio-elastic suspension would also affect the load carrying capacity of the suspension. The potential performance benefits of the torsio-elastic suspension are thus further explored through a sensitivity analysis of the ride responses to variations in suspension parameters, namely the linkage length L_0, and stiffness (k_y, k_z, k_t) and damping (c_y, c_z, c_t) properties of the torsio-elastic suspension, while assuming constant forward speed of 5 *km/h* and unloaded condition. The results attained are used to formulate an optimization problem in an attempt to seek an optimal design of the proposed torsio-elastic suspension. Each parameter was varied by ±50% about the nominal value, and the responses were obtained in terms of unweighted and frequency-weighted vertical, pitch and roll rms accelerations. The results revealed nearly negligible effect of the linkage length on the acceleration responses. The influences of variations in stiffness and damping parameters alone on the rms values are thus presented in Table 2.5.

Table 2.5: Influences of variations in torsio-elastic suspension stiffness and damping properties on the weighted and unweighted rms acceleration responses of the model.

Parameters		Unweighted rms acceleration			Weighted rms acceleration		
		z	θ	ϕ	z	θ	ϕ
Nominal value		**1.28**	**0.77**	**1.71**	**0.98**	**0.41**	**0.49**
k_z	-50%	1.21	0.67	1.72	0.95	0.34	0.49
	+50%	1.40	0.88	1.70	1.05	0.48	0.49
k_y	-50%	1.28	0.77	1.69	0.98	0.41	0.48
	+50%	1.28	0.77	1.73	0.98	0.41	0.49
k_t	-50%	1.28	0.77	1.76	0.98	0.41	0.50
	+50%	1.28	0.77	1.65	0.98	0.41	0.46
c_z	-50%	1.36	0.89	1.71	0.99	0.52	0.49
	+50%	1.26	0.72	1.71	0.98	0.37	0.49
c_y	-50%	1.28	0.77	1.73	0.98	0.41	0.50
	+50%	1.28	0.77	1.70	0.98	0.41	0.48
c_t	-50%	1.28	0.77	1.74	0.98	0.41	0.50
	+50%	1.28	0.77	1.68	0.98	0.41	0.48

The results show that both the frequency-weighted and unweighted vertical and pitch rms accelerations are strongly affected by the suspension vertical stiffness. An increase in the pitch and vertical mode resonance frequencies caused by higher vertical stiffness as well as coupling between vertical and pitch modes resulted in higher frequency-weighted and unweighted vertical and pitch accelerations. Variations in the vertical stiffness, however, do not influence the W_e-weighted and unweighted roll accelerations, suggesting that vertical and roll modes of the vehicle are mostly decoupled. While the lateral stiffness variations yield only slight effect on the W_e-weighted roll acceleration, a lower value of torsional stiffness yields higher values of unweighted and W_e-weighted roll acceleration magnitudes. This influence is greater for the unweighted roll response and is most likely caused by the properties of the W_e-weighting. The roll response is mostly affected by the torsional stiffness coefficient, while the effect of lateral stiffness is very small. While light damping of the torsio-elastic members may not yield important influences on the ride vibration responses, both the weighted and unweighted vertical and pitch accelerations tend to increase with lower vertical damping of the torsio-elastic member. A decrease in c_y and c_t results in slightly higher roll rms acceleration values. The results suggest that a suspension design with lower vertical and lateral stiffness, and higher torsional stiffness would yield lower overall weighted and unweighted rms acceleration magnitudes. Higher values of vertical damping coefficients would also be desirable, while the effects of c_y and c_t are relatively small.

2.9.3 Optimization variables and objective functions

A design optimization is undertaken to seek optimal torsio-elastic suspension parameters using the Pareto technique based on the Genetic Algorithm (GA) [216]. The W_k-weighted and unweighted rms vertical accelerations, (a_{wz}, a_z), W_e-weighted and unweighted rms pitch and roll accelerations, ($a_{w\theta}$, a_θ) and ($a_{w\phi}$, a_ϕ), are selected as the objective functions to be minimized. The results attained from the sensitivity analysis revealed that the rms acceleration responses are mostly influenced by the vertical, lateral and torsional stiffness, and the vertical damping coefficients. Two objective functions are thus formulated to seek minimal weighted and unweighted rms accelerations, respectively, with parameter design vector $X = \{ k_y, k_z, k_t, c_z \}$, such that:

$$F_w(X) = K_1 a_{wz}(X) + K_2 a_{w\theta}(X) + K_3 a_{w\varphi}(X)$$
$$F(X) = K_1 a_z(X) + K_2 a_\theta(X) + K_3 a_\varphi(X) \tag{2.20}$$

where $F_w(X)$ and $F(X)$ are the weighted and unweighted rms acceleration functions, and K_1, K_2 and K_3 are the weighting factors such that $\sum_{i=1}^{3} K_i = 1$. The minimization function $F_w(X)$ also accounts for the human sensitivity to vibration as reflected by the weighting functions. The solutions of the above minimization functions for vehicle suspensions generally converge towards lower stiffness values, which may tend to result in reduced load carrying capacity and roll stability limits, and greater relative deflections of the sprung mass with respect to the unsprung masses. Although the kinematic effect of the proposed suspension is expected to inhibit the relative deflection, limit constraints are introduced in order to seek solutions within practical ranges, such that:

$30 \leq k_y \leq 300$ *kN/m*; $70 \leq k_z \leq 300$ *kN/m*; $50 \leq k_t \leq 250$ *kNm/rad*; and $3 \leq c_z \leq 9$ *kN.s/m.*

The solutions of the minimization problems were obtained in terms of sets of Pareto optimal solutions. As an example, Fig. 2.10 illustrates the various Pareto optimal solutions in terms of the weighted acceleration values. The optimal solutions in weighted vertical, roll, and pitch accelerations suggest a positive correlation between $a_{w\theta}$ and a_{wz} attributed to greater coupling between the vertical and pitch modes. Fig. 2.10(a), however, suggests a weaker coupling between roll and vertical accelerations, while the coupling between roll and pitch responses is negligible, as seen in Fig. 2.10(c). Similar trends in optimal Pareto solutions were also observed for the unweighted rms accelerations. These solutions were subsequently explored to identify a design compromise that would yield minimal values of the multi-objective functions, defined in Eq. (2.20), using different combinations of the weighing factors. The results revealed nearly negligible effect of the roll acceleration weighting (K_3), as expected due to its relatively lower coupling with the vertical and pitch responses. The optimal solution and the corresponding design parameters were thus identified by placing greater weighting for a_{wz} ($K_1=0.5$ to 0.7) and $a_{w\theta}$ ($K_2=0.2$ to 0.4). The combination ($K_1=0.6,\ K_2=0.3,\ K_3=0.1$) resulted in minimal values of the vertical, pitch and roll acceleration responses, which resulted in the follows optimal design vectors:

$X=\{k_y, k_z, k_t, c_z\}=\{91.8, 71.3, 204.8, 8.3\}$; for the weighted function.

$X=\{k_y, k_z, k_t, c_z\}=\{36.4, 73.3, 187.5, 6.3\}$; for the unweighted function.

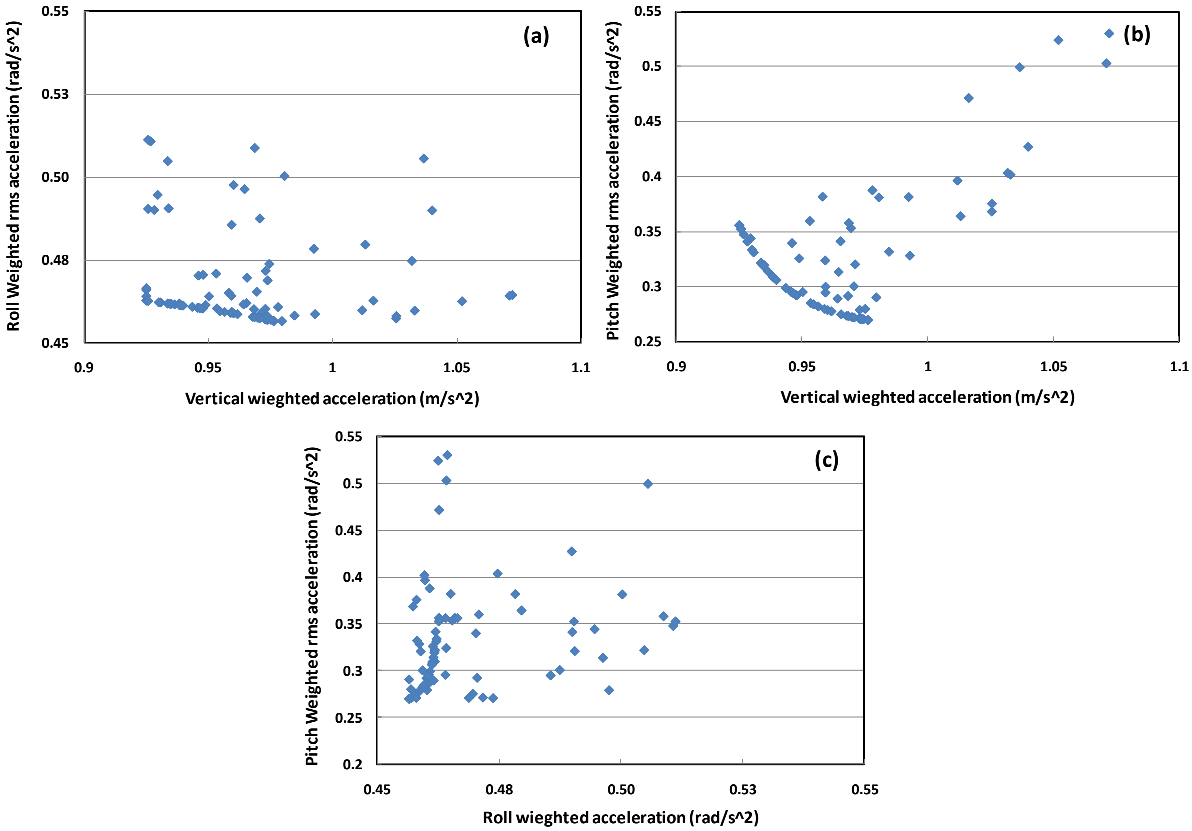

Figure 2.10: Pareto optimal solutions for weighted accelerations responses: (a) roll *vs* vertical acceleration; (b) pitch *vs* vertical acceleration; (c) pitch *vs* roll acceleration.

The above results show comparable values of the suspension parameters for both the minimization functions, except for the values of k_y. The minimization of weighted function converged towards a considerable greater value of k_y compared to that for the unweighted function. The minimization of the weighted values in roll tends to converge towards a higher value of k_y in order to achieve roll mode frequency well above the dominant frequency range of the W_e-filter (1-2 *Hz*). The resulting optimal solutions in terms of both the weighted and unweighted rms accelerations and the design parameters are summarized in Table 2.6.

Table 2.6: Optimal values of the acceleration responses.

Axis	Unweighted rms acceleration (m/s^2)			Weighted rms acceleration (m/s^2)		
	Nominal	optimal	% change	Nominal	optimal	% change
z	1.28	1.21	-5.46	0.98	0.93	-5.10
θ	0.77	0.62	-19.48	0.41	0.32	-21.95
ϕ	1.71	1.65	-3.51	0.49	0.46	-6.12

The results in Table 2.6 show that the optimal suspension design yields considerably lower values of $a_{w\theta}$ and a_θ compared to those of the model with nominal parameters, while the reductions in vertical (a_{wz}, a_z) and roll ($a_{w\phi}$, a_ϕ) acceleration values are relatively small, ranging from roughly 3.5 to 6%. The relative deflection responses of the sprung mass with respect to the rear axle were further evaluated to study the effects of optimal parameters on the vertical and roll deflections. The results revealed relatively higher relative deflections of the optimal suspension compared to the nominal suspension parameters, although the increases were considered could be small. The rms vertical relative deflection of the model with optimal suspension was 4.8 *cm* compared to 4.0 *cm* for the nominal suspension model.

2.10 Conclusions

The ride performance potentials of a novel torsio-elastic suspension were investigated for a forestry vehicle through field assessments and simulations of a ride dynamic model. The results attained from the field measurements revealed significant benefits of the rear axle torsio-elastic suspension in reducing the operator vibration exposure. In the loaded case, the suspended vehicle resulted in 35%, 43% and 57% reductions in the frequency-weighted rms accelerations along the *x*-, *y*- and *z*-axis, respectively, compared to the unsuspended vehicle. The suspended vehicle, however, revealed slightly higher unweighted pitch and roll rms accelerations, when unloaded, while the unweighted rms accelerations along the *x*-, *y*- and *z*-axis were 44%, 27% and 45% lower, respectively, compared to those of the unsuspended vehicle. The results further showed that the magnitudes of horizontal vibration transmitted to the operator's station were either comparable to or exceeded the vertical vibration magnitude. While the ride model responses agreed reasonably well with the measured responses in vertical, roll and pitch axes, the model could not be applied to predict fore-aft and lateral ride responses due to various simplifying assumptions, namely constant forward speed, negligible contributions due to articulation forces and moments, and lack of tire-terrain interaction in the shear axes.

The results obtained from sensitivity suggested that a suspension design with lower vertical and lateral stiffness but higher torsional stiffness would yield lower overall unweighted and weighted rms acceleration magnitudes. The results also suggested strong coupling between vertical and pitch mode responses, but negligible coupling between the pitch and roll modes of the vehicle. The optimal suspension parameters identified from solutions of a multi-objective minimization problem resulted in further considerable reductions in the pitch rms accelerations in the order of 20%, with only 3.5 to 6% reductions in vertical and roll accelerations. Considering the notable performance benefits of the proposed suspension, it would be desirable to develop more reliable ride and handling dynamic models of the vehicle, which could serve as a vital tool for suspension design and assessments of the ride vibration and handling/roll dynamics of a broader class of off-road vehicles.

APPENDIX 2-A: TIRE AND SUSPENSION FORCES AND MOMENTS

The vertical (F_{Ti}) and lateral (F_{TYi}) tire forces developed at the tire-road interface (F_{Ti} and F_{TYi}) are derived from the following, where $i=1,\ 2$ denote the front axle tires, and $i=3,\ 4$ refer to the rear axle tires.

$$\begin{aligned} F_{Ti} &= K_{Ti}\left[z_s + (-1)^{i+1}T\varphi_s - WB_1\theta_s - z_{0i}\right] + C_{Ti}\left[\dot{z}_s + (-1)^{i+1}T\dot{\varphi}_s - WB_1\dot{\theta}_s - \dot{z}_{0i}\right] \quad i = 1,2 \\ F_{Ti} &= K_{Ti}\left[z_{ur} + (-1)^{i+1}T\varphi_{ur} - z_{0i}\right] + C_{Ti}\left[\dot{z}_{ur} + (-1)^{i+1}T\dot{\varphi}_{ur} - \dot{z}_{0i}\right] \quad i = 3,4 \end{aligned} \tag{2-A.1}$$

$$\begin{aligned} F_{TYi} &= K_{TY\,i}[y_s - (h + h_1 + R)\phi_s] + C_{TY\,i}[\dot{y}_s - (h + h_1 + R)\dot{\phi}_s] \quad i = 1, 2 \\ F_{TYi} &= K_{TY\,i}[y_{ur} - R\phi_{ur}] + C_{TY\,i}[\dot{y}_{ur} - R\dot{\phi}_{ur}] \quad i = 3, 4 \end{aligned} \tag{2-A.2}$$

where K_{Ti} and K_{TYi} are the linear vertical and lateral stiffness and C_{Ti} and C_{TYi} are the linear vertical and lateral damping coefficients of tire i, respectively.

The vertical forces developed by the torsio elastic suspension acting on the sprung mass (F_{z3} and F_{z4}) and on the unsprung mass (F_{z3u} and F_{z4u}) are given by:

$$\begin{aligned} F_{z3} &= k_z[z_s - \left(z_3 - \frac{L_0}{2}\phi_3\right) + L_1\phi_s + WB_2\theta_s] + c_z[\dot{z}_s - \left(\dot{z}_3 - \frac{L_0}{2}\dot{\phi}_3\right) + L_1\dot{\phi}_s + WB_2\dot{\theta}_s] \\ F_{z4} &= k_z[z_s - \left(z_4 + \frac{L_0}{2}\phi_4\right) - L_1\phi_s + WB_2\theta_s] + c_z[\dot{z}_s - \left(\dot{z}_4 + \frac{L_0}{2}\dot{\phi}_4\right) - L_1\dot{\phi}_s + WB_2\dot{\theta}_s] \end{aligned} \tag{2-A.3}$$

$$\begin{aligned} F_{z3u} &= k_z[z_3 + \frac{L_0}{2}\phi_3 - z_{ur} - (L_1 + L_0)\phi_{ur}] + c_z[\dot{z}_3 + \frac{L_0}{2}\dot{\phi}_3 - \dot{z}_{ur} - (L_1 + L_0)\dot{\phi}_{ur}] \\ F_{z4u} &= k_z[z_4 - \frac{L_0}{2}\phi_4 - z_{ur} + (L_1 + L_0)\phi_{ur}] + c_z[\dot{z}_4 - \frac{L_0}{2}\dot{\phi}_4 - \dot{z}_{ur} + (L_1 + L_0)\dot{\phi}_{ur}] \end{aligned} \tag{2-A.4}$$

where k_z and c_z are the vertical stiffness and damping coefficients of the torsio-elastic suspension. The lateral forces developed by the torsio-elastic suspension acting on the sprung mass (F_{y3} and F_{y4}) and the unsprung mass (F_{y3u} and F_{y4u}) are given by:

$$\begin{aligned} F_{y3} &= k_y[y_s - h\phi_s - y_3] + c_y[\dot{y}_s - h\dot{\phi}_s - \dot{y}_3] \\ F_{y4} &= k_y[y_s - h\phi_s - y_4] + c_y[\dot{y}_s - h\dot{\phi}_s - \dot{y}_4] \end{aligned} \tag{2-A.5}$$

$$\begin{aligned} F_{y3u} &= k_y[y_3 - h_1\phi_{ur} - y_{ur}] + c_y[\dot{y}_3 - h_1\dot{\phi}_{ur} - \dot{y}_{ur}] \\ F_{y4u} &= k_y[y_4 - h_1\phi_{ur} - y_{ur}] + c_y[\dot{y}_4 - h_1\dot{\phi}_{ur} - \dot{y}_{ur}] \end{aligned} \tag{2-A.6}$$

where k_y and c_y are the lateral stiffness and damping coefficients of the torsio-elastic suspension. The roll moments developed by the torsio-elastic suspension acting on the sprung mass ($M_{\theta 3s}$ and $M_{\theta 4s}$) and the unsprung mass ($M_{\theta 3u}$ and $M_{\theta 4u}$) are defined from:

$$\begin{aligned} M_{\theta 3s} &= k_t(\phi_s - \phi_3) + c_t(\dot{\phi}_s - \dot{\phi}_3) \\ M_{\theta 4s} &= k_t(\phi_s - \phi_4) + c_t(\dot{\phi}_s - \dot{\phi}_4) \end{aligned} \tag{2-A.7}$$

$$\begin{aligned} M_{\theta 3u} &= k_t(\phi_3 - \phi_{ur}) + c_t(\dot{\phi}_3 - \dot{\phi}_{ur}) \\ M_{\theta 4u} &= k_t(\phi_4 - \phi_{ur}) + c_t(\dot{\phi}_4 - \dot{\phi}_{ur}) \end{aligned} \tag{2-A.8}$$

where k_t and c_t are the torsional stiffness and damping coefficients of the torsio-elastic suspension, respectively.

CHAPTER 3

MODELING AND VALIDATION OF OFF-ROAD VEHICLE RIDE DYNAMICS

3.1 Introduction

Ride dynamics of ground vehicles has been extensively explored in the last few decades, where the fundamentals of vehicle ride vibrations along with various types of suspension systems have been well developed [152,217-219]. In parallel, the understanding of human body vibrations and human perception of vehicle vibrations has also been considerably improved, contributing the further enhancement in vehicle ride vibration isolations and driver/passengers comfort and health [3,220,221]. However, the documented literature suggested a large majority of these efforts made on the road vehicle ride dynamics and suspension systems, while only small efforts have been devoted to those of the off-road vehicles. This may be attributed mainly to two factors: (a) It has generally been accepted that the knowledge and suspension systems developed for road vehicles can be adapted to off-road vehicles with moderate modifications; and (b) the significant difficulty in characterizing/modeling tire-terrain interactions (for either deformable or undeformable terrains).

Unlike road vehicles, off-road vehicles are known to transmit higher magnitudes of low frequency whole-body vibration (WBV) along the translational as well as rotational axes to the drivers, which can be attributed to vehicle interactions with uneven off-road terrains, and lack of adequate primary and/or secondary suspensions. A number of epidemiological studies have shown that prolonged occupational exposure to such WBV is directly associated with various health and safety risks among the vehicle drivers [5,6].

It has been reported in different field-based studies, e.g. [1,2], that WBV exposure of many off-road vehicles may exceed the health-caution guidance zone and the exposure limit defined in ISO-2631-1 [3] and EN14253 [4], respectively.

The field-based studies together with the guidelines are vital for estimating risk of musculoskeletal disorders among the occupational drivers but provide only limited data for designs of preventive measures involving primary and secondary suspension, tires and operating conditions. It has been shown that the WBV environment of off-road vehicles strongly depends upon a number of design and operating factors such as vehicle weight and dimensions, vehicle load, task, primary and secondary suspension systems, terrain roughness and driving speed [11,152,222]. Tiemessen et al. [11] evaluated the effectiveness of evidence-based preventive strategies to reduce WBV exposure using 37 different field and laboratory studies, and concluded that the dynamic characteristics of the vehicle need to be considered for design of effective strategies, apart from the driver skill and behavior. Rehn et al. [222] studied the variations in WBV exposure of 11 drivers of 7 forwarders operating on 10 different terrains in terms of vibration dose value (VDV), and showed that VDV was strongly dependent upon forwarder model, terrain type, operating load and the driver.

The most popular preventive measure of WBV exposure reduction has been the suspension at the seat, which limits only vertical vibration [8-10]. A suspension seat, however, yields limited isolation of high intensity vertical vibration encountered in many off-road vehicles, which may in-part be attributed to lack of suspension tuning with regard to the intensity and frequency contents of the target vehicle vibration [10]. A number of studies have also explored different cab suspension designs [13,14]. These suspensions, however, are not effective in limiting the transmission of fore-aft and lateral vibration, whose magnitudes are known to be either comparable to or exceed that of the vertical vibration [1,15]. In addition, performance of secondary suspensions, generally derived from subsystem models of the seat and cab suspensions [9,10,13-15], may be also limited due to lack of consideration of dynamics of the target vehicle [11]. Although axle suspensions offer greater potential to reduce translational as well as rotational vibrations, relatively fewer studies have attempted design and performance analyses of such suspensions, where the enhancements in ride have been clearly demonstrated [17-19,21,22,97]. This may in-part be attributed to design challenges associated with conflicting requirements posed by the ride and roll stability measures, and wide variations in the axle loads. Anti-roll suspension concepts with a ride-height leveling function, such as interconnected hydro-pneumatic suspensions [23,39,152], would offer a very promising alternative solution for off-road vehicle applications.

Similar to those in analyses of the road vehicle ride dynamics and suspension designs, the reported off-road vehicle ride dynamics models used for suspension designs, generally, employ either linear or nonlinear point-contact tire models that are known to be computationally efficient. Such tire models, however, cannot capture the tire-terrain interaction properties in the shear axes and thus the fore-aft and lateral ride vibration responses [22]. Furthermore, the point-contact tire models tend to overestimate contact pressure and wheel hop [223]. The study [22] demonstrated that using one-dimensional point-contact tire model would also overestimate the vertical acceleration responses. In addition, coupling of the pitch and roll modes with longitudinal and lateral dynamics, respectively, cannot be reasonably represented. Considering that off-road vehicles exhibit substantial lateral and longitudinal vibrations attributed to coupled vehicle vibration modes and horizontal tire-road interactions, it is essential to develop and integrate more efficient tire models capable of predicting multi-axis tire forces.

Although comprehensive finite element tire models have been widely reported for characterizing multi-axis tire-terrain interactions [122], such models could find only limited applications in ride dynamic analysis of vehicles due to associated complexities and high computational demands. Crolla et al. [224] proposed a three-dimensional point-contact tire model to account for horizontal and vertical tire forces in an off-road tractor model in a highly efficient manner. The model, however, does not account for the finite tire foot print and the contributions due to local gradient of the terrain, and the wheel-hop. Tire models with radial visco-elastic elements and adaptive contact patch have also been employed to determine the tire-terrain forces along the vertical and longitudinal axis [116,225].

In this chapter (paper), a comprehensive off-road ride dynamics model is derived with integrating a three-dimensional tire model, which can be conveniently used for evaluating suspension design concepts. The three-dimensional tire-terrain interaction model is formulated based on the adaptive radial representation of the tires in the pitch plane together with a lateral dynamic model based on the side-slip theory and the tire-lag. The ride dynamic responses of the model are evaluated under excitations representing an equivalent undeformable forestry terrain, and compared with the field measured data to demonstrate the model validity. The ride responses are obtained for the vehicle model with and without a rear-axle suspension to further illustrate the ride performance potentials of the torsio-elastic suspension.

3.2 Modeling of Tire-Terrain Interactions

The tire-terrain interactions along the three translational axes are characterized through formulation of a three-dimensional tire model considering undeformable terrain. The proposed model integrates an adaptive footprint tire model for describing the vertical and longitudinal forces developed by the tire, and a visco-elastic lateral model based on the side-slip theory.

3.2.1 Adaptive footprint tire model in the pitch-plane

Figure 3.1 illustrates an adaptive footprint model based on the concept of continuous radial spring representation of the tire [226], which permits computation of the net contact patch, P_1P_2, in the pitch plane and the resulting tire forces along the vertical and longitudinal axis. The resultant force developed at the tire-terrain interface is evaluated by considering the tire as a continuous ring of radial springs uniformly distributed over contact patch, P_1P_2, which varies with the local terrain profile. The dissipative property of the tire is represented by a lumped viscous damper, as shown in the Figure. Assuming that the tire-terrain contact (P_1P_2) represents the idealized deflection of the tire, the resultant force F_{wn}, assumed to act normal to the footprint, is obtained through integration of the normal components of the elemental radial forces over the footprint [225], such that:

$$F_{wn} = 2KR_w[\sin\alpha_w - \alpha_w \cos\alpha_w] + F_{dw} \tag{3.1}$$

where K is the linear stiffness constant of the radial element, R_w is undeformed tire radius and where α_w is one-half of the wheel-terrain contact patch angle, as shown in Fig. 3.2(a). $F_{dw} = C\dot{r}_w$ is the tire damping force, where C is the viscous damping coefficient and $\dot{r}_w$ is the relative velocity across the damping element which relates to the vertical motion of the wheel centre, the terrain elevation at the center of the contact patch, and the gradient of the terrain profile, such that:

$$\dot{r}_w = (\dot{z}_{wc} - \dot{z}_0)cos\,\gamma \tag{3.2}$$

where $\dot{z}_{wc}$ is the vertical velocity of the wheel center, $\dot{z}_0 = U \tan\gamma$, is the terrain imposed vertical velocity at the mid-point of the idealized tire-terrain contact patch P_1P_2, γ is the gradient of the instantaneous contact patch, and U is the constant forward speed.

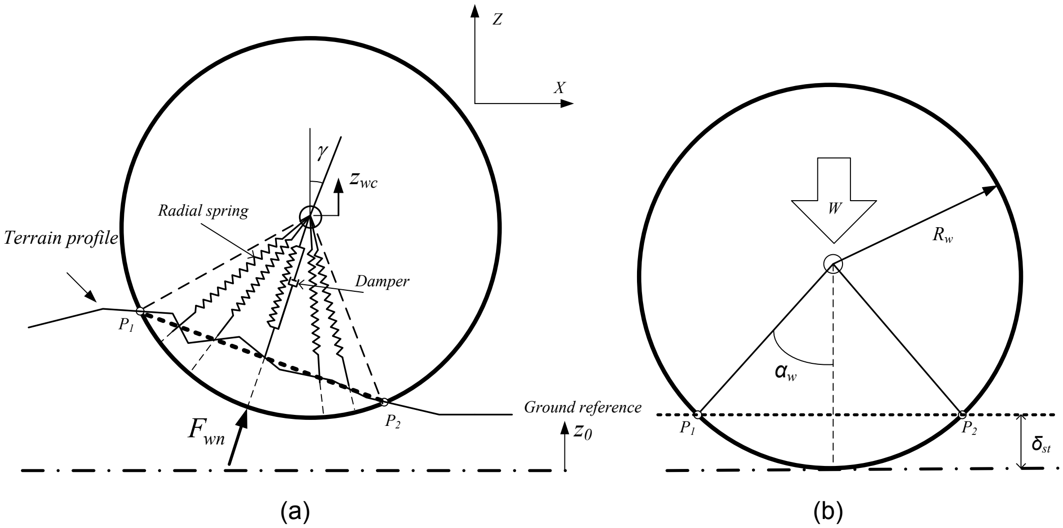

Figure 3.1: Adaptive foot-print radial tire model.

The radial spring constant of the tire is estimated from Eq. (3.1) and the static tire deflection δ_{st} subject to a static load, *W,* on a flat surface, as shown in Fig. 3.1(b), such that:

$$K = \frac{W}{2R_w[\sin\alpha_w - \alpha_{ws}\cos\alpha_w]} \tag{3.3}$$

The determination of the resultant tire force from Eq. (3.1) necessitates the instantaneous contact patch angle $2\alpha_w$ and thus the instantaneous patch length P_1P_2. The coordinates of P_1 and P_2 are derived from the circle-line interaction representation [226], shown in Fig. 3.2 (b). The algorithm initially identifies all the terrain elevation points P_s that lie within the projection of the wheel on the terrain surface, $X_{wc}-R_w \leq X_{Ps} \leq X_{wc}+R_w$, where X_{Ps} are the x-coordinates of the identified terrain points, and X_{wc} is x-coordinate of the wheel center. The elevation points within the wheel geometry are subsequently identified using the criteria: $(Z_{wc}-Z_{Ps})^2+(X_{wc}-X_{Ps})^2<R_w^2$ where Z_{wc} and Z_{Ps} are the vertical coordinates of the wheel center and terrain contact point, respectively. The coordinates of the two extreme elevation points, P_L and P_R, within the wheel geometry together with those of the preceding (P_{L-1}) and following (P_{R+1}) points are used to define the equations of the lines intersecting the tire ring at P_1 and P_2, respectively, as shown in Fig. 3.2(b). The coordinates of the intersection points, (X_1, Z_1) and (X_2, Z_2), are finally determined from the equations of the two lines and that of the tire ring, given by:

$$(X_{wc}-X)^2+(Z_{wc}-Z)^2=R_w^2$$

The instantaneous contact patch angle α_w can be derived from the angular coordinates θ_1 and θ_2 of the intersection points P_1 and P_2, respectively, as seen in Fig. 3.2(a), such that $2\alpha_w=\theta_2-\theta_1$. Using the circle-line interaction method, these can be expressed as:

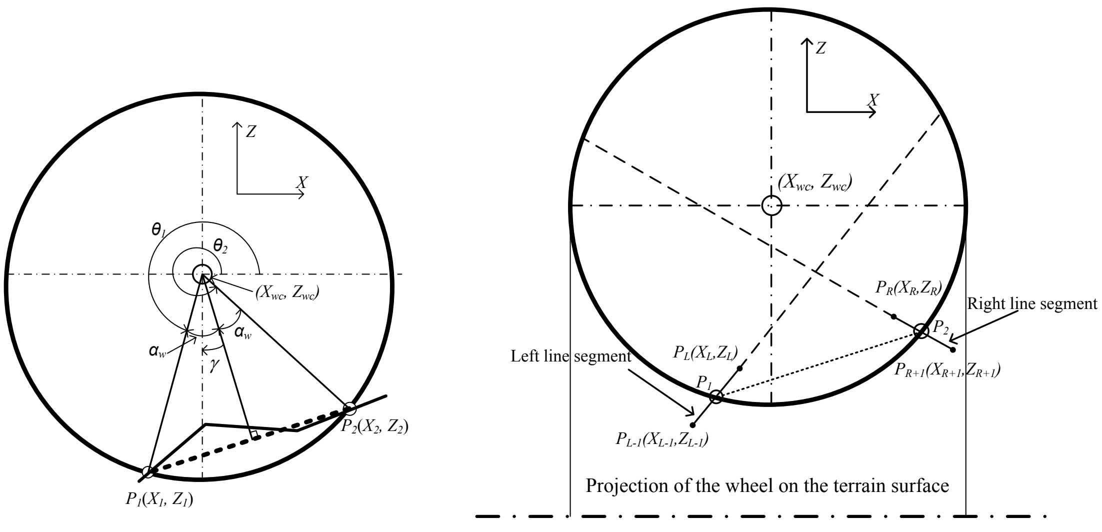

(a) (b)

Figure 3.2: (a) Wheel-terrain contact patch; and (b) Circle-line interaction representation.

$$\theta_1 = \tan^{-1}\left[\frac{Z_1 - Z_{wc}}{X_1 - X_{wc}}\right]; \quad \theta_2 = \tan^{-1}\left[\frac{Z_2 - Z_{wc}}{X_2 - X_{wc}}\right] \tag{3.4}$$

Furthermore, the gradient of the instantaneous contact patch can be computed from: $\gamma = \theta_1 + \alpha_w - 1.5\pi$. The vertical and longitudinal forces developed by the tire can be derived from Eq. (3.1) using the instantaneous contact patch angle and gradient of the idealized contact patch, such that:

$$F_{Tz} = F_{wn}\cos\gamma; \quad F_{Tx} = F_{wn}\sin\gamma \tag{3.5}$$

where F_{Tx} and F_{Tz} are the resultant longitudinal and vertical tire forces, respectively.

3.2.2 Lateral tire force

A lateral tire force model [224] based on the side-slip theory could be applied to account for contributions of the lateral tire-terrain interaction to the ride dynamics of off-road vehicles. The lateral tire force model may be integrated with the adaptive footprint tire model in order to describe the tire-terrain interactions along the three translational axes. Furthermore, the large and soft tires, popularly employed in off-road vehicles, exhibit considerable hysteresis and appreciable time lag associated with buildup of lateral force. It has been further shown that the lateral force developed by a tire can be derived considering first-order tire dynamics, where the time constant directly relates to the relaxation length σ and the forward speed U [118]. Assuming small slip angle and a constant vertical load, the tire lateral force can be related to the side-slip angle α and tire cornering stiffness C_α in the following manner:

$$\tau\dot{F}_y(t) + F_y(t) = C_\alpha\alpha(t) \tag{3.6}$$

where the time constant $\tau = \sigma/U$, $F_y(t)$ is the lateral force developed by the tire and $C_\alpha \alpha(t)$ is the steady-state lateral force developed by the tire. The reported lateral tire force model is integrated with the pitch-plane adaptive foot-print model, as shown in Fig. 3.3, to derive the tire forces along the three translational axes. In the absence of the external input ($u_y=0$), the tire lateral force can be related to the stiffness and damping coefficients in the following manner:

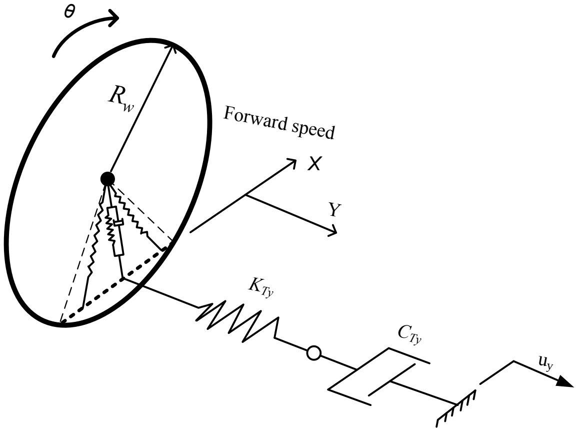

Figure 3.3 Tire lateral ride dynamic model consisting of linear spring and damper in series.

$$\frac{C_{Ty}}{K_{Ty}}\dot{F}_y(t) + F_y(t) = C_{Ty}\dot{y}(t) \tag{3.7}$$

where C_{Ty} and K_{Ty} are damping and stiffness coefficients of the model, which are related to cornering stiffness and relaxation length of the tire, such that: $C_{Ty} = C_\alpha/U$ and $K_{Ty} = C_\alpha/\sigma$, and $\dot{y}(t) = U\alpha(t)$ is the lateral velocity developed at the tire-terrain contact.

3.3 Ride Dynamics Modeling of Off-Road Vehicles

3.3.1 Unsuspended off-road vehicles

Assuming negligible contributions of the articulation mechanism to the vehicle responses, a 5 degree-of-freedom (DOF) ride dynamic model of an un-suspended off-road skidder is developed, which is an extension of the pitch-plane model presented in [22]. Figures 3.4(a) and 3.4(b) illustrate the model in the pitch and roll-planes, respectively. The forward speed is assumed to be constant, the axles are considered to be rigidly attached to the vehicle frame, and axles, frame and the cabin are considered as a rigid mass supported on four tires. The tire forces are derived using the adaptive foot-print and lateral force tire model described above. The equations of motion for the vehicle model are derived considering differential terrain excitations at the two tire tracks:

$$
\begin{aligned}
& m_s\ddot{z}_s + \sum_{i=1}^{4} F_{Tzi} = 0; \qquad m_s\ddot{x}_s + \sum_{i=1}^{4} F_{Txi} = 0; \qquad m_s\ddot{y}_s + \sum_{i=1}^{4} F_{Tyi} = 0; \\
& I_{YYS}\ddot{\theta}_s - WB_1[F_{Tz1} + F_{Tz2}] + WB_2[F_{Tz3} + F_{Tz4}] - H(\textstyle\sum_{i=1}^{4} F_{Txi}) = 0; \\
& I_{XXS}\ddot{\phi}_s - T[F_{Tz1} + F_{Tz3}] + T[F_{Tz2} + F_{Tz4}] + H(\textstyle\sum_{i=1}^{4} F_{Tyi}) = 0;
\end{aligned}
\tag{3.8}
$$

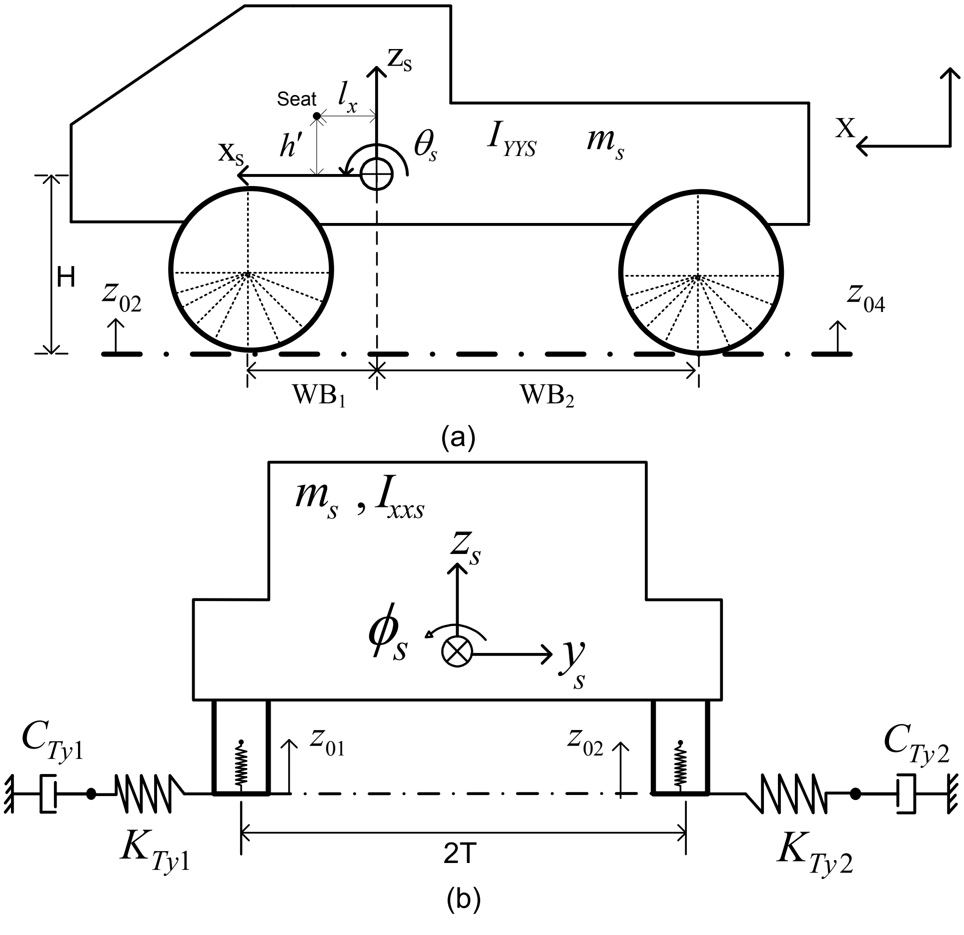

Figure 3.4: Pitch- and roll-plane representations of an unsuspended skidder: (a) Pitch-plane; and (b) Roll-plane, (front view)

where z_s, x_s, y_s, θ_s, and ϕ_s are the vertical, longitudinal, lateral, pitch and roll deflections, respectively, of the sprung mass m_s about its static equilibrium. I_{XXS} and I_{YYS} are roll and pitch mass moments of inertia of the sprung mass, respectively. The vertical (F_{Tzi}), lateral (F_{Tyi}) and longitudinal (F_{Txi}) tire forces developed by tire i (i=1, 2 for front axle tires and i=3, 4 for the rear axle tires), are derived from the tire models expressed in Eqs. (3.5) and (3.7). The lateral force (F_{Tyi}) where lateral velocity $\dot{y}_i(t)$ of the contact point is given by $\dot{y}_i(t) = \dot{y}_i + H\dot{\phi}_s$ (i=1, ..,4). WB_1, WB_2, T, and H are the geometric parameters shown in Fig. 3.4.

3.3.2 Suspended off-road vehicles with rear-axle torsio-elastic suspension

A torsio-elastic axle suspension concept has been proposed to improve the terrain-induced ride vibrations of a forestry skidder, while providing high effective roll stiffness [22]. The ride performance potential was demonstrated through field measurements and analysis of a vehicle model with a point-contact tire model. In this study, the conventional skidder retrofitted with the torsio-elastic suspension at the rear-axle is modeled considering multi-axis tire-terrain interactions, as shown in Figs. 3.5(a) and 3.5(b). The detailed linkage model is also shown in Fig. 3.5(c). The vehicle with the rear-axle suspension is modeled as a 14-DOF dynamic system, which includes: 5-DOF of the sprung mass m_s' comprising chassis, cab, front axle and the mounted equipment (x_s, y_s, z_s, ϕ_s, θ_s); 3-DOF of the real axle unsprung mass (y_{ur}, z_{ur}, ϕ_{ur}); and 3-DOF of each of the two suspension units (y_i, z_i, ϕ_i; $i=3, 4$). The equations of motion for the sprung and rear-axle unsprung masses of the vehicle subject to terrain excitations at the right- and left-tracks are formulated as:

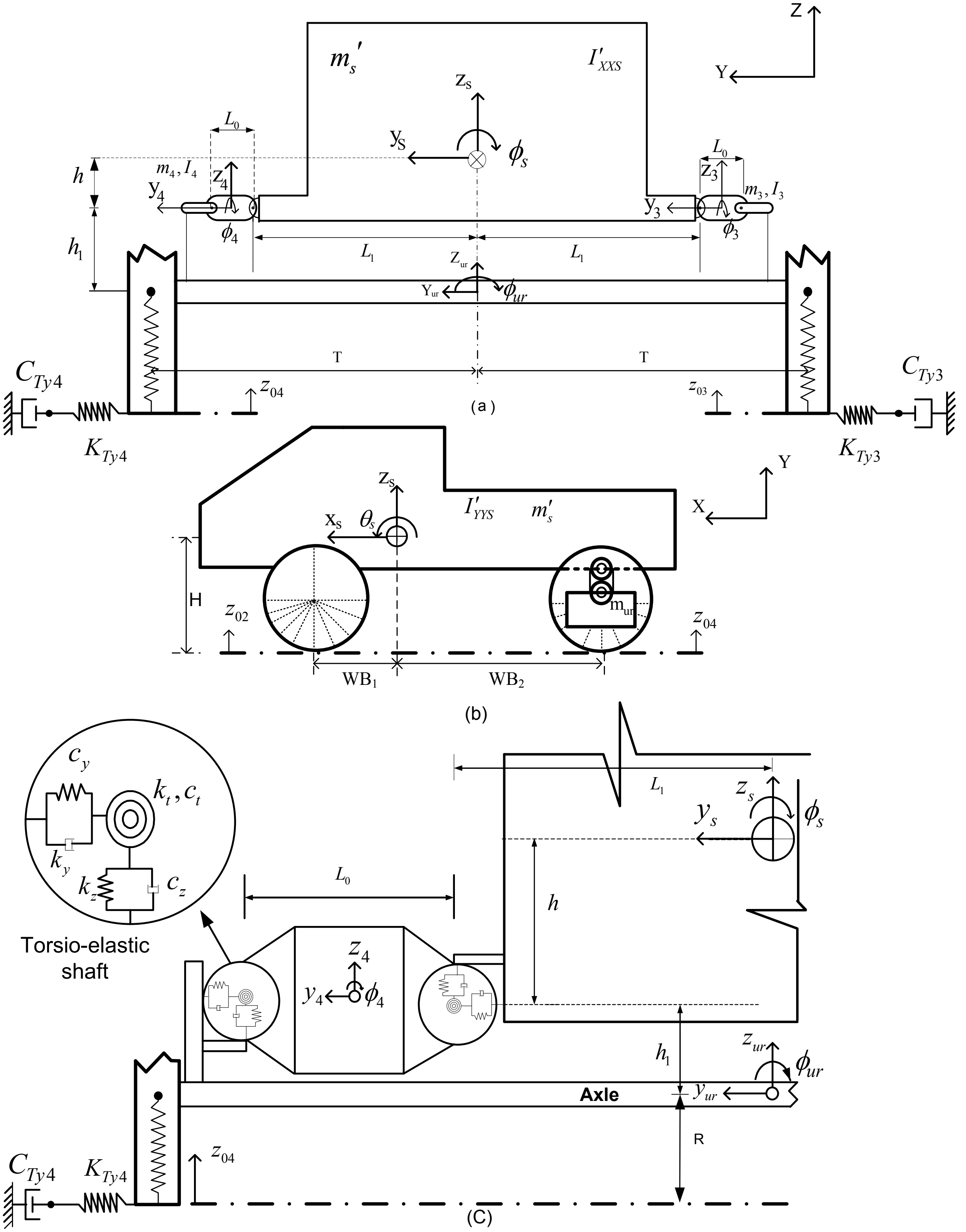

Figure 3.5: Schematic representation of the 14-DOF suspended vehicle model: (a) roll plane; (b) pitch plane; and (c) torsio-elastic suspension linkage mechanism.

$$m'_s\ddot{z}_s+\sum_{i=1}^{2}F_{Tzi}+\sum_{i=3}^{4}F_{zi}=0;\quad M\ddot{x}_s+\sum_{i=1}^{4}F_{Txi}=0;\quad m'_s\ddot{y}_s+\sum_{i=1}^{2}F_{Tyi}+\sum_{i=3}^{4}F_{yi}=0;$$

$$I'_{XXS}\ddot{\phi}_s+M_{\phi 4s}+M_{\phi 3s}+(F_{z4}-F_{z3})L_1+h\left(\sum_{i=3}^{4}F_{yi}\right)+(F_{Tz2}-F_{Tz1})T+H(\sum_{i=1}^{2}F_{Tyi})=0;$$

$$I'_{YYS}\ddot{\theta}_s+WB_2\left(\sum_{i=3}^{4}F_{zi}\right)-WB_1\left(\sum_{i=1}^{2}F_{Tzi}\right)-H\left(\sum_{i=1}^{4}F_{Txi}\right)=0; \tag{3.9}$$

$$m_{ur}\ddot{z}_{ur}+\sum_{i=3}^{4}F_{Tzi}-\sum_{i=3}^{4}F_{ziu}=0;\qquad m_{ur}\ddot{y}_s+\sum_{i=3}^{4}F_{Tyi}-\sum_{i=3}^{4}F_{yiu}=0;$$

$$I_{ur}\ddot{\phi}_{ur}-M_{\phi 3u}-M_{\phi 4u}+(F_{Tz4}-F_{Tz3})T+\sum_{i=3}^{4}(R_wF_{Tyi}+h_1F_{yiu})+(F_{z3u}-F_{z4u})(L_1+L_0)=0;$$

$$m_i\ddot{z}_i+F_{ziu}-F_{zi}=0;\qquad m_i\ddot{y}_{si}+F_{yiu}-F_{yi}=0;\qquad i=3,4$$

$$I_i\ddot{\phi}_i-M_{\phi is}+M_{\phi iu}-(F_{ziu}+F_{zi})\frac{L_0}{2}=0;\qquad i=3,4 \tag{3.10}$$

In the above equations, the vertical and lateral forces, and roll moment due to rear axle suspension are denoted by F_{zi}, F_{yi} and $M_{\phi is}$ (i=3,4), respectively, which are derived from the detailed linkage model, shown in Fig. 3.5(c). These have been developed in [22] considering 3-DOF of each of the rear axle suspension links, including vertical (z_{ur}), lateral (y_{ur}) and roll (ϕ_{ur}) of the unsprung mass, and lateral, vertical and roll (y_i, z_i and ϕ_i; i=3,4) motions of the suspension linkages. The geometric parameters L_0, L_1, R_w, h, and h_1 are illustrated in Fig. 3.6. The vertical, longitudinal and lateral tire forces are derived from Eqs. (3.5) and (3.6), while the lateral velocity of the footprint of the rear axle tires, however, is related to the unsprung mass motion such that: $\dot{y}_i=\dot{y}_{ur}+R_w\dot{\phi}_{ur}$ (i=3, 4).

3.3.3 Estimation of the terrain roughness profiles

The roughness of deformable off-road terrains has been expressed by a power regression function in spatial spectral density $G_Z(\Omega)$ representing the elevation of an equivalent undeformable terrain. The regression function for a forestry terrain, derived from the field measured responses of a conventional unsuspended forestry skidder, has been expressed as [22]:

$$G_Z(\Omega) = \alpha_r \Omega^{-\beta}; \quad \alpha_r > 0 \text{ and } \beta > 0 \tag{3.11}$$

where Ω is the spatial frequency that is related to forward speed U and the temporal frequency f, such that $f = \Omega U$, and constants α_r and β are the roughness coefficients and wavinesses of the terrain, respectively. The constants α_r and β which were identified from the measured vertical, pitch and roll ride responses of the conventional unsuspended vehicle through solution of an error minimization problem described in [22]. Compared to the other reported profiles like plowed field, pasture and the MVEE [114, 132], the identified roughness model showed lower roughness particularly at the lower wave numbers, which was in part be attributed to the soft terrain since the measurements were performed late in the fall season.

The spatial power spectral density (PSD) of the terrain roughness may also be expressed by a rational PSD function in temporal frequency ω and operating speed U [133]:

$$T(\omega) = (\frac{\mu_4}{\pi})[\frac{\mu_1 U}{\mu_1^2 U + \omega^2}] + (\frac{\mu_5}{\pi})[\frac{\mu_2 U(\mu_2^2 U^2 + \mu_3^2 U^2 + \omega^2)}{(\mu_2^2 U^2 - \mu_3^2 U^2 + \omega^2)^2 + 4\mu_2^2 \mu_3^2 U^2}] \tag{3.12}$$

where μ_i ($i=1, \ldots, 5$) are constant coefficients that were identified from the terrain profile spectrum over a range of 5 to 25 km/h forward speed, as: (0.19, 2.00, 0.76, 2.00×10^{-1}, 3.0×10^{-3}). The comparison of the spatial PSD derived from the above function with that derived from Eq. (3.11) in Fig. 3.6 shows that $T(\omega)$ can accurately describe the identified terrain spectra.

The above function permits the synthesis of time-history of the terrain roughness by applying a random white noise signal of unity power. For this purpose, the spectral density function in Eq. (3.12) is expressed as:

$$T(\omega) = b_1\left[\frac{\omega^4 + b_2\omega^2 + b_0^2}{(\omega^2 + a_1^2)(\omega^4 + a_2\omega^2 + a_0^2)}\right] \tag{3.13}$$

where a_i and b_i ($i=0, 1, 2$) are functions of the vehicle speed and coefficients μ_i, which can be applied to describe the random road irregularity $z_0(t)$ through stationary solution of a third-order differential equation subject to a random white-noise input of unity power $l(t)$ in the following manner [133]:

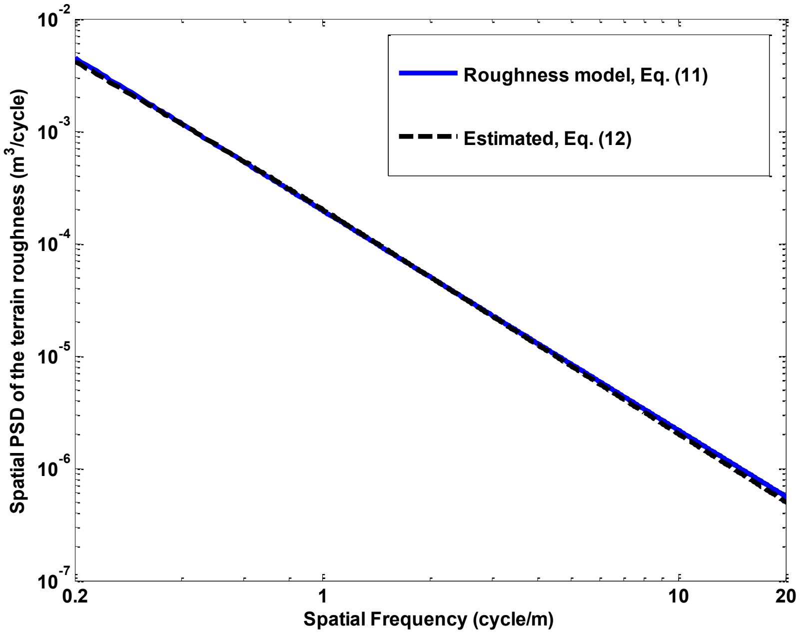

Figure 3.6: Comparison of the roughness profile with that estimated from model proposed by Hac [133].

$$\dddot{z}_0(t) + \left(a_1 + \sqrt{a_2 + 2a_0}\right)\ddot{z}_0(t) + \left(a_0 + a_1\sqrt{a_2 + 2a_0}\right)\dot{z}_0(t) + a_0 a_1 z_0(t) = \sqrt{b_1}\left[\ddot{l}(t) + \left(\sqrt{b_2 + 2b_0}\right)\dot{l}(t) + b_0 l(t)\right] \tag{3.14}$$

The above differential equation has been derived from a frequency response function $Q(\omega)$ obtained from Eq. (3.13) based on the stationary random process [227] in the following manner:

$$Q(\omega)=\sqrt{b_1}\left[\frac{-\omega^2+\sqrt{(b_2+2b_0)}i\omega+b_0}{(i\omega+a_1)(-\omega^2+\sqrt{(a_2+2a_0)}i\omega+a_0)}\right]=\frac{Z_0(\omega)}{L(\omega)} \tag{3.15}$$

where $Z_0(\omega)$ and $L(\omega)$ are the corresponding finite Fourier transforms of $z_0(t)$ and $l(t)$, respectively. $z_0(t)$ can be considered to represent average roughness profile of the terrain, assuming that the terrain tracks are statistically equivalent. In off-road operations, the two vehicle tracks are invariably subjected to different terrain elevations that contribute to the roll and lateral dynamic responses of the vehicle. The roughness profiles of the two tracks may be estimated by assuming a coherence function describing the linear dependence of two random profiles. A few studies have established coherence functions of roughness profiles of two tracks of the roadways. The analyses of measured road profiles by Bogsjo [228] showed that roughness profiles of the two tracks are highly correlated at low frequencies, while the coherence diminishes at higher frequencies. Yonglin and Jiafan [229] described the coherence by a piecewise linear function in frequency of the form:

$$\gamma_{LR}^2(\omega)=\begin{cases}1-0.9(\dfrac{\omega}{2\pi}) & ;\quad \omega\le\omega_1\\ 0.1 & ;\quad \omega>\omega_1\end{cases} \tag{3.16}$$

where $\gamma_{LR}^2(\omega)$ is the coherence between the left and right tracks of a roadway and ω_1 is the transition frequency, which was taken as 2Hz for the roadways. Considering that off-road terrains exhibit relatively low frequency components, a lower transition frequency would be more reasonable, which is considered as 1Hz in this study that is identical to the measured predominant roll frequency of the forestry vehicle [22]. The above coherence function can also be expressed accurately by a second-order function of the form:

$$|Q_1(\omega)|^2=\left[\frac{e_2^2\omega^4+(e_1^2-2e_2e_0)\omega^2+e_0^2}{d_2^2\omega^4+(d_1^2-2d_2d_0)\omega^2+d_0^2}\right]=\gamma_{LR}^2(\omega) \tag{3.17}$$

where e_i and d_i ($i=0, 1, 2$) are constant coefficients that are identified from the coherence function as: (4.47, 0.73, -0.06; and 4.47, 1.81, -0.20). The validity of the above function in describing the coherence is illustrated through comparison of the coherence values derived from Eqs. (3.15) and (3.17), as shown in Fig. 3.7.

Roughness profiles of the two tracks may be synthesized by considering the above coherence function and two uncorrelated random white noise signals, $l(t)$ and $n(t)$ applied to the spectral density function of the road profile. Assuming that Eq. (3.14) describes the roughness profile of the left track $z_{0L}(t)$, the roughness of the right track may be derived by considering a filtered random process $r(t)$, such that:

$$r(t) = q_1(t)l(t) + q_2(t)n(t) \tag{3.18}$$

where $q_1(t)$ is the coherence function and $q_2(t)$, describes the uncorrelated component of $r(t)$, which can be expressed as [227]:

$$\begin{cases} |Q_1(\omega)|^2 = \gamma_{LR}^2(\omega) \\ |Q_2(\omega)|^2 = 1 - \gamma_{LR}^2(\omega) \end{cases} \tag{3.19}$$

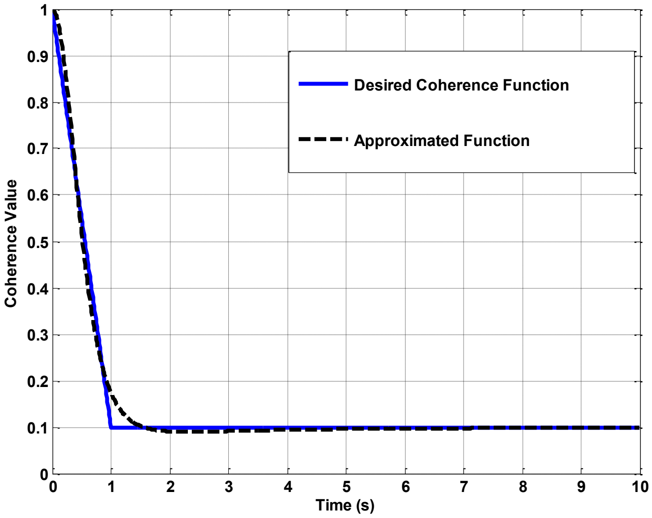

Figure 3.7: Comparison of the coherence values obtained from Eq. (3.16) with that approximated by fractional system function.

As it is shown in Fig. 3.8, schematically, the functions $q_1(t)$ and $q_2(t)$ are applied to obtain the filtered random process $r(t)$. The frequency response function $Q(\omega)$ described in Eq. (3.15) is subsequently applied to $r(t)$ to obtain random road irregularity of the right track $z_{0R}(t)$ through stationary solution of Eq. (3.14).

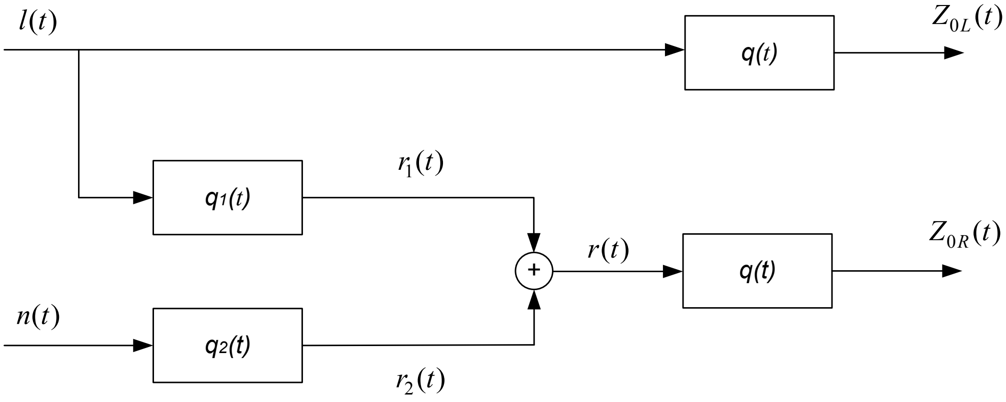

Figure 3.8 Flowchart of the proposed method to find the time series of two tracks profiles.

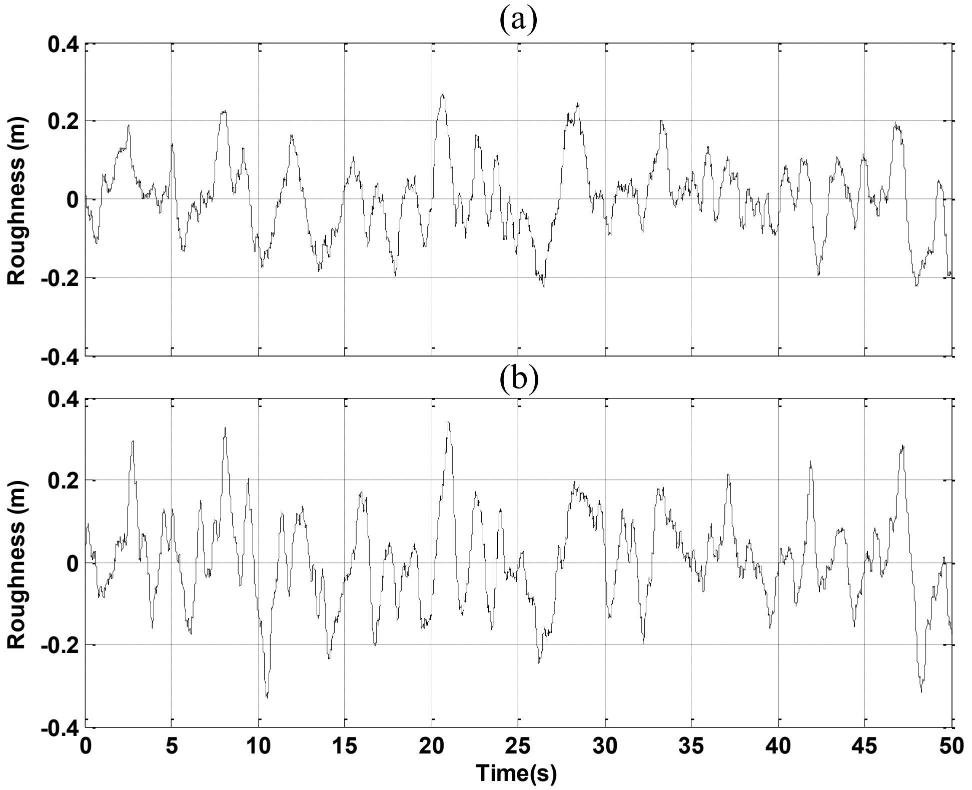

Figure 3.9: Time histories of roughness of the (a) left track; and (b) right track (U=5km/h).

Figures 3.9(a) and 3.9(b) illustrate time histories of the roughness of the left and right tracks considering a forward speed of 5km/h, respectively. Figure 3.10 illustrates the coherence of the two random terrain profiles, which is compared with the assumed target coherence. The time history of roll excitation attributed to roughness of the two tracks is further computed considering vehicle track width of 2.5m. Figures 3.11(a) and 3.11(b) illustrate the time-history and PSD of the roll displacement, respectively. The results show that the coherence of the two tracks roughness is quite close to the assumed target coherence, while the peak roll displacement excitation approaches 6 degrees.

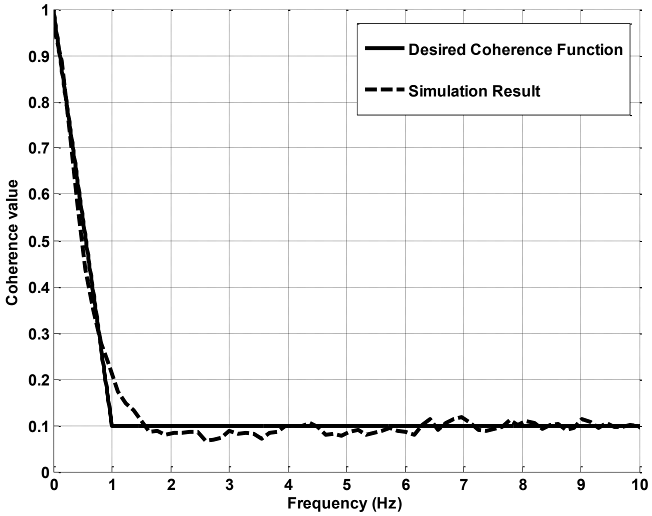

Figure 3.10: Coherence of the two track profiles compared with the target coherence.

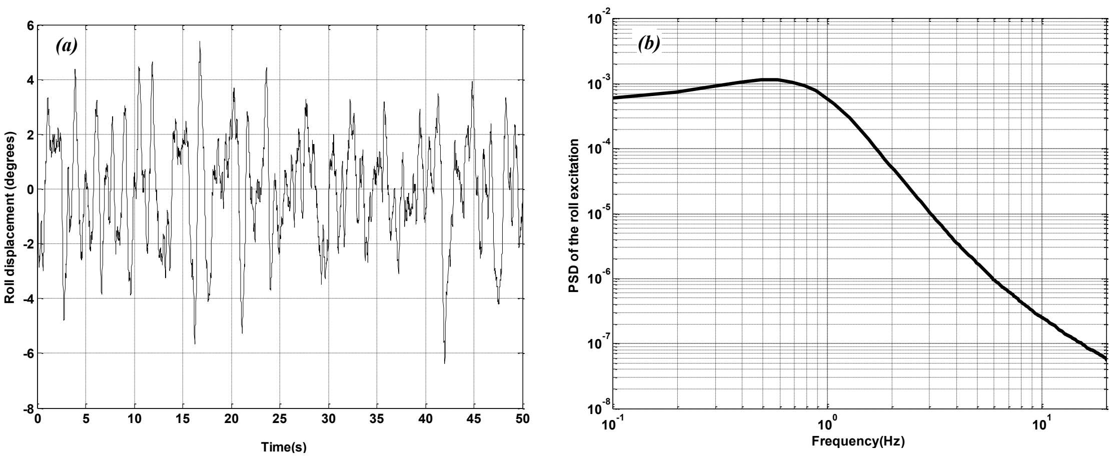

Figure 3.11: Roll displacement (a) time-history; and (b) PSD spectrum.

3.4 Method of Analysis

The unsuspended and suspended vehicle models together with the three-dimensional tire model are analyzed considering terrain excitations arising from two parallel tracks, shown in Fig. 3.9, at a constant forward speed. The simulations were initially performed at a speed of 5km/h in order examine model validity on the basis of the field-measured data that were acquired at the same speed. The simulation parameters of the vehicle models are summarized in Table 3.1 [22]. The model responses were evaluated in terms of PSD of translational and rotational accelerations, and frequency-weighted and un-weighted rms accelerations at the operator seat location. The vertical, longitudinal, and lateral acceleration responses at the seat location were derived from the following relations:

$$\ddot{z}_{seat} = \ddot{z}_s - l_x\ddot{\theta}_s; \quad \ddot{x}_{seat} = \ddot{x}_s + h'\ddot{\theta}_s; \quad \ddot{y}_{seat} = \ddot{y}_s - h'\ddot{\phi}_s \tag{3.21}$$

where h' and l_x are the vertical and longitudinal distances of the seat, respectively, from the sprung mass center of gravity (cg).

Table 3.1: Simulation parameters.

Parameter	value	Parameter	value
m'_s	8616 kg	k_z	185 kN/m
m_s	9662 kg	k_y	185kN/m
m_3	42.6 kg	k_t	125kNm/rad
m_4	42.6 kg	c_z	4000 Nm.s/rad
m_{ur}	1500 kg	c_y	4000 N.s/m
I'_{XXS}	10495 kg.m^2	c_t	3500 N.s/m
I'_{YYS}	16353 kg.m^2	K	94.5 kN/m
I_3	3500 kg.m^2	C	2000 N.s/m
I_4	3500 kg.m^2	σ	0.40 m
h'	0.43m	L_0	0.16 m
WB_1	1.23 m	h	0.60 m
WB_2	1.90 m	l_x	0.29 m
$2T$	2.50m	δ_{st}	0.20m
R_w	0.80 m	K_{Ty}	256kN/m
C_α	102 kN/m	h_1	0.21 m

The frequency-weighted accelerations were obtained using the weighting functions defined in ISO-2631-1 [3]. For this purpose, the response time-histories were analyzed to derive PSD and rms spectra using the modified Welch method [230] together with Hanning window and 50% overlap of the data segments. The total WBV exposure was also derived in terms of vibration total value, a_v:

$$a_v = \sqrt{\left(f_x^2 a_{wx}^2 + f_y^2 a_{wy}^2 + a_{wz}^2\right)} \tag{3.22}$$

where f_x and f_y are the additional weightings factors imposed on the weighted longitudinal and lateral acceleration values, as described in ISO-2631-1 [3]. a_{wx}, a_{wy} and a_{wz} are frequency-weighted longitudinal, lateral and vertical rms accelerations at the seat, respectively. The eight-hour energy equivalent frequency-weighted acceleration $A(8)$ is also computed for a daily exposure duration of T_e= 4 hours, based on the information attained from the Forestry Engineering Research Institute of Canada [231], such that $A(8) = a_v\sqrt{T_e/T_0}$, where T_0 is the reference duration of 8 hours.

3.5 Results Discussions and Model Validation

The validity of the vehicle models was examined on the basis of the field measured responses of a conventional skidder and a skidder integrated with a torsio-elastic rear suspension. The measurements and analysis of the field data have been described in [22]. The study [22] further showed that addition of the torsio-elastic suspension to the rear unit resulted in substantial reductions in overall unweighted and frequency-weighted rms accelerations measured near the operator seat. In this study the field-measured responses are used to examine validity of the vehicle models with three-dimensional tire model.

The acceleration PSD response spectra obtained along the vertical, fore-aft, lateral, pitch and roll axes at the operator seat location, derived assuming negligible effects of the seat cushion, are compared with the measured spectra in Figs. 3.12 and 3.13 for the conventional and suspended vehicles models, respectively. The results show respectively good agreements between the models and the measured data for both the models. The results suggest that the proposed three-dimensional tire model provides more accurate predictions of ride responses along all the axes compared to the results obtained with a one-dimensional point-contact tire model reported in [22].

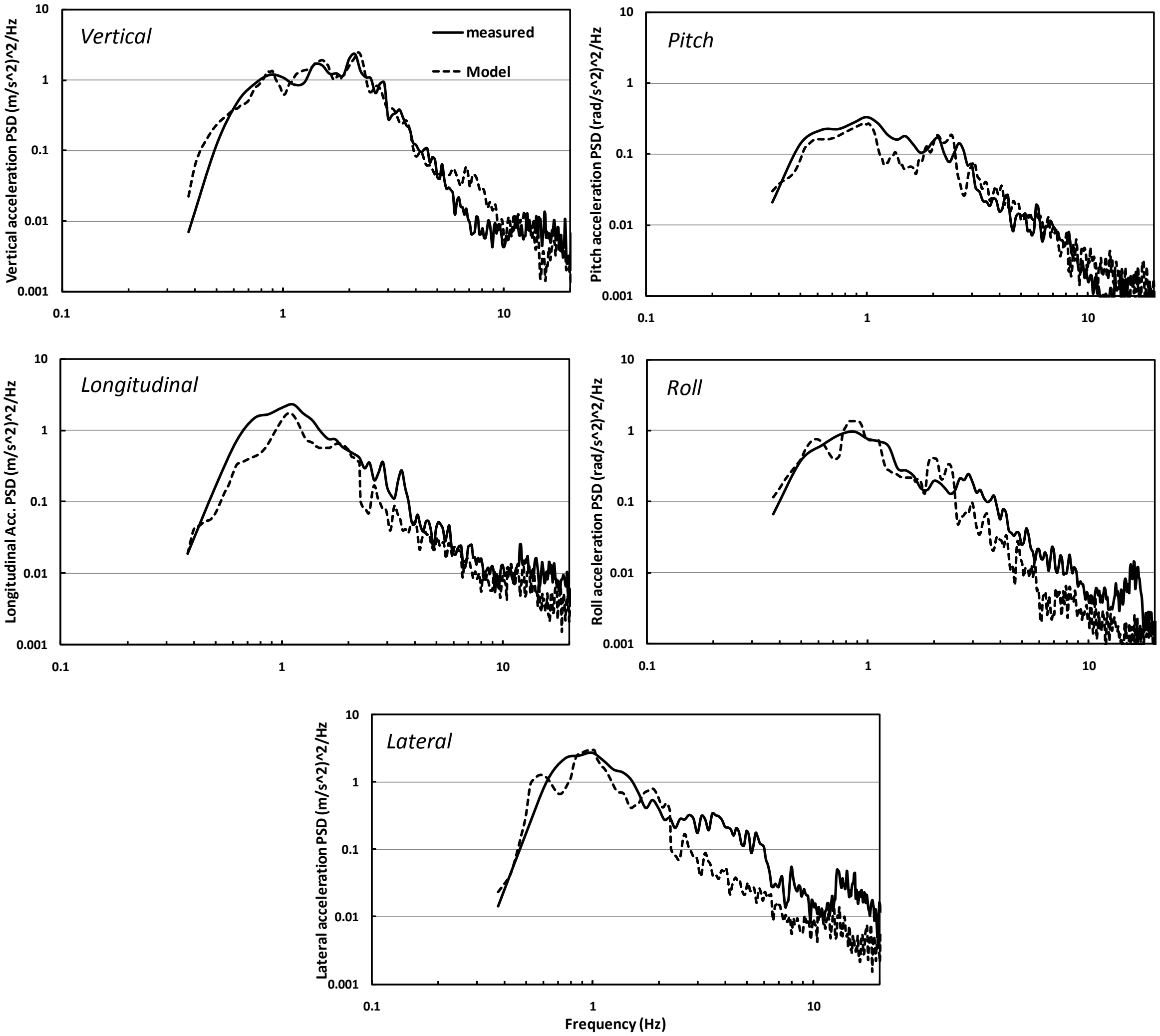

Figure 3.12: Comparisons of acceleration PSD responses of the conventional vehicle model with those of the measured data.

The results show peak responses near 1 and 2Hz, which are attributed to pitch and vertical mode resonances of the vehicle models. The predominant longitudinal vibration of the sprung mass occurs at a frequency slightly above 1Hz for both the vehicle models, which is partly associated with its coupling with the pitch mode. The roll and lateral acceleration responses also show two peaks near 0.9Hz and above 2.5Hz denoting the roll and lateral mode resonance frequencies of the sprung mass suggesting the coupling between lateral and roll modes.

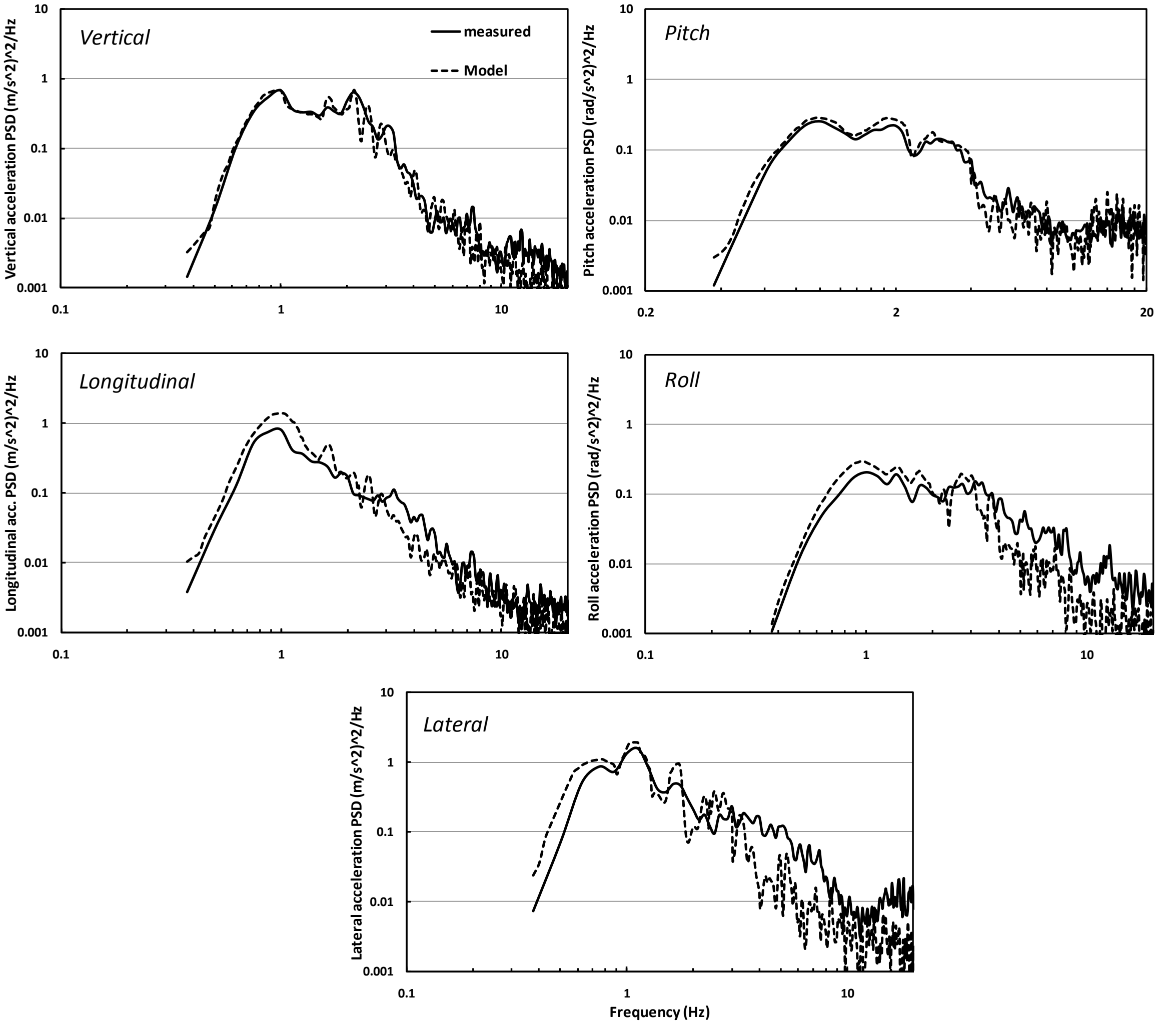

Figure 3.13: Comparisons of acceleration PSD responses of the suspended vehicle model with those of the measured data.

While the results suggest reasonably good agreements between the model responses and the measured spectra, some deviations are also evident. As it is observed in Figs. 3.12 and 3.13, the lateral and roll responses of the both suspended and unsuspended vehicle models at frequencies range above 3Hz are slightly below the measured data, which may partially be attributed to the relatively low roll excitation due to synthesized terrain profiles for the two parallel tracks at higher frequencies. The longitudinal acceleration response magnitudes of the unsuspended vehicle model are lower than the measured magnitudes at frequencies below 2Hz. The longitudinal response of the suspended vehicle, however, is greater than the measured response at frequencies below 2Hz.

The deviations in the response are also believed to be caused by various simplifying modeling assumptions, particularly the consideration of negligible contributions due to articulation forces and moments, constant forward speed, absence of wheel hop, and linear suspension properties. Despite the observed deviations, the results suggest that the vehicle models with the three-dimensional tire model can predict the ride dynamic responses along the vertical, longitudinal, lateral, roll and pitch axes, reasonably well. The models can thus serve as an effective tool to seek desirable suspension design parameters and to assess the whole-body vibration exposure of the operator.

Table 3.2: Comparisons of frequency-weighted and unweighted rms translational (m/s^2) and rotational (rad/s^2) acceleration values of the unsuspended vehicle model with the corresponding measured values.

Axis		Bounce	Longitudinal	Lateral	Pitch	Roll	a_v	*A(8)*
Unweighted	*Model*	1.97	1.39	1.53	0.67	1.00		
	Measured	1.83	1.59	1.79	0.70	1.10		
	Deviation (%)	7.6	-12.6	-14.6	-4.5	-9.1		
Weighted	*Model*	1.20	1.24	1.34	0.44	0.69	2.82	2.00
	Measured	1.12	1.43	1.52	0.46	0.75	3.13	2.22
	Deviation (%)	7.1	-13.3	-11.8	-4.3	-8.0	-9.9	-9.9

The overall frequency-weighted and unweighted rms acceleration values of the model responses are further computed and compared with those derived from the measured data in Tables 3.2 and 3.3. The frequency weighting W_d, W_k and W_e are applied to derive the overall frequency weighted rms acceleration along the horizontal (x, y), vertical (z) and rotational (θ, φ) axis, as recommended in ISO-2631-1 [3]. The results suggest good agreements between the rms acceleration values of both the models and the measured data particularly for the bounce and pitch rms acceleration responses. Slightly higher deviations, however, are observed in the lateral and longitudinal acceleration values of the unsuspended vehicle model. Similar deviations are also evident in the longitudinal rms acceleration of the suspended vehicle model, which are partly attributed to the simplifying assumptions of the models, specially the lack of consideration of the articulation force and moments. It should be noted that the previous study [22] using a one-dimensional point-contact tire model demonstrated considerable overestimates in the bounce-mode acceleration (for suspended vehicle: 28% deviation for unweighted rms acceleration and 58% deviation for weighted rms acceleration.) However, the off-road vehicle ride dynamics model developed in this study shows a considerable improvement in the bounce-mode acceleration, where deviations less than 5% were observed in Table 3.3.

Table 3.3: Comparisons of frequency-weighted and unweighted rms translational (m/s^2) and rotational (rad/s^2) acceleration values of the suspended vehicle model with the corresponding measured values.

	Axis	Bounce	Longitudinal	Lateral	Pitch	Roll	a_v	$A(8)$
Unweighted	*Model*	1.05	1.00	1.38	0.85	0.96		
	Measured	1.00	0.89	1.30	0.82	0.87		
	Deviation (%)	5.0	12.4	6.2	3.6	10.3		
Weighted	*Model*	0.65	0.89	1.17	0.44	0.48	2.16	1.53
	Measured	0.62	0.78	1.07	0.43	0.44	1.95	1.38
	Deviation (%)	4.8	14.1	9.3	2.3	9.1	10.8	10.8

The tables also present the vibration total value, a_v, derived from Eq. (3.22), and $A(8)$ values estimated from models responses and measured data. These illustrate deviations in the order of 10-11% between the model and measured responses. Comparisons of the results presented in Tables 3.2 and 3.3 confirm that the addition of a rear-axle torsio-elastic suspension yields significant reduction in the WBV exposure of the operator along all the translational axes. Both the total value and eight-hour energy equivalent frequency-weighted acceleration are nearly 38% lower for the suspended vehicle compared to the unsuspended vehicle. The results further show that the $A(8)$ value of the unsuspended vehicle exceeds the "limiting value" of 1.15m/s^2 defined in the EC guidelines [4]. While the suspended vehicle yields substantially lower $A(8)$ value, its magnitude still exceeds the "action value" of 0.5m/s^2 defined in the EC guidelines.

3.6 Parameter Sensitivity Analysis

Different vehicle design and operating parameters including the torsio-elastic suspension properties, the linkage geometry, vehicle forward speed, vehicle load, and terrain roughness would affect the ride performance potential of the torsio-elastic suspension. Among these, the suspension characteristics would also influence the load carrying capacity of the vehicle. The validated suspended vehicle model is used to study the sensitivity of ride responses to variations in the suspension parameters so as to seek desirable suspension design parameters. The analyses are performed for the unloaded vehicle operating at a constant forward speed of 5km/h. The suspension design parameters considered include: the stiffness (k_y, k_z, k_t) and damping (c_y, c_z, c_t) constants, and the linkage length (L_0) of the rear-axle torsio-elastic suspension. The stiffness and damping constant was varied by ±50% about the nominal value, and the variation in the link length was limited to ±25%, while the vehicle track width was held constant. The responses were obtained in terms of unweighted and frequency-weighted vertical, longitudinal, lateral, pitch and roll rms accelerations, which are summarized in Table 3.4.

The results revealed considerable influence of the suspension vertical stiffness on both the frequency-weighted and unweighted vertical and pitch rms accelerations. Increase in the vertical stiffness causes higher pitch and vertical mode resonance frequencies, which resulted in higher frequency-weighted and unweighted vertical and pitch rms accelerations. Same effect can be observed on the longitudinal rms acceleration due to coupling between the longitudinal and pitch dynamics. The influence of variations in the vertical stiffness, however, is negligible on the roll and lateral accelerations, suggesting relatively weak coupling of the vertical mode with roll and lateral modes of the vehicle. While the lateral stiffness variations show only minimal effect on the roll responses, the un-weighted lateral rms acceleration is strongly affected by both the torsional and lateral suspension stiffness suggesting greater coupling between the roll and lateral responses of the vehicle. Reductions in both the lateral and torsional stiffness yield relatively higher magnitude of the weighted lateral acceleration, which may be partly attributed to reduced roll and lateral mode frequencies, below 1Hz, where the effect of W_d-weighting is greater. The roll response is mostly affected by the torsional stiffness, where a reduction in the torsional stiffness results in higher roll acceleration.

The torsio-elastic suspension provides only light damping, which may not yield important influences on the ride vibration responses. However, the frequency-weighted and unweighted vertical, longitudinal, and pitch accelerations tend to increase with lower vertical damping of the torsio-elastic suspension. The roll acceleration response is only slightly affected by the torsional and lateral damping coefficients. The results obtained in terms of vibration total value, a_v, suggest that a suspension design with lower vertical stiffness and higher lateral and torsional stiffness, and higher vertical damping would yield lower overall weighted rms acceleration, while the effects of lateral and torsional damping are relatively small.

Table 3.4: Influence of variations in the torsio-elastic suspension stiffness and damping properties on the frequency-weighted and unweighted rms translational (m/s^2) and rotational (rad/s^2) acceleration responses of the model.

Parameters		Weighted rms acceleration						Unweighted rms acceleration				
		z	x	y	θ	ϕ	a_v	z	x	y	θ	ϕ
Nominal value		**0.65**	**0.89**	**1.17**	**0.44**	**0.48**	***2.16***	**1.05**	**1.00**	**1.38**	**0.85**	**0.96**
k_z	-50%	0.61	0.85	1.17	0.40	0.48	***2.11***	0.90	0.90	1.38	0.73	0.97
	+50%	0.73	0.92	1.17	0.48	0.48	***2.20***	1.25	1.16	1.38	1.02	0.95
k_y	-50%	0.65	0.89	1.26	0.44	0.47	***2.28***	1.05	1.01	1.32	0.85	0.94
	+50%	0.65	0.89	1.10	0.44	0.49	***2.07***	1.05	1.01	1.43	0.85	0.99
k_t	-50%	0.65	0.89	1.21	0.44	0.51	***2.23***	1.05	1.01	1.34	0.85	1.09
	+50%	0.65	0.89	1.14	0.44	0.43	***2.11***	1.05	1.01	1.41	0.85	0.81
c_z	-50%	0.66	0.96	1.17	0.47	0.48	***2.22***	1.17	1.12	1.38	0.97	0.96
	+50%	0.65	0.83	1.17	0.41	0.48	***2.11***	1.02	0.94	1.38	0.77	0.96
c_y	-50%	0.65	0.89	1.18	0.44	0.49	***2.17***	1.05	1.01	1.43	0.85	0.98
	+50%	0.65	0.89	1.16	0.44	0.47	***2.15***	1.05	1.01	1.36	0.85	0.95
c_t	-50%	0.65	0.89	1.17	0.44	0.49	***2.16***	1.05	1.01	1.40	0.85	1.00
	+50%	0.65	0.89	1.17	0.44	0.47	***2.16***	1.05	1.01	1.37	0.85	0.96
L_0	-25%	0.65	0.89	1.18	0.44	0.49	***2.17***	1.05	1.00	1.38	0.84	0.96
	+25%	0.63	0.90	0.92	0.48	0.37	***1.91***	1.02	1.03	1.13	0.88	0.78

The kinematic effect of the suspension mechanism is investigated from the responses sensitivity to variation in the suspension linkage length. The results (Table 3.4) suggest that an increase in L_0 yields lower roll and lateral responses, which is partly attributed to lower effective-roll stiffness, while the effects on frequency-weighted and unweighted vertical, longitudinal, and pitch responses are relatively small. A 25% increase in L_0 results in nearly 12% reduction in the vibration total value.

Apart from the suspension parameters, forestry skidders are invariably subject to high load variations during a work cycle, which could greatly affect the ride vibration responses. The ride responses of loaded vehicle are thus obtained in terms of unweighted and frequency weighted rms acceleration responses for both the conventional and suspended vehicle models. The loaded condition is realized by increasing the vehicle sprung mass by 50% of the nominal mass presented in Table 3.1. The results are compared with those of the unloaded vehicle models in Table 3.5. The results show that the loaded unsuspended vehicle yields considerably higher acceleration responses compared to the unloaded vehicle along all the axes, except in the longitudinal direction. In particular, the weighted vertical, lateral, pitch and roll rms accelerations of the loaded vehicle are nearly 25%, 15%, 55% and 110% higher than those of the unloaded vehicle.

Table 3.5: Influence of vehicle load on the frequency-weighted and unweighted rms translational (m/s^2) and rotational (rad/s^2) acceleration responses of the unsuspended and suspended vehicle models.

Parameters		Weighted rms acceleration						Unweighted rms acceleration				
		z	x	y	θ	ϕ	$\boldsymbol{a_v}$	z	x	y	θ	ϕ
Un-suspended	**Un-loaded**	1.20	1.24	1.34	0.44	0.69	***2.82***	1.97	1.39	1.53	0.67	1.00
	Loaded	1.50	1.06	1.54	0.68	1.44	***3.02***	2.42	1.20	2.02	0.96	1.92
Suspended	**Un-loaded**	0.65	0.89	1.17	0.44	0.48	***2.16***	1.05	1.00	1.38	0.85	0.96
	Loaded	0.63	0.82	1.10	0.54	0.60	***2.05***	1.06	0.96	1.31	0.78	0.91

The suspended vehicle, however, exhibits significantly lower sensitivity to variations in the load, as seen in Table 3.5. The unweighted responses of the loaded suspended vehicle are either comparable or slightly lower than those of the unloaded vehicle along all the translational and rotational axes. The weighted responses of the loaded suspended vehicle along the translational axes are also lower than those of the unloaded vehicle. The frequency-weighted roll and pitch responses of the loaded vehicle, however, are nearly

25% greater than those of the unloaded vehicle. This is caused by lower pitch and roll resonance frequencies of the loaded vehicle and contributions of the W_e-weighting. The results clearly suggest that the torsio-elastic suspension is not greatly sensitive to variations in the load, when WBV exposure of operator is concerned.

3.7 Conclusions

This study developed a comprehensive off-road vehicle ride dynamics model integrating a three-dimensional tire-terrain interaction model, which can be effectively and efficiently applied to both suspended and unsuspended vehicles. The tire-terrain interaction model comprised an adaptive radial representation for characterizing the resultant vertical and longitudinal forces within the contact patch, and a lateral dynamic model based on the side-slip theory together with the tire-lag. The forestry terrain was described by a regression roughness model of an equivalent undeformable terrain that was estimated from the field-measured responses of a conventional unsuspended skidder. The roughness profiles of the two parallel tracks of the terrain were synthesized assuming a coherence function between the random roughness of the two tracks. The synthesized roughness characteristics revealed peak roll excitation due to terrain in the order of 6 degrees.

The model responses were subsequently evaluated in terms of PSD of accelerations, and weighted and un-weighted rms accelerations along the vertical, fore-aft, lateral roll and pitch axes for both the unsuspended and suspended vehicle models. The validity of the models was demonstrated by comparing the response spectra and overall rms accelerations with the reported field-measured responses for the same vehicle with and without suspension. Both the conventional and suspended vehicle models responses agreed very well with the measured responses in all the directions considered. Good agreement was also evident in the longitudinal and lateral axis for both the vehicle models suggesting that the three-dimensional tire model can provide good prediction of the vehicle ride responses along all the translational and rotational axes. The validated vehicle ride dynamics models could thus serve as important tools for suspension design and assessments of WBV exposure of drivers of off-road vehicles. Based on the developed off-road vehicle ride dynamics model, the use of a rear-axle torsio-elastic suspension resulted in nearly 38% reduction in the vibration total value. Furthermore, the suspension revealed only little sensitivity to variations in the vehicle load.

CHAPTER 4

KINETO-DYNAMIC DIRECTIONAL RESPONSE ANALYSIS OF AN ARTICULATED FRAME STEER VEHICLE

4.1 Introduction

Articulated frame steer vehicles (ASV) with their enhanced mobility and manoeuvrability on off-road terrains are widely used in the agricultural, construction, forestry and mining sectors. These vehicles also operate on paved roads at relatively higher speeds and thus pose difficult handling and directional performance requirements. Such vehicles are known to exhibit relatively lower stability thresholds, particularly greater jack-knife and snaking tendencies, which are attributable to a number of factors [24-26]. These include the multi-axle vehicle design, large diameter tires and thus high mass vehicle centre of gravity (cg), operation on complex terrain conditions, wide range of operating speeds, and large vehicle load and load variations, in addition to the kinematics and dynamics of the articulated steering system. While the directional dynamics and stability limits of articulated freight vehicles have been extensively investigated, only a few reported studies are found on off-road articulated steering vehicles. Some of these have established that the hydraulic steering system is the most sensitive design factor in view of the vehicle steering responses and stability [25,26]. Apart from steering of the vehicle, the kinematics and dynamics of the hydraulic articulated frame steering system play a critical role in retaining directional stability of the vehicle, due to the fact that the articulated frame steer vehicles are inherently directionally unstable and exhibit jack-knife tendency about the pivot, particularly at higher speeds [25,26]. This suggests the need to enhance understanding of contributions of the steering mechanism behaviour to the directional dynamic responses of the articulated frame steer vehicles.

The articulated frame steering responses are strongly dependent on both the kinematics and dynamics of the steering system and their coupling with the dynamics of the vehicle. The vast majority of the reported studies on characterization of directional responses have employed linearized low-order vehicle models together with a simplified articulated steering model characterized by an equivalent linear torsional stiffness and damping, while the kinematics properties of the steering mechanism are entirely ignored [24-26,28,29]. The reported studies have generally investigated three modes of instabilities namely the ‘Snaking’, ‘Jack-Knife’ and ‘Oversteer’, which have been observed with articulated frame steer vehicles [25,26]. Crolla and Horton [24] investigated the steering behavior and directional responses through an eigenvalue analysis of the 3-degree of freedom (DOF) linear yaw-plane model of the articulated steer vehicle, while the steering system was described by linear torsional spring and damping constants. The study concluded that snaking and jack-knife types of instabilities could occur even at low speeds when the steering torsional stiffness is low. A higher torsional stiffness and damping of the articulated steering was thus suggested for enhanced vehicle stability limits.

Horton and Crolla [25] further extended the model by replacing the equivalent torsional stiffness and damping by a linear model of the hydraulic steering system, although the kinematics of the steering struts and the joint was not considered. The results showed that an oversteer instability could occur at a speed above 24 m/s, which would lead to snaking mode as the driver attempts steering correction. Similar observations were also made from a full vehicle test conducted by Lopatka and Muszynski [27]. The study also concluded that the stability limits are more sensitive to the steering system properties, cg positions of the front and rear vehicle bodies, and rear body inertia [25].

He et al. [26] investigated the oversteer jack-knife types of instabilities of an articulated forestry vehicle using the model reported in [25], and showed that an oversteer mode could evolve into jack-knife with low torsional stiffness at the articulation. Azad et al. [29,177,178] developed a multi-body dynamic model of the articulated forestry vehicle and showed that the rear-mounted load would negatively affect the snaking stability mode of the vehicle. The reported studies have shown that an increase in tire lateral force would yield a moderate stabilizing effect while the effects of tire longitudinal forces and aligning moments were negligible [25,177,178].

The above studies have invariably considered yaw-plane models of the vehicle, where the contributions of roll motions of the articulated units are assumed to be small. A recent study [30] has developed a three-dimensional multi-body simulation model of an articulated wheel loader with an axle suspension to study snaking and roll responses, while the steering mechanism was represented by equivalent linear stiffness and damping constants as in earlier studies. The results showed a slightly negative effect of axle suspensions on the snaking mode of the vehicle, which could be compensated by a refined design of the steering system. For a given pulse steering torque, a snaking instability could occur at speeds above 12.6 km/h, which was strongly influenced by the rear-body inertia and cg position, where the loaded vehicle with heavy rear-unit is most prone to snaking instability. The study suggested that an axle suspension would yield improved ride comfort, while the vehicle directional stability is mostly managed by the design of the steering system.

The reported studies have established that the directional stability limits of the articulated steered vehicles are strongly dependent upon the steering system design. The steering response is a nonlinear function of the steering valve flows, kinematic and dynamic responses of the steering struts together with the vehicle inertia, which may not be adequately reflected by the equivalent linear torsional spring and damping constants that have been invariably employed in the reported models. Kineto-dynamic analysis, comprising kinematic motions of the struts and dynamics of the vehicle bodies, is vital to identify desirable design of the steering system for enhancement of the lateral stability of the vehicle. The kinematic model of the articulation dampers used in the articulated highway vehicles has been investigated by Rakheja et al. [179], which showed that the additional articulation damping forces, which are strongly dependent on the geometry of the dampers, help improve the yaw stability of the articulated vehicle and reduce the side force demand on the tires. Although the study considered linear dampers at the articulation joint, the dampers configuration was similar to the hydraulic struts of the articulated frame steering system.

Furthermore, owing to increased concerns over the vibration exposure and the associated health and safety risks among the driver, the modern articulated steer vehicles call for implementations of axle suspensions, so as to enhance vehicle ride vibrations and thus the preservation of driver's comfort and health [1,22,30,232]. The integration of axle suspensions would pose additional challenges in view of vehicle roll dynamics and stability as well as the strongly coupled vehicle roll and yaw motions [152,155,233]. The development of a refined nonlinear vehicle model integrating the kineto-dynamic characteristics of the steering system and considerations of the articulation joint, struts geometry, and valve flow properties is thus considered desirable. Such a model could serve as an important tool to seek improved designs of steering mechanism and analysis of directional behaviour of the vehicle.

This chapter (paper) provides a fundamental investigation on the effects of the combined kinematic and dynamic characteristics of the steering system on the vehicle directional dynamics and stability characteristics. The mathematical formulations of the steering system kineto-dynamics are derived and integrated within a nonlinear 3-DOF yaw-plane model of an articulated dump truck. The model also captures the tire-lag effect. The proposed kineto-dynamic model is validated on the basis of the available measured data. The vehicle model integrating the kineto-dynamic steering system model is then applied to evaluate directional response of the vehicle and the influences of selected steering and vehicle system parameters.

4.2 Kineto-Dynamic Modeling of the Steering System

The steering behaviour of an articulated frame steer vehicle is determined from the kineto-dynamic of the two hydraulic struts coupling the two units of the vehicle, and steering control valve. The steering torque developed by the struts is dependent upon the kineto-dynamics of the struts together with yaw and lateral dynamics of the vehicle units. In this section, a kineto-dynamics model of the articulated steering system is derived considering fluid flows through the control valve, which is subsequently integrated within a nonlinear 3-DOF yaw-plane model of the articulated frame steer vehicle to facilitate analyses of steering and directional properties of the vehicle.

4.2.1 Steering system kinematics

Figure 4.1 illustrates the kinematic model of the right and left hydraulic struts coupling the two vehicle units in the yaw plane. In this figure, l_1l_2 and r_1r_2 represent instantaneous lengths of the left and right struts, which are attached to the front unit at pivot points l_1 and r_1, and to the rear unit at pivot points l_2 and r_2, respectively. The pivot points on the front and rear units are located at lateral distances of a and c from the longitudinal axis of the respective units, as seen in Fig. 4.1, while b and d denote the longitudinal coordinates of the articulation joint with respect to the front and rear units, respectively. Angles α_1 and α_2 are the instantaneous yaw angles of the left strut axis l_1l_2 with respect to longitudinal axes of front and rear units, respectively. Similarly, β_1 and β_2 are instantaneous yaw angles of the right strut axis r_1r_2 with respect to longitudinal axes of the front and rear units, respectively, and φ is articulation angle. From the geometry shown in Fig. 4.1, relationships between these angles are obtained as:

$$\begin{aligned} &\alpha_1 = -\varphi + \alpha_2; \quad \beta_1 = \beta_2 - \varphi \\ &\alpha_2 = -\sin^{-1}\left(\frac{(L_1A_1)\cos\varphi}{L_1L_2}\right); \quad \beta_2 = \sin^{-1}\left(\frac{(R_1A_2)\cos\varphi}{R_1R_2}\right) \end{aligned} \tag{4.1}$$

where the instantaneous strut lengths, L_1L_2 and R_1R_2, are:

$$\begin{aligned} &(L_1L_2) = [(L_1A_1)^2 + (L_2A_1)^2 - 2(L_1A_1)(L_2A_1)\cos(\frac{\pi}{2} + \varphi)]^{\frac{1}{2}} \\ &(R_1R_2) = [(R_1A_2)^2 + (R_2A_2)^2 - 2(R_1A_2)(R_2A_2)\cos(\frac{\pi}{2} - \varphi)]^{\frac{1}{2}} \end{aligned} \tag{4.2}$$

and

$$\begin{aligned} &L_1A_1 = a - \frac{c}{\cos\varphi} - f\tan\varphi; \quad L_2A_1 = g + \frac{f}{\cos\varphi} + c\tan\varphi \\ &R_1A_2 = a - \frac{c}{\cos\varphi} + f\tan\varphi; \quad R_2A_2 = g + \frac{f}{\cos\varphi} - c\tan\varphi \end{aligned} \tag{4.3}$$

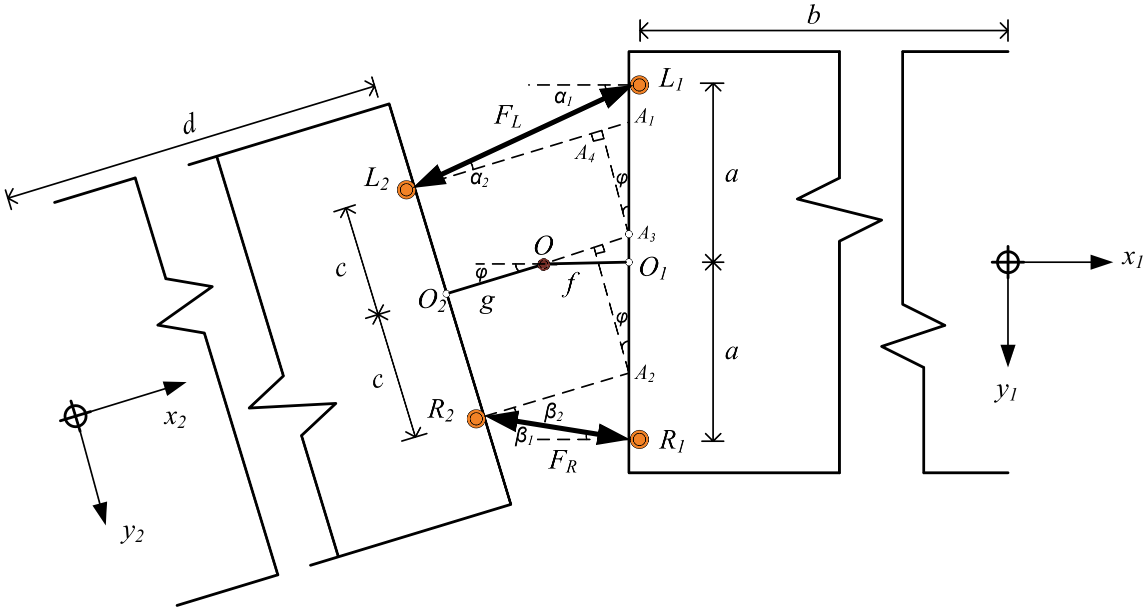

Figure 4.1: Kinematics of the articulated steering system.

4.2.2 Steering system dynamics

The above equations yield kinematic behavior of the hydraulic struts, which is further dependent upon the hydraulic flows from the control valve, and lateral dynamics of the vehicle units. Fig. 4.2 illustrates a schematic of the hydraulic steering system and directions of hydraulic flows during a right-turn maneuver. The steering system consists of a variable displacement pump with working pressure P_S. The steering control valve stem displacement X_V, caused by steering wheel rotation θ_{sw}, permits fluid flows from the pump to the struts and from the struts to the reservoir. The left- and right-struts develop forces and steering torque depending upon fluid pressure difference across the strut piston, strut geometry and strut kinematics.

Valve stem displacement

The vehicle articulation angle is directly related to displacements of the two struts, which is further influenced by motion resistances due to vehicle and tires. The steering system dynamics is thus characterized by a closed-loop system. Let φ_o be the articulation angle corresponding to a steer input θ_{sw} in the absence of the vehicle resistances, such that $\varphi_o = K_1\theta_{sw}$. The constant K_1 is termed as the open-loop articulation angle to steering gain, given by [25,26]:

$$K_1 = \frac{(\varphi_o)_{\max}}{(\theta_{sw})_{\max}} \tag{4.4}$$

where $(\theta_{sw})_{\max}$ is the maximum steering input corresponding to the locked position, and $(\varphi_o)_{\max}$ is the corresponding open-loop articulation angle.

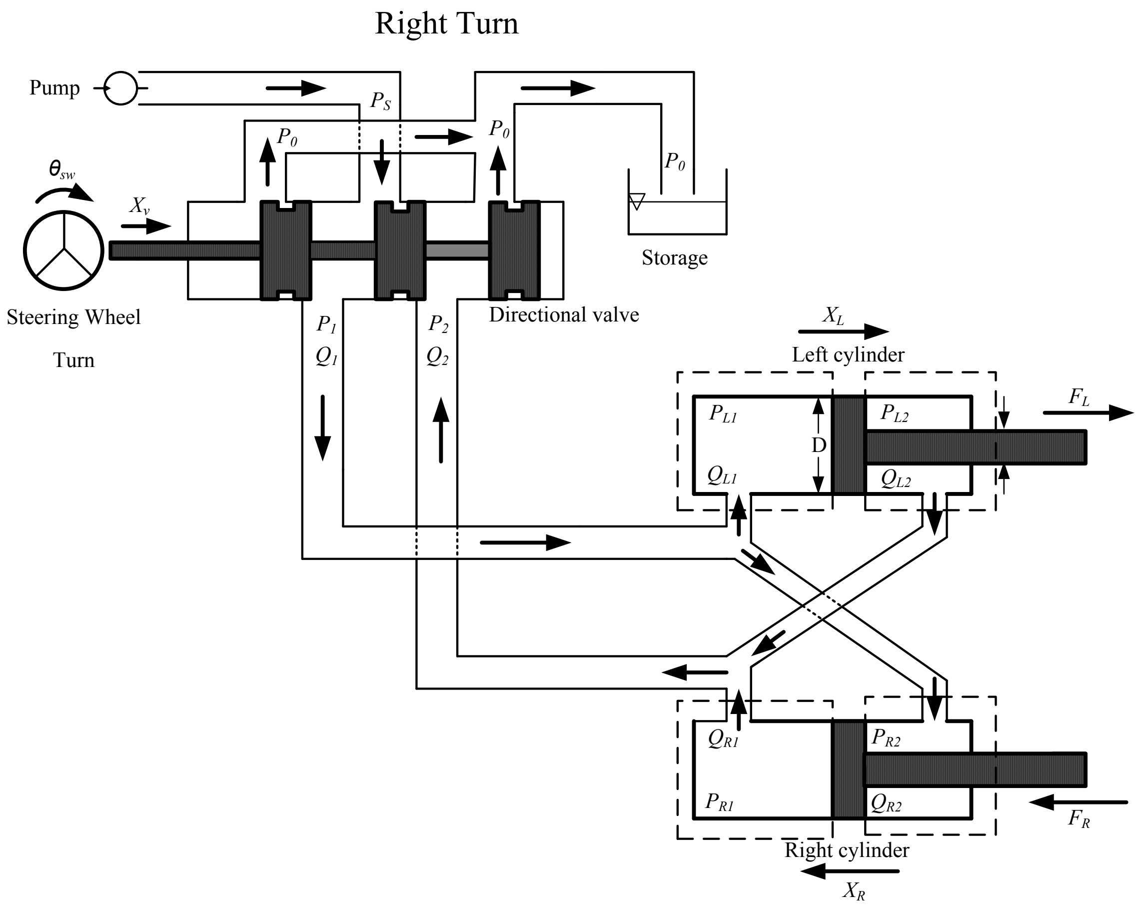

Figure 4.2: Schematic of the hydraulic steering system for a right turn.

In the closed-loop model, the vehicle articulation angle φ serves as a feedback for the steering valve. The steering valve stem displacement X_V is thus governed by the difference, $\delta = \varphi_o - \varphi$. Assuming linear relationship between X_V and δ within the permissible valve stem displacement, $-X_{Vmax} \leq X_V \leq X_{Vmax}$, as shown in Fig. 4.3, the valve stem displacement can be expressed as:

$$
\begin{aligned}
X_V &= K_2\delta; && |\delta| \leq \delta_{char} \\
X_V &= X_{V\max}\,\mathrm{sgn}(\delta); && \textit{Otherwise}
\end{aligned}
\tag{4.5}
$$

where

$$\mathrm{sgn}(\delta) = \begin{cases} +1; & \delta > 0 \\ -1; & \delta < 0 \end{cases}$$

In the above formulation, K_2 is a constant and δ_{char} is the characteristic articulation angle error corresponding to maximum valve stem displacement or saturation. This characteristic value greatly depends on the steering system design. Upon substituting for $K_2 = X_{Vmax}/\delta_{char}$ in Eq. (4.5), the normalized stem displacement $\overline{X}_V = X_V/X_{Vmax}$ can be related to θ_{sw} and φ in the following manner:

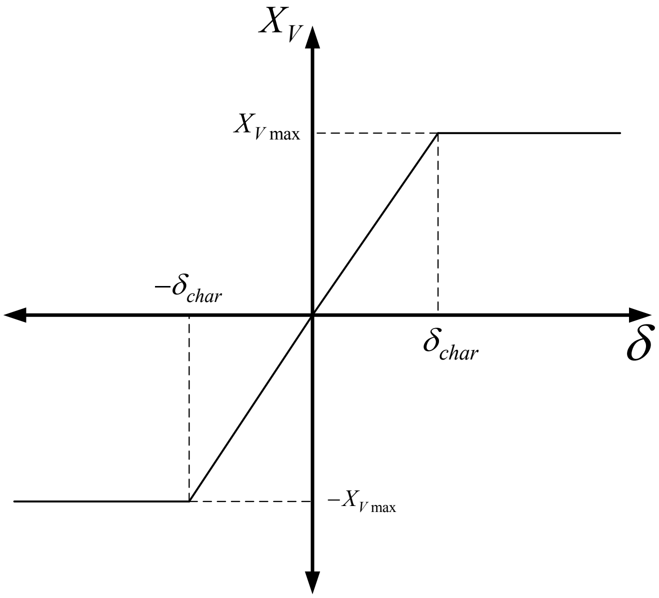

Figure 4.3: Relationship between the valve spool displacement and the articulation error.

$$\begin{aligned} &\bar{X}_V = \frac{1}{\delta_{char}}\left(K_1\theta_{sw} - \varphi\right); && |\delta| \le \delta_{char} \\ &\bar{X}_V = \operatorname{sgn}(\delta); && \mathit{Otherwise} \end{aligned} \tag{4.6}$$

Fluid flow rates

The rates of fluid flows to and from the struts, Q_1 and Q_2, are related to effective areas of valve openings and pressure drop across the valve, while the positive sign denotes the direction of the flow to the struts. The fluid flow rate from the pump to the articulation struts, Q_1, can be expressed as [234]:

$$Q_1 = C_d A_1 \sqrt{\frac{2\left(P_S - P_1\right)}{\rho_m}} \tag{4.7}$$

where C_d is the valve discharge coefficient, A_1 is effective valve opening, ρ_m is fluid mass density, and P_1 is pressures of fluid at the valve outlet (Fig. 4.2). Similarly, the rate of fluid flow from the struts to the reservoir, Q_2, can be expressed as:

$$Q_2 = -C_d A_2 \sqrt{\frac{2\left(P_2 - P_0\right)}{\rho_m}} \tag{4.8}$$

where A_2 is effective valve opening, P_2 is pressure of fluid discharged by the struts, and P_0 is the reservoir fluid pressure, considered to be atmospheric. Assuming identical opening of the valve at the inlet and the outlet, and a linear relationship between the valve stem position and the areas ($A_1=A_2=KX_V$), the fluid flow rates are expressed as:

$$Q_1 = C_T X_V \sqrt{\left(P_S - P_1\right)}\,; \qquad Q_2 = -C_T X_V \sqrt{P_2} \tag{4.9}$$

where $C_T = C_d K\sqrt{2/\rho_m}$ is a constant coefficient. Assuming negligible pressure drop in the connecting pipes, the flow continuity yields, $P_S=P_1+P_2$.

The maximum flow rate through the valve occurs for maximum stem displacement and pressure drop, such that:

$$Q_{\max} = C_T X_{V\max} \left(\Delta P_m\right)^{1/2} \tag{4.10}$$

where ΔP_m is the peak pressure drop across the steering valve. The fluid flow rates to and from the struts, normalized with respect to Q_{max} can be expressed as:

$$\bar{Q}_1 = \bar{X}_V \left(\frac{P_S}{\Delta P_m} - \bar{P}_1 \right)^{1/2}; \quad \bar{Q}_2 = -\bar{X}_V \left(\bar{P}_2\right)^{1/2} \tag{4.11}$$

where $\bar{P}_1 = P_1/\Delta P_m$, $\bar{P}_2 = P_2/\Delta P_m$, $\bar{Q}_1 = Q_1/Q_{\max}$ and $\bar{Q}_2 = Q_2/Q_{\max}$.

Hydraulic struts

Assuming negligible pressure drop across the connecting pipes and friction in the struts the fluid pressures within the piston- and rod-side chambers of the left strut, P_{L1} and P_{L2}, and the right strut, P_{R1} and P_{R2}, respectively (Fig. 4.2), can be expressed in terms of P_1 and P_2:

$$P_{L1} = P_{R2} = P_1; \quad P_{L2} = P_{R1} = P_2 \tag{4.12}$$

The rates of fluid flows to the left and right struts, Q_{L1} and Q_{R2}, respectively, are derived for the control volumes indicated by ‘dashed boxes’ in Fig. 2, considering leakage flows through the piston seals, Q_L, and fluid compressibility [234], such that:

$$Q_{L1} = Q_L + A_p \dot{X}_L + \frac{V_{L1}}{B} \dot{P}_{L1}; \quad Q_{R2} = Q_L + A_r \dot{X}_R + \frac{V_{R2}}{B} \dot{P}_{R2} \tag{4.13}$$

where A_p and A_r are the effective cross-section areas of the struts on the piston- and the rod-sides, respectively, and B is fluid bulk modulus. The leakage flow Q_L is linearly related to the pressure drop across the piston, such that: $Q_L = K_L (P_{L1} - P_{L2}) = K_L (P_{R2} - P_{R1}) = K_L (P_1 - P_2)$, where K_L is the leakage coefficient. V_{L1} and V_{R2} define the instantaneous fluid volumes in the piston- and rod-side chambers of the left and right struts, respectively, given by:

$$V_{L1} = V_{0L1} + A_p X_L \ ; \quad V_{R2} = V_{0R2} + A_r X_R \tag{4.14}$$

where V_{0L1} and V_{0R2} are the initial fluid volumes in the corresponding chambers, X_L and X_R are displacements of left and right strut pistons, respectively, $\dot{X}_L$ and $\dot{X}_R$ are the corresponding velocities, which can be derived using the derivatives of the instantaneous strut lengths, L_1L_2 and R_1R_2, presented in Eq. (4.2), such that:

$$\dot{X}_L = \frac{d}{dt}\left(L_1 L_2\right); \qquad \dot{X}_R = \frac{d}{dt}\left(R_1 R_2\right) \tag{4.15}$$

Similarly, the fluid flow rates from the left and right struts, Q_{L2} and Q_{R1}, can be expressed as:

$$Q_{L2} = -Q_L - A_r \dot{X}_L + \frac{V_{L2}}{B} \dot{P}_{L2}; \;\; Q_{R1} = -Q_L - A_P \dot{X}_R + \frac{V_{R1}}{B} \dot{P}_{R1} \tag{4.16}$$

The instantaneous fluid volumes in the rod- and piston-side chambers of the left and right struts, V_{L2} and V_{R1}, respectively, are given by:

$$V_{L2} = V_{0L2} - A_r X_L \ ; \quad V_{R1} = V_{0R1} - A_p X_R \tag{4.17}$$

where V_{0L2} and V_{0R1} are the initial fluid volumes in the corresponding chambers. The fluid flow rates to and from the struts, Q_1 and Q_2, are also related to the strut fluid flow rates from the flow continuity:

$$Q_1 = Q_{L1} + Q_{R2} \ ; \quad Q_2 = Q_{L2} + Q_{R1} \tag{4.18}$$

Upon substituting for fluid pressures in different chambers in terms of P_1 and P_2 from Eq. (4.12), the normalized fluid flow rates, $\overline{Q}_1$ and $\overline{Q}_2$, derived from Eqs (4.13) and (4.16), can be expressed as:

$$\begin{aligned}
\overline{Q}_1 &= +\left(\frac{2K_L \Delta P_m}{Q_{max}}\right)\left(\overline{P}_1 - \overline{P}_2\right) + \frac{\left(A_P \dot{\mathrm{X}}_\mathrm{L} + A_r \dot{\mathrm{X}}_\mathrm{R}\right)}{Q_{max}} + \frac{(V_{L1} + V_{R2})\Delta P_m}{B Q_{max}} (\dot{\overline{P}}_1) \\
\overline{Q}_2 &= -\left(\frac{2K_L \Delta P_m}{Q_{max}}\right)\left(\overline{P}_1 - \overline{P}_2\right) - \frac{\left(A_P \dot{\mathrm{X}}_\mathrm{R} + A_r \dot{\mathrm{X}}_\mathrm{L}\right)}{Q_{max}} + \frac{(V_{L2} + V_{R1})\Delta P_m}{B Q_{max}} \left(\dot{\overline{P}}_2\right)
\end{aligned} \tag{4.19}$$

Simultaneous solutions of Eqs. (4.11) and (4.19) yield the fluid pressures in the piston- and rod-side chambers of each strut, P_1 and P_2. Subsequently, the forces developed by the left and right struts, F_L and F_R, respectively, can be derived from:

$$F_L = P_1 A_p - P_2 A_r \; ; \quad F_R = P_2 A_p - P_1 A_r \tag{4.20}$$

The above strut forces derived from the kineto-dynamic model of the steering system are applied to the yaw-plane vehicle model, presented in the following section, to derive the steering torque applied to the two units and their directional responses to steering inputs.

4.3 Formulations of the 3-DOF Yaw Plane Vehicle Model

Assuming negligible contributions due to roll motions of the vehicle units, the directional dynamics of the ASV can be described by a 3-DOF yaw-plane model, as described in earlier studies [25, 26, 30] and shown in Fig. 4.4(a). The steering system and vehicle responses, however, would strongly depend upon the kinematics of the articulation struts, which were characterized by an equivalent linear articulation stiffness in the reported studies based on effective torque developed by the steering struts. In this study, the yaw plane vehicle model is formulated considering forces developed by the steering struts, derived from the kineto-dynamic steering system model, as shown in Fig. 4.4(b). The equations of motion for the yaw plane vehicle model are derived assuming: (*i*) small side-slip angles of tires; (*ii*) constant forward speed of the front unit; (*iii*) negligible contributions of the tire aligning moments; and (*iv*) the traction forces developed being balanced by the motion resistances, and expressed as:

Front-unit:

$$m_1(\dot{u}_1 - v_1\Omega_1) = F_{xf} + R_x$$

$$m_1(\dot{v}_1 + u_1\Omega_1) = F_{Tyf} + F_{yf} + R_y$$
$$I_1\dot{\Omega}_1 = L_{f1}F_{Tyf} - T_{sf} - L_{f2}R_y \tag{4.21}$$

Rear-unit:

$$m_2(\dot{u}_2 - v_2\Omega_2) = F_{xr} - R_x cos\varphi + R_y sin\varphi$$
$$m_2(\dot{v}_2 + u_2\Omega_2) = F_{Tyr} + F_{yr} - R_x sin\varphi - R_y cos\varphi$$
$$I_2\dot{\Omega}_2 = -L_{r1}F_{Tyf} + T_{sr} - L_{r2}(R_x sin\varphi + R_y cos\varphi) \tag{4.22}$$

where m_1 and m_2 are the masses of the front and rear units, respectively, and I_1 and I_2 are the respective yaw mass moments of inertia. (u_1, v_1, Ω_1) and (u_2, v_2, Ω_2) are the longitudinal, lateral and yaw velocities of the front and rear units, respectively. R_x and R_y are the internal forces at the articulation joint. The geometric parameters, L_{f1}, L_{r1}, L_{f2}, L_{r2} and T, are as shown in Figure 4.4. $F_{Tyf} = F_{y1}+F_{y2}$ and $F_{Tyr}= F_{y3}+F_{y4}$ are the total tire cornering forces developed at the front and rear axles, and F_{yi} ($i=1,\ldots, 4$) is the cornering force developed by tire i. (F_{xf}, F_{yf}) and (F_{xr}, F_{yr}) are the resultant strut forces acting on the front and rear units, respectively, along their body-fixed axis system, (x_1, y_1) and (x_2, y_2), given by:

$$F_{xf} = F_L \cos\alpha_1 + F_R \cos\beta_1 ; \qquad F_{yf} = F_L \sin\alpha_1 + F_R \sin\beta_1$$
$$F_{xr} = -F_L \cos\alpha_2 - F_R \cos\beta_2 ; \qquad F_{yr} = -F_L \sin\alpha_2 - F_R \sin\beta_2 \tag{4.23}$$

The steering torque acting on the front and rear units, T_{sf} and T_{sr}, are also derived from strut forces, as:

$$T_{sf} = (F_L \cos\alpha_1 - F_R \cos\beta_1)a + (-F_L \sin\alpha_1 - F_R \sin\beta_1)b$$

$$T_{sr} = (-F_L \cos\alpha_2 + F_R \cos\beta_2)c + (-F_L \sin\alpha_2 - F_R \sin\beta_2)d \tag{4.24}$$

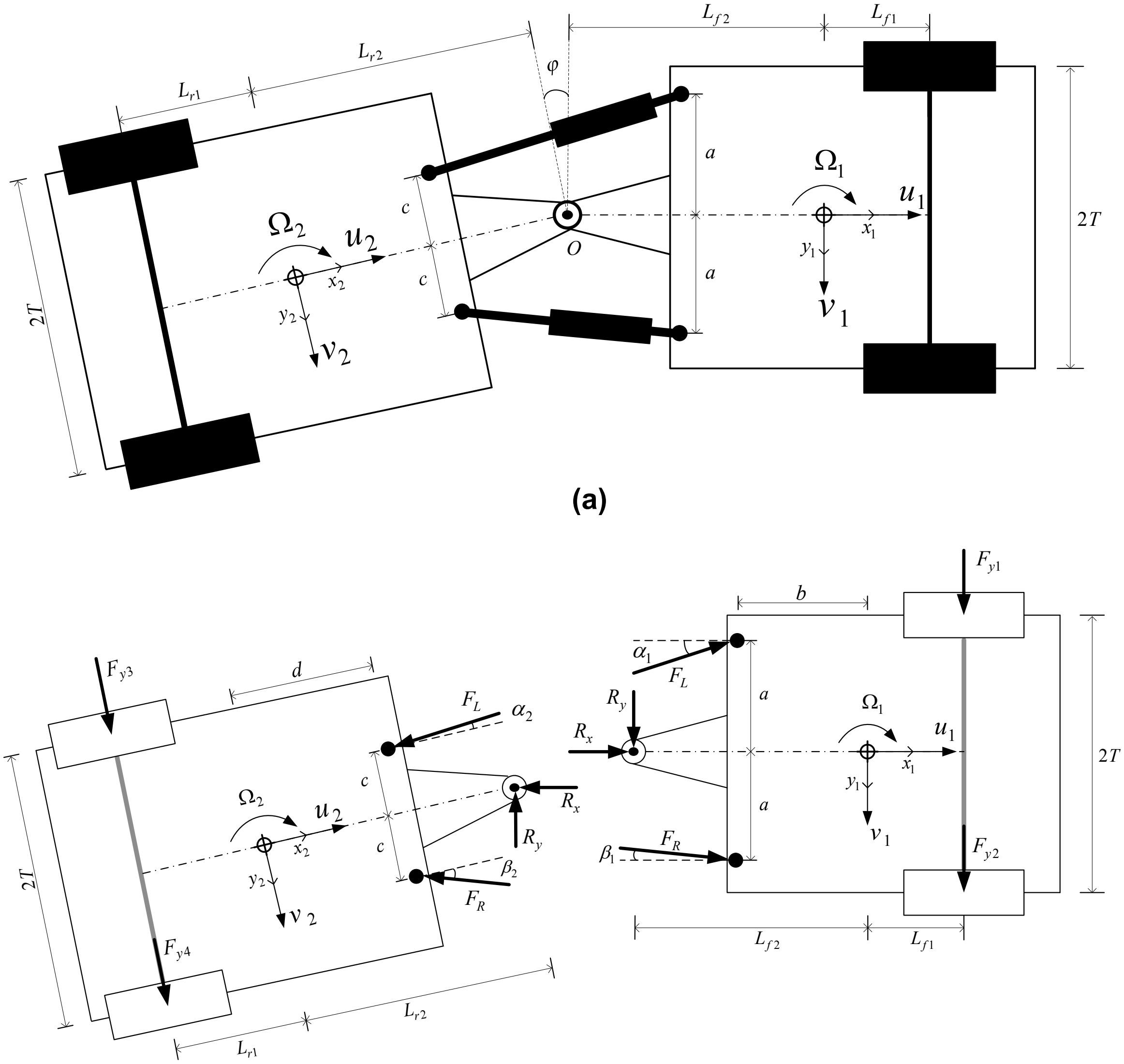

(a)

(b)

Figure 4.4 (a): Three-DOF yaw-plane model of an articulated dump truck; and (b) steering struts forces and their orientations.

The constraints posed by the articulation joint yield following relationships for the forward, lateral and yaw velocities of the two units:

$$\begin{aligned} u_2 &= u_1\cos\varphi - (v_1 - L_{f2}\Omega_1)\sin\varphi \\ v_2 &= u_1\sin\varphi + (v_1 - L_{f2}\Omega_1)\cos\varphi - L_{r2}\Omega_2 \\ \dot{\varphi} &= (\Omega_1 - \Omega_2) \end{aligned} \qquad (4.25)$$

where $\dot{\varphi}$ is the articulation rate. Assuming a constant forward speed of the front unit and eliminating the internal forces, R_x and R_y, Eqs. (4.21) to (4.25) yield the following equations of motion:

$$
\begin{aligned}
& m_0\dot{v}_1 - m_2\left(L_{f2}\dot{\Omega}_1 + L_{r2}\dot{\Omega}_2\right)cos\varphi \\
& \qquad = -m_0u_1\Omega_1 + m_2L_{r2}\Omega_2^2 sin\varphi - F_{xr}sin\varphi + \left(F_{Tyr} + F_{yr}\right)cos\varphi + F_{Tyf} + F_{yf}
\end{aligned}
$$

$$
\begin{aligned}
& \left(I_1 + m_2L_{f2}^2\right)\dot{\Omega}_1 - m_2L_{f2}\left(\dot{v}_1 - L_{r2}\dot{\Omega}_2\right)cos\varphi = m_2L_{f2}(u_1\Omega_1 - L_{r2}\Omega_2^2 sin\varphi) + T_{sf} + L_{f1}F_{Tyf} + \\
& L_{f2}F_{xr}sin\varphi - L_{f2}(F_{Tyr} + F_{yr})cos\varphi
\end{aligned}
$$

$$
\begin{aligned}
& (I_2 + m_2L_{r2}^2)\dot{\Omega}_2 - m_2L_{r2}\left(\dot{v}_1 - L_{f2}\dot{\Omega}_1\right)cos\varphi = m_2L_{r2}\left(u_1\Omega_1cos\varphi - (v_1\Omega_1 + L_{f2}\Omega_1^2)sin\varphi\right) + \\
& T_{sr} - L_{r1}F_{Tyr} - L_{r2}(F_{Tyr} + F_{yr}) \qquad (4.26)
\end{aligned}
$$

4.3.1 Tire lateral forces

Lateral force developed by an off-road tire can be derived considering first-order tire dynamics, which permits contribution of the tire relaxation (tire lag) [118, 224].The lateral force, F_{yi} (*i=1,…, 4*), is defined as a nonlinear function of the corresponding slip angle α_i, such that:

$$\tau_{yi}\dot{F}_{yi}(t) + F_{yi}(t) = -F_{zi}K_{yi}(1 - e^{-B_{yi}\alpha_i(t)})\,; \qquad (i = 1,\dots,4) \qquad (4.27)$$

where the relaxation time τ_y directly relates to relaxation length σ_y and the forward speed u such that: $\tau_y = \sigma_y/u$. In the above formulation, $K_{yi}B_{yi}$ is the cornering coefficient of tire i, which decreases with increasing normal load F_{zi}. The slip angles of the tires are derived as:

$$
\begin{aligned}
& \alpha_1 = \frac{v_1 + L_{f1}\Omega_1}{u_1 + T\,\Omega_1}; \qquad \alpha_2 = \frac{v_1 + L_{f1}\Omega_1}{u_1 - T\,\Omega_1}; \\
& \alpha_3 = \frac{v_2 - L_{r1}\Omega_2}{u_2 + T\,\Omega_2}; \qquad \alpha_4 = \frac{v_2 - L_{r1}\Omega_2}{u_2 - T\,\Omega_2}; \qquad (4.28)
\end{aligned}
$$

The kineto-dynamic model of the steering system together with the yaw dynamic model of the vehicle are solved simultaneously to determine responses of the coupled system and to seek design guidance for realizing enhanced direction performance and stability of the vehicle.

4.4 Method of Analysis

The simulations were initially performed under a 90º right-hand turn maneuver for the purpose of limited validation of the kineto-dynamic steering system model using the available measured data [197]. The simulation parameters of an un-loaded and loaded small size articulated dump truck are summarized in Table 4.1, which were mostly obtained from manufacturer specifications and personal communications [197]. Owing to the limited available data, the validation was limited only to responses of the steering struts in terms of pressure differences and piston travel. The steering wheel input, corresponding to the right-hand turn, estimated from the steering system kinematics and known strut deflection, is illustrated in Fig. 4.5(a). The validated model was subsequently used to derive response characteristics of the steering system and the vehicle under a ramp-step open-loop steady turning maneuver considering a constant forward speed of 15 km/h and a steering rate of about 0.52 rev/s, as shown in Fig. 4.5 (b).

Table 4.1 Simulation parameters.

Vehicle					
Parameter	Value	Parameter	Value	Parameter	Value
m_1	4200kg	L_{f1}	0.08m	c	0.25m
m_2 (Unloaded)	3350kg	L_{f2}	1.48m	b	1.39m
m_2 (Loaded)	13450kg	L_{r1} (Unloaded)	0.38m	d (Unloaded)	0.51m
		L_{r1}(Loaded)	0.68m	d (Loaded)	0.20m
I_1	4800 kg.m^2	L_{r2} (Unloaded)	1.16m	g	0.654m
		L_{r2} (Loaded)	0.86m		
I_2 (Unloaded)	3650 kg.m^2	T	1.0m	f	0.087m
I_2 (Loaded)	14200 kg.m^2	a	0.285m	σ_y	0.60m
		u_1	15km/h	R_w	0.65m
		K_y	0.65	B_y	6 rad^{-1}
Steering system					
Q_{max}	32 L/min	A_r	23 ×10^{-4} m^2	K_L	3×10^{-13}
P_S	230 bar	A_p	31 ×10^{-4} m^2	δ_{char}	6.70º
ΔP_m	110 bar	$(\delta_{sw})_{max}$	±2.62 rev.	$(L_1L_2)_0$	0.74m
V_{0L1}, V_{0L2}	1.5×10^{-3} m^3	φ_{max}	±35º	$(R_1R_2)_0$	0.74m
V_{0R1}, V_{0R2}	1.5×10^{-3} m^3	β	1×10^{9}Pa	$(P_1)_0$, $(P_2)_0$	100 bar

The kineto-dynamic responses of the steering system were evaluated in terms of instantaneous orientations of the left- and right-struts, (α_1, α_2) and (β_1, β_2), strut deflections (X_L, X_R), normalized steering valve opening percentage ($\overline{X}_V$) fluid pressure (P_1, P_2), and resultant strut forces (F_L, F_R) and torque developed by the resultant struts forces about the articulation joint (T_o), which are functions of the steering system geometry and instantaneous strut orientations. The vehicle responses are also evaluated in terms of tire cornering forces and slip angles using Eqs. (4.27) and (4.28), and the articulation angle. Owing to significant affects of the load, the analyses are performed for both the loaded and unloaded vehicles, assuming negligible load transfer through the articulation joint. The sensitivity of the steering system and vehicle responses to variations in selected operating and design parameters on the directional response and stability characteristics of the vehicle are further evaluated to seek design guidance. This included variations in the steering system design and operating parameters, namely steering rate ($\dot{\theta}_{sw}$), leakage flows Q_L, the maximum flow rate Q_{max}, characteristic articulation error δ_{char}, and initial orientations of the struts. The results are used to identify desirable design parameters for realizing enhanced yaw stability of the vehicle.

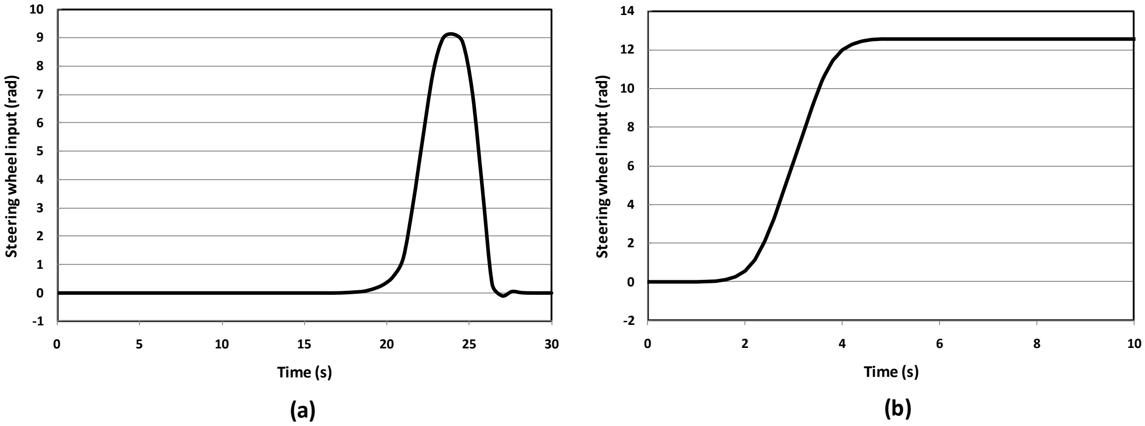

Figure 4.5: (a) Steering wheel input corresponding to the 90 degrees right-hand turn maneuver; and (b) Steady-turning (ramp-step) input.

The yaw stability of the vehicle was evaluated in terms of articulation angle response of the vehicle and its rate of decay under a pulse steering input. A smoothed trapezoidal-pulse with duration of 0.5 s and peak amplitude of 100 degrees was synthesized for this purpose. Under this pulse steering input, the articulation angle response follows an oscillatory form in which the peaks of the absolute amplitudes of the response follow an exponential curve. The rate of decay of peaks in the oscillatory articulation response is described by an exponential function of the form, $\varphi = \Phi_0 e^{\rho t}$, as presented in [30], where Φ_0 is a constant and ρ defines the exponential decay of the articulation angle. While a positive value of ρ denotes a diverging response, $\rho < 0$ would yield a stable directional response, although the response could be oscillatory. The influences of variations in the steering system parameters on ρ are also investigated for both loaded and unloaded vehicles.

4.5 Results and Discussions

4.5.1 Model validation

Figures 4.6(a) and 4.6(b) illustrate comparisons of responses of the unloaded vehicle model with the available field-measured data for the 90º right-turn maneuver, shown in Fig. 4.5(a), in terms of pressure difference (P_1 -P_2) and the left piston travel, respectively. The simulation results show zero pressure difference and piston travel up to about 20s prior to application of the steering input, while the measured data reveals small variations that are mostly attributed to corrective steering and steering system compliance. The pressure difference and the strut deflection increase rapidly with application of steering wheel input and decrease as the steering wheel input diminishes.

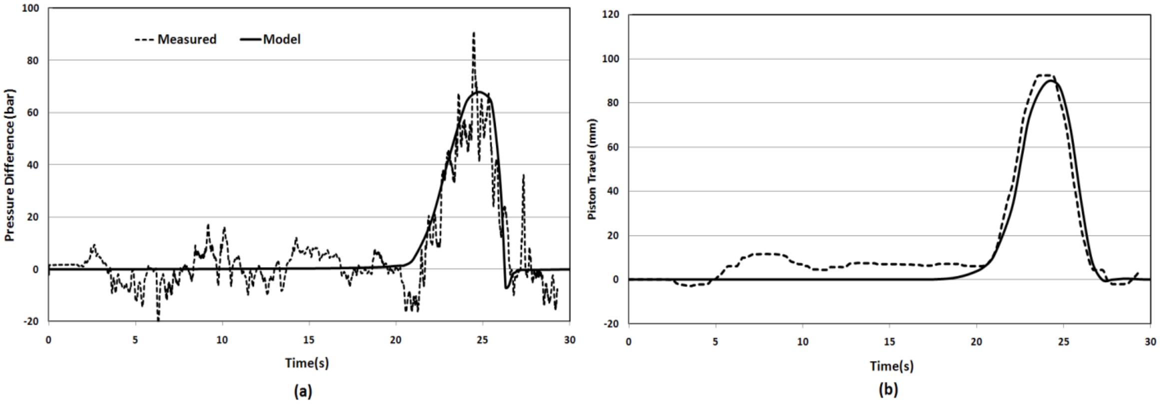

Figure 4.6: Comparisons of left strut pressure difference and piston travel responses derived from the kineto-dynamic model under the 90-degrees right-hand turn maneuver with the measured data: (a) pressure difference; and (b) piston travel (U=15 km/h).

The comparisons show reasonably good agreements of the model responses with limited available measured data, although some discrepancies between the two are also evident. In particular, the measured responses exhibit substantial high frequency variations in the strut pressure, which may be attributed to tire interactions with the terrain and compliance of the steering mechanism. The articulation angle and path trajectory of the two units obtained for the unloaded vehicle model are also shown in Figs. 4.7(a) and 4.7(b), respectively. The variations in the articulation angle follow the steer input, as it would be expected.

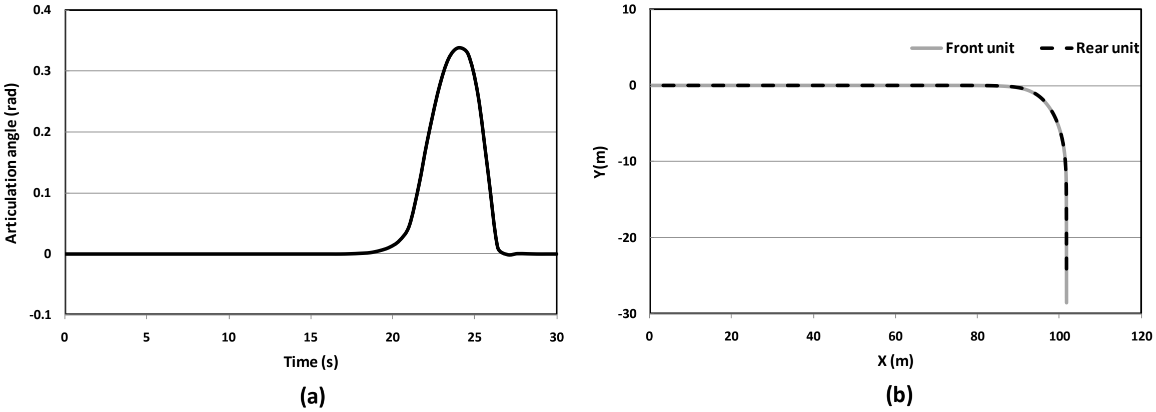

Figure 4.7: (a) Articulation angle; and (b) Path trajectories of the front and rear units of the unloaded vehicle subject to 90-degrees right-hand turn maneuver (U= 15km/h).

4.5.2 Steady-state response characteristics of the steering system

Fig. 4.8 illustrates responses in terms of articulation angle, normalized valve opening $\overline{X}_V$, and strut orientations and travel for both the unloaded and loaded vehicles under the ramp-step steer input shown in Fig. 4.5(b). The strut orientation responses, however, are presented only for the loaded vehicle, which were very close to those of the unloaded vehicle. The struts deflections and articulation angle responses of the loaded vehicle increase slightly slowly compared to the unloaded vehicle but approach identical steady values. This may be partly caused by increased flow demand of the loaded vehicle, which is evident from saturation of the valve opening in Fig. 4.8(b). In case of the unloaded vehicle, however, the valve remains only partly open during the entire maneuver to meet the articulation torque demand.

The results further show asymmetric variations in orientations of the left and right struts, as shown in Fig. 4.8(d). The orientations of the left- and right-struts with respect to the front unit (α_1 and β_1) vary far more than those of the struts with respect to the rear unit (α_2 and β_2). In a similar manner, for the given geometric configuration, the right- and left-struts also exhibit asymmetric deflections for both loaded and unloaded vehicles, as seen in Fig. 4.8(c), which is attributable to geometric nonlinearities of the frame steering mechanism. Moreover, higher pressure difference across the strut pistons results in higher leakage flows through piston seals in case of the loaded vehicle, where the valve remains slightly open in the steady conditions.

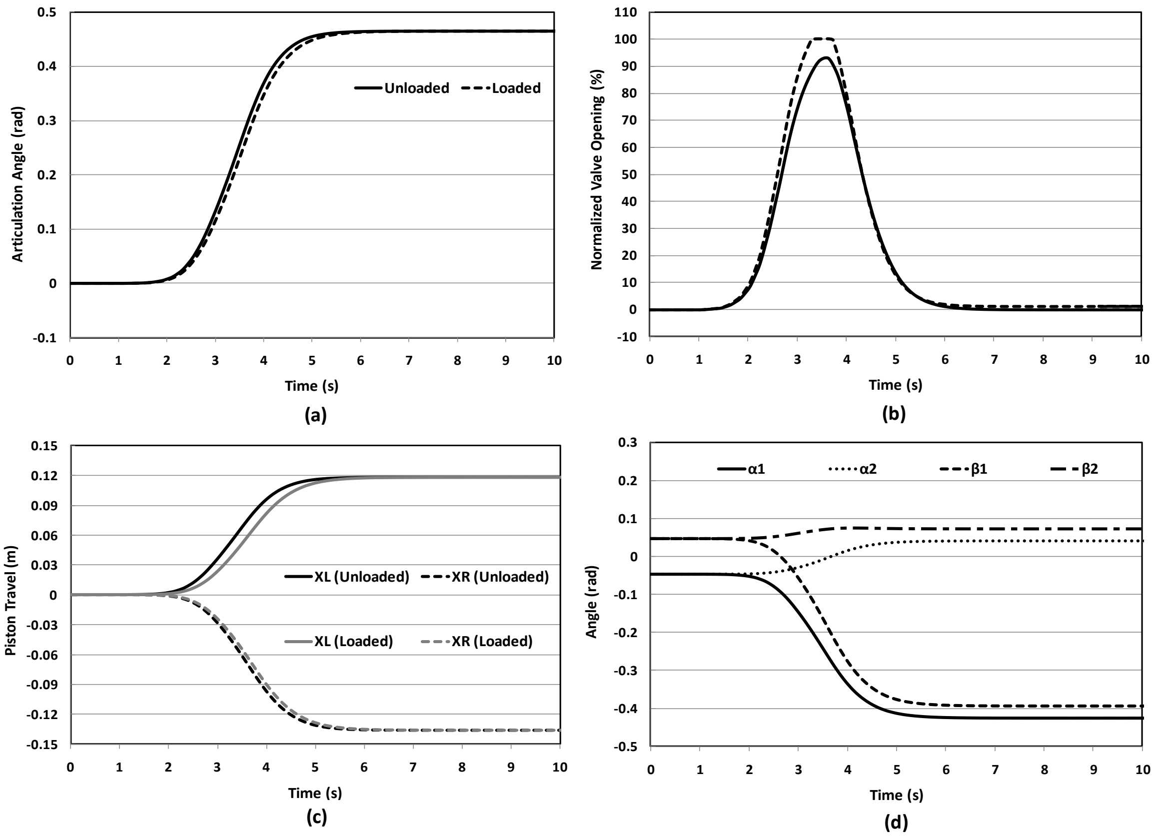

(a) (b)

(c) (d)

Figure 4.8: The steady-steer responses of the loaded and unloaded vehicles and steering struts: (a) articulation angle; (b) normalized valve opening; (c) strut deflections; and (d) strut orientations (U= 15km/h).

Asymmetry in the steering strut responses is also evident from the fluid pressure in the strut, and the resultant strut forces and steering torque at the articulation joint, as seen in Fig. 4.9. The Fig. 4.9(a) shows variations in pressure difference of the left strut, forces developed by the two struts (F_L and F_R) and effective torque developed at the articulation joint of the loaded and unloaded vehicle models. It should be noted that in the absence of a steer input both the struts impose identical forces on the two units, which is attributed to equilibrium fluid pressure and effective working area of the strut (cross-section area of the rod, A_p -A_r). The flow of fluid to/from the struts causes the pressure difference across the piston, and thus the strut forces and torque to increase until the vehicle assumes a steady trajectory.

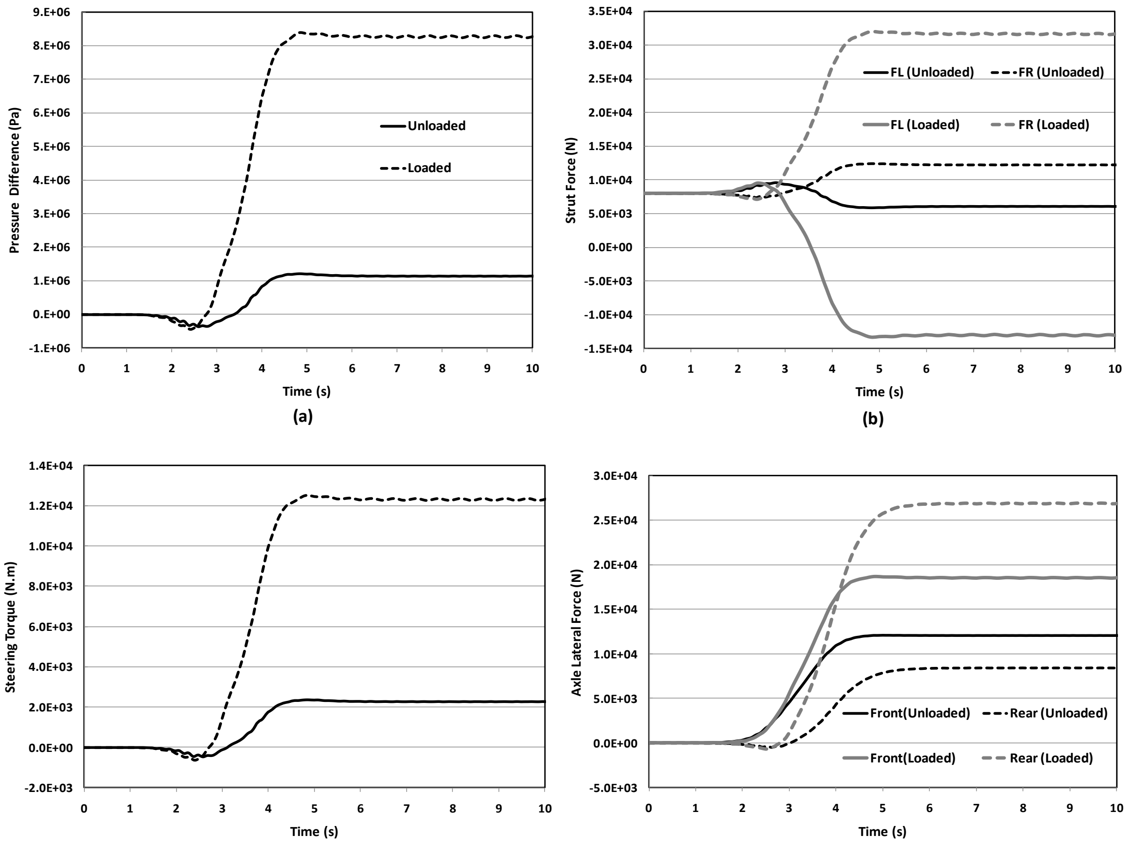

(a) (b)

(c) (d)

Figure 4.9: Responses of the steering struts of the loaded and unloaded vehicle subject a steady-turning steer input: (a) pressure difference across the strut pistons; (b) right- and left-struts forces, F_L and F_R; (c) steering torque at the articulation joint; and (d) front- and rear-axle cornering forces(U=15 km/h).

The loaded vehicle places a greater demand for the strut forces and articulation torque, as seen in Fig. 4.9(b) and 4.9(c), respectively, which causes relatively greater cornering force demand on the tires of the loaded vehicle, as seen in Fig. 4.9(d). The total cornering force developed by the tires is considerably larger for the loaded vehicle than for the unloaded vehicle, which also yields greater side-slip angles of the loaded vehicle tires. The lateral force developed by the front axle tires of the unloaded vehicle and the corresponding slip angles are higher than those for rear axle. An opposite trend, however, is evident for the loaded vehicle, which is attributed to considerably higher rear axle load of the loaded vehicle.

Parameter sensitivity analysis

In addition to the vehicle load, the steering system responses greatly depend on various operating and design parameters of the vehicle and the steering system including vehicle speed, rate of steering, maximum valve flow rate, characteristic articulation angle error, struts orientations and leakage flows through the piston seals. The influences of variations in these parameters on the steady-steering responses of the loaded vehicle are investigated by varying only a selected parameter, while retaining others to their respective nominal values (Table 4.1). The results attained could provide important guidelines on the articulated steering system.

The influence of variations in vehicle forward speed on selected responses of the loaded vehicle and the steering system are initially obtained by considering forward speeds of 10 and 20 km/h in addition to nominal speed of 15 km/h, as seen in Fig. 4.10. An increase in forward speed resulted in significant increase in lateral acceleration of the front- and rear-unit, which results in significantly larger axle cornering forces, as seen in Figs. 4.10(a) and 4.10(b). While the rear unit lateral acceleration increases relatively slowly compared to the front unit, both units approach nearly identical steady-state lateral acceleration. Greater axle forces at a higher speed also impose a higher demand for steering torque and thus the strut forces, as seen in Figs. 4.10(c) and 4.10(d), respectively. The pressure difference across struts piston thus also increases with increasing speed, as seen in Fig. 4.10(e), while the maximum steering valve openings corresponding to 15 and 20 km/h speeds remain the same due to valve saturation, as seen in Fig. 4.10(f). The valve opening increases rapidly with increase in the steering input and approaches its maximum value near 3.2 s prior to the maximum steer input that occurs near 4 s. subsequently, the valve opening saturates to its maximum value (X_{Vmax}) and diminishes as the vehicle combination approaches desired steady articulation angle.

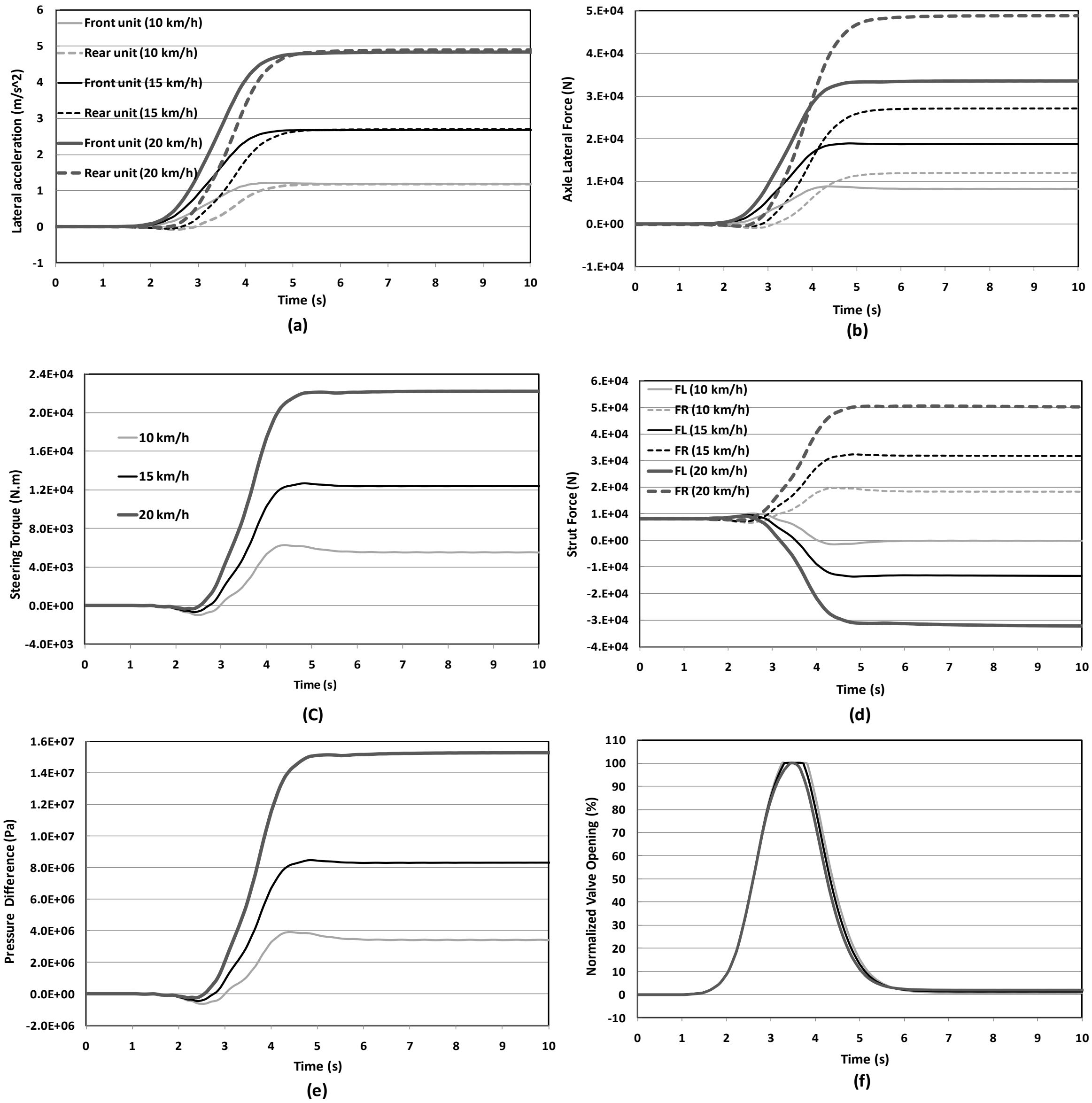

Figure 4.10: Effect of the forward speed on: (a) lateral acceleration of the front and rear units; (b) lateral forces due to front and rear unit axle tires; (c) steering torque; (d) struts forces; (e) pressure difference across the struts pistons; (f) normalized valve opening.

The steering system responses, particularly the flow demands, are most significantly affected by the rate of steering input. The influence of steering rate on the steering system and vehicle responses are evaluated by considering ±25% variations about the nominal steering rate, which rate of steering shown in Fig. 4.5(b). An increase in steering rate yields higher struts velocities and articulation rate, which poses greater flow demand, as seen in Fig. 4.11. The strut deflections and articulation angles, however, converge to identical steady values, irrespective of the steering rate, as expected. The higher flow demand corresponding to a rapid steering causes rapid valve opening and greater saturation, as seen in Fig. 4.11(c). This together with fluid compressibility yields oscillations in pressure difference across the struts pistons, and thus the articulation torque, as seen in Figs. 4.11(e) and 4.11(f). A higher steering rate may thus lead to oscillations in the articulation angle and thus weaving motion of the vehicle.

The steering valve saturation is directly related to characteristic articulation angle error δ_{char}. Fig. 4.12 illustrates dependency of the system responses on δ_{char}, which is varied by ±25% around its nominal value. The Fig. 4 shows responses in terms of normalized valve opening $\overline{X_V}$, normalized flow rate $\overline{Q_1}$, articulation angle, pressure difference across the struts pistons, and steering torque at the articulation joint. A lower value of δ_{char} causes rapid valve opening and saturation, and a higher flow rate. A rapid articulation angle response could thus be obtained with a lower δ_{char}, as seen in Fig. 4.12(b). A further decrease in δ_{char} by -50%, however, causes oscillations in the responses during valve closing and may lead to snaking instability. This is evident from the divergent pressure differential and steering torque responses, where δ_{char} is reduced by 50%, as seen in Figs. 4.12(d) and 4.12(e), respectively. This is most likely caused by relatively higher fluid pressure in the struts.

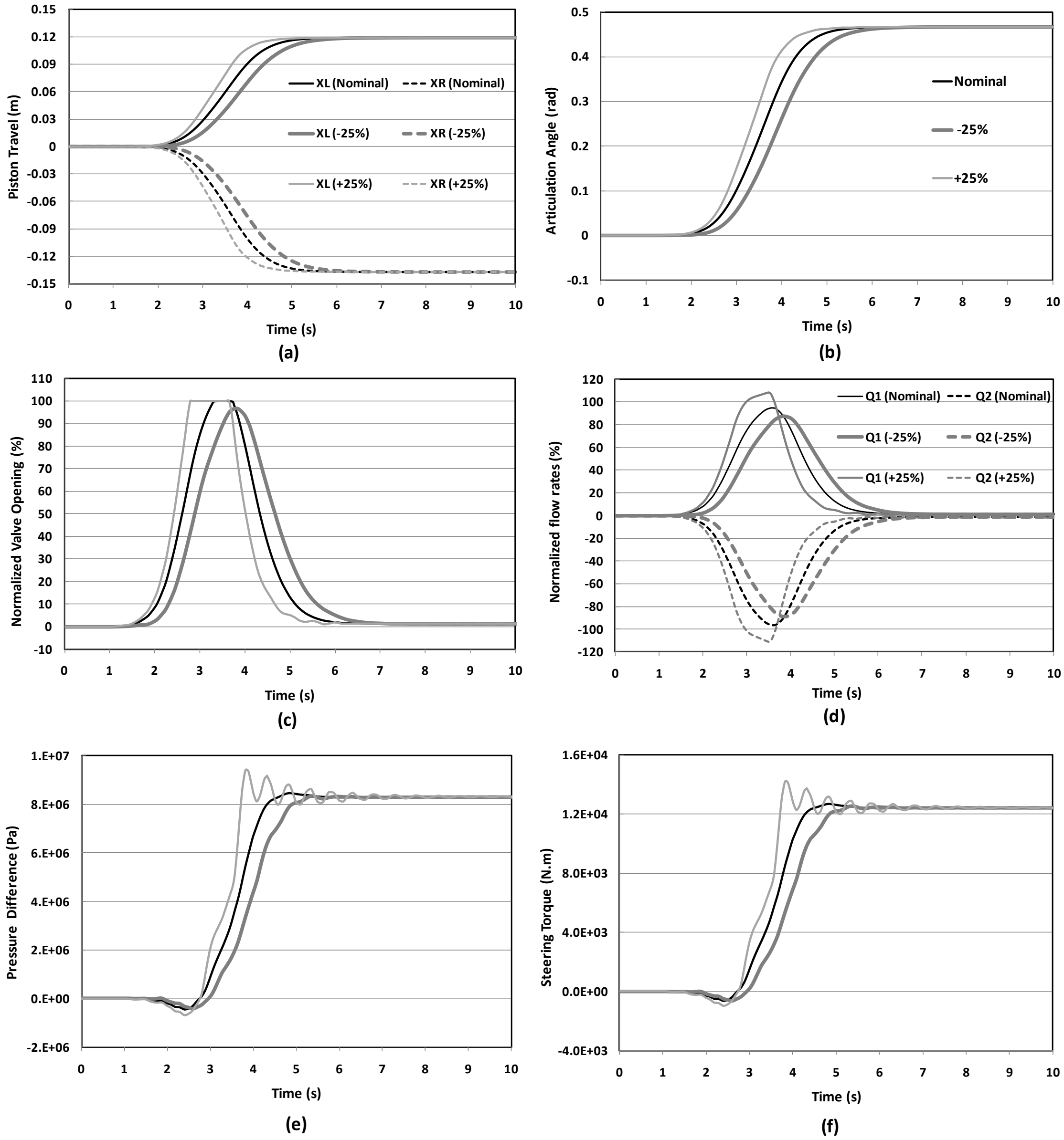

Figure 4.11: Effect of rate of steering input on: (a) struts travel; (b) articulation angle; (c) normalized valve opening; (d) normalized flow to/from the struts, $\overline{Q}_1$, $\overline{Q}_2$; (e) pressure difference across the struts pistons; and (f) steering torque at the articulation joint.

Flow saturation attributed to maximum valve opening could be circumvented by increasing the maximum valve flow rate Q_{max}, as seen in Fig. 4.13(a). The corresponding pressure differential across the strut piston increases leading to a slightly higher steering torque, as seen in Fig. 4.13 (b). With an increase in maximum valve flow-rate, the valve remains only partly open to meet the flow demand of the system, which yields slightly faster steering torque response. Conversely, a reduction in valve flow rate by 25% causes valve opening saturation for a relatively longer duration, while the steering torque and thus the articulation angles approach their respective steady-values at a slightly slower rate. Irrespective of the maximum valve flow, the vehicle and the steering system approach identical steady values. A further increase in Q_{max} by 75%, however, yields oscillatory responses during valve closing and may lead to weaving motion of the vehicle, which is also evident from the divergent pressure differential and steering torque responses, as seen in Figures 4.13(c) and 4.13(d), respectively. This is most likely caused by relatively higher fluid pressure in the struts.

The results in Figs. 4.10 to 4.13 suggest that reducing the maximum valve flow-rate or increasing the characteristic articulation angle error would result in higher steering response time. This can be associated with relatively higher effective damping of the steering system. The reported studies have characterized the hydraulic frame steering system by equivalent torsional damping and stiffness at the articulation joint [25, 26, 28-30, 177, 178]. These have shown that a higher torsional damping of the articulation system is desirable for enhanced snaking stability limits of the vehicle through the steering system.

The leakage flows through the piston seals can also significantly alter effective damping of the steering system and thus the yaw responses of the vehicle. The leakage flows across the piston are dependent upon the pressure difference, hydraulic fluid properties, and the leakage area, and are described by the flow leakage coefficient K_L considering laminar flow. The effect of leakage flows through the piston seals on the system responses is thus investigated by considering three different values of K_L: K_L=0 (no leakage); $K_L=3\times10^{-13}$ (nominal); and $K_L=15\times10^{-13}$ (greater leakage). Fig. 4.14 illustrates the influence of variations in K_L on selected kineto-dynamic responses of the steering system including normalized valve opening, normalized leakage flows $\overline{Q}_L$, normalized flow rates, $\overline{Q}_1$ and $\overline{Q}_2$ fluid pressures, P_1 and P_2, pressure difference, steering torque, and articulation angle.

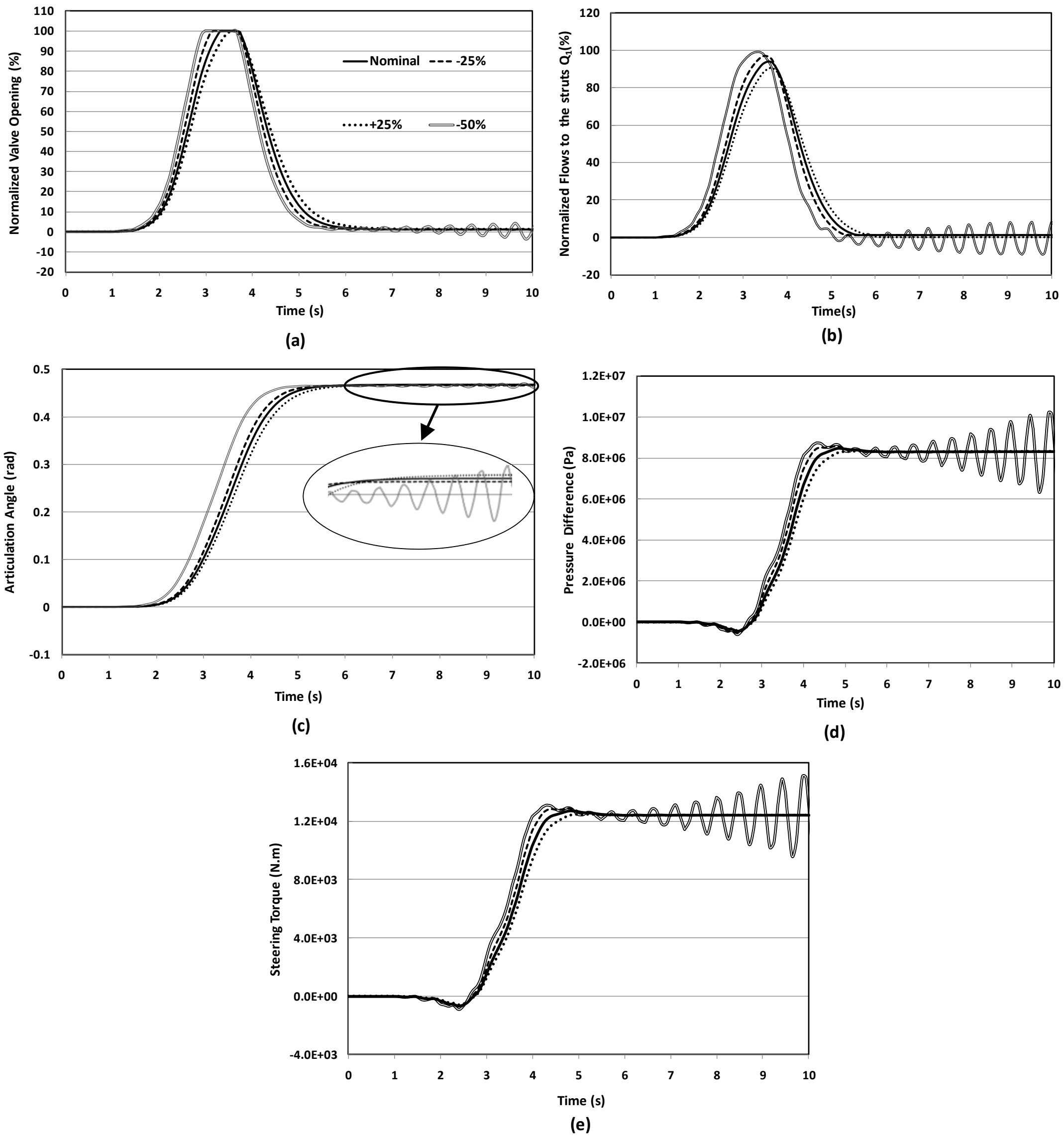

Figure 4.12: Effect of the characteristic articulation angle error δ_{char} on: (a) normalized valve opening; (b) normalized flow rate, $\overline{Q}_1$; (c) articulation angle; (d) pressure difference across the struts pistons; and (e) steering torque at the articulation joint.

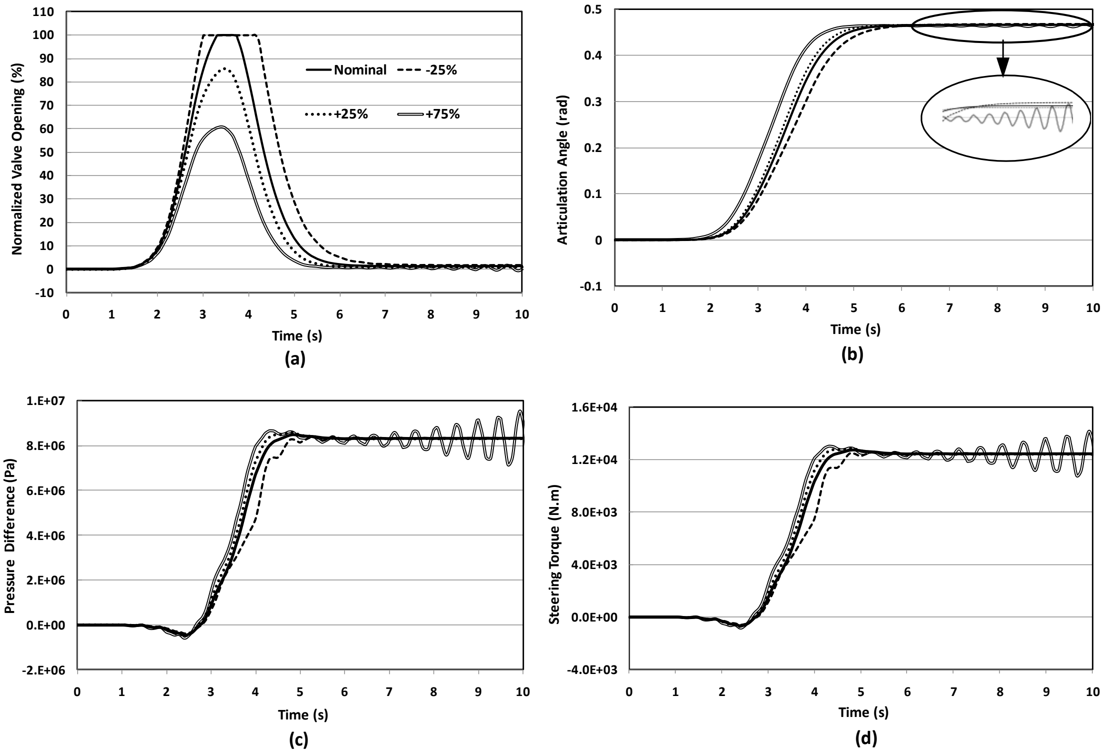

Figure 4.13: Effect of the maximum valve flow rate Q_{max} on: (a) normalized valve opening; (b) articulation angle; (c) pressure difference across the struts pistons; and (d) steering torque at the articulation joint.

As expected, variations in K_L yield only minimal changes in pressure difference across the struts pistons, while the leakage flow increases for a higher value of K_L. For a higher leakage flow, however, the flow rates, $\overline{Q}_1$ and $\overline{Q}_2$, converge to non-zero values, which suggests continued flow demand due to higher leakage apart from the fluid compressibility effect. This is also evident from Fig. 4.14(a), which shows that the valve remains slightly open in the steady-state, when a higher value of K_L is considered. In this case, the fluid pressures in the strut chambers also continue to decrease, although the pressure difference and steering torque approach their respective steady values, as seen in Figs. 4.14(d), 4.14(e) and 4.14(f), respectively. The fluid pressures in the chambers, however, approach steady values in the absence of the leakage flows (K_L=0), as seen in Fig. 4.14(d). While the leakage flows contribute to effective damping of the steering mechanism, too large a leakage imposes continued flow demand and alters the articulation angle response slightly, as seen in Fig. 4.14(g).

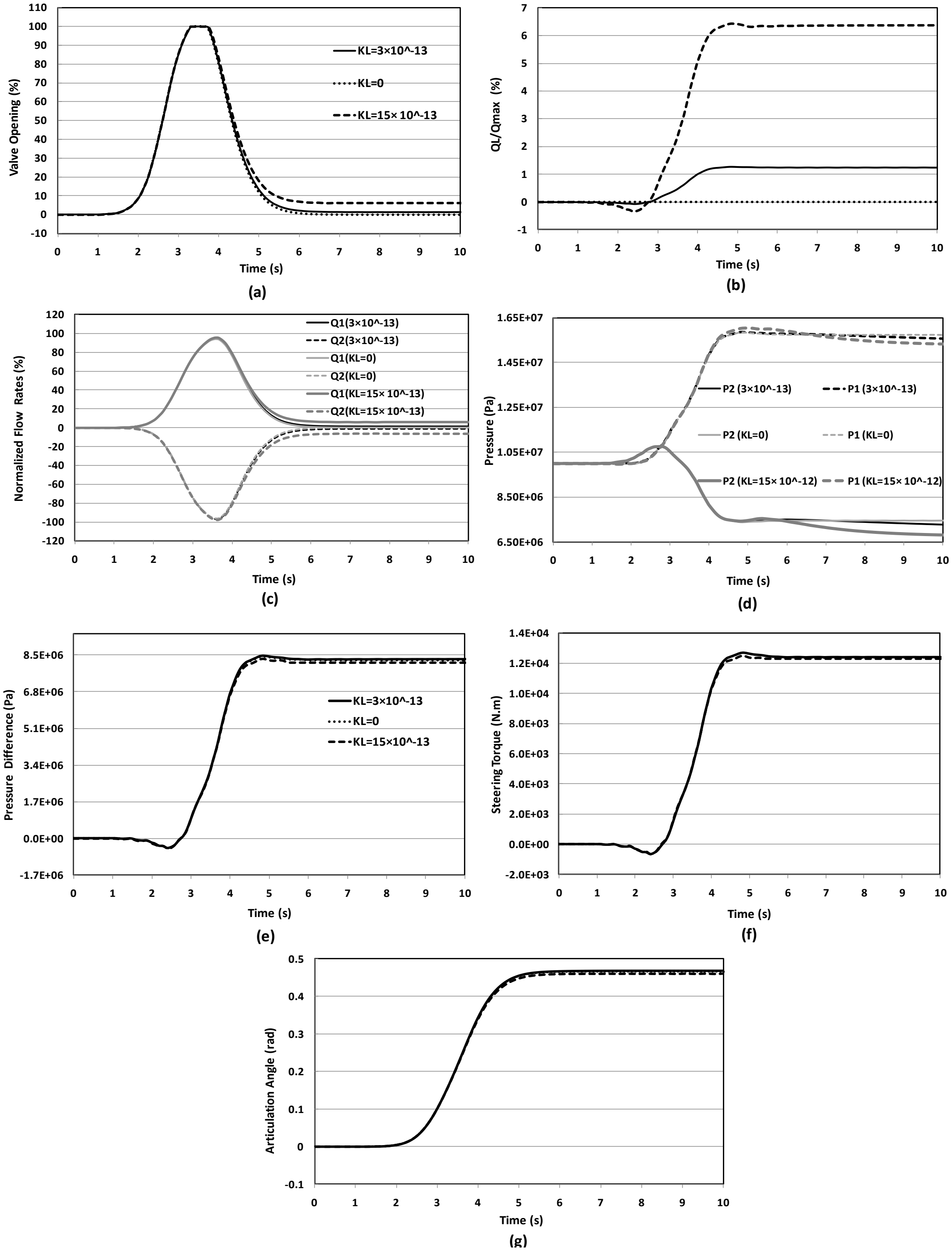

Figure 4.14: Effect of leakage coefficient on:(a) normalized valve opening; (b) normalized leakage flow $\overline{Q}_L$; (c) normalized flow rates, $\overline{Q}_1$, $\overline{Q}_2$; (d) fluid pressures P_1 and P_2; (e) pressure difference across the strut piston; (f) steering torque developed; and (g) articulation angle.

The response characteristics of the vehicle and steering system and the effective damping of the steering mechanism are also dependent upon its kinematics apart from the flow characteristics. The sensitivity of the system responses to steering system geometry is further examined by considering variations in orientations of the left- and right-struts with respect to the longitudinal axes of the front (α_1 and β_1) and rear (α_2 and β_2) units, which are function of lateral spread of the struts mounts on the front and rear units and length of the struts, as described in Eqs. (4.1) to (4.3) and shown in Fig. 4.1. The influence of variations in struts orientations is investigated considering two sets of geometric parameters. In the first case, lateral spread of strut mounts on the lead unit (parameter a) is increased by 15%, while that of the mounts on the rear unit (parameter c) is decreased by 15% from the respective nominal value. This causes the orientation angles (α_1, α_2) and (β_1, β_2) to increase to -8.8° and 8.8°, respectively from the nominal values of -2.7° and 2.7°. In the second case, parameter a is decreased by 15%, while parameter c is increased by 15%, which resulted in $\alpha_1 = \alpha_2$=3.5° and $\beta_1 = \beta_2$=-3.5°.

The effect of such variations in steering system responses are illustrated in Fig. 4.15, where the simulation runs are denoted by respective angle $\alpha = \alpha_1 = \alpha_2$. A decrease in lateral spread c (α=-8.8°) yields greater struts deformations and thus greater flow demand that causes the valve to saturate relatively rapidly, as seen in Fig. 4.15(a) to 4.15(c), respectively. This yields relatively lower pressure differential and thus lower forces developed by the struts, as seen in Figs. 4.15(d) and 4.15(e), respectively. The greater kinematic advantages, however, cause steering torque, comparable to the nominal case, to achieve the desired articulation angle. Increasing the lateral spread c (α =3.5°) results in lower initial struts lengths and struts deflections compared to the nominal case. This poses a lower flow demands and thus the valve remains only partly open during the entire maneuver. The pressure differential and thus the struts forces, however, tend to be higher.

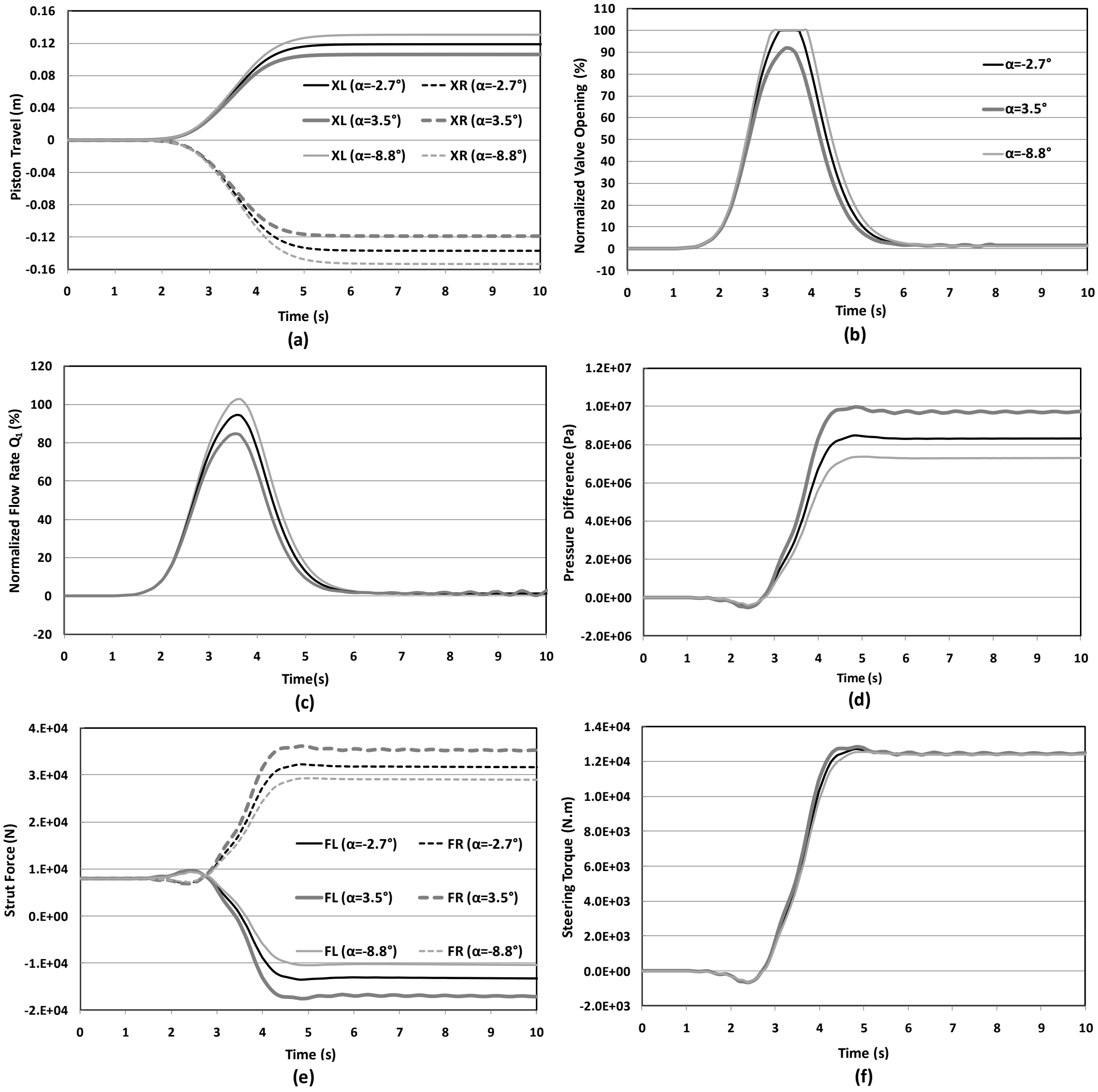

Figure 4.15: Influence of variations in struts orientations on:(a) struts deflections; (b) normalized valve opening; (c) normalized flow rate to the struts $\overline{Q}_L$; (d) pressure difference across the strut pistons; (e) resultant strut forces; and (f) steering torque developed at the articulation joint.

4.5.3 Yaw stability analysis

The snaking instability of ASVs has been evaluated through eigen-analysis of the vehicle model assuming linear equivalent stiffness and damping properties of the steering mechanism, and linear tire cornering properties [25,26,30,177]. For the non-linear kineto-dynamic model considered in this study, the snaking stability can be evaluated from articulation angle response of the combination under a pulse steering input, where a divergent response would indicate a yaw or snaking instability of the vehicle [30]. As an example, Figs. 4.16(a) and 4.16(b), respectively, illustrate articulation responses of the unloaded and loaded vehicle models subject to a pulse steering input at a forward speed of 15 km/h. The results show oscillatory yaw responses of the vehicles with oscillation frequencies of 4 Hz and 2.3 Hz for the unloaded and loaded vehicles, respectively. The amplitudes of oscillations tend to decay in an exponential manner indicating stable yaw response, while the oscillation frequency represents the snaking mode frequency. This frequency greatly depends on inertias of the two units, the steering system kinematics and flexibility, which has been characterized by an equivalent torsional stiffness at the articulation joint [25,26,30,177]. Apart from the frequency, the rate of decay of oscillations, ρ, is also an important indicator of the snaking stability, in-particular, the effective system damping, which is further dependent upon the vehicle speed. A snaking mode diagram, illustrating variations in ρ with vehicle speed, is used to study the effects of the selected kineto-dynamic design parameters of the steering system on the snaking stability of the vehicle.

The snaking mode diagrams of the unloaded and loaded vehicle models with nominal steering system parameters (Table 4.1) are illustrated in Fig. 4.17. The results suggest lightly damped snaking mode at low forward speeds. The rate of decay of oscillations increases with speed up to 30 and 45 km/h for the unloaded and loaded vehicles, respectively. The addition of load to the rear body of the vehicle would result in lower decay rate at speeds below 37km/h, as seen in Fig. 4.17. The rate of decay of yaw oscillations tends to decrease with increase in speed beyond 30 and 45 km/h for the unloaded and loaded vehicles. This suggests greater yaw oscillations or snaking tendencies of the vehicles at higher speeds. The results show that the decay rate of the loaded vehicle approaches a positive value ($\rho > 0$) at a speed of 90 km/h, where the yaw response would be divergent. The unloaded vehicle exhibits yaw instability at a relatively higher speed of 120 km/h. Relatively lower stability limit of the loaded vehicle is attributable to greater inertia of the rear unit and shifting of the rear unit center of mass toward the articulation joint, which can further deteriorate the snaking stability of the vehicle [30]. The observed stability limits are considerably higher than those reported in earlier studies [25, 26, 30, 177], which do not consider the damping effect due to leakage that tends to enhance the stability limit. The obtained trend of the obtained snaking mode diagram is comparable to that obtained by He et al. (2005) for 3 DOF model of forestry skidder with equivalent torsional stiffness of (2×10^5) at articulation joint and also with the results obtained by Rehnberg and Edrén [236] for a planar linear model of wheel loader considering no extra weights.

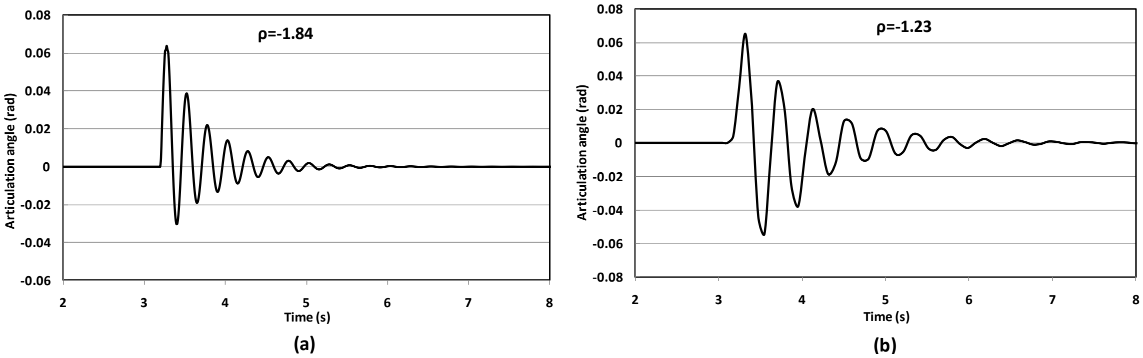

Figure 4.16: Examples of articulation angle responses corresponding to a stable snaking mode of (a) unloaded; and (b) loaded vehicle (U=15 km/h).

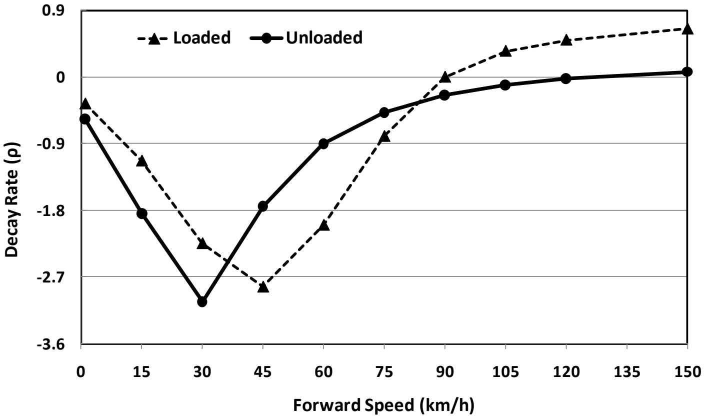

Figure 4.17: Influence of the vehicle speed on the snaking stability of the unloaded and loaded vehicles.

Parametric sensitivity analysis

The yaw oscillations and snaking stability of the vehicle greatly depend on many kineto-dynamic design parameters of the steering system, apart from the vehicle geometry and inertia, and tire properties. The influences of variations in selected kineto-dynamic design parameters of the steering system on the decay rate of yaw oscillations and snaking stability are investigated. These include the characteristic articulation angle error δ_{char}, maximum flow rate through the valve Q_{max}, leakage flows Q_L, and struts orientations, where only a selected parameter is varied at a time, as described in the previous section.

The effective damping of the steering mechanism is directly influenced by the leakage flows Q_L, characteristic articulation angle error δ_{char} and the maximum valve flow rate Q_{max}. The leakage flows across the piston seals, in-particular, affect the effective damping significantly. Figure 4.18 illustrates the effect of leakage flow coefficient on the decay rate ρ of both the loaded and unloaded vehicles. The results are presented for K_L=0 (no leakage), K_L=3×10^{-13} (nominal) and K_L=15×10^{-13} (enhanced leakage). The absence of leakage flows (K_L=0) yields lowest decay rate and thus the effective damping. The results exhibit that critical speed of the vehicles decrease to nearly 60 km/h in absence of leakage. The observed stability limits for K_L=0 are quite comparable with those reported in earlier studies considering equivalent torsional stiffness of the steering mechanism at the articulation joint [25, 26, 30, 177]. Introducing the leakage flows across the piston seals results in higher effective damping and thus considerably higher stability limits. While a higher leakage flow seems to be beneficial for enhanced snaking stability limit of the vehicle, too high a leakage flow would yield continuous valve opening to provide sufficient steering torque and may lead to failure of the hydraulic steering system.

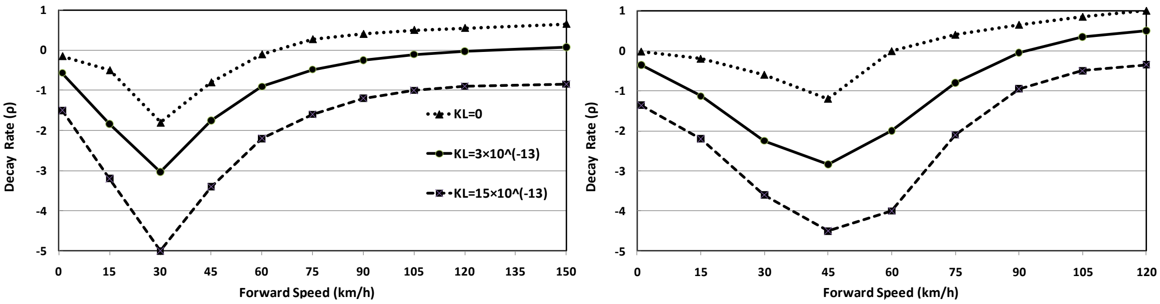

(a) (b)

Figure 4.18: Influence of variations in leakage flow on the decay rate of yaw oscillations of the: (a) unloaded; and (b) loaded vehicles.

The influences of variations in the characteristic articulation angle error and maximum valve flow rate on the yaw oscillation decay rates of the unloaded and loaded vehicles are shown in Fig. 4.19. The results are obtained considering ±25% variations in both the parameters about their respective nominal values. The results suggest that an increase in δ_{char} or a decrease in Q_{max} would yield relative greater damping effect and thereby higher yaw stability limits. This is mainly attributed to relatively slower opening of the steering valve and higher pressure drop across the steering valve. A lower value of δ_{char} or a higher Q_{max} yields lower stability limits of both unloaded and loaded vehicles, compared to those obtained for the nominal parameters. The results show that the critical speeds or yaw stability limits of the unloaded vehicle decrease to 85 and 90 km/h, respectively for -25% and +25% variations in δ_{char} and Q_{max}. For the loaded vehicle, the corresponding stability limits decrease to about 75 and 80 km/h, respectively. The maximum decay rates of yaw oscillations, however, occur at the same forward speeds, near 30 km/h and 45 km/h for the unloaded and loaded vehicles.

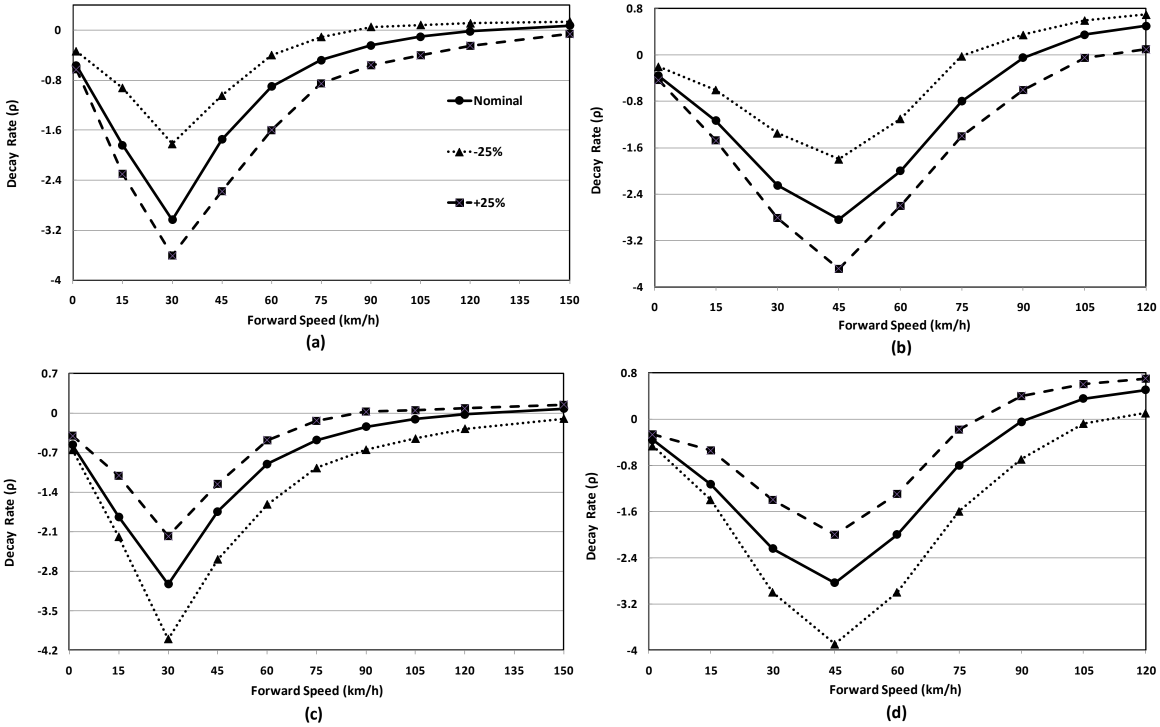

Figure 4.19: Influence of variations in characteristic articulation angle error δ_{char} and maximum valve flow-rate Q_{max} on the rate of decay of yaw oscillations of the vehicles: (a) δ_{char}-unloaded; (b) δ_{char} -loaded; (c) Q_{max}-unloaded; and (d) Q_{max} -loaded.

The results in Figs. 4.18 and 4.19 suggest that effective damping of the steering mechanism greatly depends on dynamic flow properties of the steering system coupled with dynamics of the vehicle. Such dependencies may not be adequately characterized by a linear equivalent torsional stiffness and damping model of the steering mechanism as reported in [25-27, 29, 30]. Furthermore, the reported equivalent models cannot describe the steering system kinematics, which also affects the yaw stability limits of the vehicle. The influence of the steering system kinematics on the snaking stability of the unloaded and loaded vehicles is examined by considering different orientations of the struts (α = -8.8°; -2.7°; 3.5°), as described in the previous section. Fig. 4.20 illustrates the effect of struts orientations on the decay rate of articulation angle responses of the unloaded and loaded vehicles. The results clearly show important effects of struts orientations on the decay rate and thus the stability limits. The results show that an decrease in lateral spread c (α = -8.8°) would yield higher yaw stability limits, while increasing the lateral spread c (α =3.5°) yields lower stability limits of both unloaded and loaded vehicles, compared to those obtained for the nominal orientation angles (α = -2.7°).

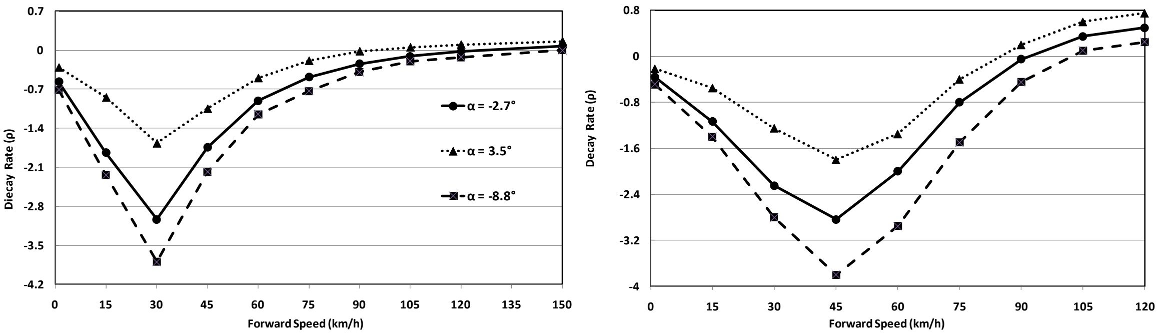

(a) (b)

Figure 4.20: Influence of variations in struts orientations on the rate of decay of articulation angle responses: (a) unloaded; and (b) loaded vehicle.

4.6 Conclusions and Design Guidance

A non-linear 3-DOF yaw plane model of an articulated steer vehicle was formulated in conjunction with the analytical model of the kineto-dynamics of the steering system, which was validated using the available field measured data. The formulated system model and thus developed simulation platform would provide a useful tool for investigating the response characteristics of the steering mechanism and yaw stability of articulated steer vehicles, contributing to enhanced design of the articulated steer vehicle system. On the basis of the detailed analyses and results discussions, some major conclusions and design guidance are summarized below:

- The directional responses of an articulated steer vehicle are strongly dependent upon the kineto-dynamic properties of the steering mechanism. The steering responses and yaw stability limits are most significantly affected by the effective damping of the steering mechanism, which is dependent upon the maximum valve flow rate, the characteristic articulation angle error, and the leakage flows within the struts and struts orientations.
- Under a rapid steering input, the struts impose greater flow demand to generate desired articulation torque leading to steering valve saturation, which may cause oscillatory articulation response and thus weaving motion of the vehicle.
- A lower value of the characteristic articulation angle error also yields rapid valve opening and saturation. Too low a value of the characteristic articulation angle error could lead to snaking instability.
- The struts geometry also affects the effective damping and the yaw stability limits of the vehicle. Increasing the struts orientation angle yields greater strut travel and thus greater flow demand and valve saturation.
- The steering valve saturation should be avoided since it results in relatively lower pressure difference across the strut piston and thus lower strut forces and articulation torque. The valve flow saturation could be circumvented by increasing the maximum valve flow rate, while too large a valve flow rate could also yield weaving motion of the vehicle due to large pressure differential across the strut piston.
- Reducing the maximum valve flow-rate or increasing the characteristic articulation angle error would result in increased steering response time, which is

attributable to relatively higher effective damping of the steering system. Leakage flows across the strut piston help enhance effective damping substantially and thus the yaw stability limits of the vehicle. Too large a leakage, however, imposes continued flow demand from the steering valve and may lead to failure of the struts.

Chapter 5

A Three-Dimensional Model of an Articulated Frame-Steer Vehicle for Coupled Ride and Handling Dynamic Analyses

5.1 Introduction

Articulated frame steer vehicles (ASV) with their enhanced mobility and maneuverability on paved as well as off-road terrains are widely used in the construction, forestry, agricultural and mining sectors. Such vehicles exhibit complex ride and directional performance attributed to their high mass center (cg), relatively soft tires, wide variations in load and load distribution, and kineto-dynamics of the frame steering mechanism. Furthermore, these vehicles are generally unsuspended; the soft and large diameter tires coupled with high mass center cause comprehensive magnitudes of low frequency translational and rotational whole-body vibration (WBV), when operating on off-road terrains. Prolonged occupational exposure to such WBV has been strongly associated with various health and safety risks among the drivers [5,6]. A number of studies have shown that the ride vibration of such vehicles exceed the health caution guidance zone defined in ISO-2631-1 [3], and the 'action' and/or 'limit' values defined in the EC guidelines [1,2,4,7,51]. The control of terrain-induced vibration is generally limited to elastic cabin mounts that provide attenuation of only higher frequency vibration and a suspension seat to isolate only vertical vibration, when adequately tuned to the target vehicle. Furthermore, the ride vibration attenuation performance of secondary suspensions (seat and cab), generally derived from the subsystem models [9,10,13-15], are limited due to lack of consideration of dynamics of the target vehicle [11]. While the superior performance potentials of axle suspension have been widely demonstrated in limiting the translational as well as rotational vibration, the suspension designs and implementations have been attempted in only a few studies [17-21]. This may in-part be attributed to design challenges associated with conflicting requirements posed by the ride and roll stability measures, and wide variations in the axle loads.

Apart from the complex ride, such vehicles also yield relatively lower directional stability limits, particularly greater jack-knife and snaking tendencies, and reduced roll stability, due to high cg and vehicle load coupled with kinematics and dynamics of the steering system [29,157-159]. While the wide and large diameter soft tires are beneficial in realizing improved traction and ride performance during off-road operations, the lower effective tire roll stiffness and track width tend to lower the roll stability limit. This would be of greater concern when operating on paved roads at relatively higher speeds.

Compared to the heavy road vehicles, the ride and handling properties of ASVs have been addressed in very few studies. The ride properties of such vehicles have been mostly evaluated through field measurements. The reported off-road vehicles analysis models focus either on ride properties assuming constant forward speed, non-deformable terrain, and negligible contribution due to steering system and vehicle articulation [17-23,232], or directional responses assuming smooth terrain surface and thereby neglecting the contributions of vertical tire interactions with the terrain [29,157-159,235]. A number of ride dynamic models of different off-road vehicles have been employed to explore performance potentials of axle suspensions, and influences of various design and operating factors on the ride performance [17-23,232]. These have mostly focused on different passive and semi-active axle suspensions for agricultural and military vehicles [43,93-100]. Rehnberg and Drugge [21] developed virtual multi-body models of an articulated wheel loader with and without axle suspensions using MSC/ADAMS software to investigate the effects of front and rear axle suspensions on vehicle ride, which revealed significant reductions in the longitudinal and vertical accelerations.

In a similar manner, the analyses of directional stability limits of off-road vehicles have been limited to very simple models [174,175]. The extensive studies on heavy road vehicles, on the other hand, have evolved into not only comprehensive simulation models but also a series of directional performance measures [45,170,173, 180,195,236,237]. This may be partly attributed to low operating speed of off-road vehicles. The ASVs, however, also operate on paved roads at relatively higher speeds, where the roll stability limit would be of concern. Furthermore, roll instability may occur even at lower speeds. Uneven sinkage of left and right wheels on deformable terrains could yield greater lateral load transfers and sprung mass roll displacement moment, and thus lower roll stability limit. Furthermore, it has been shown that the slope stability of an ASV could be 13° less when steered to full-lock position compared to that observed during straight driving [175]. The yaw stability limits of ASVs have been investigated using simple 3-DOF yaw-plane linear models, where the contributions due to kinematics and dynamics of the frame steering, the roll motions of the articulated units and vertical tire-terrain interaction are ignored. The steering system is characterized by equivalent linear torsional stiffness and damping elements, while the kinematic properties of the steering mechanism are entirely ignored [28,29,157-159]. The yaw stability limit of an ASV is most significantly affected by the effective damping of the steering mechanism, which is dependent upon kineto-dynamics of the steering struts, leakage flows and the characteristic steering valve flow rate [235]. A few studies have also investigated static stability of ASVs on slopes/cross-slopes for developments in rollover protection structures and rollover early-warning devices [34-38,174-176].

Unlike the heavy road vehicles, the vertical tire interactions with off-road terrains could cause substantially higher variations in tire vertical and lateral forces, and thereby affect the vehicle directional performance, particularly the roll stability limits. Owing to increasing demands on the high speed ASVs for both on- and off-road operations, the roll stability analysis of these vehicles becomes an important issue in addition to the ride dynamics. The analyses of both the ride and directional properties of ASVs require simulation models incorporating kineto-dynamics of the frame steering system and dynamic tire interactions with random off-road terrains. Such models could provide important design guidelines for the suspension and steering mechanism for realizing improved compromises in ride and roll performance.

In this study, a comprehensive three-dimensional model of an articulated frame steer vehicle with and without a rear axle suspension is developed to investigate ride and directional responses of the vehicle. The model incorporates kineto-dynamic properties of the frame steering mechanism and tire interactions with the random terrain tracks, while assuming constant forward speed. The proposed model is validated on the basis of the field-measured ride vibration data, and the steering strut responses under a steady-turn steering input. The yaw and roll dynamic responses of the vehicle are evaluated under different dynamic maneuvers. The influences of variations in the selected design and operating parameters including suspension and steering system parameters and vehicle load on the ride performance and stability limits are further presented through a parametric study.

5.2 Vehicle Model:

A three-dimensional ride and yaw/roll directional dynamics model of an ASV with and without a rear axle suspension is developed. For the unsuspended ASV, each unit together with the axle is considered as a rigid body with 6 degrees-of-freedom (*x*-longitudinal; *y*-lateral; *z*-vertical;Φ-roll; Θ-pitch; and Ψ-yaw). For the suspended ASV, a torsio-elastic rear-axle suspension is considered that can provide softer ride with greater roll stiffness [22].

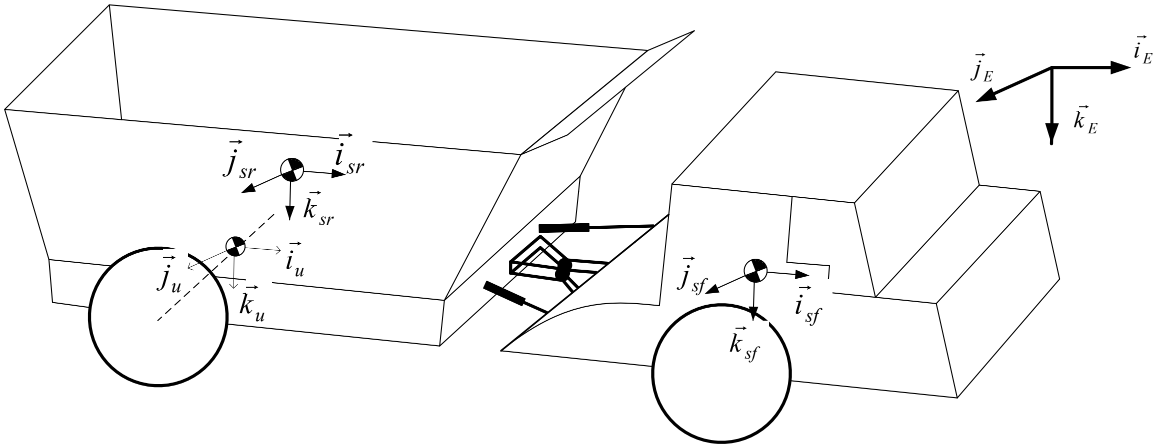

Figure 5.1: Body-fixed axis systems defined for the articulated frame steer vehicle with two sprung masses and one unsprung mass.

The coupled differential equation of motion for the front and rear units ($i =f, r$) are derived considering respective body-fixed coordinate system (i_{si}, j_{si}, k_{si} ; $i =f, r$), as shown in Fig. 5.1. Figures 5.2 and 5.3 illustrate the unsuspended ASV model in the pitch, roll and yaw planes, while the roll plane model of the rear unit with a torsio-elastic suspension is shown in Fig. 5.4. Each suspension unit comprises two elastic torsion bars, reinforced with a steel rod, attached to the sprung and unsprung units (shown with grey shading in Fig. 5.4). The two torsion bars are coupled through a link of nearly elliptical cross-section. Each link is modeled as a rigid body with three-DOF: lateral, y_j; roll,Φ_j;

and vertical z_j, where j=L, R denote left- and right-suspension unit. The equations of motion for the front $(i = f)$ and rear $(i = r)$ units are derived as:

Longitudinal: $m_{si}\dot{u}_{si} - m_{si}(r_{si}v_{si} - q_{si}w_{si}) = F_{x_{Ti}} + F_{x_{Sr}} + F_{x_{Hi}} + F_{x_{Ci}} + F_{x_{Gi}}$

Lateral: $m_{si}\dot{v}_{si} - m_{si}(p_{si}w_{si} - r_{si}u_{si}) = F_{y_{Ti}} + F_{y_{Sr}} + F_{y_{Hi}} + F_{y_{Ci}} + F_{y_{Gi}}$

Vertical: $m_{si}\dot{w}_{si} - m_{si}(q_{si}u_{si} - p_{si}v_{si}) = F_{z_{Ti}} + F_{z_{Sr}} + F_{z_{Ci}} + F_{z_{Gi}}$

Roll: $I_{xx_{si}}\dot{p}_{si} - (I_{yy_{si}} - I_{zz_{si}})q_{si}r_{si} = M_{x_{Ti}} + M_{x_{Hi}} + M_{x_{Sr}} + M_{x_{Ci}}$

Pitch: $I_{yy_{si}}\dot{q}_{si} - (I_{zz_{si}} - I_{xx_{si}})p_{si}r_{si} = M_{y_{Ti}} + M_{y_{Hi}} + M_{y_{Sr}} + M_{y_{Ci}}$

Yaw: $I_{zz_{si}}\dot{r}_{si} - (I_{xx_{si}} - I_{yy_{si}})q_{si}p_{si} = M_{z_{Ti}} + M_{z_{Hi}} + M_{z_{Sr}}$ (5.1)

where m_{si} is mass of unit i $(i = f, r)$, and $I_{xx_{si}}$, $I_{yy_{si}}$ and $I_{zz_{si}}$ are the mass moments of inertia about the fixed axis (i_{si}, j_{si}, k_{si}), respectively. For the rear unit, these represent the total values of the sprung and unsprung units in the absence of the suspension. (u_{si}, v_{si}, w_{si}) are the longitudinal, lateral and vertical velocities of unit i, respectively; and (p_{si}, q_{si}, r_{si}) are the corresponding roll, pitch and yaw velocities. $F_{k_{Tf}} = F_{k_{T1}} + F_{k_{T2}}$ and $F_{k_{Tr}} = F_{k_{T3}} + F_{k_{T4}}$are the total tires forces acting on the front and rear unit, respectively, and $F_{k_{Tl}}$is the force developed by tire l (l=$1,\ldots, 4$) along the corresponding body-fixed axis k $(k = x, y, z)$, and $M_{k_{Ti}}$ are the corresponding moments. ($F_{x_{Hi}}$ and $F_{y_{Hi}}$) are the forces imposed on unit i $(i = f, r)$ by the hydraulic steering struts along the respective body-fixed x- and y-axis, respectively. $M_{k_{Hi}}$ are the moments due to steering strut forces about the corresponding body-fixed axis k $(k = x, y, z)$ of unit i $(i = f, r)$. $F_{k_{Sr}}$ are the forces acting on the rear unit due to rear axle suspension, when present, along the axis k $(k = x, y, z)$, and $M_{k_{Sr}}$ are the corresponding moments. $F_{k_{Ci}}$ and $M_{k_{Ci}}$ are the articulation constraint forces and moments acting on unit i $(i = f, r)$ along axis k $(k = x, y, z)$, respectively. $F_{k_{Gi}}$ are the components of the gravity force of unit i along the corresponding body-fixed axis k ($k = x, y, z$). Assuming small side-slip angles of tires, constant forward speed of the front unit and that the traction force developed is balanced by the motion resistances, the equation of motion along the x-axis may be omitted.

For ASV with the rear axle suspension, the equations of motion for the unsprung mass are derived using the body-fixed coordinate system (i_u, j_u, k_u) attached to the center of mass (*cg*) of the rear axle, while those of the linkages are formulated with respect to an axis system fixed to center of each linkage (i_j, j_j, k_j); j= *L*, *R*, where subscripts "*L*" and "*R*" refer to the right- and left-suspension linkage, respectively.

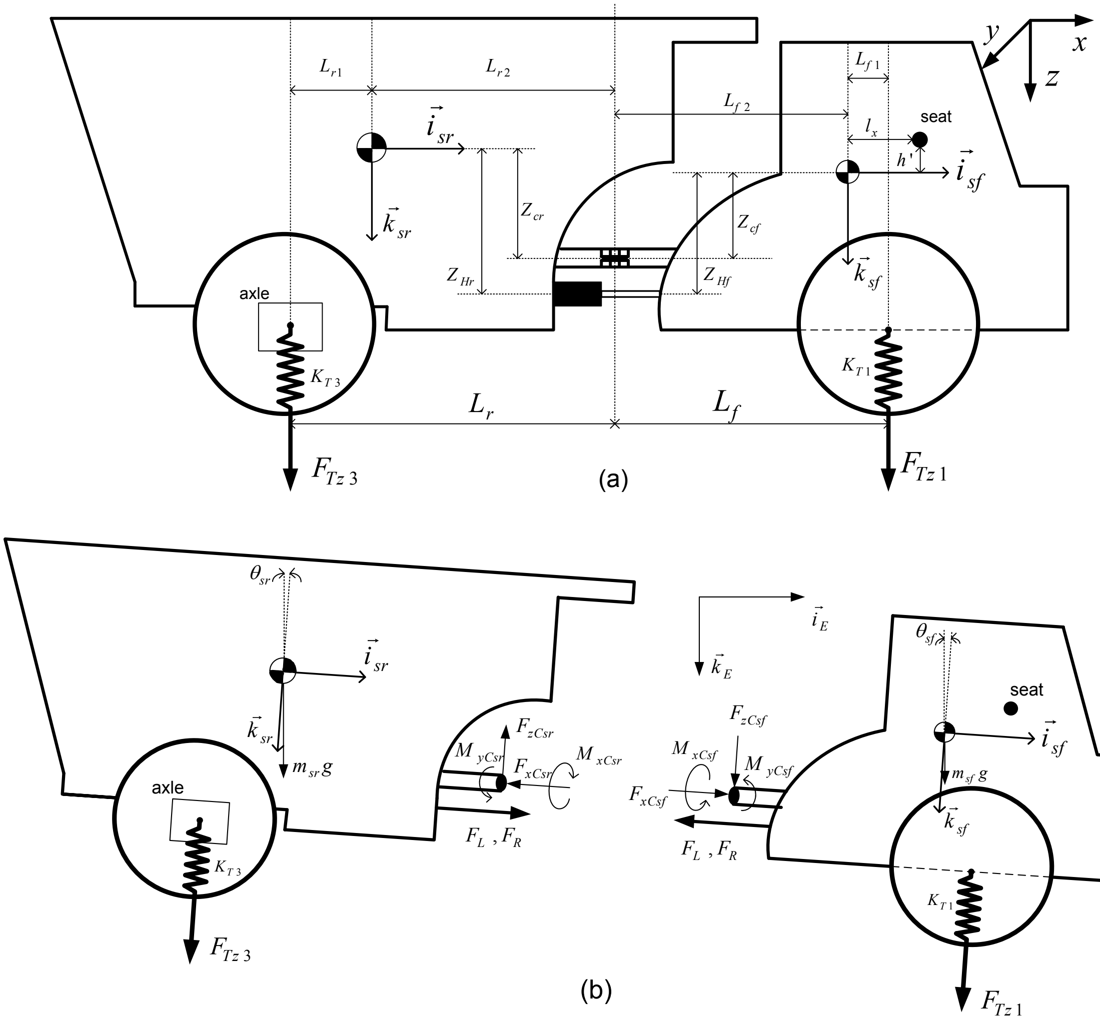

Figure 5.2: Schematic representation of the unsuspended vehicle models in the pitch plane

Unsprung mass:

$$m_u\dot{v}_u - m_u(p_u w_u) = F_{y_{Tu}} + F_{y_{Su}} + F_{y_{Gu}}$$

$$m_u\dot{w}_u + m_u(p_u v_u) = F_{z_{Tu}} + F_{z_{Su}} + F_{z_{Gu}}$$

$$I_{xx_u}\dot{p}_u = M_{x_{Tu}} + M_{x_{Su}} \tag{5.2}$$

Suspension linkage masses:

$$m_j\dot{v}_j - m_j(p_j w_j) = F_{y_{Sj}} + F_{y_{Gj}}$$

$$m_j\dot{w}_j + m_j(p_j v_j) = F_{z_{Sj}} + F_{z_{Gj}}$$

$$I_{xx_j}\dot{p}_j = M_{x_{Sj}} \qquad (j = R, L) \tag{5.3}$$

where m_u and I_{xx_u} are the mass and roll mass moment of inertia of the unsprung mass, respectively, and v_u, w_u and p_u are the lateral, vertical and roll velocities of the unsprung mass, respectively. $F_{y_{Tu}}$and $F_{z_{Tu}}$ are the total forces due to right- and left tires along the y- and z-axis of the axis system attached to the unsprung mass, respectively, and $M_{x_{Tu}}$ is the corresponding roll moment. $F_{y_{Su}}$and $F_{z_{Su}}$ are the total forces developed by the left- and right-suspension acting on the unsprung mass along the y- and z-axis, respectively, and $M_{x_{Su}}$ is resulting roll moment. $F_{y_{Gu}}$and $F_{z_{Gu}}$ are the components of the gravity force along the y- and z-axis of the unsprung mass. m_j and I_{xx_j} are the mass and roll mass moment of inertia of the suspension link *j*, *j*=*L*, *R*, respectively. v_j, w_j and p_j, respectively, denote the lateral, vertical and roll velocities of the link j. $F_{y_{Sj}}$, $F_{z_{Sj}}$ and $M_{x_{Sj}}$ are the total suspension forces and moment due to suspension linkage *j* (*j*=*L*, *R*) acting along y-, z- and x-axis of the coordinate system fixed to the linkage mass, and $F_{y_{Gj}}$and $F_{z_{Gj}}$ are the components of the gravity force along the respective axis.

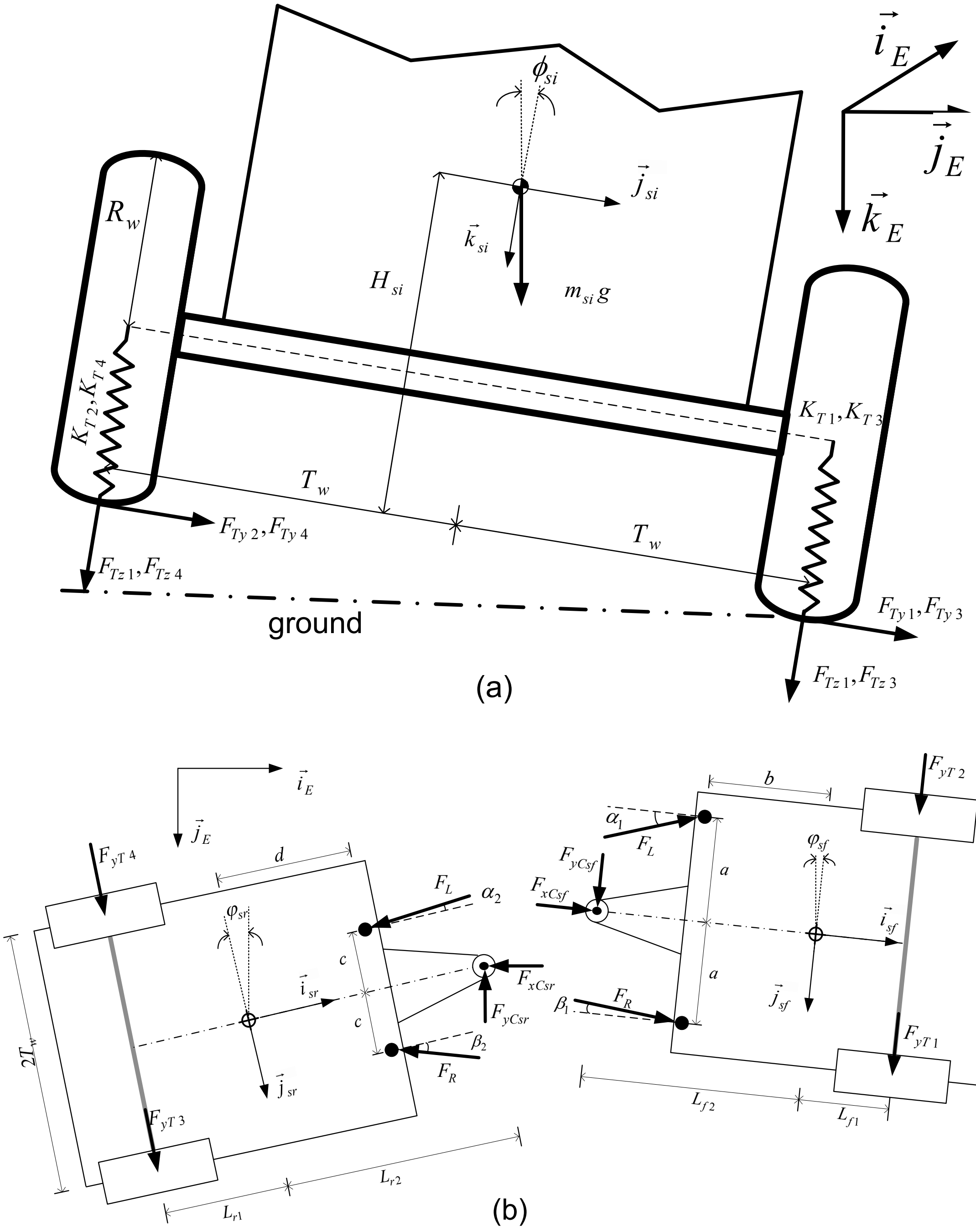

Figure 5.3: Schematic representation of the vehicle models: (a) roll-plane; and (b) yaw plane.

The vehicle attitude and trajectory are defined with respect to a fixed inertial coordinate system (i_E, j_E, k_E), as shown in Figs. 5.1 to 5.4. The relationship between each of the body-fixed axis system and the inertial axis system are obtained using the corresponding Euler angles, which define the transformation matrices between the body-fixed and inertial axis systems. Euler angles, describing yaw (φ), pitch (θ), and roll (ϕ) rotations of each rigid body, are thus defined for formulating the transformation matrices, which also define angular displacements of each body with respect to the inertial axis system. The Euler angular velocities of the sprung mass ($\dot{\phi}_{si}, \dot{\theta}_{si}, \dot{\varphi}_{si}\,; i = f, r$), unsprung mass ($\dot{\phi}_u$) and the suspension linkage mass ($\dot{\phi}_j; j = L, R$) with respect to the inertial axis system can be related to the rotational velocities in the fixed-body coordinated system [189], such that:

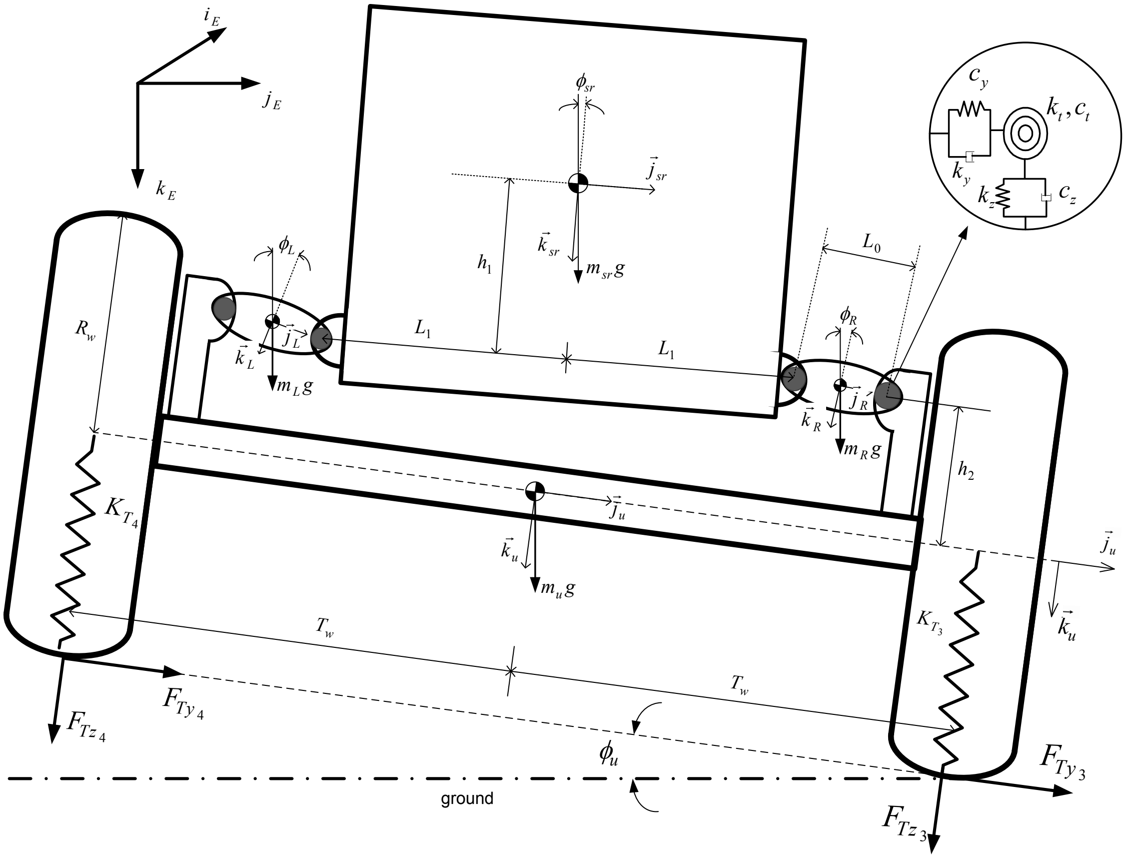

Figure 5.4: Roll plane model of rear unit with a torsio-elastic suspension (rear view)

$$\dot{\phi}_{si} = p_{si} + (q_{si} sin\phi_{si} + r_{si} cos\phi_{si}) tan\theta_{si}$$

$$\dot{\theta}_{si} = (q_{si} cos\phi_{si} - r_{si} sin\phi_{si}); \qquad \dot{\varphi}_{si} = \frac{1}{cos\theta_{si}}(q_{si} sin\phi_{si} + r_{si} cos\phi_{si})\ ;$$

$$\dot{\phi}_u = p_u + \dot{\varphi}_{sr} sin\theta_{sr;} \qquad \dot{\phi}_j = p_j + \dot{\varphi}_{sr} sin\theta_{sr} \tag{5.4}$$

Equation (5.4) can be integrated numerically to obtain the Euler angles and thus the angular displacements of the rigid bodies, $\phi_{si}, \theta_{si}, \varphi_{si}$, ϕ_u and ϕ_j . The transformation matrices relating different axis systems can thus be derived from the corresponding rotational matrices about the z-, y-, x-axis of the sprung masses, unsprung mass and the linkage masses [189].

5.2.1 External forces and moments:

Suspension forces and moments

The torsio-elastic suspension, as described in details in [22], is characterized by its radial and torsional visco-elastic properties. Each torsion bar is modeled using equivalent linear stiffness and damping along the vertical (k_z, c_z) and lateral (k_y, c_y) axes, and the torsional stiffness and damping (k_t, c_t), as shown in Fig. 5.4. The total rear-axle suspension forces (F_{yS_r}, F_{zS_r}), and moments, (M_{xS_r}, M_{yS_r}, M_{zS_r}), developed by the right (R) and left (L) torsio-elastic suspension, acting on the sprung mass in the corresponding coordinate system (i_{sr}, j_{sr}, k_{sr}), can be expressed as:

$$\begin{aligned}
&F_{yS_r} = -F_{yS_{sR}} - F_{yS_{sL}}; \qquad F_{zS_r} = -F_{zS_{sR}} - F_{zS_{sL}};\\
&M_{xS_r} = -M_{xS_{sR}} - M_{xS_{sL}} + h_1 F_{yS_r} + L_1(F_{zS_{sL}} - F_{zS_{sR}})\\
&M_{yS_r} = -L_{r1} F_{zS_r}\,; \quad M_{zS_{sr}} = L_{r1} F_{yS_r}
\end{aligned} \tag{5.5}$$

Similarly, the total suspension forces and moments acting on the unsprung mass along its coordinate system (F_{yS_u}, F_{zS_u}, M_{xS_u}) are obtained as:

$$\begin{aligned}
&F_{yS_u} = F_{yS_{uR}} + F_{yS_{uL}}; \qquad F_{zS_u} = F_{zS_{uR}} + F_{zS_{uL}};\\
&M_{xS_u} = M_{xS_{uR}} + M_{xS_{uL}} + h_2 F_{yS_u} + (L_1 + L_0)(F_{zS_{uR}} - F_{zS_{uL}})
\end{aligned} \tag{5.6}$$

where $F_{yS_{kj}}$and $F_{zS_{kj}}$ are the forces developed by suspension j (j=L, R) acting on the mass k (k=s,u; where s and u denote the sprung and unsprung mass, respectively). $M_{xS_{kj}}$, $M_{yS_{kj}}$ and $M_{zS_{kj}}$ are the moments developed by suspension j (j=L, R) acting on the sprung mass and $M_{xS_{uj}}$ are the roll moments acting on the unsprung mass, as shown in Fig. 5.5. h_1, h_2, L_1, L_0 and L_{r1} are the geometric parameters shown in Figs. 5.2 to 5.4.

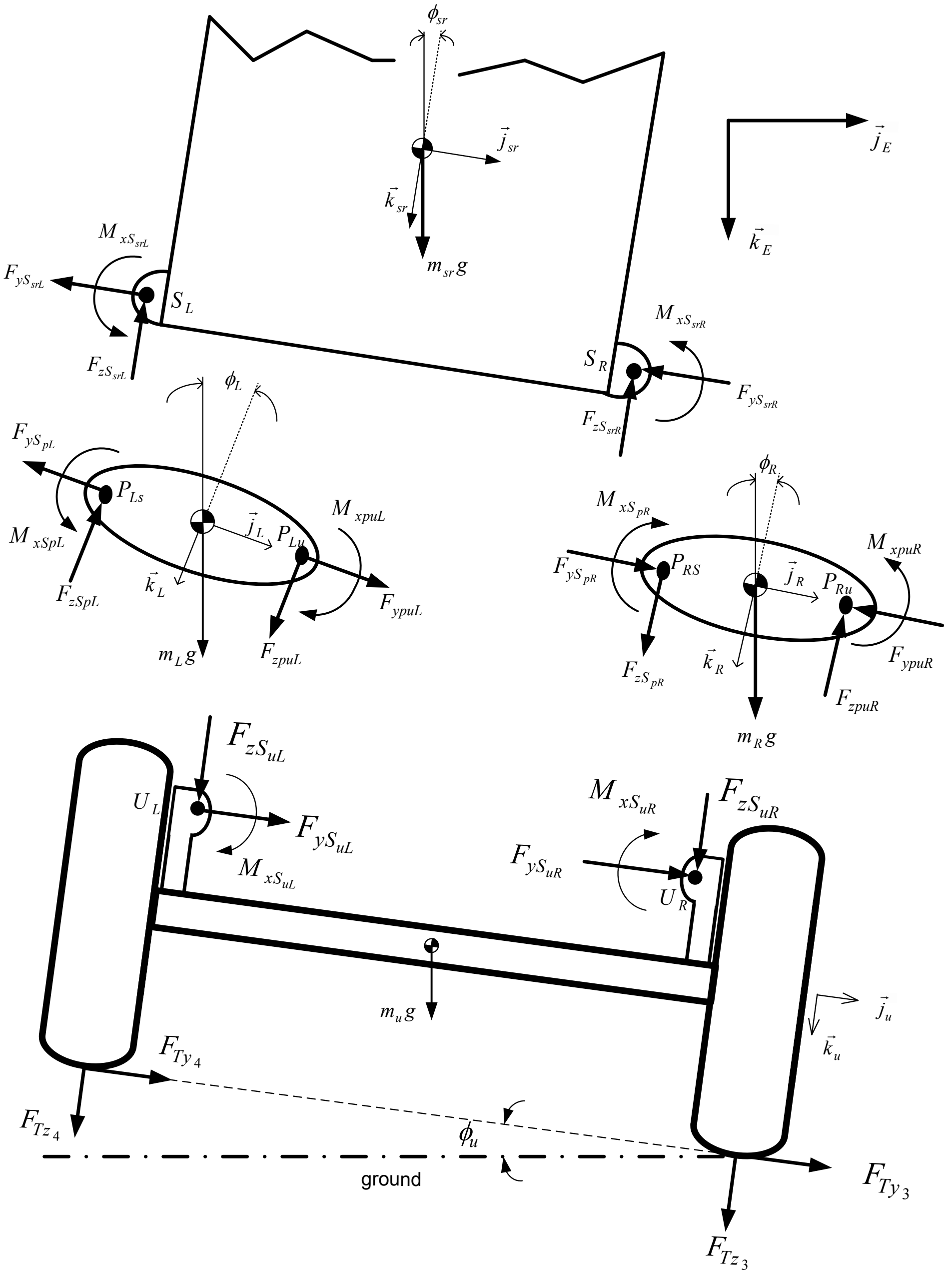

Figure 5.5: Suspension and tire forces and moments acting on the sprung mass and rear axle

The suspension forces are derived from the relative velocities and displacements across torsion bars coupling the sprung mass to the link, $F_{yS_{pj}}$and $F_{zS_{pj}}$(denoted by joints S_R-P_{RS} and S_L-P_{LS} in Fig. 5.5), and across the link and the unsprung mass, $F_{ypuj}$and F_{zpuj} (denoted by joints P_{Ru}-U_R and P_{Lu}-U_L in Fig. 5.5). The torsional moments due to each torsion bar attached to the sprung and unsprung mass, $M_{xS_{pj}}$and M_{xpuj} (j=L, R) are also derived in a similar manner from the relative roll velocities and displacements. The resultant suspension forces and moments acting on each suspension link are obtained as:

$$F_{yS_j} = F_{yS_{pj}} - F_{ypuj}; \quad F_{zS_j} = F_{zS_{pj}} - F_{zpuj}$$
$$M_{xS_j} = M_{xS_{pj}} - M_{xpuj} \pm \tfrac{L_0}{2}(F_{zS_{pj}} + F_{zpuj}); \qquad (j = R, L) \qquad (5.7)$$

<u>Constraint forces and moments</u>

The two units are rigidly coupled along the translational axes, i.e., the accelerations along the *x*-, *y*- and *z*-axis at the articulation joint are the same for both the units. The constraint forces transmitted to each unit ($F_{x_{Ci}}$, $F_{y_{Ci}}$, $F_{z_{Ci}}$; i=f, r) are determined from the kinematic constraints. The two units, however, can yaw, pitch and roll relative to each other. While the yaw moment imposed on each unit is derived from kineto-dynamics of the steering struts [235], the roll and pith constraint moments are calculated by considering the roll and pitch compliance of the coupling mechanism, as seen in Fig. 5.6. The effective pitch and roll stiffness at the articulation joint are assumed to be considerably large, primarily attributed to articulation and vehicle structures. The roll and pitch constraint moments are thus derived as functions of the relative roll and pitch displacements between the front and the rear units.

A reference coordinate system (i_1', j_1', k_1') is defined at the articulation joint, where the roll rotation is identical to that of the front unit ($\varphi_1' = \varphi_{sf}$) while the pitch and roll rotations, $\theta_1'$and ϕ_1', differ, as shown in Fig. 5.6. The vertical axis (k_1') is parallel to that of the rear unit (k_{sr}), such that: $i_1' \cdot k_{sr} = 0$ and$j_1' \cdot k_{sr} = 0$. Applications of transformation matrices relating the body-fixed and inertial coordinate systems yield following relations in the Euler angles:

$$\theta_1' = tan^{-1}\left[tan\,\theta_{sr}\cos(\varphi_{sr} - \varphi_{sf}) + \frac{\tan\phi_{sr}}{cos\theta_{sr}}\sin(\varphi_{sr} - \varphi_{sf})\right];$$

$$\phi_1' = tan^{-1}\left[\frac{sin\,\phi_{sr}\cos(\varphi_{sr}-\varphi_{sf}) - \sin\theta_{sr}\,cos\,\phi_{sr}\sin(\varphi_{sr}-\varphi_{sf})}{sin\theta_1' sin\,\phi_{sr}\sin(\varphi_{sr}-\varphi_{sf}) + sin\theta_1' sin\,\theta_{sr}\,cos\,\phi_{sr}\cos(\varphi_{sr}-\varphi_{sf}) + cos\theta_1' cos\,\theta_{sr} cos\,\phi_{sr}}\right] \tag{5.8}$$

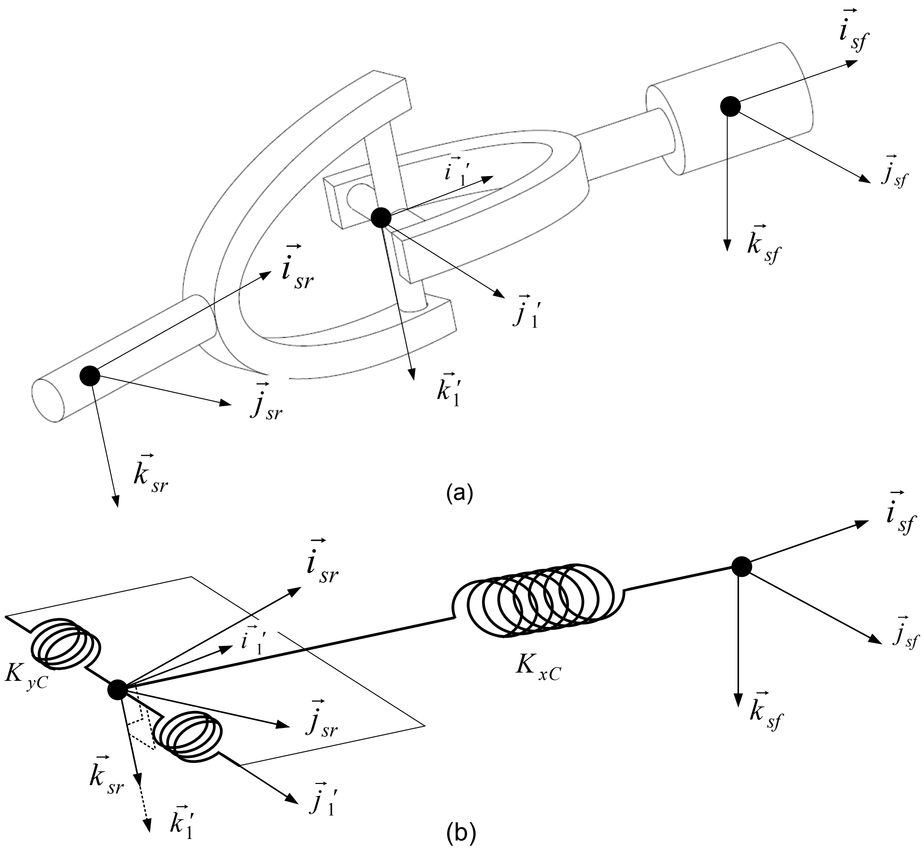

Figure 5.6: Articulation mechanism and the coordinate systems

Assuming linear roll and pitch stiffness, $K_{\varphi_c}$and K_{θ_c}, respectively, the constraint moments acting on the front unit are derived as:

$$M_{xC_f} = K_{\varphi_c}\big(\phi_1' - \phi_{sf}\big) - Z_{cf}F_{y_{Csf}}$$
$$M_{yC_f} = K_{\theta_c}(\theta_1' - \theta_{sf}) + Z_{cr}F_{x_{Csf}} + L_{f2}F_{z_{Csf}} \tag{5.9}$$

where Z_{cf} and Z_{cr} are the vertical distances between the articulation joint and the cg of the front and rear unit, respectively, and L_{f2} is the longitudinal distance between the front unit cg and the articulation joint, as shown in Fig. 5.2. The moments acting on the rear unit, M_{xC_r} and M_{yC_r}, are derived in a similar manner using transformation matrices relating (i_{sf}, j_{sf}, k_{sf}) and (i_{sr}, j_{sr}, k_{sr}) axis systems.

Tire forces:

a. Vertical forces

The vertical force developed by each tire is obtained considering linear stiffness and a non-linear point-contact model, such that:

$$F_{zT_l} = -K_{T_l}\Delta_l \; ; \quad (l = 1, \dots, 4) \tag{5.10}$$

where K_{T_l} is the vertical stiffness of tire l and $\varDelta_l = z_l - z_{0l} + z_{st_l}$ is the total vertical deflection of tire l. z_l and $\mathrm{z}_{\mathrm{st}_l}$ are the vertical dynamic and static deflections of tire l, and z_{0l} is the terrain elevation at the tire-terrain contact point. The dynamic vertical deflection of each tire z_l is obtained considering the roll and pitch motions of the unit to which it is attached.

b. Lateral forces

The lateral force developed by an off-road vehicle tire is nonlinearly dependent upon the side-slip angles and the normal load. Furthermore, the lateral force exhibits a tire lag. A first-order tire dynamic model, described in [118,224], is applied to derive the lateral force developed by each tire F_{Ty_l}(*l= 1,…, 4*), such that:

$$\tau_{y_l}\dot{F}_{y_{Tl}}(t) + F_{y_{Tl}}(t) = -F_{zT_l}K_{y_l}(1 - \mathrm{e}^{-B_{yl}\alpha_l(t)}) \; ; \quad (\mathrm{l} = 1, \dots, 4) \tag{5.11}$$

where $K_{y_l}B_{y_l}$ is the cornering coefficient of tire *l*, which decreases with increasing normal load F_{zT_l}. The relaxation time τ_{y_l} directly relates to relaxation length σ_{y_l} and the forward speed of the wheel, V_{xT_l}, such that: $\tau_{y_l} = \sigma_{y_l}/V_{xT_l}$. The tire slip angle α_{sl} can be derived as the ratio of the lateral and longitudinal velocity, $V_{xT_l}$and V_{yT_l}, at the tire-terrain contact point, such that:

$$\alpha_{sl} = \frac{V_{yT_l}}{V_{xT_l}} \; ; \quad (l = 1, \dots, 4) \tag{5.12}$$

The lateral and longitudinal velocity of each tire is obtained considering the yaw, roll and pitch motions of the unit to which it is attached.

Steering strut forces and moments:

The forces and moments developed by the frame steering system are dependent upon the kineto-dynamics of the struts together with dynamics of the vehicle units.The forces and moments imposed on each unit were derived from the kineto-dynamic model of the frame steering mechanism, presented in [235]. The model incorporates the kinematic motions of the right- and left-steering struts, hydraulic flows through the struts and the steering valve flows, as shown in Fig. 5.7. The forces developed by the left- and right-struts, F_L and F_R, are derived from the fluid pressures in the piston- and rod-side chambers of each strut, P_1 and P_2, and the effective working area of the struts, such that:

$$F_L = P_1A_p - P_2A_r \; ; \quad F_R = P_2A_p - P_1A_r \tag{5.13}$$

where A_p and A_r are cross-section areas on the piston- and the rod-side of the strut, respectively. The fluid pressures are derived from the flow continuity equations considering the flow rate through the steering valve and the leakage flows through the piston seals, $Q_L = K_L(P_1 - P_2)$, where K_L is the leakage coefficient:

$$\overline{Q}_1 = +\left(\frac{2K_L \Delta P_m}{Q_{max}}\right)\left(\overline{P}_1 - \overline{P}_2\right) + \frac{\left(A_P \dot{\mathrm{X}}_{\mathrm{L}} + A_r \dot{\mathrm{X}}_{\mathrm{R}}\right)}{Q_{max}} + \frac{(V_{L1} + V_{R2})\Delta P_m}{B Q_{max}} (\dot{\overline{P}}_1)$$
$$\overline{Q}_2 = -\left(\frac{2K_L \Delta P_m}{Q_{max}}\right)\left(\overline{P}_1 - \overline{P}_2\right) - \frac{\left(A_P \dot{\mathrm{X}}_{\mathrm{R}} + A_r \dot{\mathrm{X}}_{\mathrm{L}}\right)}{Q_{max}} + \frac{(V_{L2} + V_{R1})\Delta P_m}{B Q_{max}} (\dot{\overline{P}}_2)$$

(5.14)

where $\overline{Q}_1$and $\overline{Q}_2$ are the flow rates to and from the struts, respectively, normalized with respect to maximum valve flow rate, Q_{max}. B is the fluid bulk modulus, and V_{L1}, V_{L1}, V_{R2} and V_{R2} define the instantaneous fluid volumes in the piston- and rod-side chambers of the left and right struts, as shown in Fig. 5.7. $\dot{X}_L$ and $\dot{X}_R$ are the velocities of the left- and right-struts, respectively, obtained from the kinematic expressions relating lateral and yaw motions of the two units [235]. The fluid flow through the valve is related to the steering wheel input θ_{sw} and the articulation angle φ in a closed-loop manner, the valve stem displacement X_V and the valve flow characteristics, Fig. 5.7(b), as:

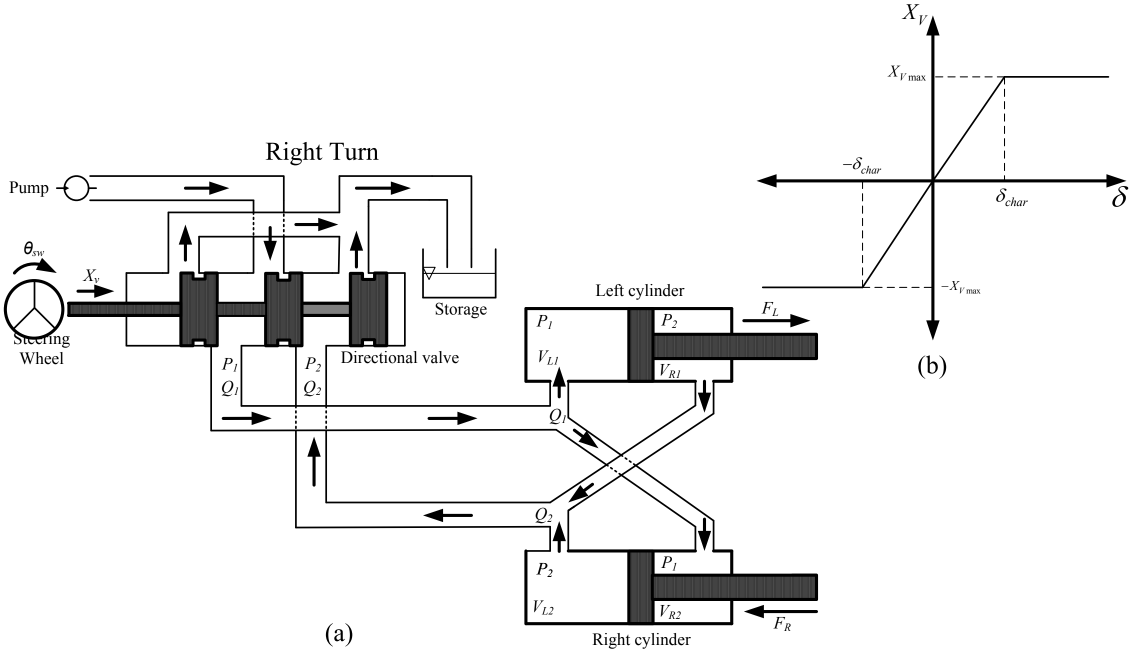

Figure 5.7: (a) Schematic of the hydraulic steering system for a right turn; and (b) Relationship between the valve spool displacement and the articulation error.

$$X_V = \frac{X_{Vmax}}{\delta_{char}}(\delta); \qquad |\delta = K_1\theta_{sw} - \varphi| \le \delta_{char}$$
$$X_V = X_{Vmax}\, sgn\,(\delta); \qquad Otherwise \qquad (5.15)$$

In the above equation, X_{Vmax} is maximum valve stem displacement, $\delta = K_1\theta_{sw} - \varphi$ is the articulation error, K_1 is the steering gain and δ_{char} is the characteristic articulation angle error corresponding to X_{Vmax} or valve flow saturation , as shown in Fig. 5.7(b).

The resultant steering strut forces can be subsequently derived as:

$$F_{x_{Hsf}} = (F_L cos\alpha_1 + F_R cos\beta_1); \qquad F_{y_{Hsf}} = (F_L sin\alpha_1 + F_R sin\beta_1)$$
$$F_{x_{Hsr}} = (-F_L cos\alpha_2 - F_R cos\beta_2); \qquad F_{y_{Hsf}} = (-F_L sin\alpha_2 - F_R sin\beta_2) \qquad (5.16)$$

The steering torques acting on the front and rear units, ($M_{x_{Hsi}}, M_{y_{Hsi}}, M_{z_{Hsi}}$), are obtained from the strut forces in the following manner:

$$M_{x_{Hsi}} = -Z_{Hi}F_{y_{Hsi}}\,; \qquad M_{y_{Hsi}} = Z_{Hi}F_{x_{Hsi}}\,; \qquad i = f, r$$
$$M_{z_{Hsf}} = (F_L cos\alpha_1 - F_R cos\beta_1)a + (-F_L sin\alpha_1 - F_R sin\beta_1)b$$
$$M_{z_{Hsr}} = (-F_L cos\alpha_2 + F_R cos\beta_2)c + (-F_L sin\alpha_2 - F_R sin\beta_2)d \qquad (5.17)$$

where angles (α_1, α_2) and (β_1, β_2) are the instantaneous yaw angles of the left and right strut with respect to longitudinal axes of front and rear units, respectively, as shown in Fig. 3(b) and a, b, c, d and Z_{Hi} are the geometric parameters of the frame steering mechanism shown in Figs. 5.2 and 5.3.

5.3 Method of Analysis

The equations of motion for the unsuspended and suspended vehicle models are solved to determine the vehicle ride under terrain excitations, and yaw/roll responses to steady and transient steering inputs. A small size articulated dump truck with and without the load is considered, whose simulation parameters are summarized in Table 5.1, which were mostly obtained from manufacturer specifications and personal communications [197].

The ride, yaw and roll response measures are defined to evaluate the influences of selected design and operating parameters, including the rear-axle suspension and steering system parameters, and vehicle load.

Ride Response Analysis

The ride responses are evaluated in terms of root mean square (rms) and power spectral density (PSD) of translational and rotational accelerations at the operator seat location in the absence of a steering input considering roughness profiles of two tracks of a plowed field and constant forward speed of 30 km/h. The frequency weighting defined in ISO-2631-1 [3] are applied to determine the whole body vibration exposure of the operator in terms of frequency-weighted rms accelerations due to ride vibration responses. These include W_k-weighting for vertical, W_d-weighting for lateral and W_e-weighting for rotational accelerations. The responses along the fore-aft axis, however, were not attempted due to lack of consideration of the tire-terrain interactions in the fore-aft direction by the non-linear point contact tire model. The roughness profiles of the right- and left-tire tracks of the plowed field were obtained from the reported model [114]:

$$G_Z(\Omega) = \alpha_r \Omega^{-\beta} \; ; \tag{5.18}$$

where G_Z is spatial PSD of the terrain roughness, Ω is the spatial frequency, and $\alpha_r = 6.5 \times 10^{-4}$ and $\beta = 1.6$ are the roughness coefficient and waviness constant, respectively. The above regression model was described by a frequency response function, $Q(\omega)$, which permits a synthesis of time-history of the roughness profile, when convolved with a white-noise random signal, $r(t)$ [232]. The roughness profiles of the two tire-tracks were subsequently estimated assuming the coherency between the two tracks, $\gamma_{LR}^2(\omega)$, of following form, using the method described in [232] and shown in Fig. 5.8:

$$\gamma_{LR}^2(\omega)=\begin{cases}1-0.9(\frac{\omega}{2\pi}) & ; \quad \omega\le\omega_1\\ 0.1 & ; \quad \omega>\omega_1\end{cases} \tag{5.19}$$

where $\gamma_{LR}^2(\omega)$ is the coherence between the left- and right-tracks of the terrain, $z_{0L}(t)$ and $z_{0R}(t)$, and ω_1 is the transition frequency, which was taken as 1 Hz for the off-road terrain. Figures 5.9(a) to 5.9(c) illustrate time histories of roughness of the left- and right-tracks of the plowed field considering a forward speed of 30km/h and the corresponding roll displacement, respectively.

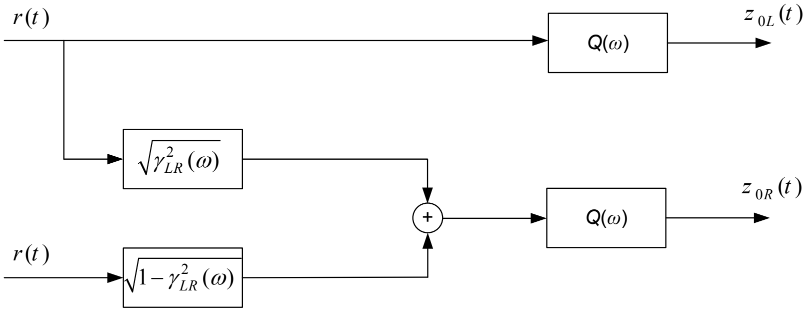

Figure 5.8: Method used to synthesize the roughness time-histories of the two terrain tracks considering coherency between the two.

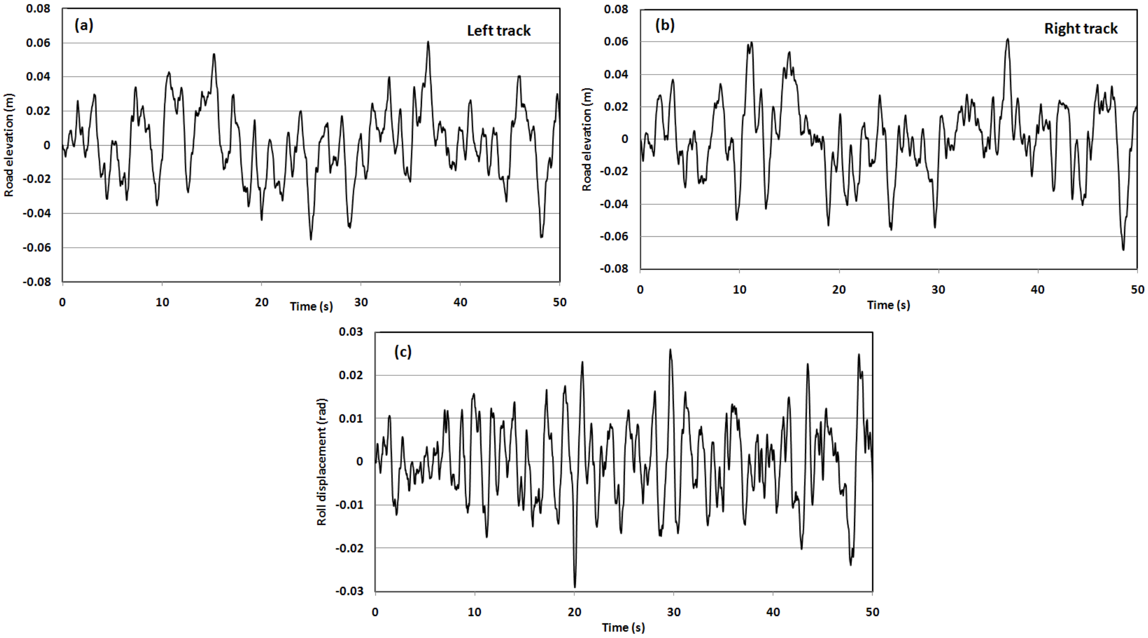

Figure 5.9: Time histories of (a) left track roughness; and (b) right track roughness; and (c) roll displacement (U=30km/h).

Static and Dynamic Roll Response Analyses

The roll stability limits of the ASVs can be evaluated in terms of static and dynamic measures commonly used to describe relative roll stability of articulated heavy road vehicles [170,180-183]. Owing to significantly higher inertia of the rear unit of the loaded dump truck, the relative roll instability of the ASV is identified on the basis of the lateral load transfer ratio (LTR) of the rear axle. Relative roll instability can also be characterized in terms of the Roll Safety Factor (RSF) of the rear axle, which is similar to the LTR and expressed as [190]:

$$RSF_r = \frac{(F_{Tz_3} - F_{Tz_4})}{(F_{Tz_3} + F_{Tz_4})} \tag{5.20}$$

The vehicle is considered to approach its relative roll instability limit when LTR or RSF value approaches ±1, as one of rear wheel lifts off the ground under a steering input. The RSF can be applied to determine both the static and dynamic rollover thresholds of the ASV. The static rollover threshold (SRT) refers to the relative roll stability limit, expressed in terms of lateral acceleration, under a constant-speed steady turning maneuver, idealized by a ramp-step steering input shown in Fig. 5.10(a), when the RSF approaches unity value.

The roll response of the vehicle combination, however, is known to depend upon the steering frequency [170]. The dynamic rollover threshold (DRT is thus obtained from the RSF response to a path-change type of maneuver, idealized by a single-sinusoid steering input at 0.25 Hz, as shown in Fig. 5.10(b). For the purpose of determining SRT and DRT, the simulations are initiated at a relatively low speed of 5 km/h and the RSF response to the chosen steering input is computed. The speed is gradually increased until the relative roll instability is identified on the basis of the RSF. The vehicle responses corresponding to the final speed are subsequently analyzed to drive the SRT and DRT accelerations of the ASV [190,238].

Table 5.1: Simulation parameters [197]

Vehicle (Front Unit)					
Parameter	**Value**	**Parameter**	**Value**	**Parameter**	**Value**
m_{sf}	4200kg	L_{f1}	0.08 m	Z_{cf}	0.04 m
I_{XXsf}	2329 kg.m^2	L_{f2}	1.48 m	H_{sf}	1.0765m
I_{YYsf}	3739 kg.m^2	f	0.087m	Z_{Hf}	0.15 m
I_{ZZsf}	3813 kg.m^2	l_x	0.85m	$\mathrm{K_y}$	0.65
T_w	0.95 m	a	0.285 m	$\mathrm{K_{Ti}}$ (i=1,...,4)	800kN/m
R_w	0.65 m	b	1.39 m	B_y	6 rad^{-1}
σ_y	0.60m	h'	0.49 m		
Vehicle (Rear Unit - Loaded)					
m_{sr}(unsuspended)	13450kg	I_{XXL}	50 kg.m^2	h_2	0.15m
m_{sr} (suspended)	12500kg	Z_{cr}	0.87m	$K_{\theta y}$	5000KN/rad
I_{XXsr} (nsuspended)	9655 kg.m^2	Z_{Hr}	1.00m	$K_{\varphi x}$	1000KN/rad
I_{XXsr} (suspended)	8650kg.m^2	H_{sr}	1.906m	k_z	150kN/m
I_{YYsr}	12655kg.m^2	d	0.203m	k_y	200kN/m
I_{ZZsr}	11905 kg.m^2	L_{r1}	0.665m	k_t	125KN/rad
mu	1050 kg	L_{r2}	0.872m	c_z	4000N.m/s
I_{XXu}	1100 kg.m^2	L_0	0.16m	c_y	4000N.m/s
m_R	50kg	L_1	0.40m	c_t	3500N.m/s
I_{XXR}	50 kg.m^2	c	0.25m		
m_L	50kg	h_1	1.34m		
Vehicle (Rear Unit - Unloaded)					
m_{sr}(Un-suspended)	3450kg	I_{ZZsr}	3087 kg.m^2	L_{r1}	1.16m
m_{sr}(Suspended)	2500kg	$\mathrm{Z_{cr}}$	0.1423m	L_{r2}	0.38m
I_{XXsr} (Un-suspended)	2331 kg.m^2	$\mathrm{Z_{Hr}}$	0.2513m	H	1.40m
I_{XXsr} (Suspended)	2000kg.m^2	H_{sr}	1.1763m	h_1	0.5663m
I_{YYsr}	2822kg.m^2	h_s	0.5063m	D	0.50m

SRT is defined as the magnitude of lateral acceleration of the rear unit under the steady turning maneuver, when the vehicle approaches the relative roll instability condition ($RSF = \pm 1$). The DRT of the vehicle is expressed as the effective lateral acceleration (ELA) of the vehicle subject to a path-change type of maneuver, given by [190]:

$$ELA = \frac{(m_{sf}h_{sf}a_{ysf} + m_{sr}h_{sr}a_{ysr}) + m_u h_u a_{yu}}{(m_{sf}h_{sf} + m_{sr}h_{sr}) + m_u h_u} \tag{5.21}$$

where h_{sf}, $h_{sr}$and h_u are the instantaneous *cg* heights of the front unit, rear unit and rear axle (for the suspended vehicle model), respectively. a_{ysf}, a_{ysr} and a_{yu} are the lateral accelerations experienced by the sprung masses and rear unsprung mass, when $RSF = \pm 1$.

Critical Speed and Yaw Response Analyses

Articulated vehicles also exhibit frequency-dependent rearward amplification (RA) of the yaw velocity response under path-change type of steering maneuvers. The RA describes the amplification or attenuation of the yaw response of the rear unit with respect to the lead unit, such that:

$$RA = \left| \frac{r_{sr(peak)}}{r_{sf(peak)}} \right| \tag{5.22}$$

where $r_{sr(peak)}$ and $r_{sf(peak)}$ are the peak yaw velocity responses of the rear and the front units, respectively. A greater value of RA suggests greater yaw oscillations of the rear unit and potential yaw instability.

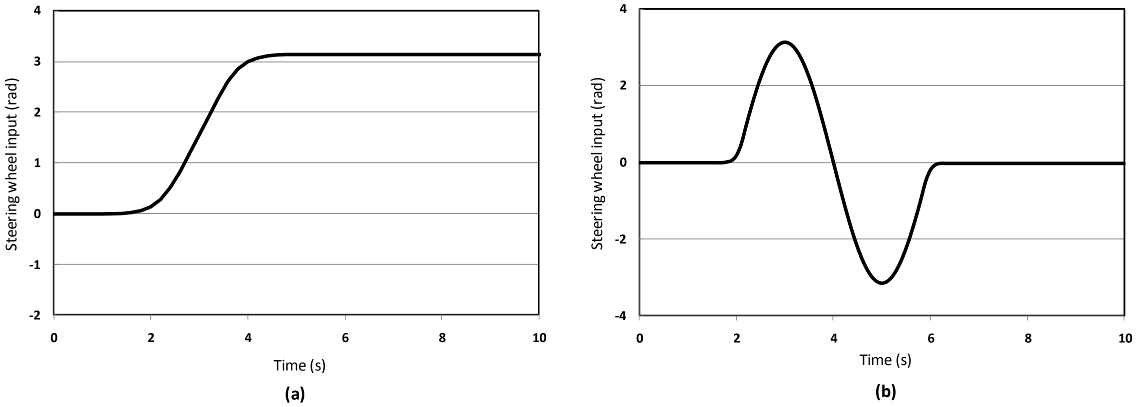

Figure 5.10: (a) Steering wheel input corresponding to a steady-turn (ramp-step) input; and (b) a path-change maneuver, idealized by a sinusoid.

The yaw or snaking stability limit of the ASV is also evaluated from the rate of decay of the articulation angle response under a pulse steering input, as described in [235]. The oscillatory articulation response is described by an exponential function of the form: $\varphi_d = \Phi_0 e^{\rho t}$, where Φ_0 is a constant and ρ represents the rate of decay. A positive value of ρ indicates a diverging response or snaking instability of the vehicle. The speed at which ρ approaches a positive value ($\rho > 0$) is denoted as the critical speed attributed to snaking tendency of the vehicle.

5.4 Results and Discussions

5.4.1 Model validations

The validity of the three-dimension vehicle model was examined on the basis of: (i) the measured ride vibration data obtained from field-tests performed on an articulated forestry skidder with and without the torsio-elastic suspension operating at a speed around 5km/h [22]; and (ii) the available measured steering strut responses of an articulated dump truck in terms of pressure differences and piston travel under a 90º right-hand turn maneuver [197]. The simulations were thus initially performed considering the parameters of the forestry skidder without the load and the corresponding terrain roughness of the two parallel tracks of the forestry terrain [232]. Figure 5.11 compares the PSD of acceleration responses of the suspended and unsuspended forestry skidder models along the vertical, lateral, yaw, pitch and roll axes at the operator seat location with the corresponding measured acceleration spectra. Reasonably good agreements between the model results and the measured data are obtained for both the suspended and unsuspended vehicles. Some deviations, however, are evident, which are likely caused by various simplifying assumptions, particularly the constant forward speed and linear properties of tires and suspension, and lack of consideration of terrain deformations and precise terrain roughness. The results show pitch and vertical mode resonance frequencies near 1 and 2 Hz, while the predominant lateral and roll vibration occur at frequencies near 0.9 Hz and above 2.5Hz, suggesting coupling between the lateral and roll modes.

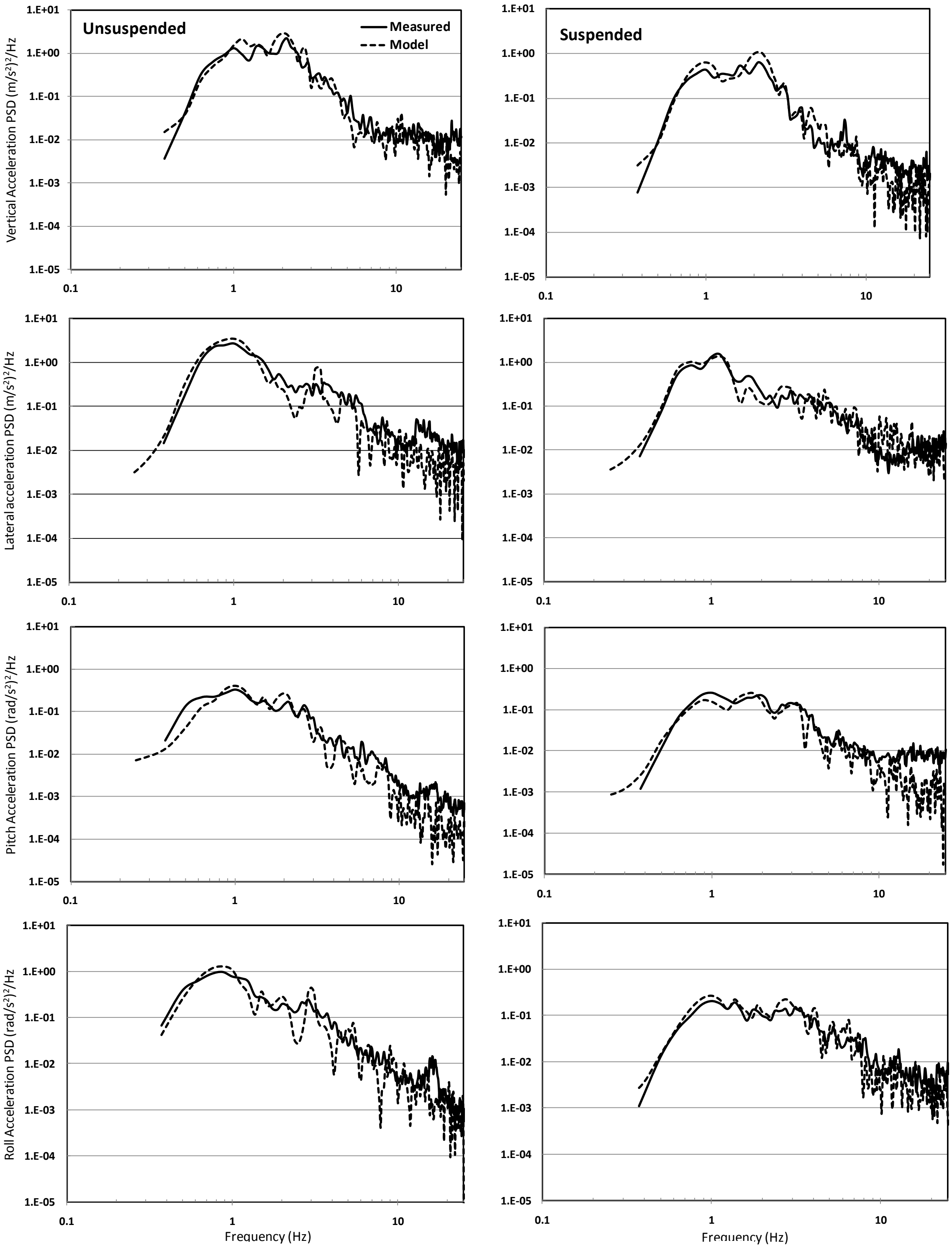

(a) (b)

Figure 5.11: Comparisons of vertical, lateral, pitch and roll acceleration PSD responses of vehicle models with spectra of the measured acceleration data at a forward speed of 5 km/h: (a) unsuspended vehicle; and (b) vehicle with rear axle torsio-elastic suspension.

The overall frequency-weighted and unweighted rms acceleration responses of the unsuspended and suspended skidder models are further computed with those derived from the measured data in Table 5.2. The results suggest good agreements between the rms accelerations of both the vehicle models and the measured data, particularly for the lateral, roll and pitch rms accelerations. Slightly higher deviations, however, are observed in the vertical rms acceleration. The rms of the measured vertical accelerations of both the unsuspended and suspended vehicles are consistently lower compared to the model results, which may be partly attributed to the undeformable terrain and point-contact tire model considered in the study. The model results suggest that the three-dimensional model can effectively predict the ride dynamic responses of ASVs, and can serve as a tool to seek desirable suspension design parameters for limiting the WBV exposure of the drivers.

Table 5.2: Comparisons of unweighted and frequency-weighted rms acceleration responses of the model with those obtained from the measured data [22]

Unsuspended	Unweighted rms acceleration (m/s^2 or rad/s^2)				Frequency-weighted rms acceleration (m/s^2 or rad/s^2)			
	Vertical	*Lateral*	*Pitch*	*Roll*	*Vertical*	*Lateral*	*Pitch*	*Roll*
Model	2.05	1.66	0.63	1.13	1.24	1.44	0.42	0.76
Measured	1.83	1.79	0.70	1.10	1.12	1.52	0.46	0.75
Deviation (%)	12.0	-7.3	-10.0	2.7	10.7	-5.3	-8.7	1.3
Suspended	*Vertical*	*Lateral*	*Pitch*	*Roll*	*Vertical*	*Lateral*	*Pitch*	*Roll*
Model	1.08	1.26	0.78	0.94	0.67	1.03	0.41	0.47
Measured	1.00	1.30	0.82	0.87	0.62	1.07	0.43	0.44
Deviation (%)	8.0	-3.1	-4.9	8.0	8.1	-3.7	-4.7	6.8

The available steering struts response data for an unloaded articulated dump truck permitted only limited validation of the three-dimensional model, particularly the kineto-dynamic steering system model. The simulations results were obtained under the steering input used during the measurements [197], i.e., a 90° right-hand turn applied at t=20s, while operating on a smooth road at a forward speed of 15 km/h. The simulation results are compared with available field-measured data in terms of pressure difference across the strut piston (P_1- P_2) and the left piston travel (X_L), respectively, in Figs. 5.12(a) and 5.12(b). The comparisons show reasonably good agreements of the model responses with the limited available measured data, although some discrepancies between the two are also evident, which are mostly attributed to corrective steering, steering system compliance, and contributions of the terrain roughness. The simulation results show that both the pressure difference and the strut deflection responses increase rapidly with application of steering wheel input at about t=20s and decrease as the steering wheel input diminishes.

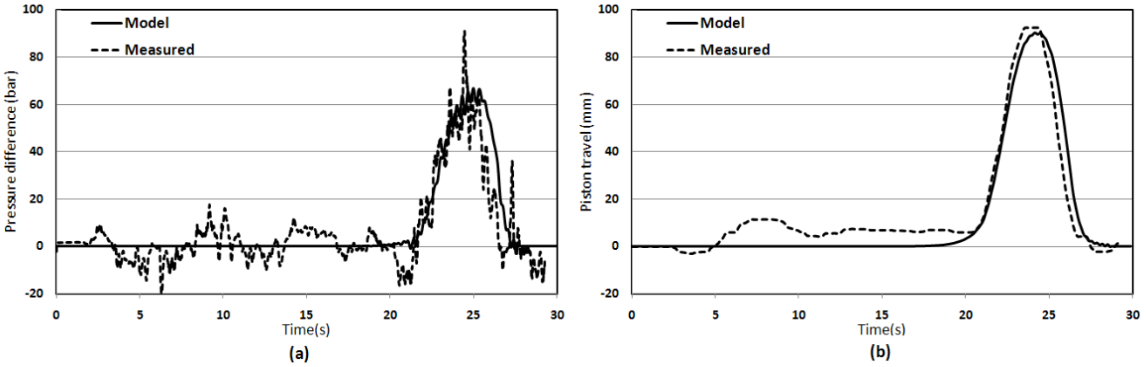

Figure 5.12: Comparisons of pressure difference and piston travel responses of the left steering strut derived from vehicle model with the measured data: (a) pressure difference; and (b) piston travel (90-degrees right-hand turn; speed=15 km/h)

5.4.2 Ride dynamics responses of the articulated dump truck

The validated model together with simulation parameters of the articulated dump truck is used to determine the ride and directional dynamic responses under the chosen terrain and steering inputs. The PSD of acceleration responses along the vertical, lateral, pitch, roll and yaw axes at the seat location of the unsuspended and suspended vehicle models are compared in Fig. 5.13. The results are obtained considering constant forward speed of 30 km/h and terrain excitations described in Fig. 5.9. The vertical and pitch response spectra of the unsuspended vehicle show peaks near 2.2 and 0.85 Hz, which are the respective resonance frequencies. A study of responses obtained by varying tire lateral stiffness suggested roll, lateral and yaw mode resonances near 0.875, 3.125 and 4.75 Hz, respectively. The roll, lateral and yaw responses of the vehicle model with rear axle suspension suggest even stronger coupling with peaks near 0.7, 1-1.25, 1.625 and 3.175 Hz.

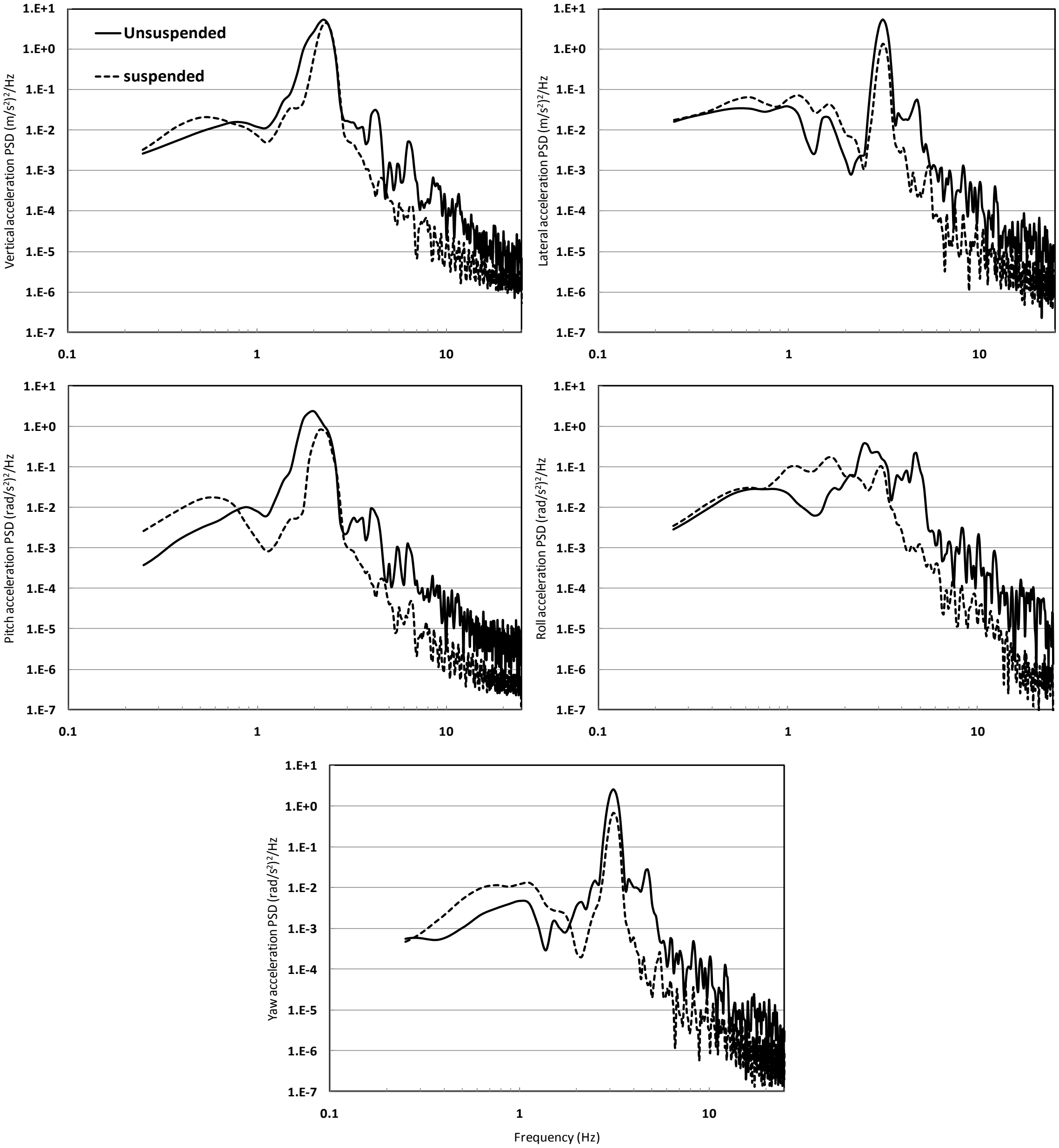

Figure 5.13: Comparisons of PSD of vertical, lateral, pitch, roll, and yaw acceleration responses of the unsuspended and suspended articulated dump truck models (speed = 30 km/h).

The addition of rear axle suspension resulted in relatively lower pitch mode frequency near 0.63 Hz but comparable vertical mode frequency near 2.2 Hz. The suspended vehicle also yields relatively lower roll and yaw mode frequencies. It should be noted that the ride dynamics of the unsuspended front unit contributes strongly to ride responses near the operator seat, particularly around 2.2 Hz and 3.175 Hz. The responses, however, show additional peaks near the above noted frequencies, which can be attributed to resonance frequencies of the rear suspended unit. The results suggest that the vehicle model with suspended rear unit yields lower vertical response at frequencies above 3 Hz, while the pitch acceleration is lower in the 0.75-2.2 Hz range and above 2.5 Hz. The lateral, yaw and roll acceleration responses of the ASV with suspended rear unit are considerably lower at frequencies above 2 Hz compared to the unsuspended ASV model, while the magnitudes at lower frequencies are generally higher.

The potential ride performance benefits of the rear-axle suspension are subsequently evaluated from the unweighted and frequency-weighted rms acceleration responses at the driver seat location in accordance with ISO-2631-1[3]. Table 5.3 compares the W_k-weighted vertical, W_d-weighted lateral, and W_e-weighted roll, pitch and yaw rms acceleration responses of the unsuspended and suspended ASV models under the loaded condition. The results suggest that implementation of the torsio-elastic rear axle suspension could significantly reduce the vibration exposure of the operators in all the directions. The suspended vehicle model yields 36, 22, 21, 54 and 37% reductions in the frequency-weighted lateral, vertical, roll, pitch and yaw vibration exposures, respectively, compared to the unsuspended vehicle model, when loaded. Compared to the relative benefits of the suspension observed for the articulated forestry skidder model (Table 5.2), the ride benefits for the dump truck model are relatively smaller in all directions, except in pitch. This can be partly attributed to a number of vehicle design factors. Unlike the skidder, the operator seat in a dump truck is located ahead of the front unit axle, which yields greater contribution of pitch and yaw motions to vertical and lateral acceleration responses, respectively. Higher cg height of the dump truck compared to the skidder would also cause higher vertical, roll and lateral acceleration responses. Furthermore, the torsio-elastic suspension retrofitted to the skidder was adequately tuned considering the load distributions.

Table 5.3: Comparisons of frequency-weighted and unweighted rms translational (m/s^2) and rotational (rad/s^2) acceleration responses near the driver seat location of the unsuspended and suspended ASV models.

	Vehicle Model	rms Acceleration				
		Vertical	*Lateral*	*Pitch*	*Roll*	*Yaw*
Unweighted	*Unsuspended*	1.62	1.32	1.08	0.77	0.90
	Suspended	1.25	0.81	0.56	0.46	0.54
Frequency-Weighted	*Unsuspended*	0.93	0.85	0.56	0.34	0.30
	Suspended	0.73	0.54	0.26	0.27	0.19

5.4.3 Roll and yaw stability analysis of articulated dump truck

The transient yaw and roll responses of the suspended and unsuspended vehicle models are obtained under the idealized path-change maneuver, shown in Fig. 5.10(b), at a constant forward speed of 30km/h on a perfectly smooth road surface. The time histories of the roll safety factor (RSF), roll angle, lateral acceleration and yaw velocity responses of the front and rear unit of the loaded dump truck are shown in Figs. 5.14(a) and (b), respectively. The results illustrate relatively higher load transfer at the rear unit axle, which is attributed to higher cg and load of the rear unit of the loaded dump truck. The load transfer is even greater for the suspended rear unit compared to the unsuspended unit, as it would be expected. The suspended vehicle also yields higher roll response of both the units compared to the unsuspended vehicle model, which is attributable to lower effective roll stiffness of the suspended vehicle. This is also evident from the lateral acceleration and yaw velocity responses, where the suspended vehicle shows higher peak values for both the front and rear units compared to the unsuspended vehicle. The yaw velocity responses also show only slight rearward yaw amplification (RA) tendency of the suspended vehicle. At the forward speed of 30 km/h, considered in the study, the suspended vehicle revealed peak RA of nearly 1.01, while that the unsuspended vehicle is in the order of 0.96 (Table 5.4).

The articulation angle responses of the suspended and unsuspended vehicle models are further evaluated under a pulse steering input applied at different speeds up to 120 km/h. The oscillatory articulation angel responses are analyzed to identify the rate of decay ρ to study the effect of suspension on the critical velocity associated with the snaking instability. Figure 5.15 presents the snaking mode diagrams of the suspended and unsuspended vehicle models, illustrating variations in ρ with the vehicle speed. The results suggest lightly damped snaking mode at low forward speeds. The rate of decay of oscillations increases with speed up to 45km/h and increases with speed above 45km/h for the both the unsuspended and suspended vehicles. At higher speeds, the rate of decay approaches a positive vale (ρ >0), suggesting a snaking instability. The speed corresponding to ρ=0 is denoted as the critical speed, V_{crit}, associated with snaking instability of the vehicle, which are summarized in Table 5.4. The results show that the V_{crit} of the suspended vehicle (72km/h) is lower than that of the unsuspended vehicle (81km/h). These are lower than 90km/h earlier study that considered a three-DOF yaw plane model of the vehicle [235]. The observed difference is attributable to considerations of the suspension and roll motions of the vehicle units in the present study.

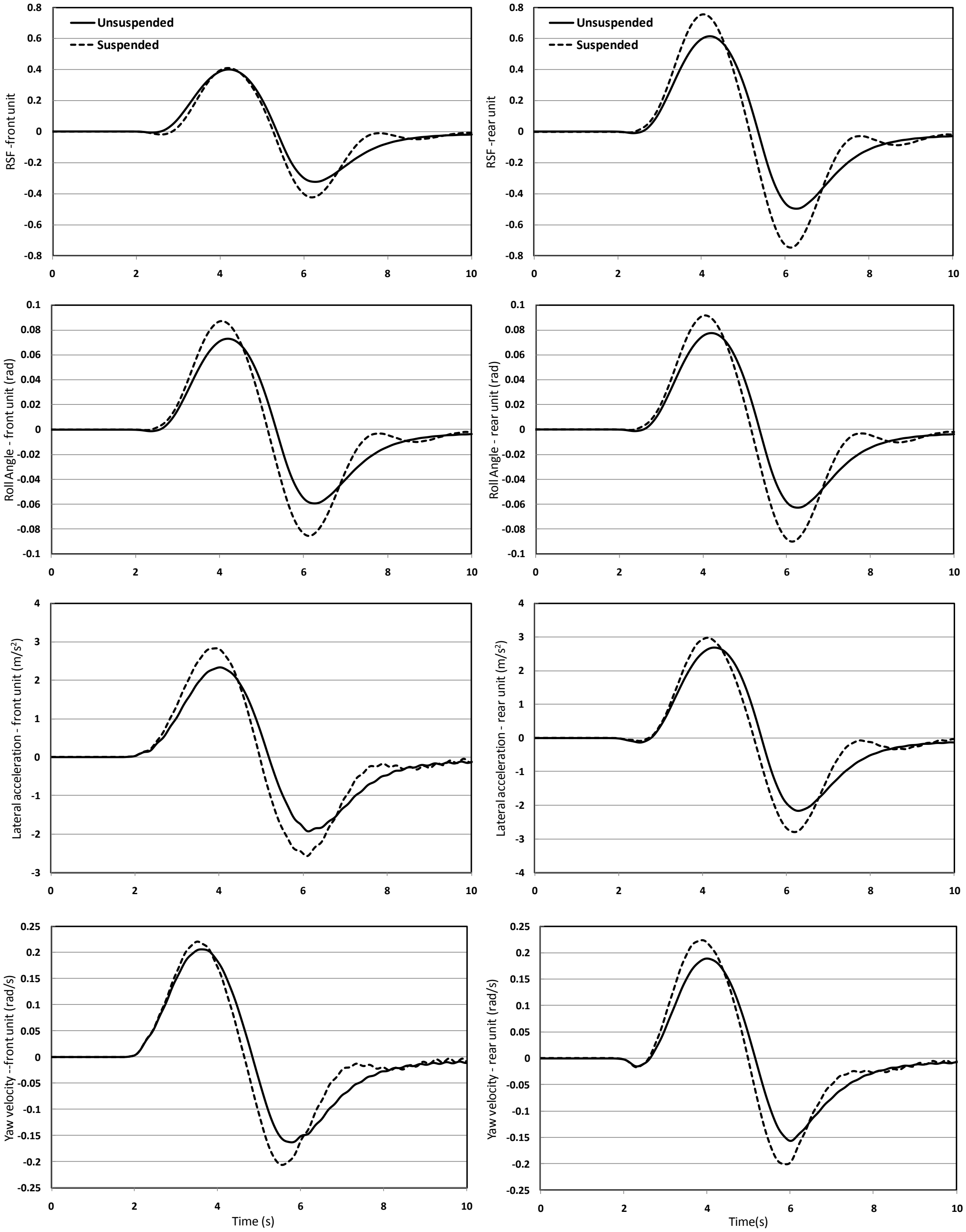

(a) **(b)**

Figure 5.14: Comparisons of RSF, roll angle and lateral acceleration responses of unsuspended and suspended articulated dump truck models subject to the idealized path-change maneuver at a forward speed of 30 km/h: (a) front unit; and (b) rear unit.

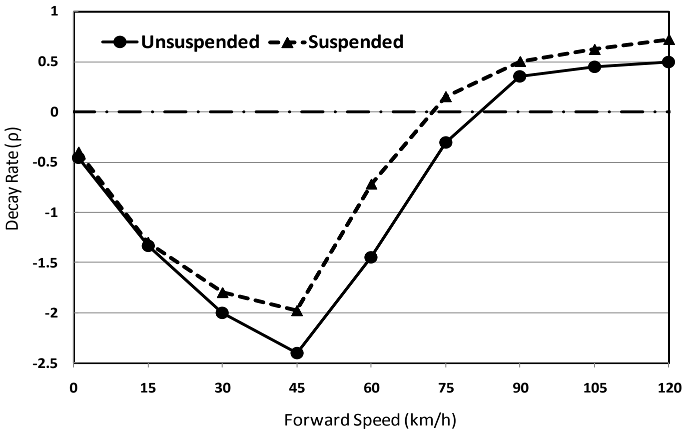

Figure 5.15: Snaking mode diagrams of the suspended and unsuspended vehicle models

The static and dynamic roll stability characteristics of the suspended and unsuspended vehicle models are subsequently evaluated under the steady (ramp-step) and path-change maneuvers at varying forward speeds, respectively. The static rollover thresholds (SRT) of the models are taken as the lateral accelerations corresponding to the speed when the vehicle approaches the relative roll instability (RSF=±1). Similarly, the DRT is taken as the effective lateral acceleration (ELA) when the vehicle approaches relative roll instability under the path-change maneuver. Both the SRT and DRT of the suspended vehicle model are lower than those of the unsuspended vehicle model, as seen in Table 5.4. The SRT and DRT of the vehicle model with torsio-elastic suspension are nearly 10.1% and 9.4% lower than those of the unsuspended vehicle, respectively. These suggest that addition of the rear-axle suspension yields relatively small reductions in the roll stability limits of the vehicle, which is attributable to relatively higher roll stiffness of the torsio-elastic suspension. The results also show that the DRT of the vehicle models are lower compared to the SRT, suggesting relatively lower dynamic roll stability limits of the vehicle. The ratios of DRT to SRT are 0.927 and 0.934, respectively, for the unsuspended and suspended vehicle models. These suggest that SRT could also provide a reasonable estimation of the dynamic rollover propensity of the vehicle. The difference between the SRT and DRT values, however, is smaller for the suspended vehicle compared to the unsuspended vehicle.

Table 5.4 Static (SRT) and dynamic (DRT) rollover thresholds, yaw velocity rearward amplification ratios (RA) and snaking mode critical speeds (V_{crit}) of the unsuspended and suspended vehicle models

	Steady Turning	Path-change		
	***SRT*(*g*)**	***DRT*(*g*)**	***RA***	**V_{crit}**
Unsuspended	0.424	0.393	0.96	81
Suspended	0.381	0.356	1.01	72

5.4.4 Effect of terrain roughness on roll and yaw directional stability

The directional response characteristics and stability limits of heavy vehicles are generally evaluated considering smooth road surface. The tires interactions with rough terrains could yield greater vehicle roll and lateral load transfer responses, and thereby affect the roll as well as yaw stability limits in a highly adverse manner. The simulations are performed under the steady and path-change steering inputs (Fig. 5.10) in the presence of tire interactions with the rough terrain (Fig. 5.9). The simulation results are analyzed to establish the effect of terrain roughness on the yaw and roll stability measures (RA, V_{crit}, SRT and DRT), which are summarized in Table 5.5. The results clearly show considerably lower roll and yaw stability limits in the presence of tires interactions with the rough terrain. The SRT of the unsuspended and suspended vehicle models decrease by about 15% and 12%, respectively, when the terrain profile is considered. The respective DRT values are around 11% and 8% lower. The critical speed also decreased from 81 to 72 km/h for the unsuspended vehicle and from 72 to 65km/h for the suspended vehicle, while the RA values increased in the presence of terrain roughness. The results thus suggest greater snaking tendency of the vehicle on rough terrains, and relatively lower sensitivity of the suspended vehicle to terrain roughness.

Table 5.5 Influence of road elevation on the roll and yaw stability measures of the vehicle models.

Vehicle model	Road condition	*Roll stability*		*Yaw stability*	
		SRT	**DRT**	***RA***	V_{crit} **(*km/h*)**
Unsuspended	*Smooth*	0.424	0.393	0.96	81
	Plowed-field	0.360	0.350	1.02	72
Suspended	*Smooth*	0.381	0.356	1.01	72
	Plowed-field	0.336	0.326	1.07	65

5.4.5 Effect of vehicle load on ride and yaw/roll responses

The ASVs generally encounter wide variations in vehicle load during a work cycle, which could significantly affect the ride performance and roll/yaw stability limits. The simulations were thus performed for the unloaded and fully loaded suspended and unsuspended vehicles under identical steering inputs at 30km/h, and the results are analyzed to evaluate the effect of load on ride, and yaw and roll stability limits. Table 5.6 summarizes the frequency-weighted rms accelerations, and roll and yaw stability limits of loaded and unloaded vehicle models. The results show significantly higher frequency-weighted rms accelerations and lower stability limits of the loaded unsuspended vehicle compared to the unloaded vehicle. The ride vibration exposure tends to be substantially higher along all the axes for the loaded vehicle due to greater inertia and cg height. The frequency-weighted vertical, lateral, pitch, roll and yaw rms accelerations of the loaded vehicle are nearly 36%, 29%, 70%, 55% and 30% higher than those for the unloaded vehicle. The suspended vehicle, however, shows substantially lower sensitivity to vehicle load in the context of vehicle ride performance. The weighted acceleration responses of the loaded suspended vehicle are either comparable or slightly lower than those of the unloaded vehicle along all the translational and rotational axes, which suggests beneficial kinematic advantage of the torsio-elastic suspension.

Table 5.6: Influence of variations in vehicle load on the frequency-weighted rms acceleration responses, static (SRT) and dynamic (DRT) rollover thresholds, rearward amplification ratio (RA), and snaking mode critical speed (V_{crit})

Model	Load	rms acceleration (m/s^2 or rad/s^2)					*SRT* (*g*)	*DRT* (*g*)	*RA*	V_{crit} (km/h)
		Vertical	*Lateral*	*Pitch*	*Roll*	*Yaw*				
Unsuspended	No-load	0.68	0.66	0.33	0.22	0.23	0.501	0.457	0.89	95
	Loaded	0.93	0.85	0.56	0.34	0.30	0.360	0.350	1.02	72
Suspended	No-load	0.76	0.59	0.23	0.30	0.16	0.434	0.401	0.95	83
	Loaded	0.73	0.54	0.26	0.27	0.19	0.336	0.326	1.07	65

Owing to the higher load and cg height, the yaw and roll stability limits of the loaded vehicle are substantially lower than those of the unloaded vehicle, as seen in Table 5.6. For the unsuspended model, the loaded vehicle yields 28% and 23% lower values of the SRT and DRT, respectively, compared to the unloaded vehicle. The corresponding reductions for the suspended vehicle are 23% and 19%. Addition of load also caused the rear unit cg to shift closer to the articulation joint, which further contributed to reduced snaking and yaw stability limits [30]. This is evident from the lower V_{crit} and higher RA of loaded vehicle (Table 5.6). The V_{crit} of the unloaded suspended and unsuspended vehicle models increased to 83 and 95km/h, respectively, compared to 65 and 72km/h for the loaded vehicles.

5.4.6 Effect of suspension parameters on ride and yaw/roll responses

Apart from the vehicle load and terrain roughness, the ride and directional dynamic performance of a vehicle are strongly affected by the suspension design parameters. The load carrying capacity, ride and directional performances, however, impose conflicting requirements on the suspension design. The influences of variations in the suspension design parameters on the ride and yaw/roll stability measures are investigated. The results could provide important suspension design guidance to realize a better compromise among the ride and roll/yaw stability performance measures of the vehicle. Simulations are performed considering full vehicle load, roughness profiles of the two parallel terrain tracks and forward speed of 30 km/h. Influences of variations in different suspension parameters are considered. These include: the suspension stiffness (k_y, k_z, k_t) and damping (c_y, c_z, c_t) constants of the torsion bars, and length of link (L_0) coupling the sprung and unsprung masses. The stiffness and damping constants are varied by ±50% about the nominal value, while the variation in the link length is limited to ±25%. The vehicle track width, however, is held constant, irrespective of the link length.

Table 5.7 summarizes the influences of variations in above-stated suspension parameters on: (i) the ride performance expressed in terms of frequency-weighted rms accelerations at driver seat location; and (ii) roll and yaw stability measures in terms of SRT, DRT, RA and V_{crit}. The results revealed that increase in the vertical stiffness, which causes higher pitch and vertical mode resonance frequencies, resulted in higher frequency-weighted vertical and pitch rms accelerations. The results suggest that reducing the vertical suspension stiffness (k_z) yields 5.5% and 15% reductions in frequency-weighted vertical and pitch rms accelerations, respectively, while the effects on yaw, roll and lateral accelerations are very small. These suggest relatively weak coupling of the vertical mode with the roll and lateral modes of the vehicle. Reducing the torsio-elastic vertical suspension stiffness also yields relatively small effects on the roll and yaw stability measures. While the SRT value decreases by 3.3%, the corresponding changes in dynamic stability measures (DRT, RA and V_{crit}) are within 1.5%, where the lateral and torsional suspension stiffness plays an important role. Increasing the vertical stiffness by 50%, however, could yield 5% higher SRT coupled with considerably higher pitch and vertical accelerations.

Table 5.7: Influence of variations in the torsio-elastic suspension properties on the frequency-weighted rms acceleration responses, static (SRT) and dynamic (DRT) rollover thresholds, rearward amplification ratio (RA), and snaking mode critical speed (V_{crit})

Parameters		rms acceleration (m/s^2 or rad/s^2)					SRT(g)	DRT(g)	*RA*	V_{crit}(km/h)
		Vertical	Lateral	Pitch	Roll	Yaw				
Nominal value		**0.73**	**0.54**	**0.26**	**0.27**	**0.19**	**0.336**	**0.326**	**1.07**	**65**
k_z	-50%	0.69	0.53	0.22	0.26	0.17	0.325	0.324	1.08	64
	+50%	0.77	0.55	0.30	0.28	0.18	0.353	0.327	1.06	67
k_y	-50%	0.73	0.63	0.26	0.30	0.22	0.332	0.323	1.10	60
	+50%	0.74	0.47	0.26	0.26	0.17	0.340	0.328	1.04	69
k_t	-50%	0.73	0.56	0.26	0.32	0.19	0.304	0.305	1.09	62
	+50%	0.73	0.52	0.26	0.21	0.18	0.361	0.347	1.04	69
c_z	-50%	0.74	0.55	0.29	0.28	0.19	0.335	0.326	1.07	65
	+50%	0.73	0.53	0.23	0.27	0.19	0.336	0.326	1.07	65
c_y	-50%	0.73	0.56	0.26	0.29	0.19	0.336	0.330	1.06	66
	+50%	0.73	0.52	0.26	0.25	0.18	0.336	0.322	1.08	64
c_t	-50%	0.73	0.56	0.26	0.30	0.20	0.337	0.326	1.07	65
	+50%	0.73	0.53	0.26	0.25	0.18	0.335	0.326	1.07	65
L_0	-25%	0.73	0.56	0.26	0.29	0.19	0.339	0.326	1.07	66
	+25%	0.72	0.50	0.27	0.21	0.19	0.333	0.326	1.08	63

Reducing the lateral stiffness (k_y) yields notably lower yaw stability measures, while the effects on roll stability measures are very small, within 1.2%. The V_{crit} and RA decrease by 7.7% and 2.8%, respectively. The variations in k_y affects only the lateral, roll and yaw accelerations, which increase by 16.7, 11.1 and 15.8%, respectively. The increase accelerations is mostly attributed to lower resonance frequencies and higher magnitudes of W_d- and W_e-weighting in the lower frequency range. Reductions in the torsional stiffness (k_t), on the other hand, yields lower mode frequency and thereby considerably higher W_e-weighted roll acceleration (18.5%). Relatively small effect is also observed on the lateral acceleration, which is due to coupling between the roll and lateral modes. Lower value of k_t, however, reveals most detrimental effect on the SRT and DRT, in the order of 10.1 and 6.4%, respectively. The V_{crit} also decreases notably by 4.6%, while the effect on RA is small.

The torsio-elastic suspension yields only minimal suspension damping attributed to hysteretic damping of the elastic torsion bars. Increasing the damping constants by 50% revealed nearly negligible changes on all of the ride and stability measures. Higher damping in the lateral and torsion modes (c_y, c_t), however, resulted in slightly lower magnitudes of lateral and roll accelerations, while higher vertical damping (c_z) caused lower pitch and vertical accelerations. An increase in c_y, however, resulted in slightly higher DRT and V_{crit}.

Apart from the torsion bars properties, the suspension kinematics could also affect the vehicle performance. The kinematic effect in this study is considered by varying the length of the suspension link (L_0), which would alter the suspension spring track and thus the effective roll stiffness. The results show that increasing L_0 yields nearly negligible to very small effects on the roll and yaw stability measures, even though the effective roll stiffness would be lower. This suggests that the stability measures are more strongly affected by torsional stiffness of the suspension, which is also evident from the results in table 5.7. An increase in L_0, however, yields substantially lower weighted roll acceleration, in the order of 22%, while the effects on vertical, yaw, and pitch responses are relatively small.

The results in Table 5.7 suggest that the static rollover threshold of the vehicle is more sensitive to variations in k_z and k_t, while the DRT and V_{crit} exhibit greater sensitivity to k_y and k_t. Higher vertical stiffness could help realize greater yaw and roll stability at the expense of poor ride along all the axis, particularly along the vertical and pitch axis. A higher lateral stiffness could yield higher yaw stability limits coupled with moderate gains in SRT and DRT, and lateral and roll accelerations. Higher torsional stiffness, on the other hand, could yield roll stability measures (SRT and DRT) quite similar to those of the unsuspended vehicle coupled with higher RA and V_{crit}. Furthermore, higher torsional stiffness yields beneficial effect on the lateral and roll accelerations, and no effect on the vertical and pitch ride. A suspension design with higher lateral and torsional stiffness is thus expected to provide an improved compromise among the ride performance, and yaw and roll directional stability measures of the articulated dump truck.

5.5 Conclusions

A comprehensive 3-dimensional articulated steer vehicle model was formulated and validated, which was then employed for vehicle ride and handling dynamics, and stability analyses under different driving scenarios. Articulated steer vehicles with and without a rear-axle torsio-elastic suspension were analyzed. The use of the rear-axle torsio-elastic suspension revealed substantial ride performance benefits but relatively lower yaw and roll stability limits. From the parametric sensitivity analyses, it is concluded that the suspension design with greater lateral and torsional stiffness could yield roll and yaw stability limits similar to those of the unsuspended dump truck, while retaining the ride performance benefits of the torsio-elastic suspension. Furthermore, the suspended vehicle showed very low sensitivity to variations in vehicle load in view of the ride performance. The loaded vehicle, however, revealed considerably lower yaw and roll stability limits, attributed to higher inertia, cg height and shifting of the rear unit cg closer to the articulation joint. Furthermore, the tire interactions with the rough terrain affected the stability limits in a highly adverse manner. It is thus concluded that the directional performance analyses of ASVs, which operate on both the paved and unpaved surfaces, need to be evaluated under representative terrain excitations. The yaw and roll stability limits, obtained in this study, however, may be considered conservative when operating on deformable terrains. The results further showed that the dynamic rollover threshold of the vehicle is less sensitive to variations in the torsio-elastic suspension parameters compared to the static rollover threshold, which is mostly affected by suspension torsional stiffness. The dynamic rollover threshold of the vehicle was observed to be lower than the static rollover threshold, while the ratio of dynamic to static rollover threshold ranged from 0.91 to 1.0 for both the suspended and unsuspended vehicle models, irrespective of the load and terrain roughness. The static rollover threshold could thus be employed to attain a reasonable estimation of the dynamic rollover propensity of the vehicle. The results suggest that the proposed three-dimension model could serve as an effective tool to assess ride and directional stability performance of articulated frame steer vehicles operating on rough terrains, and provide essential guidance on suspension design and tuning.

CHAPTER 6

CONCLUSIONS AND RECOMMENDATIONS

6.1 Highlights and major contributions of the dissertation research

This dissertation research presents systematic analytical and field studies of an advanced passive suspension concept to achieve enhanced ride performance while preserving the roll/directional stability performance of articulated frame steer vehicles (ASV). A comprehensive kineto-dynamic analysis of the frame steering mechanism is also presented and the critical design features affecting the snaking stability are identified. A comprehensive analytical model of an ASV is formulated for integrated ride and stability analysis, and axle suspension design and tuning. The major highlights of the dissertation work are summarized below:

- The ride performance potentials of a torsio-elastic suspension concept are investigated for a forestry skidder. The ride performance analyses are performed through development of ride dynamic model and simulations, and field measurements.

- The 13-DOF vehicle model is used for sensitivity analyses to study the effects of various suspension design parameters.

- A three-dimension tire model is proposed and integrated to ride dynamic model to account for tire interactions along the fore-aft, lateral and vertical axes. the model is based on an adaptive radial representation for characterizing the resultant vertical and longitudinal forces within the contact patch, and the side-slip theory together with the tire-lag to estimate lateral forces.

- A methodology is proposed to synthesize roughness profiles of the two terrain tracks considering coherency between the left and right tracks. A coherence function was proposed to describe the linear dependence of two random profiles of the off-road so as to synthesize relatively low frequency components of the off-road terrains.

- A kineto-dynamic model of the articulated frame steering mechanism is proposed to account for kinematics and dynamics of the hydraulic steering struts, leakage flows and steering valve characteristics. The steering model is integrated into a nonlinear yaw-plane model of an articulated dump-truck to study the roles of steering system kinematics and dynamics on critical vehicle speeds associated with snaking stability performance. For this purpose, a methodology based on decay rate of the yaw response oscillations is proposed for identifying the critical speed.

- A comprehensive three-dimensional model of an articulated frame steer vehicle with and without a rear axle suspension is proposed for integrated ride and directional stability of the vehicle. Performance measures are defined to evaluate static and dynamic roll stability limits, and rearward yaw amplification of the ASV.

- A comprehensive parametric analysis is performed to study the influences of axle suspension design parameters on the vehicle ride and directional stability under a wide range of operating conditions.

6.2 Conclusion

The major conclusion drawn from the simulation results and the field-measured data are summarized below:

- The results attained from field measurements clearly show that the proposed torsio-elastic suspension could offer considerable benefits in reducing the WBV exposure of the off-road vehicle operators under loaded as well as unloaded conditions. The frequency-weighted rms accelerations along the translational axes at the operator location were 35% to 57% lower for the vehicle with rear-axle torsio-elastic suspension compared to the conventional unsuspended vehicle.

- The magnitudes of horizontal vibration transmitted to the operator’s station of the conventional vehicle were either comparable to or exceeded the vertical vibration magnitude, suggesting the need for an effective axle suspension.

- The ride dynamic responses obtained from the linear model considering simple point contact tire model agreed reasonably well with the measured responses, while the fore-aft and lateral ride responses could not be predicted.

- The optimal suspension parameters identified from solutions of a multi-objective minimization revealed further reductions of 6% in the frequency-weighted vertical accelerations.

- The radial tire model coupled with a lateral spring model based on side-slip theory and tire lag could effectively simulate the tire-terrain interactions along the three translational axes. The vehicle ride model incorporating the three-dimensional tire model provided very good estimations of ride responses along the fore-aft and lateral axes.

- Both the frequency-weighted and unweighted vertical and pitch rms accelerations were strongly affected by the suspension vertical stiffness, while the lateral and roll responses were mostly affected by suspension torsional and lateral stiffness. A suspension design with lower vertical stiffness and higher lateral and torsional stiffness, and higher vertical and lower lateral and torsional damping would be beneficial in limiting the ride vibration exposure of the vehicle operators.

- The vehicle fitted with the torsio-elastic rear axle suspension showed significantly lower sensitivity to variations in the vehicle load. The kinematic advantage of the torsio-elastic suspension is thus most beneficial in limiting the ride dynamic of the vehicle.

- The directional responses of an articulated steer vehicle were strongly dependent upon the kineto-dynamic properties of the steering mechanism. The steering responses and yaw stability limits were most significantly affected by the effective damping of the steering mechanism, which is dependent upon the maximum valve flow rate, the characteristic articulation angle error, and the leakage flows within the struts and struts orientations.

- The greater load on the rear axle of the frame steer vehicle resulted in lower snaking stability limit of the vehicle, while the yaw oscillations or snaking tendencies increased with speed. Minor leakage flows could yield substantially high yaw damping and thus a higher critical speed.

- Both the unsuspended and suspended vehicles show relatively higher load transfer at the rear unit axle, which is attributed to higher cg and load of the rear unit of the loaded dump truck. The suspended vehicle, however, resulted in greater roll motion, lateral acceleration, lateral load transfer and yaw velocity responses compared to the unsuspended vehicle.

- The suspended vehicle revealed only slightly lower static rollover threshold (10%) compared to the unsuspended vehicle due to lower effective roll stiffness of the suspended vehicle. This was attributed to high effective roll stiffness and kinematic effect of the torsio-elastic suspension, which provide higher roll stability of the vehicle compared to linear beam axle suspensions.

- The results generally revealed relatively lower values of (DRT) compared to (SRT) values for both the suspended and unsuspended vehicles. The ratio of DRT to SRT ranged from 0.91 to 0.98 for different load conditions. The static rollover threshold can thus be used to obtain reasonable estimates of the dynamic rollover propensity of the vehicle.

- The static and dynamic stability limits are significantly influenced by the vehicle load. The loaded vehicle revealed considerably lower yaw and roll stability limits, attributed to higher inertia, cg height and shifting of the rear unit cg closer to the articulation joint.

- The tire interactions with the rough terrain affected the stability limits in a highly adverse manner. The SRT of the unsuspended and suspended vehicle models decrease by about 15% and 12%, respectively, when the terrain profile is considered. The respective DRT values are around 11% and 8% lower.

- The suspension design with greater lateral and torsional stiffness could yield roll and yaw stability limits similar to those of the unsuspended dump truck, while retaining the ride performance benefits of the torsio-elastic suspension.

- The three-dimensional vehicle model can be effectively applied for integrate ride and directional stability analyses, design and tuning of axle suspensions, and design and analyses of the steering mechanism.

6.3 Recommendations for Future Studies

The proposed three dimensional model can serve as an effective tool for predicting the ride dynamic responses and directional stability limits of vehicle, and thereby facilitate axle suspension and steering system designs. The proposed passive torsio-elastic suspension introduced at the rear-axle of ASVs also offers a good compromise between the ride comfort and the stability performance of the vehicle. The models developed in the study and the suspension design thus offer attractive potentials for off-road vehicles, particularly the articulated frame steer vehicles that are designed for higher speed operations in road as well as off-road sectors. Considering that such vehicles yield high magnitudes of ride vibration and relatively lower directional stability limits, the vehicle operations at higher speeds poses greater safety risks. Additional efforts on suspension and steering designs so as to achieve higher speeds are thus highly desirable. Particular topics of future work may include the following:

- Experimental study and field measurement on the high-speed dump truck. An articulated dump truck, as a high-speed ASV, can be instrumented to measure the vibration responses at the seat location along the translational and rotational axis during the transport operation under loaded and unloaded conditions.

- Evaluations of ride and roll stability limits of an ASV with both suspended axles is desirable for realizing further improvements in ride: Alternate suspensions with high roll stiffness need to be explored to preserve roll stability. These may include the torsio-elastic suspension and roll and/or pitch connected hydro-pneumatic suspensions.

- It is essential to develop tire models to incorporate tire-interactions with deformable terrains. A ring model of the tire together with elastic-plastic model of the deformable terrain would likely provide a good starting point.

- A more refined model of the steering mechanism is most desirable to fully describe the nonlinear steering valve flows and flow saturation, fluid pressure drop in connecting pipes, struts seals and joints friction, and leakage flows.

- Field measurements of the steering system responses to various steering inputs are vital to develop an effective model that can be considered valid over a wide range of operating conditions, which can help derive steering system design for higher critical speeds.

- A virtual multi-body model of the vehicle with and without the axle suspensions incorporating suspension kinematics and dynamics would be most beneficial to seek improved axle suspension designs.

- A multi-objective optimization study is recommended to seek a set of design parameters of the proposed suspensions that can yield an enhanced compromise in both the ride and roll/directional stability characteristics of ASV.

- In order to improve the roll/directional stability of the vehicle, the stability control systems including dynamic stability control (DSC) and electronic stability program (ESP) could be developed to improve the control over the vehicle traction and to minimize the loss of control during high-speed maneuvers.

REFERENCES

1. Cation, S., Jack, R.J., Dickey, J.P., Lee-Shee, N. and Oliver, M. (2008) Six degree of freedom whole-body vibration during forestry skidder operations, *International Journal of Industrial Ergonomics*, 38, 739-757.

2. Neitzel, R. and Yost, M. (2002) Task-based assessment of occupational vibration and noise exposure in forestry workers, *American Industrial Hygiene Association* (*AIHA*) *Journal*, 63, 617-627.

3. ISO 2631-1 (1997) Mechanical vibration and shock-evaluation of human exposure to whole-body vibration - part 1: general requirements, ISO, Geneva, Switzerland.

4. European Committee for Standardization (CEN) (2003) Mechanical vibration. Measurement and evaluation of occupational exposure to whole-body vibration with reference to health. Practical guidance (Standard No. EN 14253:2003). Brussels, Belgium: CEN.

5. Seidel, H. (2005) On the relationship between whole body vibration exposure and spinal health risk, *Industrial Health*, 43, 361-377.

6. Bovenzi, M., Rui, F., Negro, C., D'Agostin, F., Angotzi, G., Bianchi, S., Bramanti, L., Festa, G., Gatti, S., Pinto, L., Rondina, L. and Stacchini, N. (2006) An epidemiological study of low back pain in professional drivers, *Journal of Sound and Vibration*, 298, 514-539.

7. Cann, A. P., Salmoni, A. W., Vi, P. and Eger, T. R. (2003) An exploratory study of whole-body vibration exposure and dose while operating heavy equipment in the construction industry, *Applied Occupational and Environmental Hygiene*, 18, 999-1005.

8. Donati, P. (2002) Survey of technical preventative measures to reduce whole-body vibration effects when designing mobile machinery, *Journal of Sound and Vibration*, 251, 169-183.

9. Ma, X.Q., Rakheja, S. and Su, C-Y. (2008) Damping requirement of a suspension seat subject to low frequency vehicle vibration and shock, *International Journal of Vehicle Design*, 47, 133-156.

10. Ma, X.Q., Rakheja, S. and Su, C-Y. (2008) Synthesis of a semi-active suspension seat for attenuation of whole-body vibration and shock, *International Journal of Vehicle Design*, 47, 157-175.

11. Tiemessen, I. J., Hulshof, C. T. J. and Frings-Dresen, M. H. W. (2007) An overview of strategies to reduce whole-body vibration exposure on drivers: a systematic review, *International Journal of Industrial Ergonomics*, 37, 245-256.

12. Rehn, B., Nilsson, T., Olofsson, B. and Lundström, R. (2005) Whole-body vibration exposure and non-neutral neck postures during occupational use of all-terrain vehicles, *Annals of Occupational Hygiene*, 49(3), 267-275.

13. Boulanger, P., Lemerle, P. and Poirot, R. (2002) A simplified method to design a suspension cab for counterbalance trucks, *Journal of Sound and Vibration*, 253, 283-293.

14. Ahmadian, M. and Patrico, P. S. (2004) Effect of panhard rod cab suspensions on heavy truck ride measurements, *SAE Transactions*, 113, 551-559.

15. Rakheja, S., Mandapuram, S. and Dong, R. G. (2008) Energy absorption of seated occupants exposed to horizontal vibration and role of back support condition, *Industrial Health*, 46, 550-566.

16. Yisa, M. G., Terao, H., Noguchi, N. and Kubota, M. (1998) Stability criteria for tractor-implement operation on slopes, *Journal of Terramechanics*, 35, 1-19.

17. Lehtonen, T. J. and Juhala, M. (2005) Predicting the ride behavior of a suspended agricultural tractor, *International Journal of System Modeling and Testing*, 1, 131-142.

18. Uys, P. E., Els, P. S. and Thoresson, M. (2006) Suspension setting for optimal ride comfort of off-road vehicles travelling on roads with different roughness and speeds, *Journal of Terramechanics*, 44, 163-175.

19. Mazhei, A., Uspenskiy, A., Ermalenok, V. (2006) Dynamic analysis of the hydro-pneumatic front axle suspension of agriculture tractor, *SAE Paper 2006-01-3526*, PA, USA.

20. Hansson, P-A. (1996) Rear axle suspension with controlled damping on agricultural tractors, *Computers and Electronics in Agriculture*, 15, 123–147.

21. Rehnberg, A. and Drugge, L. (2008) Ride comfort simulation of a wheel loader with suspended axles, *International Journal of Vehicle System Modeling and Testing*, 3, 168-188.

22. Pazooki, A., Cao, D., Rakheja, S. and Boileau, P- É. (2011) Ride dynamic evaluations and design optimization of a torsio-elastic off-road vehicle suspension, *Vehicle System Dynamics*, 49, 1455-1476.

23. Cao, D., Rakheja, S. and Su, C-Y. (2010) Roll- and pitch-plane coupled hydro-pneumatic suspension. Part 1: feasibility analysis and suspension properties, *Vehicle System Dynamics*, 48, 361-386.

24. Crolla, D.A., Horton, D.N.L. (1983) The steering behavior of articulated body steer vehicles, In paper C123/83, *International Mechanical Engineering Conference on Road Vehicle Handling*, MIRA, Nuneaton.

25. Horton, D.N.L. and Crolla, D.A. (1986) Theoretical analysis of the steering behaviour of articulated frame steer vehicles, *Vehicle System Dynamics*, 15, 211-234.

26. He, Y., Khajepour, A., McPhee, J. and Wang, X. (2005) Dynamic modelling and stability analysis of articulated frame steer vehicles, *International Journal of Heavy Vehicle Systems*, 12, 28-59.

27. Loptka, M. And Muszunski, T. (2003) Research of high speed articulated wheel tool-carrier steering system, *9th European Regional Conference of the International Society for Terrain-Vehicle Systems* (*ISTVS*)*,* September 8-11, Newport, United Kingdom.

28. Azad, N. L., Khajepour, A. and McPhee, J. (2009) A survey of stability enhancement strategies for articulated steer vehicles, *International Journal of Heavy Vehicle Systems*, 16, 26-48.

29. Azad, N. L., Khajepour, A. and McPhee, J. (2005) Analysis of jack-knifing in articulated steer vehicles, *IEEE Conference on Vehicle Power and Propulsion*, USA, 216-220.

30. Rehnberg, A., Drugge, L. and Stensson T. A. (2010) Snaking stability of articulated frame steer vehicles with axle suspension, *International Journal of Heavy Vehicle Systems*, 17, 119-138.

31. Eriksson, M., Edren, J. (2007) A radio controlled 1:10 scale articulated test vehicle for vehicle dynamic studies, Master thesis, department of aeronautical and vehicle engineering, royal institute of technology (KTH), Stockholm, Sweden.

32. Rakheja, S., Sankar, S. and Ranganathan, R. (1988) Roll plane analysis of articulated thank vehicles during steady turning, *Vehicle System Dynamics*, 17, 81-104.

33. Fancher, P. S. (1989) Directional dynamics considerations for multi-articulated, multi-axled heavy vehicles, *SAE Paper 892499*.

34. Blankenship, J. W., Means, K. H. and Biller, C. J. (1984) Side slope static stability of double articulated logging tractor, *SAE Paper 841140*.

35. Gibson, H. G., Benjamin, C., Thomas, J. W. (1981) Slope stability warning device for articulated tractors, *US Patent 428498*.

36. Gibson, H. G., Elliott, K. C., Persson, S. P. E. (1971) Side slope stability of articulated-frame logging tractors, *Journal of Terramechanics*, 8(2), 65-79.

37. Grecenko, A. (1984) Operation on steep slopes: State-of-the art report, *Journal of Terramechanics*, 21, 181-194.

38. Wary G., Nazalewiez, J. and Kwitowski, A. J. (1984) Stability indicators for front end loaders, *Proceedings of the 8th International Conference International Society for Terrain-Vehicle Systems* (*ISTVS*), Cambridge, 655-671.

39. Cao, D., Rakheja, S. and Su, C-Y. (2010) Roll- and pitch-plane coupled hydro-pneumatic suspension. Part 2: dynamic response analysis, *Vehicle System Dynamics*, 48, 507-528.

40. Holm, I.C. (1970) Articulated wheeled off-the road vehicles, *Journal of Terramechanics*, 7(1), 19–54.

41. Paddan, G. S. and Griffin, M. J. (2002) Evaluation of whole body vibration in vehicles, *Journal of Sound and Vibration*, 253 (1), 195-213.

42. Eger, T., Stevenson, J., Boileau, P-É., Salmoni, A. and Vib, RG. (2008) Health risks associated with the operation of load-haul-dump mining vehicles: Part 1- Analysis of whole-body-vibration exposure using ISO 2631-1 and ISO-2631-5 standards, *International Journal of Industrial Ergonomics*, 38, 726-738.

43. Matthews, J., Talamo, J. D. C. (1965) Ride comfort for tractor operators, *Journal of Agricultural Engineering Research*, 10(2), 93-108.

44. Crolla, D. A. and MacLaurin, E. B. (1985) Theoretical and practical aspects of the ride dynamics of off-road vehicles-Part 1, *Journal of Terramechanics,* 22, 17–25.

45. Peters, G. A. and Peters, B. J. (1993) Automotive Engineering and litigation, John Wiley & Sons Inc., NY.

46. Boileau, P-É. (1995) A study of secondary suspensions and human driver response to whole-body vehicular vibration and shock, Ph.D. Thesis, Concordia University, Canada.

47. Salmoni, A. W., Cann, A. P., Gillin, E. K. and Eger, T. R. (2008) Case studies in whole-body vibration assessment in the transportation industry- Challenges in the field, *International Journal of Industrial Ergonomics*, 38(9-10), 783-791.

48. Bovenzi, M., Hulshof, C. T. J. (1998) An updated review of epidemiologic studies on the relationship between exposure to whole-body vibration and low back pain, *Journal of Sound and Vibration*, 215, 595-611.

49. British Standards Institution BS 6841(1987) Measurement and evaluation of human exposure to whole-body mechanical vibration and repeated shock.

50. EN 2002/44/EC Directive 2002/44/EC of the European Parliament and of the Council of 25 June 2002.- [s.l.], *Official Journal of the European Communities*, 06 25, 2002.- Vol. L 177. - 2002/44/EC.

51. Teschke, K., Nicol, A., Davies, H. and Ju, S. (1999) Whole body vibration and back disorders among motor vehicle drivers and heavy equipment operators, Technical Report, University of British Columbia.

52. Holmlund, P. (1999) Absorbed power and mechanical impedance of the seated human within a real vehicle environment compared with single-axis laboratory data, *Journal of Low Frequency Noise, Vibration, and Active Control*, 18(3), 97-110.

53. Adams, B. T., Reid, J. F., Hummel, J. W., Zhang, Q. and Hoeft, R. G. (2004) Effects of central tire inflation systems on ride quality of agricultural vehicles, *Journal of Terramechanics*, 41(4), 199-207.

54. Eger, T., Stevenson, J., Grenier, S., Boileau, P-É. and Smets M. (2006) Whole-body vibration exposure and driver posture evaluation during the operation of LHD vehicles in underground mining, *American Conference on Human Vibration*, (1st : June 5-7, 2006 : Morgantown, U.S.A., 119-120.

55. Bongers, P. M, Boshuizen, H. C. (1990) Back disorders and whole-body vibration at work, Thesis: University of Amsterdam, Holland.

56. Bongers, P. M., Boshuizen, H. C., and Hulshof, C. T. J. (1988) Back disorders in crane operators exposed to whole-body vibration, *International Archives of Occupational and Environmental Health*, 60, 129-137.

57. Bovenzi, M., Pinto, L. and Stacchini, N. (2002) Low back pain in port machinery operators, *Journal of Sound and Vibration*. 253(1), 3-20.

58. Rehn, B., Nilsson, T., Olofsson, B. and Lundström, R. (2005) Whole-body vibration exposure and non-neutral neck postures during occupational use of all-terrain vehicles, *Annals of Occupational Hygiene*, 49(3), 267-275.

59. Boshuizen, H. C, Bongers, P. M. and Hulshof, C. T. (1990). Self-reported back pain in tractor drivers exposed to whole-body vibration, *International Archives of Occupational and Environmental Health*, 62(2), 109-115.

60. Barbieri, N. (1995) The optimal performance index for an off-road vehicle with passive and active suspension systems, *Heavy Vehicle Systems*, 2(3–4), 225–237.

61. Bovenzi, M, Betta, A. (1994) Low-back disorders in agricultural tractor drivers exposed to whole body vibration and postural stress, *Applied Ergonomics* 35:231-241.

62. Sandover, J., Gardner, L., Stroud, P. and Robertson, N. (1994). Some epidemiological issues regarding vibration and tractor driving, *Presented at the United Kingdom Informal Group Meeting on Human Response to Vibration*, Institute of Naval Medicine, Alverstoke, Gosport, Hants.

63. Village, J. and Morrison, J. B. (1989) Whole-body vibration in underground load-haul dump vehicles, *Ergonomics*, 32(10), 1167-1183.

64. Kumar, S. (2004) Vibration in operating heavy haul trucks in overburden mining, *Applied Ergonomics*, 35, 509-520.

65. Scarlett, A. J., Price, J. S. and Stayner, R. M. (2007) Whole-body vibration: Evaluation of emission and exposure levels arising from agricultural tractors, *Journal of Terramechanics*, 44(1), 65-73.

66. Servadio, P., Marsili, A. and Belfiore, N. P. (2007) Analysis of driving seat vibrations in high forward speed tractors, *Biosystems Engineering*, 97, 171-180.

67. Okunribido, O. O., Magnussin, M. and Pope, M. (2006) Low back pain in drivers: The relative role of whole-body vibration and manual materials handling, *Journal of Sound and Vibration*, 298, 540-555.

68. Futatsuka, M., Maeda, S., Inaoka, T., Naganoi, M., Shono, M. and Miyakita, T. (1998) Whole-Body Vibration and Health Effects in the Agricultural Machinery Drivers, *Industrial Health*, 36, 127-132.

69. Kumar, A., Mahajan, P., Mohan, D. and Vargese, M. (2001) Tractor vibration severity and driver Health: a study from Rural India, *Journal of Agricultural Engineering Research*, 80(4), 313-328.

70. Burdorf, A. and Swuste, P. (1993) The effect of seat suspension on exposure to whole-body vibration of professional drivers, *Annals of Occupational Hygiene,* 37:45-55.

71. Tiemessen I. J. H., Hulshof, C. T. J. and Frings-Dresen, M. H. W. (2008) Two way assessment of other physical work demands while measuring the whole body vibration magnitude, *Journal of Sound and Vibration*, 310(4-5), 1080-1092.

72. Newell, G. S, Mansfield, N. J. and Notini, L. (2006) Inter-cycle variation in whole-body vibration exposures of operations driving track-type loader machines, *Journal of Sound and Vibration*, 298, 563-579.

73. Mansfield, N. J. (2003) Effect of increasing measurement duration on accuracy of whole-body vibration field measurements, *Proceedings of the 38th UK Group Meeting on Human Response to Vibration*, Gosport, UK.

74. Notini, L. and Mansfield, N. (2004) evaluation of digital implementations of whole-body vibration frequency weighting filters and the effect of filter phase response on whole-body vibration metrics. *Proceedings of the 39th UK Conference on Human Response to Vibration*, Ludlow, Shropshire, England, 15 – 17 September.

75. Golsse, J-M. and Hope, P.A. (1987) Analysis of whole-body vibration levels during skidding, *Forest Engineering Research Institute of Canada (FERIC) Technical Report No. TR-77*, Quebec, Canada.

76. Jack, R., Oliver, M., Dickey, J., Cation, S., Hayward, G. and Lee, S. (2010) Six-degree-of-freedom whole-body vibration exposure levels during routine skidder operations, *Ergonomics*, 53, 696-715.

77. Mansfield, N. J. and Griffin, M. J. (2002) Effects of posture and vibration magnitude on apparent mass and pelvis rotation during exposure to whole-body vertical vibration, *Journal of Sound and Vibration*, 253, 93-107.

78. Sherwin, L. M., Owende, P. M. O, Kanali, C. L., Lyons, J. and Ward, S. M. (2004) Influence of forest machine function on operator exposure to whole-body vibration in cut-to-length timber harvester, *Ergonomics*, 47(11), 1145-1159.

79. Boileau, P-É., Rakheja, S. and Wang, Z. (2002) Ride vibration environment of tracked sidewalk snowplows: Spectral Classification, *International Journal of Vehicle Design*, 30(4), 309-326.

80. Kordestani, A., Rakheja, S., Marcotte, P., Pazooki, A. and Juras, D. (2010) Analysis of Ride Vibration Environment of Soil Compactors, *SAE International Journal of Commercial Vehicles* December 2010 3:259-272.

81. Dupuis, H. and Zerlett, G. (1987) Whole body vibration and disorders of the spine, *International Archives of Occupational and Environmental Health,* 59, 323-336.

82. Ruppe K. and Mucke, R. (1993). Functional disorders at the spine after long lasting whole-body vibration. In VR Nielsen and K Jorgensen (editors), *Advances in Industrial Ergonomics and Safety,* 483-486.

83. Calvo, A. (2009) Musculoskeletal disorders (MSD) risks in forestry: a case study to propose an analysis method, *Agricultural Engineering International: CIGR Journal*, 6, 1-9.

84. Crolla, D. A. and Pitcher, R. H. (1987) Active suspension control for an off-road vehicle, *Journal of Automobile Engineering,* 201, 1-10.

85. Adams, B. T., Reid, J. F., Hummel, J. W., Zhang, Q. and Hoeft, R. G. (2004) Effects of central tire inflation systems on ride quality of agricultural vehicles, *Journal of Terramechanics*, 41(4), 199-207.

86. Elmadany, M. M. and Abduljabbar, Z. (1990) Design evaluation of advanced suspension systems for truck ride comfort*, Journal of Computers & Structures*, 36(2), 321-331.

87. Cole, D. J. and Cebon, D. (1992) Validation of an articulated vehicle simulation, *Vehicle System Dynamics,* 21, 1992.

88. Dhir, A. and Sankar, S. (1994) Analytical Model for Ride Dynamic Simulation of Tracked Vehicles, *Journal of Terramechanics,* 31 (2), 107-138.

89. Besinger, F. H., Cebon, D. and Cole, D. J. (1995) Damper models for heavy vehicle ride dynamics, *Vehicle System Dynamics,* 24 (1), 35-64.

90. Boileau, P-É. and Rakheja, S. (2000) Characterization of the vibration environment of urban buses, *Proceedings of the 35th UK Informal Group Meeting, Southampton, UK*, 11-15, 305-316.

91. Hilton, D. J. and Moran, P. (1975) Experiments in improving tractor operator ride by means of a cab suspension, *Journal of Agricultural Engineering,* 20, 433-448.

92. Crolla, D. A. and Dale, A. K. (1980) Ride vibration measurements of agricultural tractor and trailer combinations, *Vehicle System Dynamics*, 9 (5). 261-279.

93. Crolla, D. A. (1980) A theoretical analysis of the ride vibration of agricultural tractor and trailer combinations, *Vehicle System Dynamics*, 9 (5). 237-260.

94. Claar, P. W., Sheth, P. N., Buchele, W. F. and Marley, S. J. (1980) Agricultural tractor chassis suspension system for improved ride comfort, *ASAE Paper 80-1565*.

95. Sankar, S., and Dhir, A. (1991) On the Ride Dynamics of a Tracked Multi-Wheeled Vehicle, *Proceedings of the Canadian Congress of Applied Mechanics* (*CANCAM'91*) *Conference*, University of Manitoba, Winnipeg, Canada, June 2 - 6, 734735.

96. Sankar, S., Rakheja, S. and Afonso, M. (1992) Dynamic Analysis of Tracked Vehicles with Trailing Arm Suspension and Assessment of Ride Vibrations, *International Journal of Vehicle Design, 13(1),* 56-77.

97. Hansson, P-A. (2002) Working space requirement for an agricultural tractor axle suspension, *Biosystems Engineering*, 81(1), 57-71.

98. Bester, R. (2006) The ride comfort versus handling decision for off-road vehicles, Master Thesis, University of Pretoria.

99. Els, P. S. (2005) The applicability of ride comfort standards to off-road vehicles, *Journal of Terramechanics*, 42, 47-64.

100. Els, P. S. Theron, P. E., and Thoresson, M. J. (2007) The ride comfort vs. handling compromise for off-road vehicles, *Journal of Terramechanics*, 44(4), 303-317.

101. Crolla, D. A., Horton, D. N. L. and Stayner, R. M. (1990) Effect of tire modeling on tractor ride vibration prediction, *Journal of Agricultural Engineering*, 47, 55-77.

102. Hansson, P-A. (1996) Control algorithms for active cab suspensions on agricultural tractors, *Vehicle System Dynamics*, 25(6), 431-461.

103. Hansson, P-A. (1995) Optimization of agricultural tractor cab suspension using the evolution method, *Computers and Electronics in Agriculture,* 12, 35–49.

104. Horton, D. N. L. and Crolla, D. A. (1986) Theoretical analysis of a semi-active suspension fitted to an off-road vehicle, *Vehicle System Dynamics*, 15, 351-372.

105. Crolla, D. A. and Pitcher, R.H. (1987) Active suspension control for an off-road vehicle, *Journal of Automobile Engineering,* 201, 1-10.

106. Crolla, D. A. and MacLaurin, E. B. (1985) Theoretical and practical aspects of the ride dynamics of off-road vehicles-Part 1, *Journal of Terramechanics,* 22, 17–25.

107. Wegscheid, E. (1994) Another look at skidder ride vibration**,** *Journal of Forest Engineering*, 5(2), 21-32.

108. Schalkels, P. and Niekerk, V. (1999) Dynamic modeling of an off-road vehicle for the design of a semi-active, hydropneumatic spring-damper system, *Vehicle System Dynamics (Supplement)*, 33, 566–577.

109. Niranjan, P., Tewari, V. K. and Yadav, R. (1995) Tractor ride vibration- a review, *Journal of Terramechanics*, 32(4), 205-2019.

110. Lines, J. A. (1987) Ride vibration of agricultural tractors: transfer function between the ground and the tractor body, *Journal of Agricultural Engineering Research*, 37, 81-91.

111. Lines, J.A. and Murphy, K. (1991) The stiffness of agricultural tractor tires, *Journal of Terramech*anics, 28, 49-64.

112. Lines, J. A., Peachey, R. O. and Collins, T. S. (1992) Predicting the ride vibration of an unsuspended tractor using the dynamic characteristics of rolling tyres, *Journal of Terramech*anics, 29, 307-315.

113. Transportation Research Board (2006) Tire and passenger vehicle fuel economy, Committee for the National Tire Efficiency Study Board on Energy and Environmental Systems, Report 286.

114. Wong, J.Y. (2002) Theory of ground vehicles. John Wiley & Sons, New York, 4th edition.

115. Captain, K. M., Boghani, A. B., Wormley, D. N. (1979) Analytical tire models for dynamic vehicle simulation, *Vehicle System Dynamics*, 8, 1–32.

116. Xiding, Q., Jude, L. and Yongxin, M. (1993) A modified point contact tire model for the simulation of vehicle ride quality, *Journal of Terramechanics*, 30(3), 133-141.

117. Zegelaar, P. W. A. (1998) The dynamic response of tires to brake torque variations and road unevennesses, Ph.D. Thesis, Delf University of Technology, Netherlands, ISBN 90-370-0166-1

118. Crolla, D.A. and El-Razaz A.S.A. (1987) A review of the combined lateral force generation of tires on deformable surfaces, *Journal of Terramechanics*, 24(1), 25-82.

119. Peng, C., Cowell, P. A., Chisholm, C. J. and Lines, J. A. (1994) Lateral tire dynamic characteristics, *Journal of Terramechanics*, 31(6), 395-414.

120. Andersson Patrik, B. U. (2007) Modeling non-linear contact stiffness in tire/road contact, *International Congress on Acoustics*, Madrid, Spain.

121. Davis, D. C. (1975) A radial-spring terrain-enveloping tire model, *Vehicle System Design*, 4(1), 55-60.

122. Lescoe, R., El-Gindy, M., Koudela, K., Oijer, F., Trivedi, M. and Johansson, I. (2010) Tire-soil modeling using finite element analysis and smooth practical hydrodynamics techniques, *Proceedings of ASME International Design Engineering Technical Conference*, DETC2010-28002, Montreal, Canada.

123. Pacejka, H. B. and Bakker, E. (1993) The magic formula tire model: tire models for vehicle dynamic analysis, *In Proceedings of 1st International Colloquium on Tire Models for Vehicle Dynamic Analysis*, Delft, 1–18.

124. Pacejka, H. B. (2006) Tire and Vehicle Dynamics, Second Edition, Society of Automotive Engineers Inc.

125. Metz, L. D. (1993) Dynamics of four-wheel-steer off-highway vehicles, *SAE Paper 930765*.

126. Blundell, M. and Harty, D. (2004) The multibody systems approach to vehicle dynamics, Elsevier, ISBN 0750651121.

127. Laib, L. (1995) Analysis of the vibration-excitation effect caused by deformable soil surfaces, *Journal of Terramechanics,* 32(3):151-163.

128. Park, S., Popov, A. A. and Cole, D. J. (2004) Vehicle suspension optimization for heavy vehicles on deformable ground, *Vehicle System Dynamics (Supplement)*, 41, 3–12.

129. Park, S., Popov A. A. and Cole, D. J. (2004) Influence of soil deformation on off road heavy vehicle suspension vibration, *Journal of Terramechanics*, 41, 41-68.

130. Robson, J. D. (1979) Road surface description and vehicle response, *International Journal of Vehicle Design,* 9, 25–35.

131. Maclaurin, B. (1983) Progress in British tracked vehicle suspension system. *SAE Paper No. 830442*, International Congress and Exposition, Detroit, Mich.

132. Logdanoff, J. L., Kozin, F. and Cote, L. J. (1996) Atlas of off-road ground roughness PSDs and report on data acquisition techniques, *ATAC Components Research and Development Laboratories Technical Report No.9387 (LL109)*, U.S. Army Tank-Automotive Center, Warren, Mich.

133. Hac, A. (1987) Adaptive control of vehicle suspension, *Vehicle System Dynamics*, 16, 57-74.

134. Bogsjo, K. (2008) Coherence of road roughness in left and right wheel-path, *Vehicle System Dynamics*, 46(supp), 599-609.

135. Yonglin, Z. and Jiafan, Z. (2006) Numerical simulation of stochastic road process using white noise filtration, *Mechanical Systems and Signal Processing*, 20, 363-372.

136. Rakheja, S. and Sankar, S. (1984) Improved Off-Road Tractor Ride via Passive Cab and Seat Suspension. Trans. ASME, *Journal of Vibration, Acoustic, Stress and Reliability in Design*, 106(2), 305-313.

137. Boileau, P-É., Emile, P. and Rakheja, S. (1990) Vibration attenuation performance of suspension seats for off-road forestry vehicles, *International of Industrial Ergonomics*, 5, 275-291.

138. Lemerle, P., Boulanger, P. and Poirot, R. (2002) A simplified method to design suspended cabs for counterbalance trucks, *Journal of Sound and Vibration* 253(1), 283-293.

139. Wu, X. and Griffin, M. J. (1998) The influence of end-stop buffer characteristic on the severity of suspension seat end-stop impacts, *Journal of Sound and Vibration*, 215(4), 989–996.

140. Wu, X., Rakheja, S. and Boileau, P-É. (1998) Study of human-seat interface pressure distribution under vertical vibration, *International Journal of Industrial Ergonomics*, 21, 433–449.

141. Tewari, V. K. and Prasad, N. (1999) Three-DOF modeling of tractor seat-operator system, *Journal of Terramechanics*, 36, 207–219.

142. Rebelle, R. (2004) Methology to improve the performance of the end-stop buffers of suspension seats, *Vehicle System Dynamics*, 42(4), 211-233.

143. Xiao Qing, M., Rakheja, S. and Yi S. C. (2008) Damping requirement of a suspension seat subject to low frequency vehicle vibration and shock, *International Journal of Vehicle Design*, 47(1/2/3/4), 133-156.

144. Young, R. E. and Suggs, C. W. (1973) Seat-suspension system for isolation of roll and pitch in off-Road vehicles, *ASAE Transaction*, 16(5), 873.

145. McManus, S., Clair, K., Boileau, P-E., Rakheja, S. and Boutin, J. (2000) Evaluation of the vibration and shock attenuation performance of a semi-active magneto-rheological fluid damper, *Journal of Sound and Vibration*, 253(1), 313-327.

146. Rakheja, S., Afework, Y. and Sankar, S. (1994) An analytical and experimental investigation of the driver-seat suspension system, *Vehicle System Dynamics*, 23(1), 501-524.

147. Hill, K. and Dhingra, A. (2003) Modeling analysis of a scissors linkage seat suspension, *Engineering Optimization*, 35(4), 341-357.

148. Kusahara, Y., Li, X. S., Hata, N. and Watanabe, Y. (1994) Feasibility study of active roll stabilizer for reducing roll angle of an experimental medium-duty truck, *Proceedings of International Symposium on Advanced Vehicle Control*, 9438501.

149. Cebon, D. (1999) Handbook of vehicle-road interaction, Swets & Zeitlinger, the Netherlands.

150. Cole, D. J. (2001) Fundamental issues in suspension design for heavy road vehicles, *Vehicle System Dynamics*, 35, 319-360.

151. Barbieri, N. (1995) Optimal active suspension systems for an off-road vehicle, *International Journal of Vehicle Design*, 16(2–3), 219–228.

152. Cao, D., Song, X. and Ahmadian, M. (2011) Editors' perspectives: road vehicle suspension design, dynamics, and control, *Vehicle System Dynamics*, 49, 3-28.

153. Cao, D., Rakheja, S. and Su, C. Y. (2010) Roll- and pitch-plane coupled hydro-pneumatic suspension. Part 1: feasibility analysis and suspension properties, *Vehicle System Dynamics*, 48, 361-386.

154. Cao, D., Rakheja, S. and Su, C. Y. (2010) Roll- and pitch-plane coupled hydro-pneumatic suspension. Part 2: dynamic response analysis, *Vehicle System Dynamics*, 48, 507-528.

155. Cao D., Rakheja S. and Su C. Y. (2008) Dynamic analyses of roll plane interconnected hydro-pneumatic suspension systems, *International Journal of Vehicle Design*, 47, 51-80.

156. Cao D., Rakheja S. and Su C. Y. (2009) Handling and braking analyses of a heavy vehicle with cross-axle fluidically-coupled suspension, *SAE International Journal of Commercial Vehicles*, 117-2.

157. Crolla, D. A., Horton, D. N. L. (1983) The steering behavior of articulated body steer vehicles. In paper C123/83. *International Mechanical Engineering Conference on Road Vehicle Handling*, MIRA, Nuneaton.

158. Horton, D. N. L. and Crolla, D. A. (1986) Theoretical analysis of the steering behaviour of articulated frame steer vehicles, *Vehicle System Dynamics*, 15, 211-234.

159. He, Y., Khajepour, A., McPhee, J. and Wang, X. (2005) Dynamic modelling and stability analysis of articulated frame steer vehicles, *International Journal of Heavy Vehicle Systems*, 12, 28-59.

160. Ma, W. H. and Peng, H. (1999) Worst-case vehicle evaluation methodology-example on truck rollover/jackknifing and active yaw control system, *Vehicle System Dynamic*, 32, 389-408.

161. Hac, A. (2002) Influence of active chassis systems on vehicle propensity to maneuver-induced rollovers, *SAE Paper 2002-01-0967*.

162. Mashadi, B. and Crolla, D. A. (2005) Influence of ride motions on the handling behavior of a passenger vehicle, *Journal of Automobile Engineering*. 219, 1047-1058.

163. Chen, D. C. and Crolla, D. A. (1998) Subjective and objective measures of vehicle handling: drivers & experiments, *Vehicle System Dynamics Supplement*, 28, 576-597.

164. Louca, L. S., Rideout, D. G, Stein, J. L. and Hulbert, G. M. (2004) Generating proper dynamic models for truck mobility and handling, *International Journal of Heavy Vehicle System*, 11, 209-236.

165. Gillespie, T. D. and Sayers, M. W. (1999) A multibody approach with graphical user interface for simulating truck dynamics, *SAE Paper 1999-01-3705*.

166. Sherman, M. and Myers, G. (2000) Vehicle dynamics simulation for handling optimization of heavy trucks, *SAE Paper 2000-01-3437*.

167. Ledesma, R. and Shih, S. (2001) The effect of kingpin inclination angle and wheel offset on medium-duty truck handling, *SAE Paper 2001-01-2732*.

168. Ledesma, R. (2002) Ride performance comparison of trailer suspension systems using computational methods, *SAE Paper 2002-01-3103*.

169. Rakheja, S., Piche, A. and Sankar, T. S. (1991) On the development of an early warning safety monitor for articulated freight vehicles, *International Journal of Vehicle Design*, 12, 420-449.

170. Liu, P., Rakheja, S. and Ahmed, A. K. W. (1998) Dynamic rollover threshold of articulated freight vehicles, *International of Heavy Vehicle Systems*, 5, 300-322.

171. Blundell, M. V. (1999) The modeling and simulation of vehicle handling. Part 1: analysis methods, *Journal of Multi-Body Dynamics*, 213, 103-118.

172. Sharp, R. S. (1991) Computeer codes for road vehicle dynamic models, *Proceeding of Autotech 91*, Birmingham, UK.

173. Goldman, R. W., El-Gindy, M. and Kulakowski, B. T. (2001) Roll over dynamics of road vehicles: Literature survey, Heavy Vehicle Systems, *International Journal of Vehicle Design*, 8(2), 103-141.

174. Newland, D. E. (1981) The roll stability of frame-steered two axle vehicles during steady cornering, *Proceedings of the 8th International Society for Terrain-Vehicle Systems* (*ISTVS*), Cambridge, 821-833.

175. Hunter, A.G.M. (1993) A review of research into machine stability on slopes, *Safety Science*, 16, 325-339.

176. Chen, B. and Peng, H. (2005) Rollover warning for articulated heavy vehicles based on a time-to-rollover metric, *Journal of Dynamic Systems, Measurement and Control*, 127(3), 406-414.

177. Azad, N. L., Khajepour, A. and McPhee, J. (2005) The effects of front and rear tires characteristics on the snaking behavior of articulated steer vehicles, *IEEE Conference on Vehicle Power and Propulsion*, USA, 221-226.

178. Azad, N. L., Khajepour, A. and McPhee, J. (2005) The Effects of drive configuration on undesirable behaviors of articulated steer vehicles, *Vehicle Power and Propulsion* (*VPP*), IEEE Conference, USA, 322-326.

179. Rakheja, S., Vallurupalli, R. K. and Woodrooffe, J. (1995) Influence of articulation damping on the yaw and lateral dynamic response of the vehicle, *International Journal of the Heavy Vehicle Design*, 2(2), 105-123.

180. Preston-Thomas, J. and El-Gindy, M. (1992) Static rollover threshold of heavy vehicles, *Proceedings of CSME Forum*, Montreal, 946-951.

181. Winkler, C. B. (1993) Repeatability of the tilt-table test method, *SAE Paper 930832*.

182. Chrstos, J. P. and Guenther D. A. (1992) The measurement of static rollover metrics, *SAE Paper 920528*.

183. El-Gindy, M. and Hosamel-deen, Y. H. (1989) Sensitivity parametric analysis of UMTRI static roll model, *International Journal of Vehicle Design*, 10(2), 187-189.

184. Vlk, F. (1985) Handling performance of truck-trailer vehicles: a state-of-the-art survey, *International Journal of Vehicle Design*, 6(3), 323-361.

185. Jones, I. S. and Penny, M. B. (1990) Engineering parameters related to rollover frequency, *SAE Paper 900104*.

186. Klein, T. M. (1992) A statistical analysis of vehicle rollover propensity and vehicle stability, *SAE Paper 920584*.

187. Piche, A. (1990) Detection of onset of instabilities for an early warning safety monitor for articulated freight vehicles, Master Thesis, Concordia University, Montreal, Canada.

188. Verma, M. K. and Gillespie, T. D. (1980) Roll dynamics of commercial vehicles, *Vehicle System Dynamics*, 9, 1-17.

189. Gillespie, T. D. and MacAdam, C. C. (1982) Constant velocity yaw/roll program, User's manual, The University of Michigan Transportation Research Institute.

190. Wong, J. Y. and El-Gindy, M. (1985) Computer simulation of heavy vehicle dynamic behavior, User's Guide to the UMTRI model, Technical Report 3, vehicle weights and dimensions study, Road and Transportation Association of Canada.

191. El-Gindy, M. and Wong, J. Y. (1987) A comparison of various computer simulation model for predicting the directional responses of articulated vehicles, *Vehicle System Dynamics*, 16, 249-268.

192. Nalecz, A. G. (1989) Influence of vehicle and roadway factors on the dynamics of tripped rollover, *International of Vehicle Design*, 10(3), 321-345.

193. Hinch, J. (1992) NHTSA's rollover rulemaking program-results of testing and analysis, *SAE Paper 920581*.

194. Lund, Y. I and Bernard, J. E. (1995) Analysis of simple rollover metrics, *SAE Paper 950306*.

195. El-Gindy, M. (1995) A overview of performance measures for heavy commercial vehicles in north America, *International Journal of Vehicle Design*, 16(4/5), 441-463.

196. Winkler, C. B. and Fancher, P. S. (1996) Scenarios for regulation of commercial vehicle stability in the US, *4th International Heavy Vehicle Seminar Inst. Road and Dimensions*, Cambridge UK.

197. Thomas H. L., Personal communication, Ph.D. R&D Engineer Development Department, Hydrema Co.

198. Commission of the European Communities (1992) Proposal for a council directive on the minimum health and safety requirements regarding the exposure of workers to the risks arising from physical agent. Brussels, Belgium.

199. Korhonen O, Nummi J, Nurminen M, Nygard K, Soininen H and Wiikeri M. (1980) Finnish Lumberjacks. Part 3: The Health of Forest Tractor Drivers, *Institute of Occupational Health*, Helsinki.

200. Bovenzi M, Zadini A, Franzinelli A and Borgogni F. (1991) Occupational musculoskeletal disorders in the neck and upper limbs of forestry workers exposed to hand-arm vibration, *Ergonomics*, 34 (5), 547-562.

201. Springfeldt B. (1996) Rollover of tractors - international experiences, *Safety Science*, 24 (2), 95-110.

202. Franklin R., Mitchell R., Driscoll T. and Fragar L. (2000) Farm related fatalities in Australian, 1989–1992, *Australian Centre for Agricultural Health and Safety and Rural Industries Research and Development Corporation*, Moree, Australia.

203. Wu X., Rakheja S. and Boileau, P. E. (1999) Dynamic Performance of Suspension Seats Under Vehicular Vibration and Shock Excitations, *SAE Transactions, Passenger Car Journal*, 108 (6), 2398-2410.

204. Boileau P.-É., Wu X. and Rakheja S. (1998) Definition of a set of idealized values to characterize seated body biodynamic response under vertical vibration, *Journal of Sound and Vibration*, 215(4), 841-862.

205. Marcu F. M., Ahmadian M., Southward S. and Jansson S. (2009) A methodology for laboratory testing of truck cab suspension, *SAE Paper 2009-01-2862*.

206. Ahmadian M., Patricio P. (2004) Effect of panhard rod cab suspension on heavy truck ride measurements. *SAE Paper 2004-01-2710*.

207. Wu Qi-Ya, Qing-Za S, Jin-Wen W., and Yong-Fa F (1988) The simplified dynamic model, measurement and evaluation of ride vibration for the combination unit of agricultural hand tractor and trailer, *Vehicle System Dynamics*, 13, 367-385.

208. Cole D. J., and Cebon D. (1998) Front-rear interaction of a pitch-plane truck model, *Vehicle System Dynamics*, 30, 117-141.

209. Park S., Popov A. A., and Cole D. J. (2004) Influence of soil deformation on off-road heavy vehicle suspension vibration, *Journal of Terramechanics*, 41, 41-68.

210. Matlab Optimization Toolbox User’s Guide (1990 – 2001) by The MathWorks, Inc.

211. FERIC/FP Innovations (1979) The forestry engineering research institute of Canada. Montreal, Canada.

212. Cao D., Rakheja S., and Su C-Y. (2008) Heavy vehicle pitch dynamics and suspension tuning. Part I: unconnected suspension, *Vehicle System Dynamics*, 46(10), 931-953.

213. Sharp R. S. (2002) Wheelbase filtering and automobile suspension tuning for minimization motion in pitch, *Journal of Automobile Engineering*, 216, 933-946.

214. Best A. (1984) Vehicle ride-stages in comprehension, *Physics in Technology*, 15, 205-210.

215. Haupt R. L., Haupt S. E. (2004) Genetic Alghorithms. A John Wiley & Sons, INC., Publication, second edition.

216. Boileau P. E., Emile P. and Rakheja S. (1996) Évaluation et étude du comportement dynamique d'un système de suspension torsio-élastique pour véhicules tout terrain, Études et recherches, Rapport R-124, Montréal, IRSST.

217. Gillespie, T.D., 1985, Heavy truck ride, *SAE Paper 850001, PA, USA*.

218. Su, H., Rakheja, S. and Sankar, T. S. (1992), Random response analysis of a non-linear vehicle suspension with tunable shock absorber, *Mechanical Systems and Signal Processing*, 6, 363-381.

219. Priyandoko, G., Mailah, M. and Jamaluddin, H.(2009), Vehicle active suspension system using skyhook adaptive neuro active force control, *Mechanical Systems and Signal Processing*, 23, 855-868.

220. Griffin, M. J. (2007) Discomfort from feeling vehicle vibration, *Vehicle System Dynamics*, 45, 679-698.

221. Rakheja, S., Dong R. G., Patra, S., Boileau, P.-E., Marcotte, P. and Warren, C. (2010) Biodynamics of the human body under whole-body vibration: synthesis of the reported data, *International Journal of Industrial Ergonomics*, 40, 710-732.

222. Rehn, B., Olofsson, B., Lundstrom, R., Nilsson, L., Liljelind, I. and Jarvholm, B. (2005) Variation in exposure to whole-body vibration for operators of forwarder vehicles - aspects on measurement strategies and prevention, *International Journal of Industrial Ergonomics*, 35, 831-842.

223. Andersson, P. B. U. and Kropp, W. (2008) Time domain contact model for tyre/road interaction including nonlinear contact stiffness due to small-scale roughness, *Journal of Sound and Vibration*, 318, pp. 296-312.

224. Crolla, D. A., Horton, D. N. L. and Stayner, R. M. (1990) Effect of tire modeling on tractor ride vibration prediction, *Journal of Agricultural Engineering*, 47, 55-77.

225. Rakheja, S., Wang, K., Bhat, R. B. and Boileau, P.-E. (2002) Enhancement of ride vibration environment of tracked snowplows: vehicle modeling and analysis, *International Journal of Vehicle Design*, 30, 193-222.

226. Wang, K. (2000) Dynamic analysis of a tracked snowplowing vehicle and assessment of ride quality, Master Thesis, Concordia University, Montreal, Canada.

227. Bendat, J. S. and Piersol, A. G. (2000) Random data analysis and measurement procedures, 3rd Edition, John Wiley & Sons, New York, USA.

228. Bogsjo, K. (2008) Coherence of road roughness in left and right wheel-path, *Vehicle System Dynamics*, 46(supp), 599-609.

229. Yonglin, Z. and Jiafan, Z. (2006) Numerical simulation of stochastic road process using white noise filtration, *Mechanical Systems and Signal Processing*, 20, 363-372.

230. Welch, P. D. (1967) The use of fast fourier transform for the estimation of power spectra: a method based on time averaging over short, modified periodogram, *IEEE Transaction Audio Electroacoustics*, 15, 70-73.

231. FERIC/FP Innovations (1979) The forestry engineering research institute of Canada. Montreal, Canada.

232. Pazooki, A., Rakheja S. and Dongpu C. (2012) Modeling and Validation of Off-Road Vehicle Ride Dynamics, *Mechanical Systems and Signal Processing*, 28, 679–695.

233. Cao, D., Rakheja, S. and Sandu, C. (2011) Editorial: Special Issue on interdisciplinary aspects of vehicle system dynamics integration, *Mechanical Systems and Signal Processing*, 25, 3113-3215.

234. Akers A., Gassman M., Smith R. (2006), Hydraulic power system analysis, Taylor & Francis Group LLC.

235. Pazooki, A., Rakheja, S. and Dongpu, C. (2012) Kineto-Dynamic Directional Response Analysis of an Articulated Frame Steer Vehicle, *Journal of Vehicle System Dynamics,* accepted, IJVD-38698.

236. Kar S., Rakheja S. and Ahmed A. K. W (2006) Normalized measure of relative roll instability for open-loop rollover warning, *International Journal of Heavy Vehicle System*s, 13(1/2), 74-97.

237. Preston-Thomas, J. and Woodrooffe, J. H. F, (1990) A feasibility study of a rollover warning device for heavy trucks, Technical Report, TP 16010E, *National Research Council*, Canada.

238. MacAdam, C. C. (1982) A computer-based study of the yaw/roll stability of heavy trucks characterized by high centers of gravity, *SAE Paper 821260*.